Novel intramolecular diastereoselective flp-type activation for aldehydes

Angelica Mejia Fajardo

Université Fédérale
Toulouse Midi-Pyrénées

THÈSE

En vue de l'obtention du
DOCTORAT DE L'UNIVERSITÉ DE TOULOUSE

Délivré par l'Université Toulouse 3 - Paul Sabatier

Présentée et soutenue par

ANGELICA MEJIA FAJARDO

Le 18 mai 2021

Nouveau type de paires de Lewis frustrées (FLP) pour l'activation intramoléculaire diastéréoselective des aldéhydes

---

Ecole doctorale : **SDM - SCIENCES DE LA MATIERE - Toulouse**

Spécialité : **Chimie Organométallique et de Coordination**

Unité de recherche :
LCC - Laboratoire de Chimie de Coordination

Thèse dirigée par
Sébastien BONTEMPS

Jury
Dr. Raluca MALACEA KABBARA, Rapporteure
Dr. Frédéric LAMATY, Rapporteur
Prof. Frédéric GUILLEN, Examinateur
Dr. Sébastien BONTEMPS, Directeur de thèse

Our greatest weakness lies in giving up.
The most certain way to succeed is always to try just one more time.
Thomas A. Edison

It always seems impossible until it is done.
Nelson Mandela

Acknowledgments

First of all, I would like to thank the Jury for accepting my thesis and taking the time to read, review, and give me constructive feedback. Dr. Raluca Malacea, thank you for your kind guidance during my corrections; you encourage me to give my best. Dr. Frédéric Lamaty, I really appreciate your comments and your interest in clean energies; which is my motivation in this field. Professor Frédéric Guillen, as a president of the committee, you were neutral and fair. In the reading of the document, you went through helping me clarify some concepts.

I also want to thank my Supervisor, Sébastien Bontemps. He played a big part in my thesis; I believe I am a better person thanks to him. He is a good scientist and taught me new things in chemistry. He did all he could with the tools he had during this period. He taught me the difference between being a leader and a boss. Both are based on authority. A boss demands blind obedience; he depends only on authority and needs to inspire fear. A leader earns his authority being strong but not rude and inspires enthusiasm and understanding. The boss drives people; the leader coaches them. A true leader fixes the breakdown, does not blame others, has the courage to accept mistakes, learn from them, and works without resentfulness. The leader is emotionally intelligent, taking responsibility for their own behavior and emotions. The leader understands situations and tries to find solutions objectively. For all of these learnings, dear Sébastien, I am genuinely thankful. I have learned that knowledge is not enough; we live in a society and interact with human beings. It is fundamental to improve the four

pillars of emotional intelligence self-awareness, self-management, motivation, and empathy. I will work every day to improve myself, and success will continue coming as a result.

The completion of this study could not have been possible without the Doctoral School, especially to Agnès Lavande and Eric Benoist. They took additional time to check the document and guide me during the manuscript's writing in the absence of a supervisor. Furthermore, they surpass the willingness to be helpful and neutral, offering me appropriate guidance and thoughtful advice when I really need it. Thanks to COLFUTURO, who provide me the loan/scholarship.

Additionally, I would like to thank team N, especially Michel Etienne and Nicolas Queyriaux. Michel always took the time to teach me and guide me like a coach. Without a doubt, he is a role model for me as a scientist, professor, and human being. Nicolas was incredibly kind and good at handling all the situations. As a postdoctoral researcher, he helped me in the academic field. Sylviane, thank you for your kindness and example as a team leader; it was always inspiring to see how you can be an excellent scientist with a fantastic personality. I was always amazed every time you told us stories about yourself and all the activities you can do besides chemistry.

Thank you, dear Dan; you were my colleague, roommate, and friend who always give me advice in any aspect, even in chemistry or cooking. You always were willing to hear me and offer me a smile any time; I am really going to miss you. Cynthia, thank you because I find in you a wonderful person and friend.

Amal, you really surprise me, you are such a beautiful person, and I will always remind your empathy. For the rest of the team members, I always appreciate the atmosphere at work. Thanks to Ramaraj for his jokes and happiness, Carlos for his kindness, and Sara for her advice and love stories. Thank you, Sameh, for sharing all your dreams for the future; I am sure you will succeed in all. Thank you all, SMAC group, really.

In the LCC, there are so many people to be grateful. The director Azzedine Bousseksou thank you for your support. Marie-Louise, thank you for encouraging me to keep going and for being such a great listener. Laure, thank you for all your happiness every time I worked with you. Thank you to all the technical staff in the Laboratory. In LPCNO, I would like to thank Iskander for the theoretical studies on my work. I am sure you will keep succeeding; you are one of the most intelligent and disciplined people I know.

Thank you to all my friends in Toulouse because they were my family here. There are too many things to say about how they positively impact my life, but it would be endless, so I would try to be concise. Elias, thank you for being my best friend in the laboratory; you always helped me to keep myself calm and focus, no matter the events. Kasia, you have no idea how grateful I am to find you; you are one of my best friends for life; you give me strength every time and defended me against the world; thank you so much. Lenka, thank you so much; you are a beautiful friend. You and Andreij were great, and you always have so much empathy with me. I love spending time with you and now with Dominic. Mario, my favorite Colombian in Toulouse, you are a loyal and honest friend. That is not

easy to find; thank you really, you are a good friend, even if you are sometimes not the most subtle, which is an aspect I love about you.

Alejandro, I have not enough words to thank you, you are a terrific person. It is rare to find someone willing to help as you, taking the time even with a thousand things to do. When it was the researcher's time, the postdoc was there, when it was the time to hear an overwhelmed friend, Alejo was there. You make me believe that everything is possible if you keep going and you do the right thing. So honestly, thank you so much for this incredible support.

Mayra, thanks for your words in the last days before the defense; you really touch my heart. Elena, thank you for your support in the distance; I hope to see you soon for our trip. Thank you, Julien, Valentin, Emmanuel, Pablo, Ayman, Montse, Natalie, Oleskander and Camila, for cheering me up every time and share incredible moments with me.

Thank you so much for my old friends Pau Pau, Andre, Osqui, Munir, Sista, Jhon, Migue, Carlos, Andres and Julito. They were always there to share with me their stories, listen to me, and most of all, persuade me to continue no matter the situation.

My life sisters, Marti, Lilos, and Meli, thank you so much for being there like no one. In my most difficult moments, you were there, giving me all the strength I could possibly have. In My joy moments, you celebrate like it was your own achievement. You are always proud of me and always inspiring me to be a better person.

Last but not least, thanks to my family. My parents Patricia and Alvaro, you are the best parents every person can imagine. You are kind and strong; you always taught me that I should continue fighting for my goals and be an honorable person no matter the circumstances. You always let me decide my path and make my own mistakes because all the obstacles and difficulties were experiences and wisdom that a good learner would no miss. Thank you so much for your support; to teach me that good manners and kindness are essential in any field. It would not be possible this work without you.

Thanks to my abuelitos (grandparents) Justo y Blanca. You are the biggest fans I can imagine. Always calling me and cheering me up. The happiness and love you give me are incommensurable; you are like my parents to me. Aunt Haydi, thank you for your support and your jokes at any time; your laugh is something that I remember when I want to feel happy. Thank you so much to all my family.

Finally, Fadi, there are not enough words to thank you, you were by my side during this process. You were there when I laughed when I cried, whenever I needed a hand. You support me in every way possible. For example, when I have no scholarship, no place to live, and even you stayed awake when I had to give parallel classes in the middle of the night (Colombia time) to earn some extra money. You are the most patient, kind and lovely person I know. I feel fortunate that I met you, and now you are part of my family.

For everyone to make in a way this work possible, thank you so so much.

NOVEL INTRAMOLECULAR DIASTEREOSELECTIVE FLP-TYPE ACTIVATION FOR ALDEHYDES

I. TABLE OF CONTENTS

GENERAL INTRODUCTION

GENERAL INTRODUCTION

The overexploitation of fossil fuels has led to an excess of carbon dioxide in the atmosphere creating an imbalance in the carbon cycle. As a consequence, an increase in global temperature and ocean acidification has directly impacted all the ecosystems and, therefore, the economy and quality of human life.[1] International agreements have been addressed to mitigate these emissions. The most relevant, the Paris Agreement, United Nations Framework Convention on Climate Change's (UNFCCC) 21st Conference of Parties (COP 21), adopted on December 12, 2015.[2] In this historic meeting for the first time, 195 nations agreed on limiting the global average temperature rise in this century to well below 2 degrees Celsius and being carbon neutral no later than the second half of the century—all of them under international funding and obligations with specific actions.

In this context, the scientific community is driven to find new possibilities and methods for capture and reduce carbon dioxide for energy storage.[3,4] In the chemistry field, the approach to solving these new challenges of climate change is towards green and sustainable chemistry solutions, aiming to design and synthesize cost-competitive products with better processes, reducing pollution and its source. Some of the principles include preventing waste, provide less hazardous synthesis, design for energy efficiency, the use of removable feedstocks, reduce derivatives, and improve catalysis over stoichiometric, among others.[5,6]

The present work is embedded in the Small Molecules Activation Group (SmAC), from the Coordination Chemistry Laboratory (LCC-CNRS). This group studies the fundamentals of homogeneous catalysis and their reaction performance, activating abundant and stable molecules such as carbon dioxide, oxygen, nitrogen carbon dioxide, and other types of readily available feedstock, including formaldehyde, alkanes, alkenes, and simple aromatics. In this regard, the team could provide fundamental studies to reduce the footprint and use CO_2 as a carbon source.

Frustrated Lewis Pairs systems (FLP) are a new concept in green chemistry due to their ability to function as the free metal catalyst for small molecules activation like hydrogen[7], carbon dioxide, aldehydes, and all kinds of small molecules. Although one of the most prominent summaries with development and perspectives in FLP was in a review in 2015 by Stephan[8], the area has grown substantially since then. These systems have found new reactivities under mild conditions, making them attractive to a practical and safe chemical process solution.

The present document seeks to study the reactivity and potential use of the C02 adduct = compound **1** (Figure 1) (named this way because it comes from 2 molecules of CO_2). This molecule is particularly fascinating because of its inner features that include:

1. A Lewis base carbon-based that is not coming from a carbene **F1**.

2. A Lewis acid, borane **F2**.

These characteristics lead to explore the potential use of the compound as a new FLP system, mentioned for Bontemps group[9], opening these questions to address in the present work (Figure 1):

1. Could it be considered as a masked FLP form **Q1**?
2. Could it have the potential to activate small molecules such as carbonyl functions **Q2**?

Chapter one presents two main sections. The first one is about the general concepts that will be used during the present study. The second part is about state of the art, including the most relevant reactions and publications.

Chapter two is divided into two essential parts. The first one is dedicated to exploring the scope of CO_2 adduct reactivity with polar and carbonyl functions and the synthesis of new compounds. The second is devoted to the electronic and kinetic study of the benzaldehyde adduct reaction.

Chapter 3 is the experimental compilation of the present study.

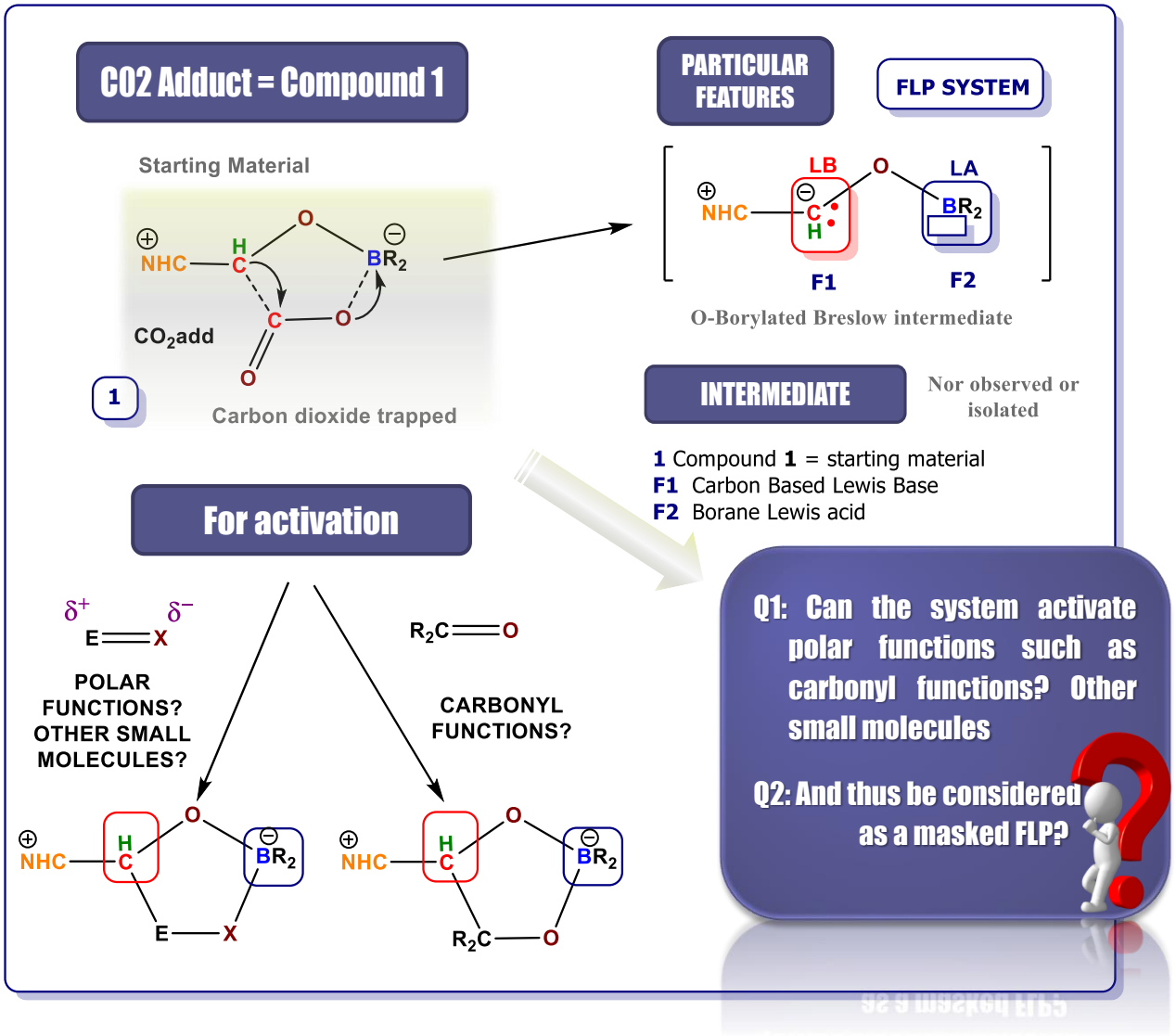

Figure 1. CO2 Adduct =CO2add. Potential new FLP type activation and its particular features. Present work.

CHAPTER I

CHAPTER I

BIBLIOGRAPHIC BACKGROUND

I. INTRODUCTION

Frustrated Lewis Pair's ability to activate small molecules in a metal-free manner has drawn the attention of researchers interested in green chemistry, broadening the Lewis acid/base combinations.[10]

This chapter will concentrate primarily on the FLP systems with carbonyl functions. It will be described the synthesis of the FLP system and its modifications for the study. Following, generalities of the reactivity of carbonyl compounds will be the base for the system's activation. Concepts as chirality and stereoisomerism would be essential to understand the possible results. Therefore, features of various Breslow intermediates and their studies related to FLP activation will be explored. Finally, it will be described the state of the art of related studies in FLP.

II. SYNTHESIS

The CO_2 adduct, (**CO_2add**), was obtained following the main protocol[9] (Figure 2), and it is prepared in two main steps, the reduction step and the C-C coupling step.

The first part comprises the double hydroboration of CO2 from 2 equivalents of **9-BBN** under dynamic CO2 at room temperature. 1% of Iron Catalyst **FeCat** was necessary to afford the 4e-reduction product Bis (boryl) acetal (**BBA**) (Figure 2).

Without further purification, the Enders Carbene (**E-carb**) is added to the fisher porter in stoichiometric ratio at 60°C in which the carbene attacks the methylene of

the **BBA** with a simultaneous migration of the **O-BBN** fragment to the other borane, resulting in compound intermediate A (**int-A**). When **Int-A** is subjected to CO2, the methylene is internally deprotonated and the borinic acid is released, which results in the **OBB-int**, in simple words E-carb mediated an umpolung event in the methylene group from **1** to the **OBB-int**, now the carbon center is a nucleophilic carbon. The new generated nucleophilic center attacks the CO2 generating the final product.

To obtain the product **CO2add**, it is washed with Et2O and filtrate. The white solid obtained as a residue is the purified compound (yield= 50%).

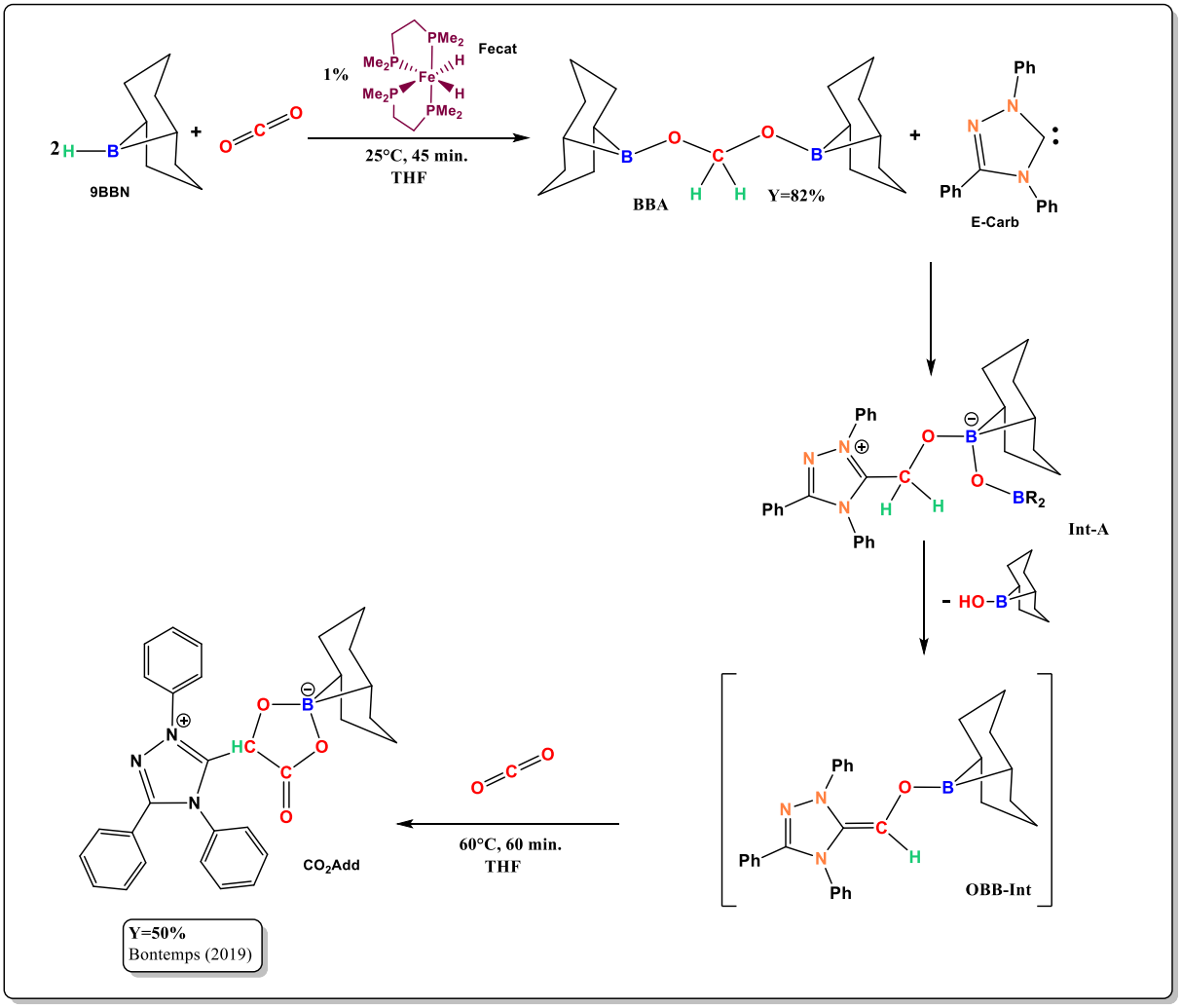

Figure 2. CO2 adduct synthesis.

III. GENERALITIES

1. CARBONYL GROUP

1.1. Carbonyl functional group

Aldehydes, ketones, carboxylic acids, esters, amides, and acid halides, contain the carbonyl functional group (C=O) (Table 1)[11]. However, some functions like carboxylic acid can have more than one function, carbonyl and hydroxyl group being considered a derivative of the carbonyl group, the carboxyl group. In the same way, esters are alkyl derivatives of carboxylic acids. Esters contain alkoxy carbonyl group as a functional group, being a combination of carbonyl and alkoxy group. [12]

Keeping in mind that the acyl group strongly affects the reactivity of the carbonyl compounds, it is possible to divide it into two classes: class I and class II. In the class I carbonyl compounds, the acyl group is bonded to an atom or group that can be substituted by a nucleophile.[13] Acyl halides, carboxylic acids, esters, acid anhydrides, and amides can undergo nucleophilic acyl substitution reactions, and are called carboxylic acid derivatives. On the other hand, Class II carbonyl compounds include those in which the acyl group is attached to a group that can not be substituted by a nucleophile, such as ketones and aldehydes.[14]

Table 1. Principal functions cointaining carbonyl functional group C

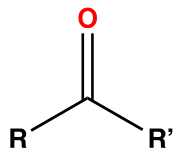 KETONE	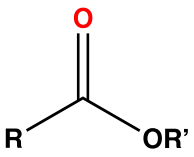 ESTER	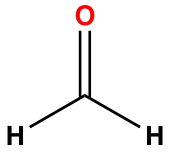 FORMALDEHYDE	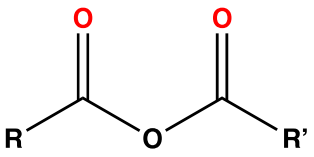 ACETIC ANHYDRIDE
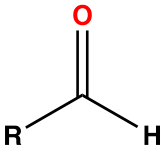 ALDEHYDE	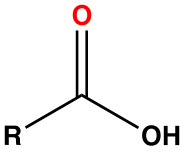 CARBOXYLIC ACID	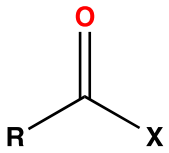 X= Cl, Br, F (halides) ACYL HALIDE	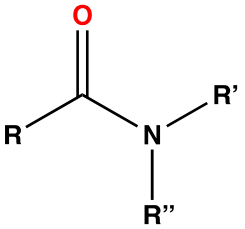 AMIDE

The carbonyl group comprises a double bond between the oxygen and the carbon atoms: one with σ-character and one with π-character.[15] The carbon-oxygen double bond is polar: the oxygen atom is more electronegative than carbon, so the electron density is higher on the bond's oxygen side and lowers on the carbon side (Figure 3).

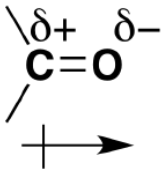

Figure 3. The polarization of the carbonyl group.

Carbonyl carbons present sp^2 hybridization. The three sp^2 orbitals on the carbon overlaps with one sp^2 orbital on the oxygen and one sp^3 orbital of each of the two adjacent carbons or the *s* orbital in the case of hydrogen atoms.[16] These three bonds adopt a trigonal planar geometry with three angles of 120° (Figure 4). The remaining unhybridized *2p* orbital on the central carbonyl carbon is perpendicular to this plane and forms a π bond with a *2p* orbital on the oxygen. Two of the sp^2 hybrid orbitals on the oxygen contain a lone pair of electrons that are not used to bond with another atom. The carbon and oxygen then bond in much the same way as the two carbons do in ethylene (Figure 4, Figure 5).[17]

It is essential to notice that while the bonding is similar between C=C and C=O, they are different because of the electronegativity difference, the distribution of electrons in the π bond is highly distorted towards the oxygen end of the bond, this distortion in the π bond causes significant differences in the reactions of compounds containing carbon-oxygen double bonds.[18]

Another difference lies in the length of the C=O bond. It is shorter than C=C due to the greater s-character in the oxygen atom. The closer the electrons are held to the nucleus, the shorter and stronger the bond. [19,20]

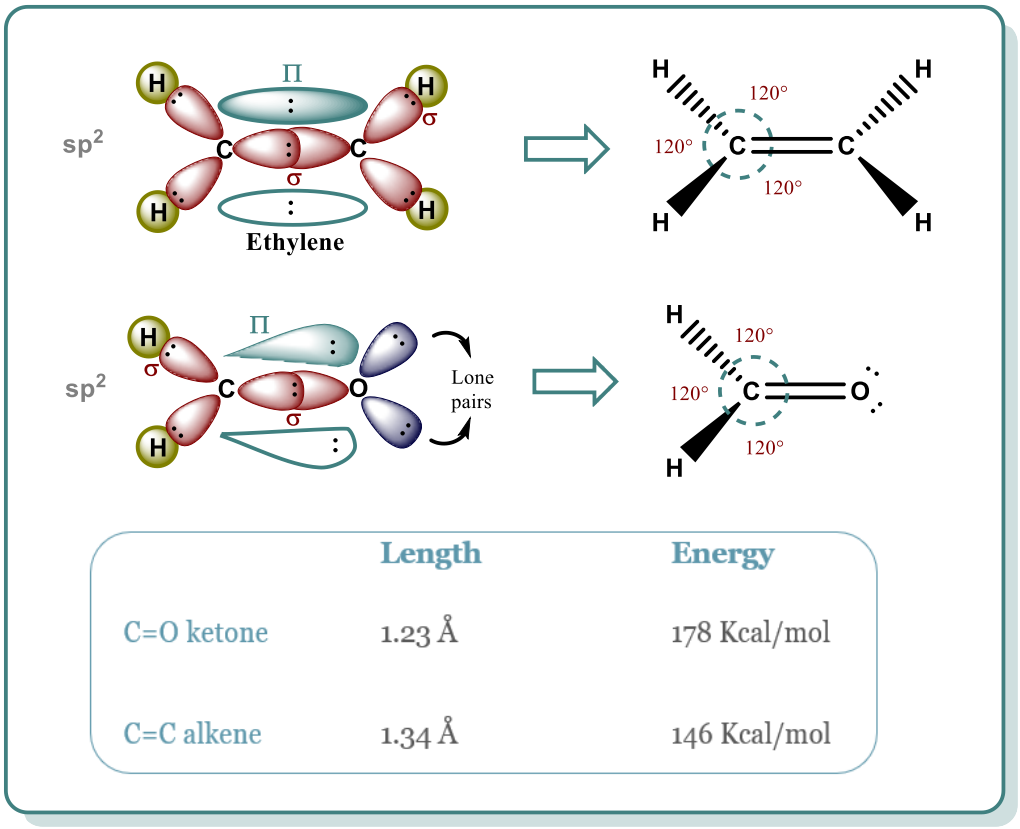

Figure 4. General configuration of the carbonyl function.

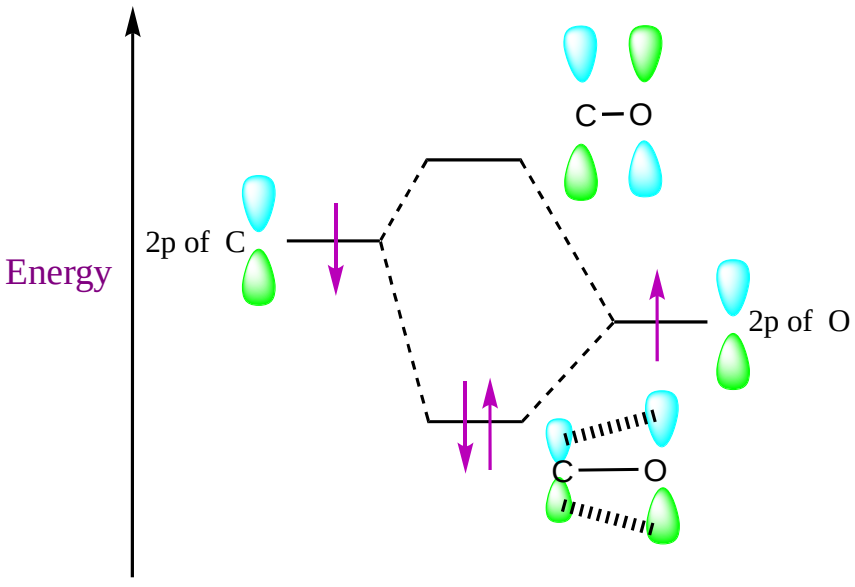

Figure 5. Molecular Orbitals π and π* of the carbonyl group.

1.2. Nucleophilic addition reactions to the carbonyl group.

The carbonyl group's reactivity results from the electronegativity difference between the carbon atom and the oxygen atom. This functional group's most common reaction is the nucleophilic addition, which consists of adding a nucleophile to the carbon atom.[21]

A nucleophile is a specie that brings a pair of electrons in order to form a new covalent bond; there are three majors criteria to determine how strong is a nucleophile:

-The size: the linear/smallest it is, the strongest it will be.

-The electronegativity: Good nucleophilic species are not electronegative

-The polarizability: the more polarizable it is, the more nucleophilic it will be.

Because of this group's geometric configuration, the system has relatively low steric hindrance and is open to attack from both sides of the double bond. When a nucleophilic species attacks the carbonyl group's carbon atom, the electrons of the π bond are displaced toward the oxygen atom, creating an ion alkoxide. In this process, the carbon atom changes its sp^2 hybridization to sp^3. In a later step, the alkoxide is protonated, giving the product of the reaction.[22,23]

There are two fundamental events in a nucleophilic addition reaction (Figure 6):

- ✓ Formation of the new sigma bond between the nucleophile (Nu) to the electrophilic C of the C=O group.
- ✓ Breaking of the π bond to the O resulting in the formation of an intermediate alkoxide.

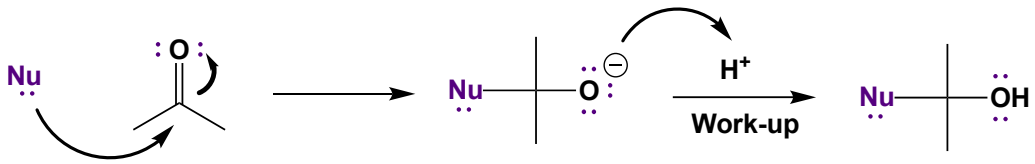

Figure 6. General nucleophilic addition.

Depending on the reactivity of the nucleophile, there are two possible general scenarios: Strong nucleophiles (anionic) add directly to the C=O to form the intermediate alkoxide. The alkoxides are then protonated on work-up with dilute acid.[11]

Weaker nucleophiles (neutral) require that the C=O be activated before the attack of the **Nu**. This can be done using an acid catalyst that protonates the oxygen on the carbonyl and makes the system more electrophilic.[24,11] This can also be achieved by using a Lewis acid. Examples of strong nucleophilic systems ranking from strongest to weakest are: NH_2^- > Ph_3C- > $PhNH^-$ > ArS^- > RO^- .[25,26]

In ketones, although the alkyl groups are a weak electron-donating group, they compensate for the withdrawal offset of electron density by the oxygen atom, in contrast to aldehydes which contain only one alkyl group. This partial positive charge does not provide enough electron density as in ketones, which means that the aldehydes are slightly more electrophilic and less stable than ketones. Consequently, formaldehyde is the most reactive of the three due to the carbon's lack of electron density (Figure 7).[27]

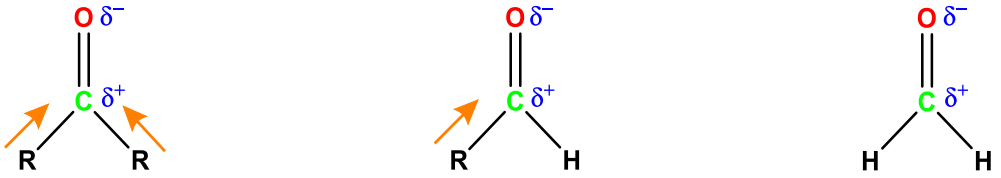

KETONE	ALDEHYDE	FORMALDEHYDE
Two alkyl groups	One alkyl group	None alkyl group
Donating Group EDG	Lower stabilization	Relatively unstable

Figure 7. Comparison of the stability between ketones, aldehydes, and formaldehyde.

The carbonyl group's stability effects are reflected in the equilibrium constants for the hydration of aldehydes and ketones (Figure 8). The equilibrium constants of ketones' hydration reaction have values between 10^{-4} and 10^{-2}. For the majority of aldehydes, this constant is close to 1. The formaldehyde, which does not have alkyl groups attached to the carbonyl, has a constant hydration of 2,000.[28,29]

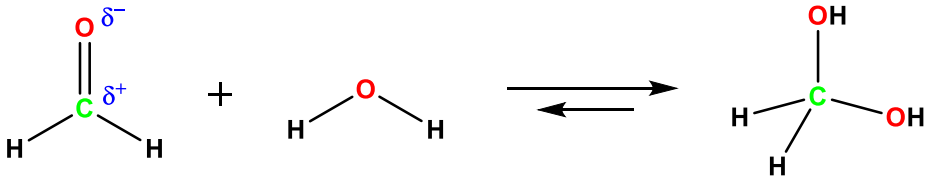

at equilibrium: $\frac{\text{concentration of methylene glycol}}{\text{concentration of formaldehyde}} > 1000$

Figure 8. Hydration for methylene glycol

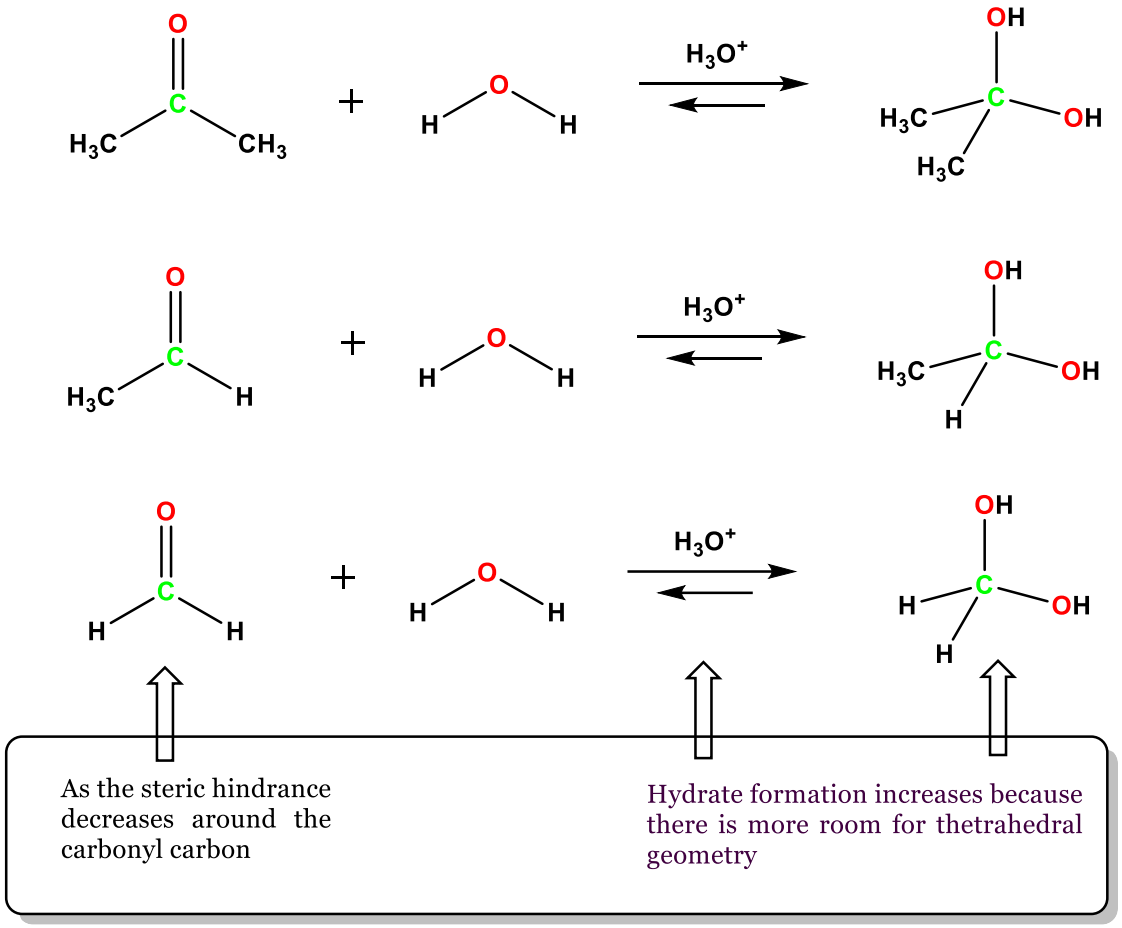

Figure 9. Steric effect for hydrate formation stability.

There is also a steric effect. The carbonyl carbon atom has a larger bond angle than the tetrahedral product. As a result of increased steric hindrance, the addition product is less stable for ketones than for aldehydes (Figure 9).[12,26]

1.3. *Addition of Hydride: Reduction to Alcohols*

Certain metal hydrides can add to the carbonyl group of aldehydes and ketones. The result of this nucleophilic attack is an alkoxide, which provides alcohol after protonation (Figure 10) .[11]

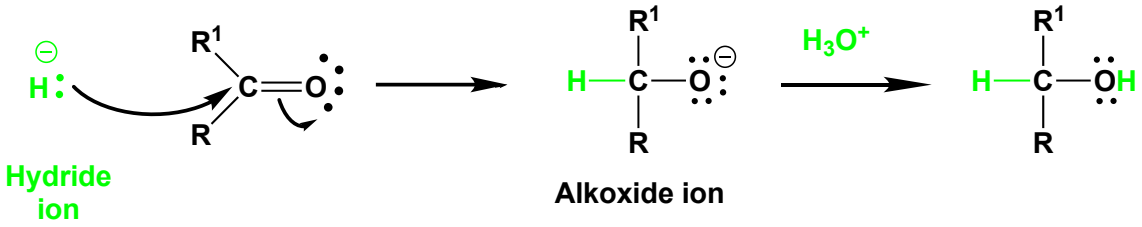

Figure 10. Hydride addition reaction.

1.4. *Oxidation of aldehydes and ketones.*

Aldehydes can be oxidized by strong oxidizing agents, such as $KMnO_4$ and soft oxidant as the Ag_2O. In these oxidations, the aldehyde is transformed into a carboxylic acid. Ketones are resistant to oxidation because of the absence of a C-H bond (Figure 11).

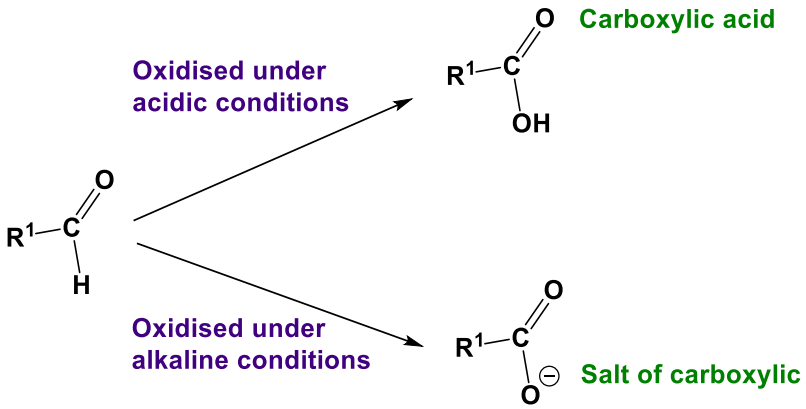

Figure 11. Oxidation of aldehydes and ketones scheme.

The ease with which aldehydes are oxidized is the basis of chemical tests that allow differentiating them from the ketones. When silver nitrate ($AgNO_3$) and aqueous ammonia are mixed, it generates a solution known as *the reagent of Tollens*. The reagent contains the diamminosilver (I) ion $Ag(NH_3)_2^+$. Although this ion is a very weak oxidizing agent, it is able to oxidize the aldehydes into the corresponding carboxylate. The Ag(I), which is the oxidant, is reduced to metallic silver, Ag(0). If the test of *Tollens* is carried out in a test tube, the metallic silver is deposited on the walls forming a silver mirror. Sometimes, the oxidation of the aldehyde is very fast, and then the metallic silver is deposited in the form of dark gray precipitate[26].

1.5. The Baeyer-Villiger oxidation reaction.

The aldehydes and ketones are converted to esters by reaction with peracids (RCO_3H). The reaction is beneficial with ketones because it allows the obtention of esters' in good yields[21] (Figure 12).[30]

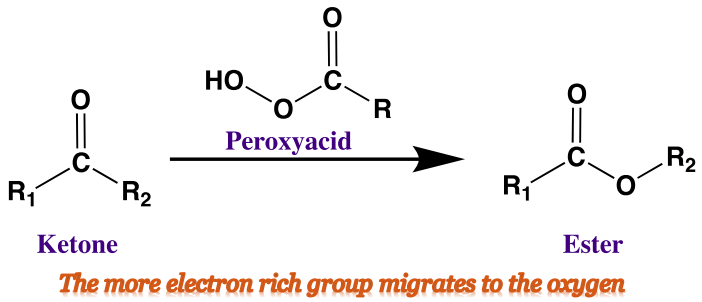

Figure 12. Baeyer-Villiger oxidation reaction scheme.

This reaction's mechanism begins with the carbonyl oxygen protonation, making it much more reactive (1b). Then there is the nucleophilic attack of the peroxide oxygen as a result (2b). The hydronium ion is easily deprotonated to give a neutral compound (3). The peroxide's carbonyl oxygen is protonated, which facilitates its elimination as

a leaving group (4). Finally, the carbonyl group's regeneration forces the migration of the phenyl group, and the free pair of electrons to the oxygen atom produces a simultaneous elimination of the carboxylic acid[31] (Figure 13).

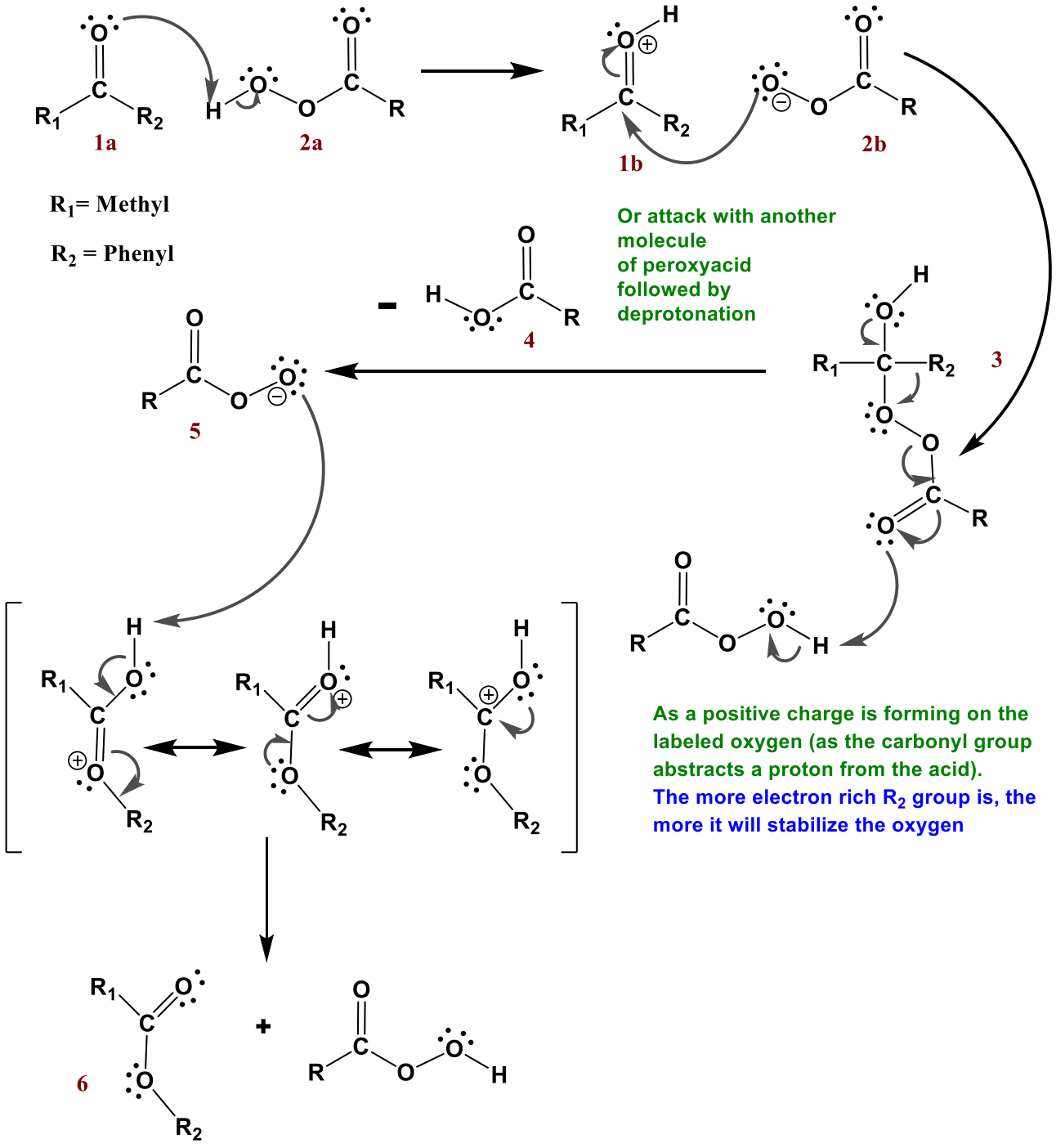

Figure 13. Mechanism of the Baeyer-Villiger oxidation reaction.

The product of this reaction (6) shows that the aromatic group has a greater tendency to migrate than the methyl group because it stabilizes better his positive charge; otherwise, it would have obtained the methyl benzoate. This tendency to migrate is called migratory aptitude. The migration aptitude of different groups in the reaction of Baeyer-Villiger is described in the following list: H > tertiary alkyl > cyclohexyl > secondary alkyl, aryl > primary alkyl > methyl.[30]

2. CHIRALITY AND STERREOISOMERISM

In this section, concepts of stereoisomerism and chirality will be explained to analyze diastereoselectivity in the reactions. Previous studies suggest that FLP related systems, with phosphine/borane and enamine/borane system, do not present diastereoselectivity.[32–34] However, as will be discussed in the next chapter, the present study seems to present unprecedented diastereoselectivity.

In order to understand our system, concepts such as chirality and absolute configuration will be explained in the following lines as other notions, including enantiomers and diastereoisomers (Figure 14).[26,11]

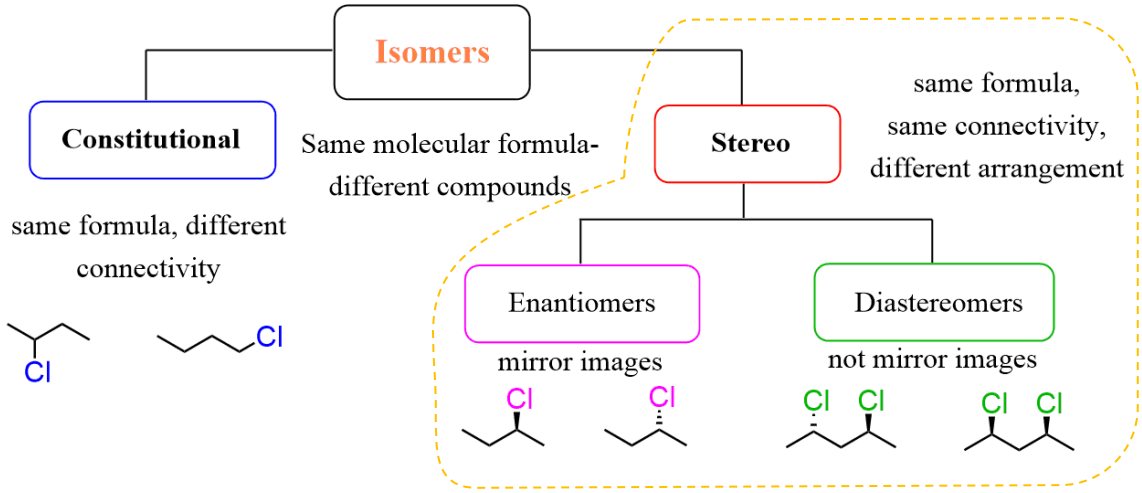

Figure 14. General classification of isomers.

2.1. Chirality

A molecule is chiral if no symmetry plane can be found. The presence of an asymmetric carbon is a sufficient condition but not necessary. Two molecules are chiral if they are non-superimposable like the reflection of one another in a mirror. The most common example is the hand that cannot be superimposed on its image in a mirror. While achirality is the absence of chirality, meaning that it is possible to superimpose (Figure 15).[11,35]

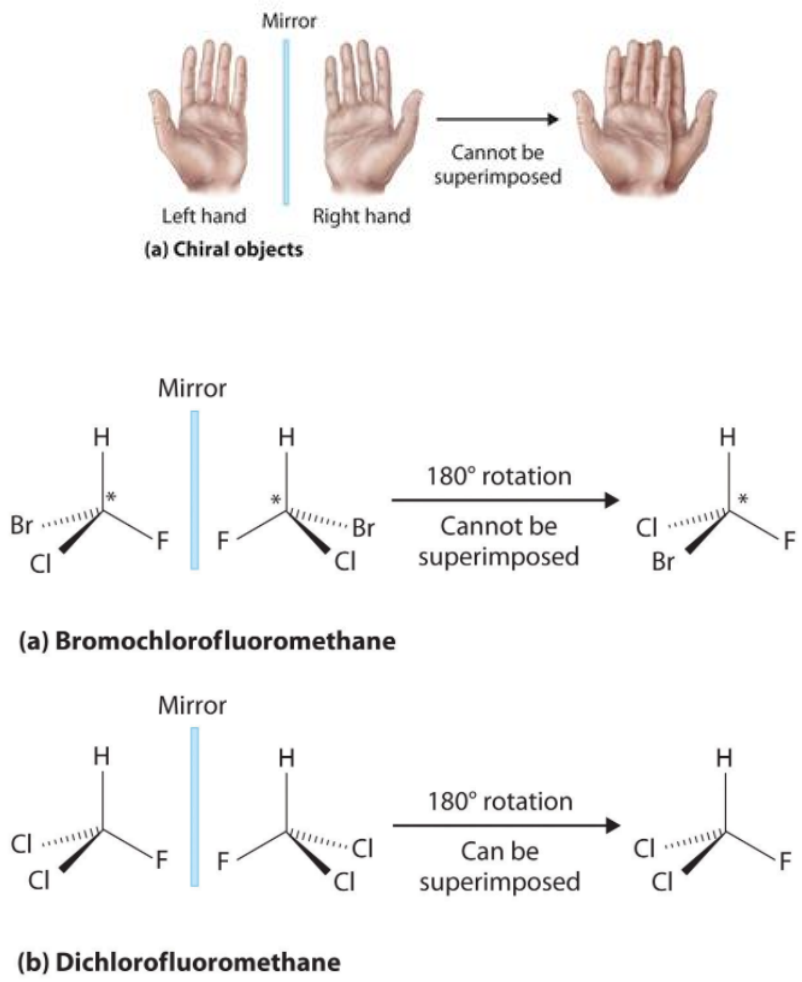

Figure 15. Chirality vs. achirality

2.2. *Absolute and relative configuration of chiral centers*

Absolute configuration: Refers to the chiral molecule arrangement in the three dimensions, no matter the other molecules. It can be determined by Cahn–Ingold–Prelog priority rules or optical rotation experiment.[35]

The Cahn-Ingold-Prelog rules of priority are based on the atomic numbers of the atoms of interest. For chirality, the atoms of interest are the atoms bonded to the chiral carbon. The atom with higher atomic number has higher priority (I > Br > Cl > S > P > F > O > N > C > H).

When comparing isotopes, the atom with the higher mass number has higher priority [$^{18}O > {}^{16}O$ or $^{15}N > {}^{14}N$ or $^{13}C > {}^{12}C$ or T (^{3}H) > D (^{2}H) > H].

When there is a tie in (2) above, establish relative priority by proceeding to the next atom(s) along the chain until the first difference is observed.

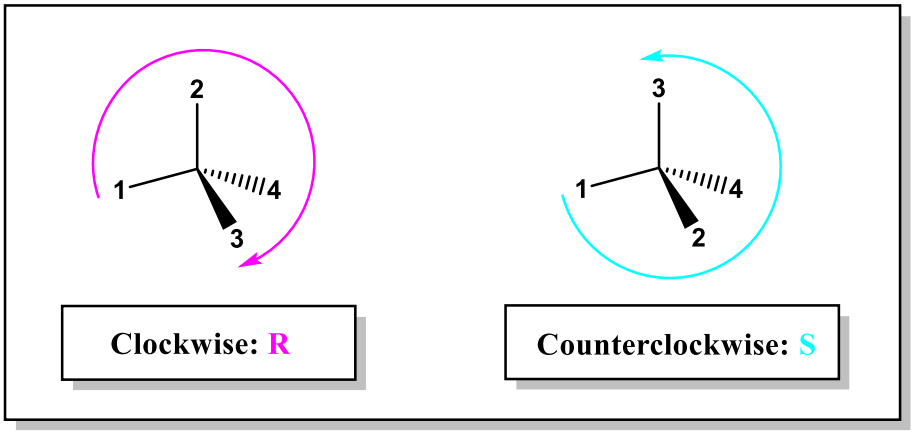

Figure 16. Scheme for the determination of S and R according to the priory rules of Cahn-Ingold- Prelog

Relative configuration: The relative configuration is the experimentally determined relationship between two enantiomers; it is independent of the absolute configuration.[36]

While relative configuration compares the arrangement of atoms in space of one compound with those of another, the absolute configuration is the precise arrangement of atoms in space.[37]

Cis/trans nomenclature is adequate only when the alkene has two different groups on each carbon atom of the double bond, and each carbon has one of the same group. If the isomer is on the same side, it is a cis isomer, and if it is on the opposite side is a trans isomer.[11]

In the case of tetrahedral atoms, sp^3 hybridization, the substituents are in a geometrical equivalent position. That means that, if the four substituents are different, there are two possibilities to be arranged: they are the reflection of each other, and they cannot be superimposed (Figure 17). This situation is defined as a chiral molecule, previously defined before in the present document. [36,38]

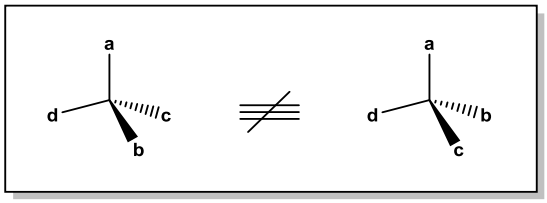

Figure 17. Chiral molecule in a tetrahedral molecule

2.2.1. Compounds with multiple chiral centers

It is pretty common in the compounds to find more than one stereocenter, which opens the possibilities for new types of isomers inside the molecule. The enantiomers, as mentioned before, are a non-superimposable mirror image. However, when it is more than one stereocenter, finding an isomer (same molecular formula, same connectivity, a different configuration in space) is non-superimposable and no longer a mirror image a diastereoisomer. [35,39]

For example, the threonine (Figure 18) (2-amino-3-hydroxybutanoic acid) present four projection formulas from the two chiral carbons :

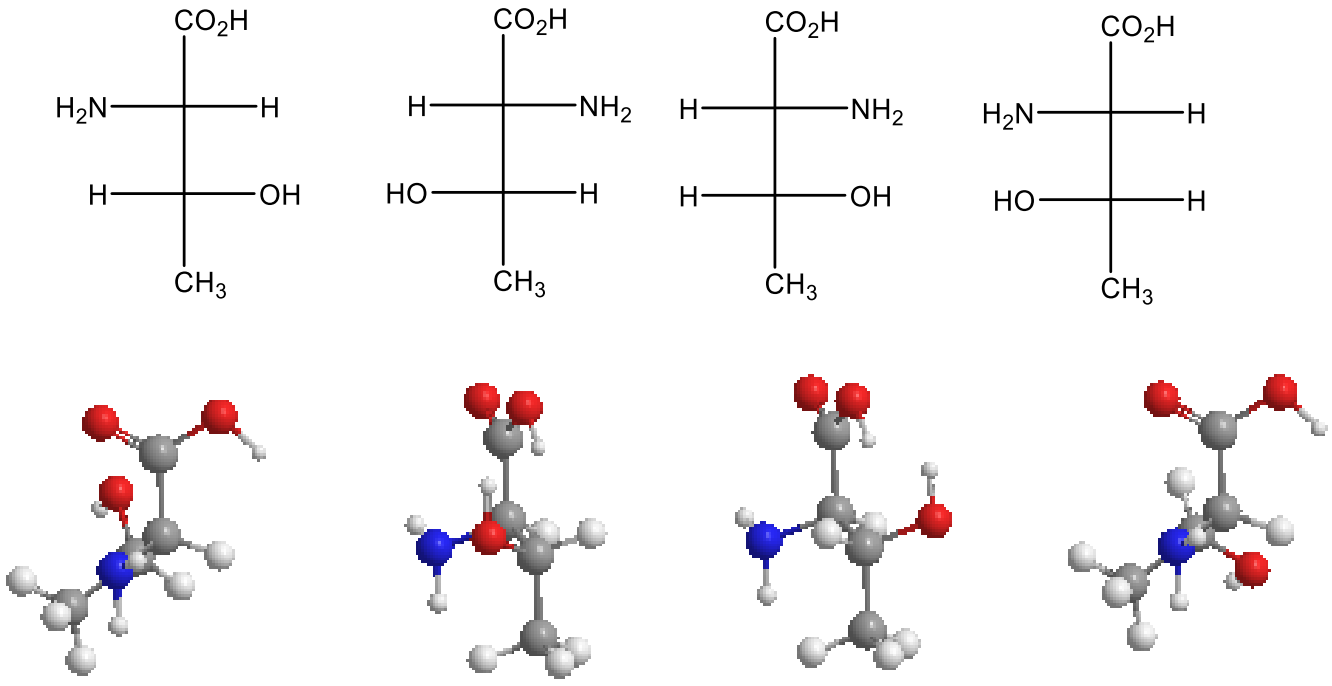

Figure 18. Chiral molecules of threonine.

2.3. Stereoisomers

It refers to isomers with the same functional group and connectivity, but the atoms' arrangement in their space is different.[26,37]

2.3.1. Enantiomers

It is a subgroup of stereoisomers, where a pair of stereoisomers are the reflection of each other. In other words, they are non-superimposable mirror images (Figure 19).

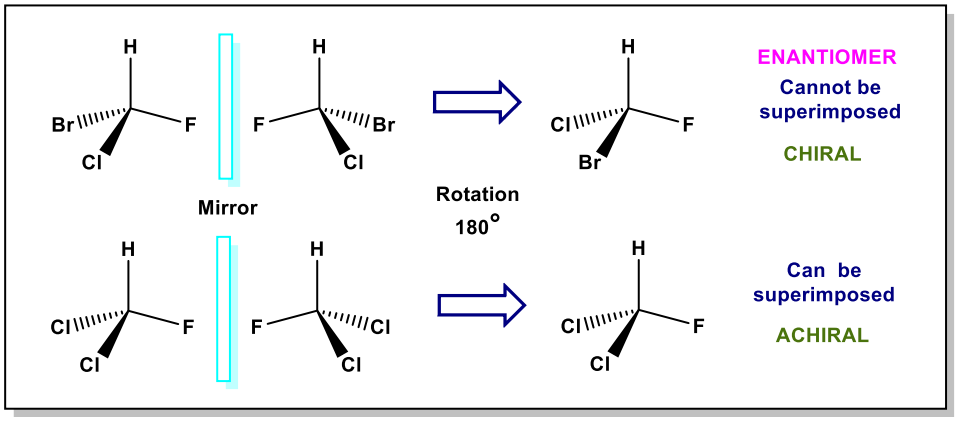

Figure 19. Enantiomer example (above). Chiral structure (above) and achiral (under).

2.3.2. Diastereoisomers

Diastereoisomers are optical isomers that are not enantiomers. Enantiomers are chemically identical because they are the reflection of the other; meanwhile, diastereoisomers are stereoisomers that are not the mirror images of the other and are non-superimposable. They are characterized by having more than one chiral center. A diastereomer with n chiral centers has 2^n possible stereoisomers. Thus for a diastereomer with two chiral centers, they are four possible stereoisomers: a pair of diastereomers with two pairs of enantiomers (Figure 20).[26,40]

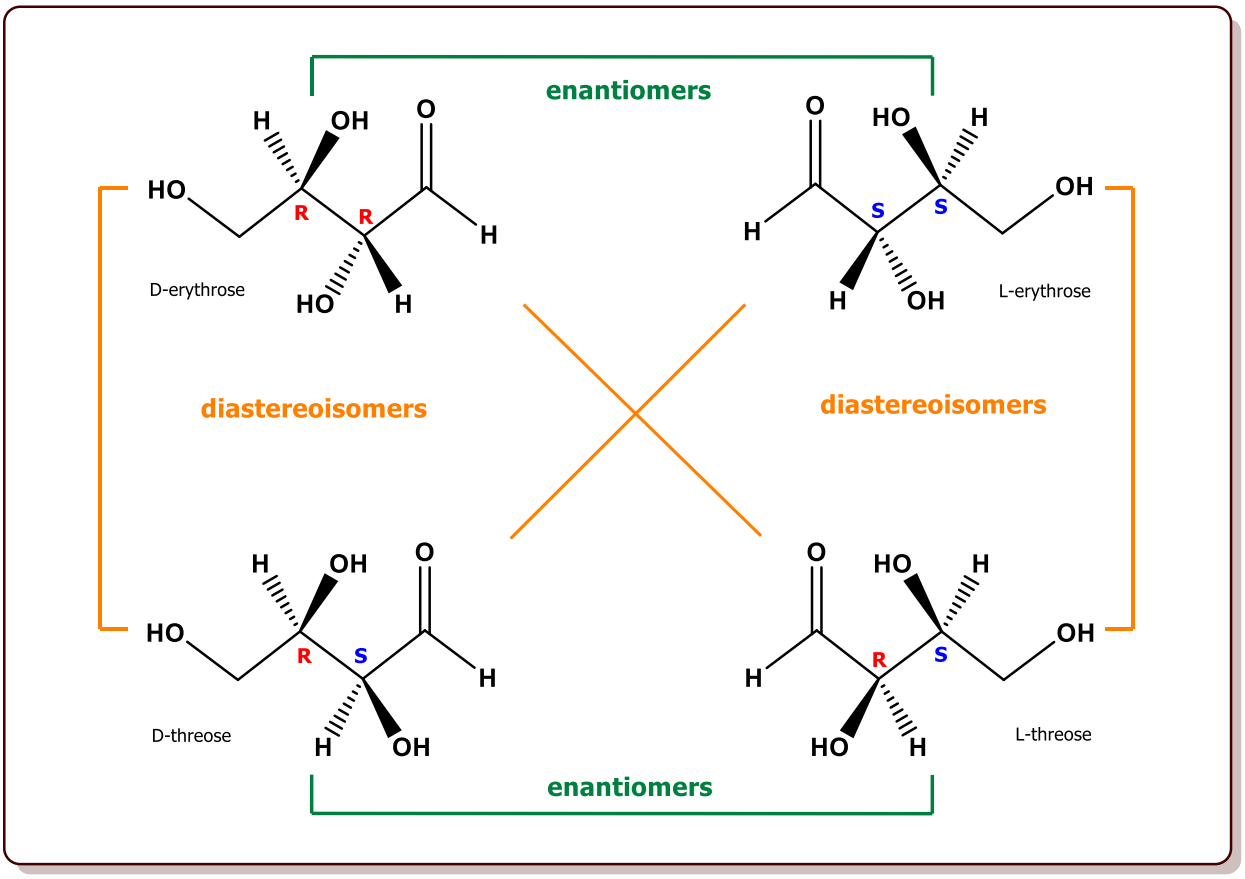

Figure 20. Diastereoisomers and enantiomers.

The physical and chemical properties of diastereoisomers are different, in contrast to the properties of the enantiomers which are identical.[41]

2.3.3. Stereoselectivity

It is defined by the preferential formation of one stereoisomer over another in a reaction. It is divided into enantioselectivity and diastereoselectivity. The selectivity could be applied by the preference in the consumption of one stereoisomer or, in the most common situation, by the isomer predilection in the product formation.[40]

Several factors combined could determine the stereoselectivity, such as stereoelectronics, steric hindrance, torsion, conformational, and temperature effects. Each of these effects can be linked to a particular aspect of the structure. In the case of stereoelectronic effects, they are geometry-dependent; orbital interactions favor one stereoisomer's formation or consumption over another. Steric effects are from repulsions between valence electrons or non-bonded atoms. The repulsive interactions develop between closely approaching species (e.g., a neutral molecule and a free radical) or between two groups within the same structure. Steric effects complement electronic effects, which dictate the shape and reactivity of molecules. Conformational effects are differences in stereoselectivity due to differences in the population of various conformers. Torsional effects are the destabilizing interactions that develop as electrons in bonds on adjacent atoms move closer to each other. [37,42]

In a chemical reaction, there are two possible paths, thermodynamic control, and kinetic control. Those not necessarily are separated in the product; they always depend on the specific reaction and could also favor an isomer's selectivity.[43] The reaction conditions as the solvent, temperature, pressure, and the factors mentioned above can affect the pathway competition. As a basic definition, the kinetic product is formed faster, and the thermodynamic product is the more stable product (Figure 21).[44]

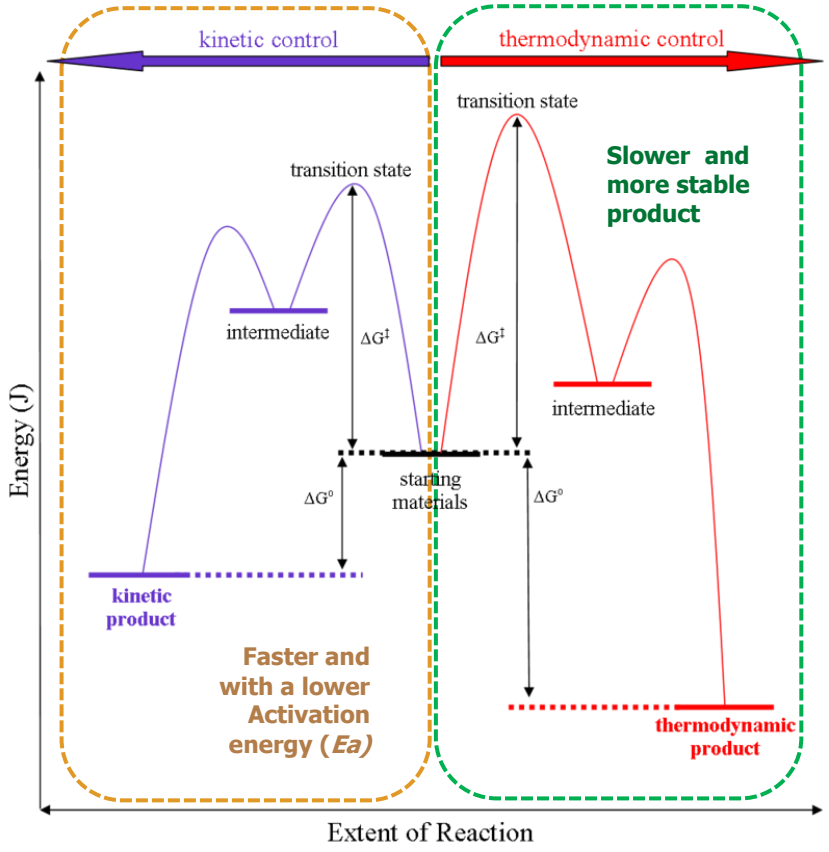

Figure 21. Kinetic vs. thermodynamic control.

IV. BRESLOW INTERMEDIATE

In 1832, Wöhler and Liebig discovered the cyanide-catalyzed coupling of benzaldehyde to benzoin.[45] Later in 1903, a mechanism for this reaction in which an intermediate carbanion is formed by hydrogen cyanide addition to benzaldehyde followed by deprotonation was revealed by Lapworth.[46]

Based on Lapworth's studies, in 1958,[47] Breslow proposed a mechanistic model for the thiazolium salt-catalyzed benzoin condensation (Figure 22). In this

mechanism, the catalytically active free carbene is generated under basic conditions. The nucleophilic attack of an aldehyde's carbonyl function generates the tetrahedral intermediate **I**, which generates nucleophilic Breslow intermediate in the resonance-stabilized form enaminol-type **II** after a proton transfer. Breslow intermediate **II** reacts with an electrophilic substrate of an aldehyde's second molecule to give intermediate **III**. From intermediate **III**, a proton transfer followed by elimination of free NHC furnishes the benzoin product via the intermediate **IV**.

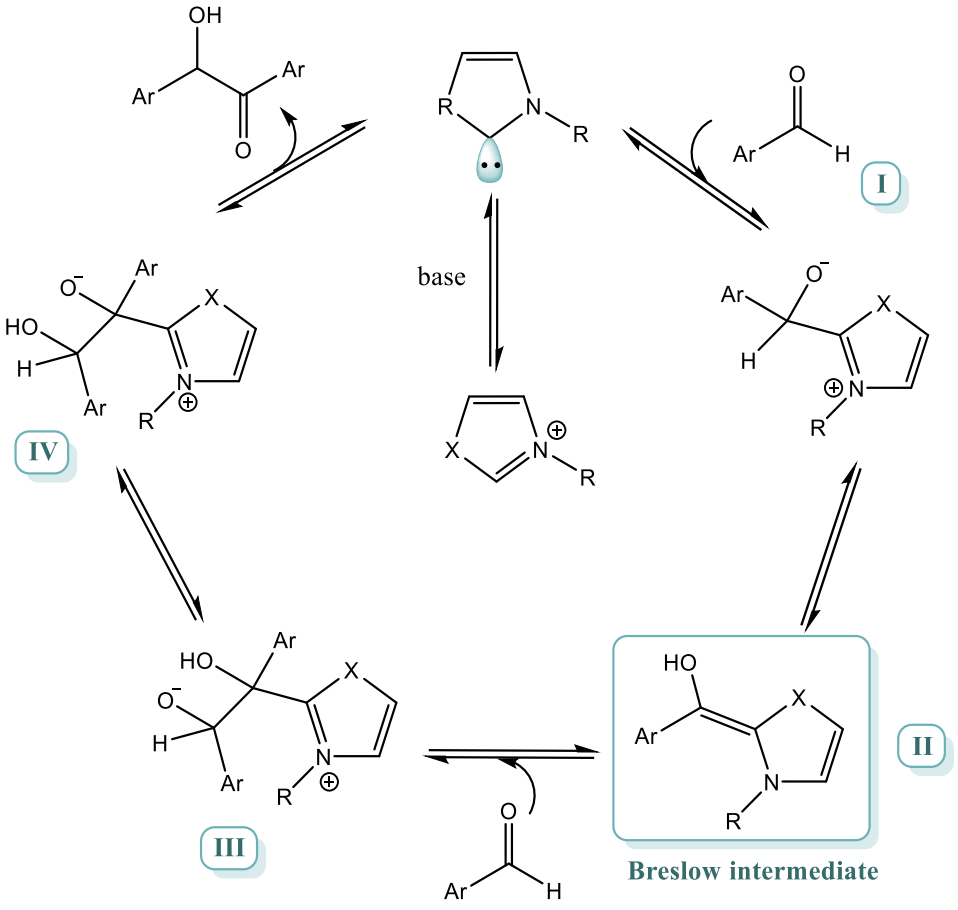

Figure 22. Benzoin condensation proposed by Breslow.

In the 1970s, the Stetter reaction,[48] named in honor of his author, reported using a thiazolium-catalyst (umpolung chemistry) to add aldehydes to α,β-unsaturated

carbonyl compounds, catalyzed by cyanide or a thiazolium salt, resulting in 1,4-dicarbonyl products. This reaction competes with the corresponding 1,2-addition, which is the Benzoin Condensation. However, the Benzoin-Condensation is reversible, and since the Stetter Reaction leads to more stable products, the main product will be derived from 1,4-addition. Since this discovery, the asymmetric synthesis of this transformation has been developed. In general, catalysts capable of enforcing conformational stability of the key intermediate (the Breslow intermediate) have successfully achieved high degrees of enantiocontrol. In the 1990s, Arduengo and Enders[46,49] isolated and characterized several NHCs, providing new opportunities to expand this field in organocatalysis.

During the past years, new Breslow intermediates had been characterized by NMR or Crystal isolation. In 2012, Mayr and coworkers[50] developed a method to synthesize and isolate stable O-methylated Breslow intermediates where they found that they were less reactive than deoxy Breslow intermediates and that O-methylated Breslow intermediates derived from thiazoles (Figure 23.a). In the same year, Rovis and coworkers reported the isolation and complete characterization of nitrogen analogs of the Breslow intermediate derived from the reaction of chiral triazolylidene carbenes and iminium salts, including their catalytic properties (Figure 23.b).[50] Soon after, in 2013, Berkessel and coworkers characterized by NMR and X-ray the selective generation and characterization of diamino enols, diamino dienols, azolium enolates, and an azolium enol providing better understanding and new data to discover futures NHC-catalyzed umpolung reactions (Figure 23.c).[51,52]

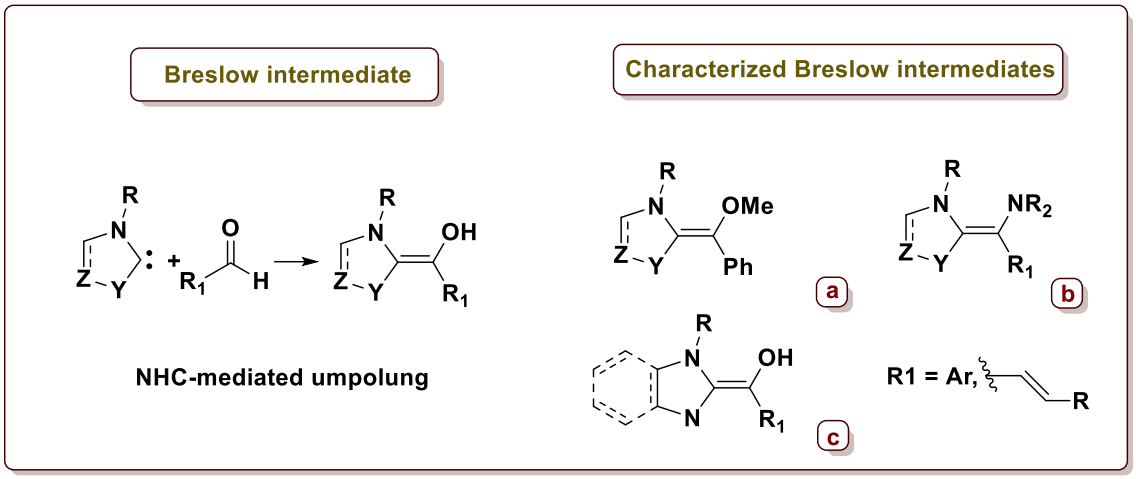

Figure 23. Types of Breslow intermediates characterized.

As a remark, no other O-substituent analog has been described, nor the C-unsubstituted Breslow intermediate has never been characterized experimentally. The present work will study a Breslow intermediate version, the O-Borylated Breslow intermediate (**OBB-int**) hidden in product **1** (Figure 24). This intermediate formed with boron in one site and with the triazol-5-ylidene carbene (also known as Enders carbene) in the other site, affords a nucleophilic carbon in one site and acid boron in the other, providing a Lewis acid base pair.

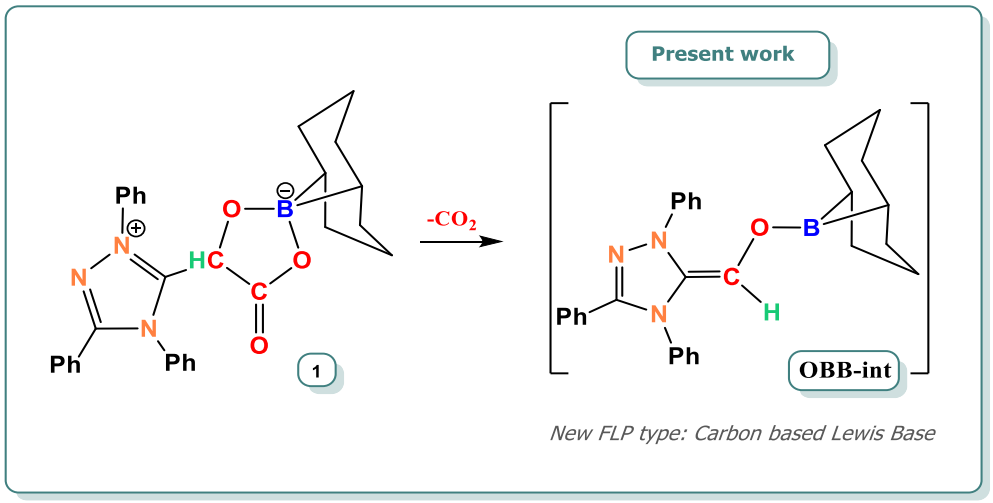

Figure 24. O-Borylated Breslow Intermediate hidden in product 1.

V. STATE OF ART: FRUSTRATED LEWIS PAIR AND CARBONYL GROUP ACTIVATION

1. FLP CONCEPT

In order to understand Frustrated Lewis Pair, it is essential to explain the concept of electron donors and acceptors given by Gilbert Lewis in 1923 in his work "Valence and the Structure of Atoms and Molecules"[53] and further in 1942, the application of the concept as an axiom of Lewis acid bases by Brown[54] and coworkers. A Lewis acid refers to the chemical species with an empty orbital capable of accepting an electron pair that is not involved in a bond; thus, a Lewis base is the donor of a free electron pair forming a dative bond.

The classical Lewis acid-base adduct is the reaction between borane and ammonia (Figure 25).[55]

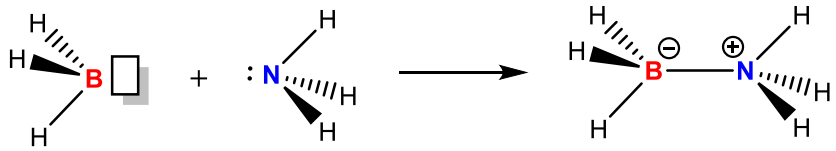

Figure 25. Classical Lewis acid/base adduct.

In terms of molecular orbitals, Lewis bases have a high energy HOMO compared to Lewis acids, which are molecules with a low-lying LUMO.[56] This is an important principle to understand the mechanism of several organic and inorganic reactions. However, some exceptional cases where the Lewis base and Lewis acid cannot form an adduct due to geometry or steric hindrance are called Frustrated Lewis Pair (FLP), opening a new type of small molecule activation (Figure 26).[57]

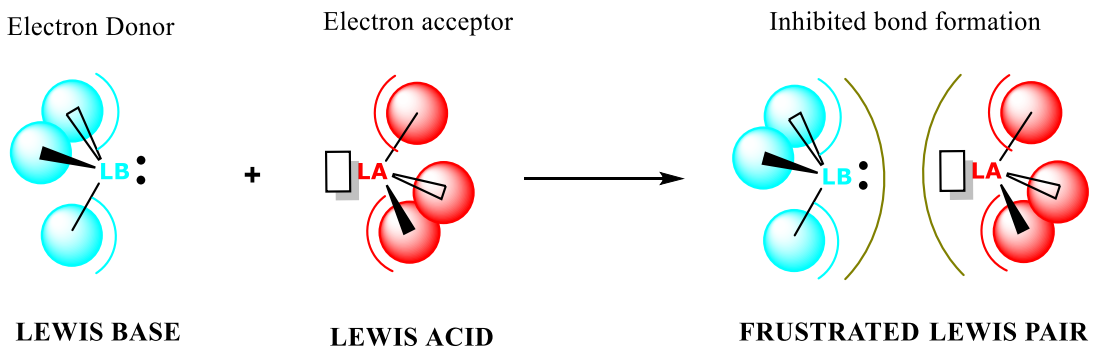

Figure 26. Frustrated Lewis pair FLP scheme.

Although in the 40s, Brown[54] developed early studies in this field observing that lutidine and BF_3 could not form a dative lewis pair due to steric hindrance of lutidine, it was not until 2006 that this particular system was exploited for synthetic purposes. Stephan's research group[58] observed that the phosphine-borane **I-1** could activate a hydrogen molecule under very mild conditions (25 ° C, 1atm H_2) (Figure 27). Moreover, the product **I-2** deriving from the heterolytic rupture of the H_2 molecule can release the dihydrogen and regenerate compound **I-1** in a reversible process above 100°C. The heterolytic breaking of the dihydrogen molecule in the absence of transition metals, is the real significance of this work, very unusual for that decade.

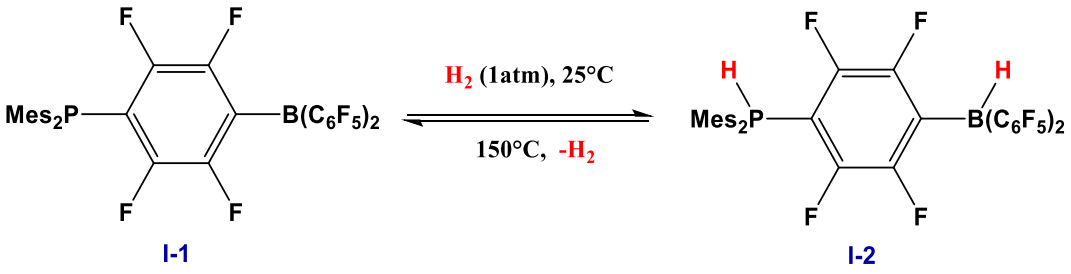

Figure 27. First FLP system reported.

Since this field's birth (2006), if we search in the Sci-finder database, using "Frustrated Lewis Pairs" as a query, 3095 research papers and 41 patents have been published, (I obtained this information from this database on June 10/21),[59] with more than 1000 publications only between 2019 and 2020.[60] Two volumes of *Topics in Current Chemistry*[32,61] develop various aspects of the area, and it has been written several reviews[62,63,64] and papers have been written from the general scope to more specialized aspects of FLP type systems.[64,65]

2. LEWIS BASE/LEWIS ACID INTERACTION

Although the first interest of FLP was its utility to cleave dihydrogen without the intervention of a metal, nowadays, the activation of small polar molecules lead to explore new opportunities in the reactivity of FLP. Functional groups such as alkynes, olefins, ketones, aldehydes[66,67], and more specific small molecules such as SO_2, N_2O, NO, CO, and CO_2, are examples of the wide variety that generate multiple possibilities of new reactivities.[62]

While currently FLPs have been studied by several experimental methods, including calorimetry and the most known by NMR spectrometry, the beginning of the studies towards the understanding of LB/LA interaction began with computational models.[62,63,68,69,70]

In a general way, the FLP could be classified into two main groups: intermolecular and intramolecular systems (Figure 28). In essence, the intermolecular system is a bimolecular reaction between the adduct and the molecule to activate, in contrast to the intramolecular system, which refers to the Lewis pair's internal interaction molecule.[61]

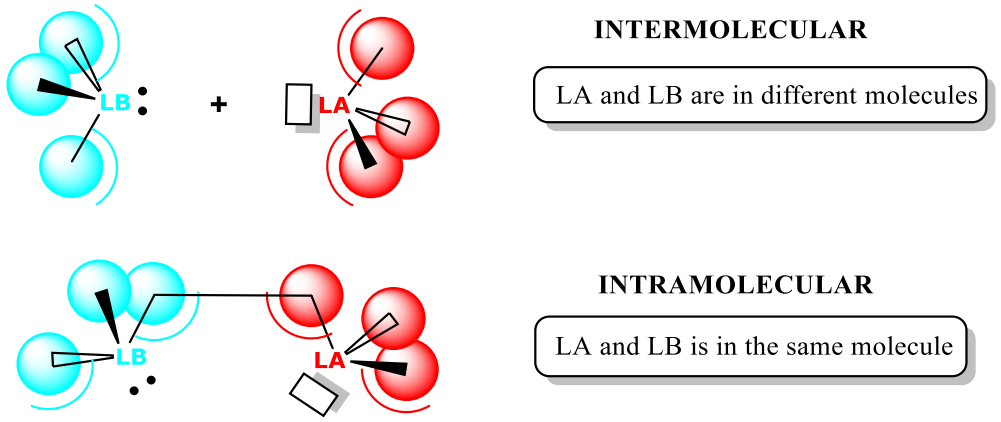

Figure 28. General scheme for intermolecular and intramolecular FLP.

3. RELATED STUDIES ON FLP: ACTIVATION OF CARBONYL GROUP

3.1. FLP Capture of CO_2

In 2009,[34] The first CO_2 reactions of interest in FLP were between **I-3** and **I-4**. This system, when interacts with CO_2, forms the species **I-5**. These products are also capable of releasing CO_2 and activating H_2. Related intermolecular reactions[71] have resulted in the species **I-8** (R= iPr, tBu) and **I-12** (R= hexyl, Cy, (norbornyl), Cl, and Ph) (Figure 29).

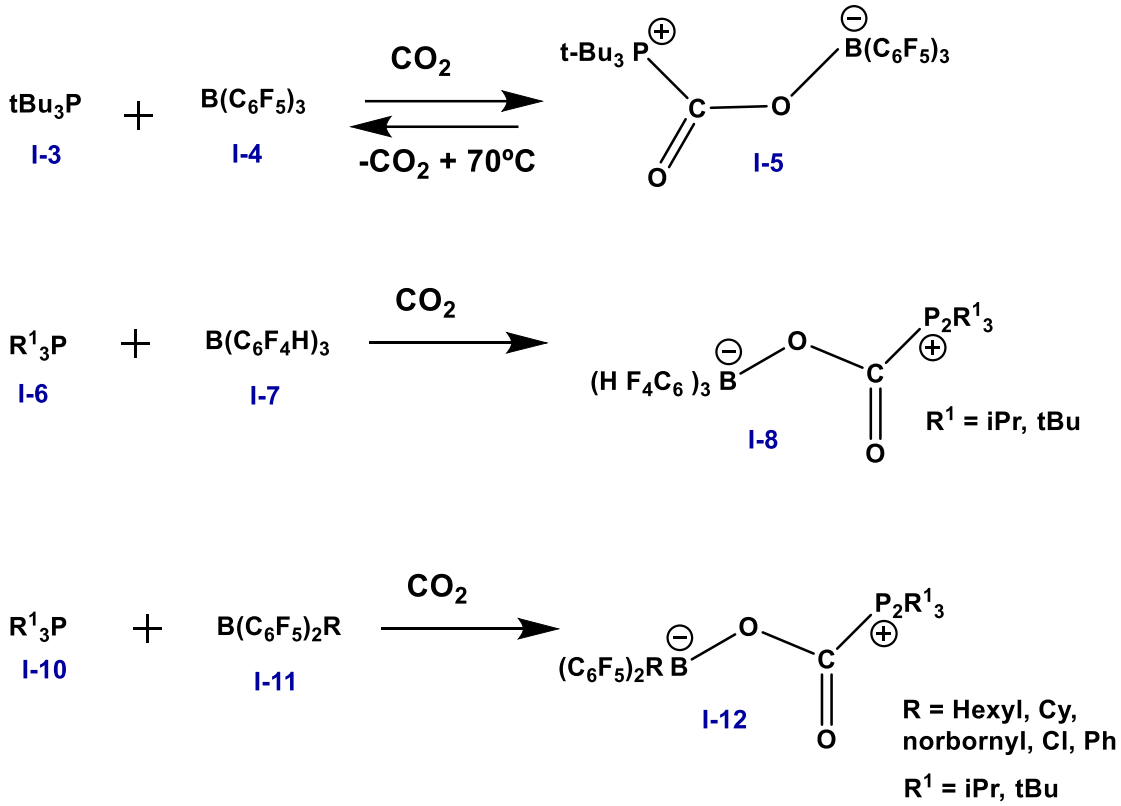

Figure 29. First FLP reactions with CO_2 reported.

In 2012,[72] other reactions were made with **I-13** and **I-14** to produce **I-15**. Likewise, **I-16** and **I-18** generate the products: **I-17** and **I-19** (Figure 30).

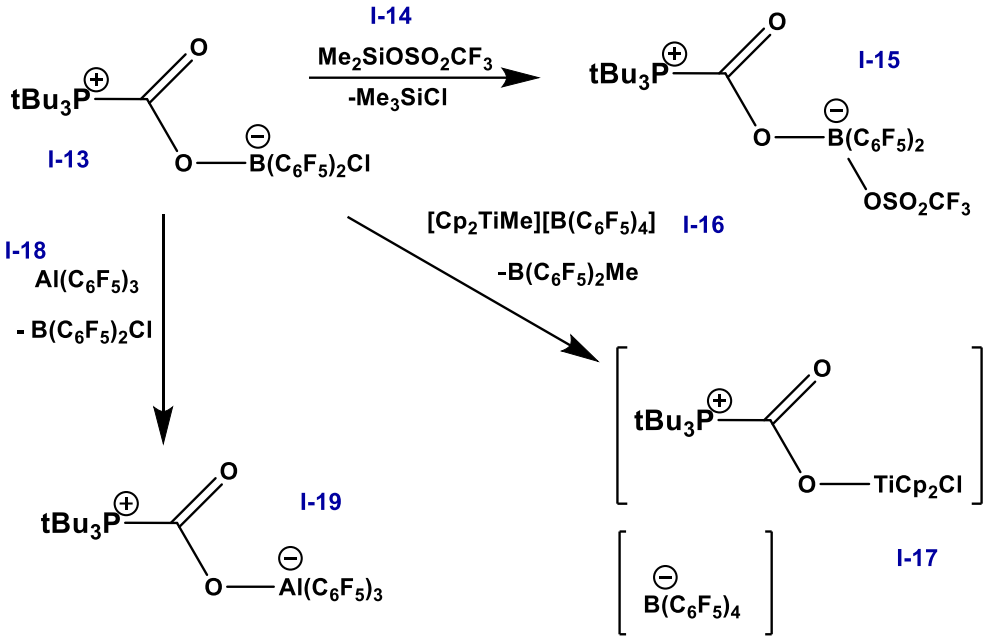

Figure 30. FLP reaction with $tBu_3P(CO_2)B(C_6F_5)_2Cl$ (CI-13) in 2012.

On the other hand, to prove the bis-boranes' advantage for stronger CO_2 bindings, **I-20** was used with CO_2 and **I-21**. The product obtained was **I-22**. Similarly, bis-boranes **I-23** (R=Cl, C_6F_5) react with CO_2 and **I-21** from the cyclic species **I-24**. When the temperature is over 15°C, the CO_2 is released (Figure 31). In the present work, the FLP system type shows a bond also between the Boron and the Oxygen of one CO_2 molecule and is not released at high temperatures, suggesting good stability.

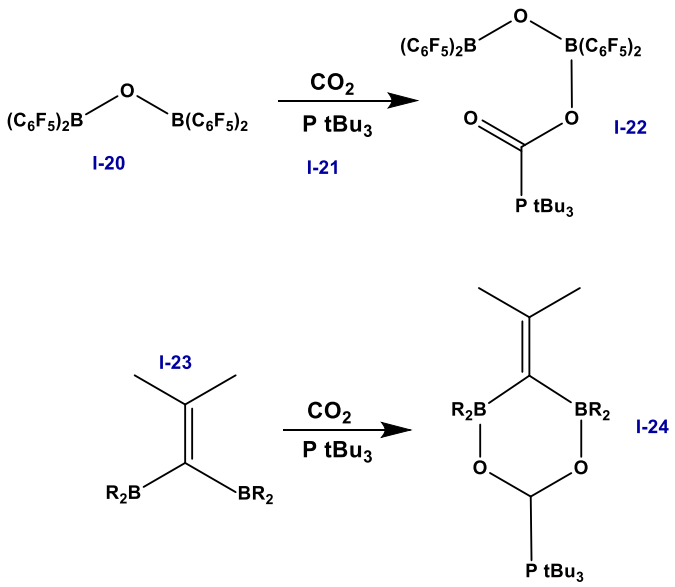

Figure 31. Reactions between CO_2 and bisboranes.

3.2. FLP in a stoichiometric reduction of CO_2

In 2009, Ashley and O'Hare[73] presented the FLP between tetramethylpiperidine (TMP, Me_4C_5NH) and $B(C_6F_5)_3$ that reacted with CO_2 and H_2. As a result, there is a conversion of CO_2 into methanol with a 24% yield.

When the phosphine-borane FLPs **I-25/I-3** (R= hexyl, Cy, norbornyl) react with CO_2 the formyl derivatives **I-30** is produced. The reaction of this FLP with formic acid **I-28** produces the compounds **I-29** (Figure 32).[71] These results showed similar behavior with the study made by Tran and coworkers (2011) using N-bases.[74]

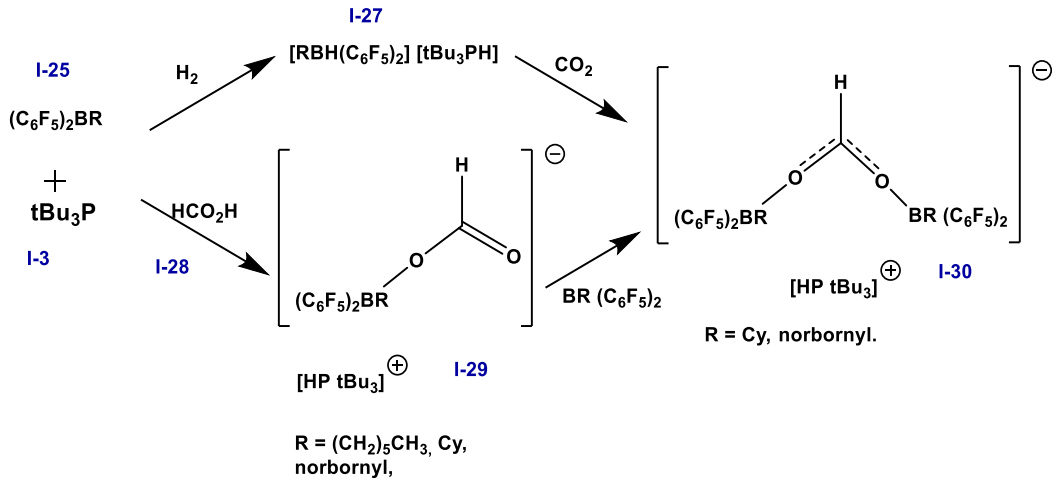

Figure 32. Reduction of CO_2 with phosphine/borane FLPs.

Another FLP system, **I-31** with **I-3**, binds with CO_2 and afford the product **I-33**. This product is incredibly stable because even under 80ºC for 24h, the CO_2 is not released[75]. Subsequently, the reaction with the amine borane **I-34** plus the quenching with D_2O forms methanol-d **I-36** in 34% yield. Equally, if the reaction is carried out with the compounds **I-35**, methanol yield raises 57% in 1 hour[75] (Figure 33).

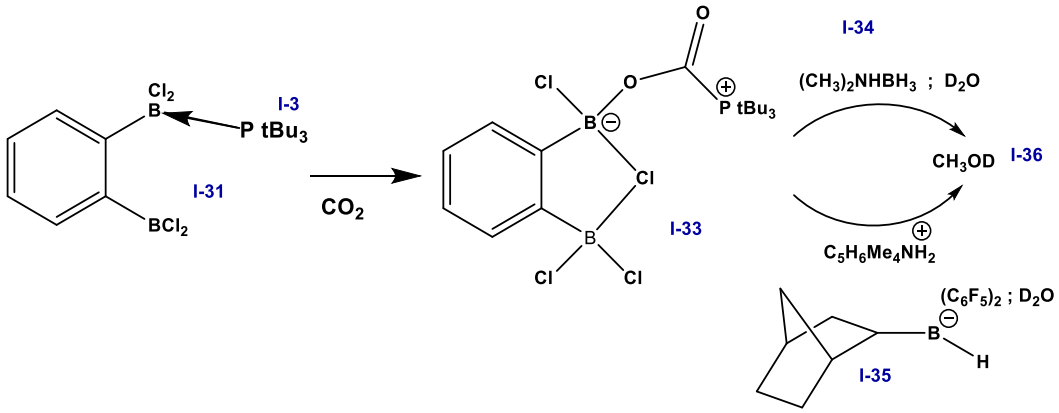

Figure 33. Reduction of CO_2 with phosphine/bis-borane FLPs.

The Phosphine/alane FLP, **I-37** and **I-38** (X= Cl, Br, I), reacts with CO_2 forming **I-39**. The addition of **I-40** provides Al-methoxide species, which upon hydrolysis gives methanol in 50% yield[76] **I-42**. When **I-39** is exposed to CO_2 for 18h, the products are **I-43** and **I-44**[77] (Figure 34).

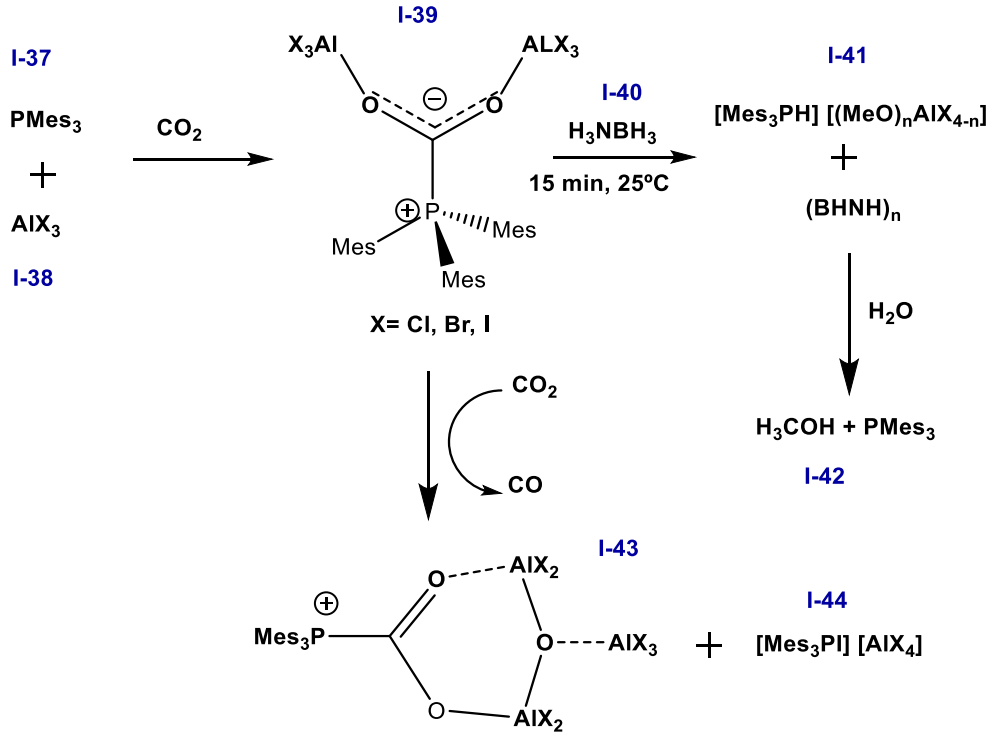

Figure 34. Reaction between $PMes_3$ (CI-37) and AlX_3 (CI-38) with CO_2.

3.3. Activation of Aldehydes

One of the first studies concerning the activation of aldehydes was performed by Momming *et al.* (2009).[78] In benzaldehyde **I-46** and cinnamaldehyde **I-48**, both are polar molecules that could potentially react with this intramolecular FLP system **I-45**. However, this addition reaction (Figure 35) showed a direct competition between the two aldehydes, strongly driven towards the trans-cinnamaldehyde **I-49** than **I-47**. The resonance effect on the cinnamaldehyde could explain this reactivity, which presents six resonance structures (one more than benzaldehyde), providing a more stable carbocation, favoring the product **I-49**.

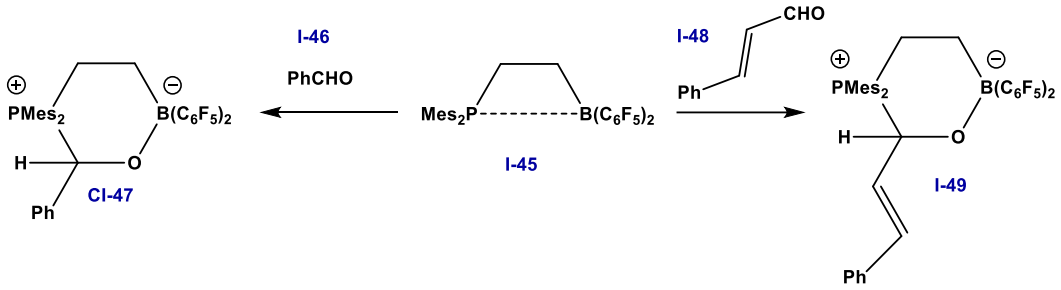

Figure 35. FLP system with benzaldehyde and cinnamaldehyde.

3.4. Carbon-Based Lewis Base

This group is constituted mainly by NHC´s reactivities and following fewer examples: the enamines and ylides. They provide a resonance effect in the structures, delocalizing the charges and giving more reactive compounds (Figure 36). The ylides afford stronger bases; the importance of the dipolar resonance form accounts for the

strongly nucleophilic character of the carbon atom of the ylide, which implies a broader application than enamides in this field.[79]

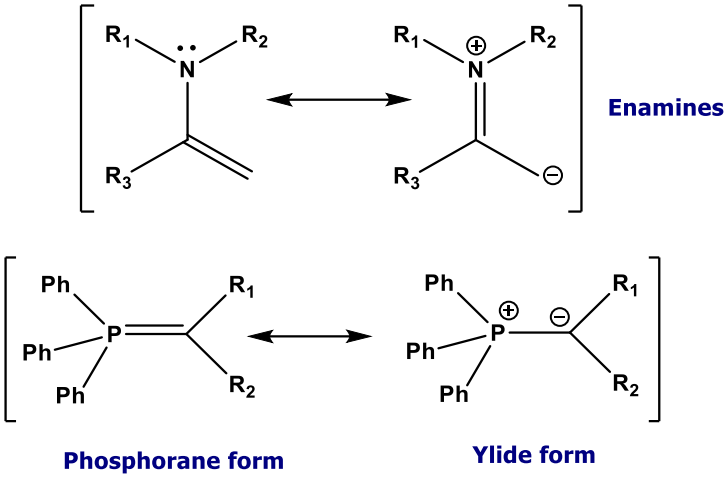

Figure 36. Resonance forms of phosphorus ylides and enamines.

In 2017, Erker and coworkers,[79,80] formed a C/B FLP system **I-52** with conjugated dienamine (enamine) and Piers´borane, activating small molecules such as nitriles, sulfur dioxide, and benzaldehyde.

I-51 and **I-52** react with benzaldehyde **I-53** resulting in the product **I-54**, by a B-O and C-O formation. This kind of bond can be comparable in the present work where **CO2add** is formed by B-O and C-C formation when interacting with CO_2 and potentially reacting with other carbonyl functions. **I-54** produced different stereoisomers due to lower steric interaction, in which the trans-CH-CH configuration is obtained (Figure 37). Particularly in this study, there was no diastereomeric control.

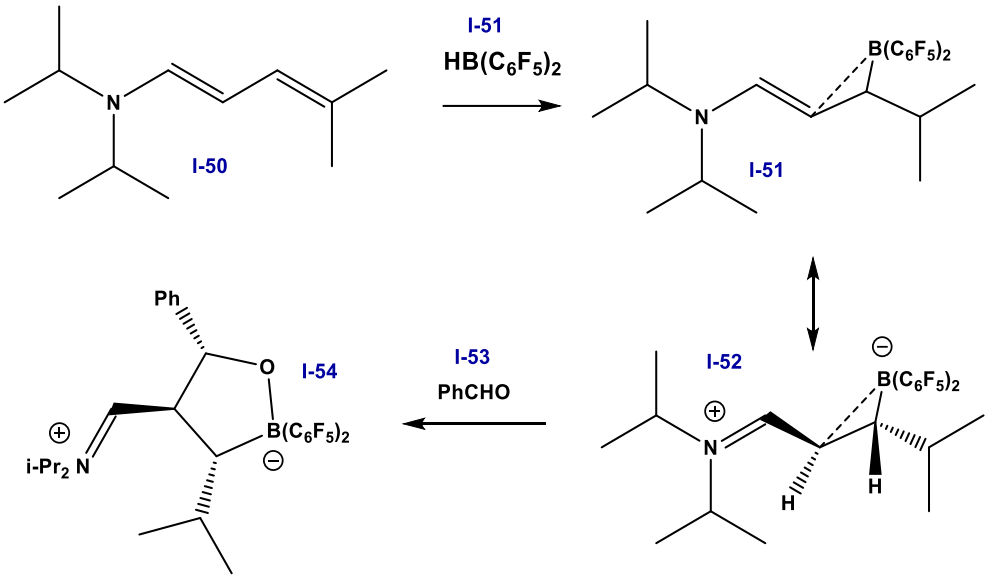

Figure 37. FLP system with benzaldehyde.

3.4.1. Carbenes as a Carbon-Base Lewis Bases

Arduengo and coworkers (2011),[81] Stephan (2008,[82] 2009[83]), and Tamm (2008)[84] worked with the interaction with Carbenes/Boranes, especially with activation of H_2. Stephan and Tamm, reported that the reaction between $B(C_6F_5)_3$ **I-54** and **I-55,** in the presence of hydrogen, forms an FLP at low-temperature **I-56**. Tamm and coworkers described that if the reaction carbene/borane FLPs is done at room temperature using THF instead of hydrogen results in **I-53** (Figure 38). This intermolecular reaction could afford the FLP at 20°C.

Unsurprisingly, the N-substituents in these strong Lewis bases are directed towards the carbene lone pair, generating significant "steric pressure" for an FLP towards a suitable Lewis acidic reactant. When **I-54** is added, these systems' interaction has undergone C–H activation in the 4-position with a strong B–C bond's irreversible formation.

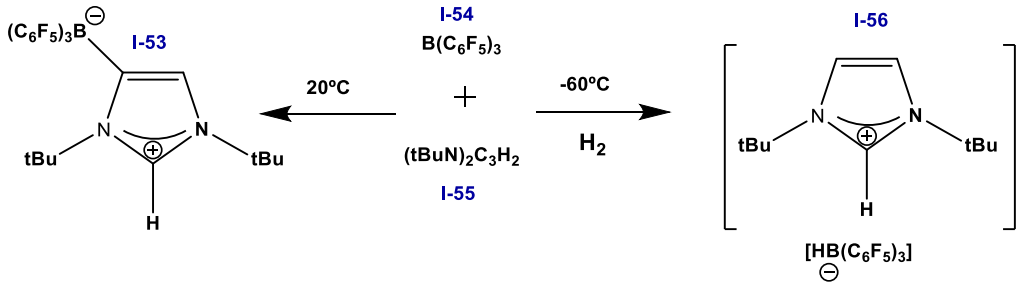

Figure 38. Reactions between carbenes and $B(C_6F_5)_3$ CI-54.

Although there is a widespread use of CO_2 fixation in FLP systems phosphine/borane, only a few examples are with the carbene/borane systems.[85] Tamm's team in 2012[87] reported a new FLP **I-59** from **I-58** that reacts and traps CO_2 by a carbene/borane system. This adduct was remarkably stable in solution and solid-state (Figure 39).

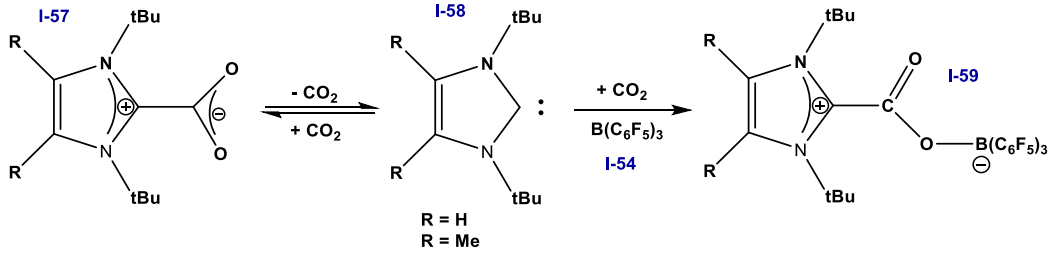

Figure 39. Reactions with carbenes.

3.5. *Masked FLP systems*

Masked FLP systems contain the Lewis acid and Lewis base but can only be seen as an FLP system when the activated molecule is trapped.[32] This kind of system is used to be unstable until they form the product, making its isolation difficult. One example is the complex **I-60,** which forms a classical Lewis pair between Phosphorus and aluminum.[88] However, this complex is in equilibrium with an open form without the Lewis pair interaction (**I-61**). The equilibrium is largely displaced towards the Lewis pair formation, but in the presence of CO_2, the open forms behave like an FLP system. This case leads to two isomers, a cis configuration (**I-62**) and a trans configuration (**I-63**). This reaction can activate small dipolar molecular such as phenyl isocyanate and carbon dioxide. In the case of carbon dioxide, two isomers are generated, compound **I-62** and **I-63**. The **I-62** includes a cis arrangement of Al and H at the C=C, while the **I-63** has a trans configuration (Figure 40). This shows that the FLP system can derive from the Classical Lewis acid-base complex, which shows no evidence for dissociation and can display Masked FLP system behavior.

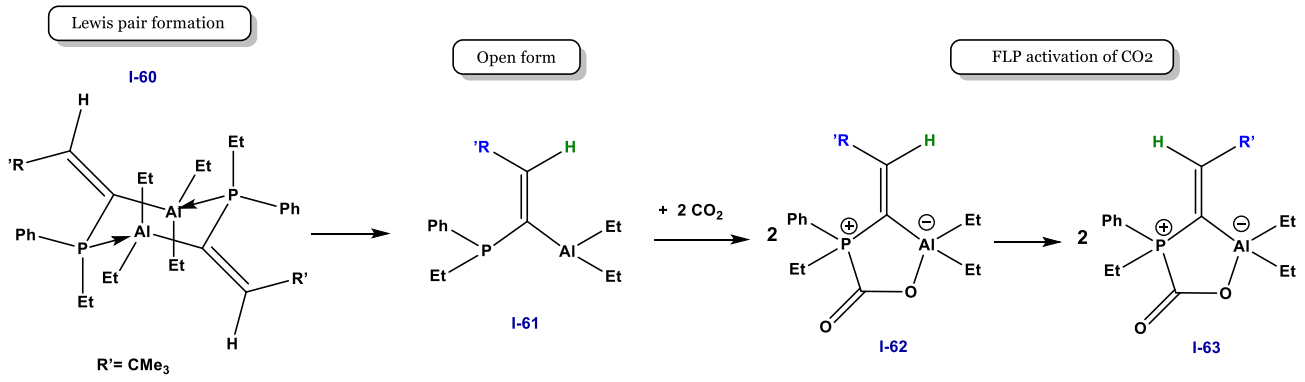

Figure 40. Masked FLP system with CO_2.

In contrast to the present work, **CO2add** does not present a Lewis pair interaction because of geometric constraints. Lewis sites are already involved with another molecule; in this case, CO_2, already trapped in a possible masked FLP system that could be activated with another small molecule. Additionally, the product is intramolecular as opposed to the P/Al example here.

CHAPTER II

CHAPTER II

STUDY OF CO_2 ADDUCT AS A FLP TYPE

I. INTRODUCTION

As was discussed in chapter 1, **CO2add** could be used as a precursor of an FLP-type activation. These systems open new thriving research for the activation of small molecules being potentially used for new applications. In this sense, this particular adduct as an FLP could activate other types of small functions besides carbon dioxide.[62,89] This statement leads us to the main question to address in this chapter: what other types of small molecules can activate this system? If it does, which kind of polar functions? Carbonyl functions? (Figure 41).

This chapter will explore different small molecules, including polar and non-polar functions, with the aim to test the capacity of **CO2add** as a novel FLP-type activation.

Once the system is tested, the scope of the reactivity will be studied to understand how the novel FLP system is activated, observing the possibilities and the insights about the mechanism of the chemical process. Why is it activating certain functions and not others? What are the optimal conditions? Is there a favorable barrier to activation? Likewise, is the **OBB-int** ever released in the process? Can it be observed during the reaction or even be isolated?

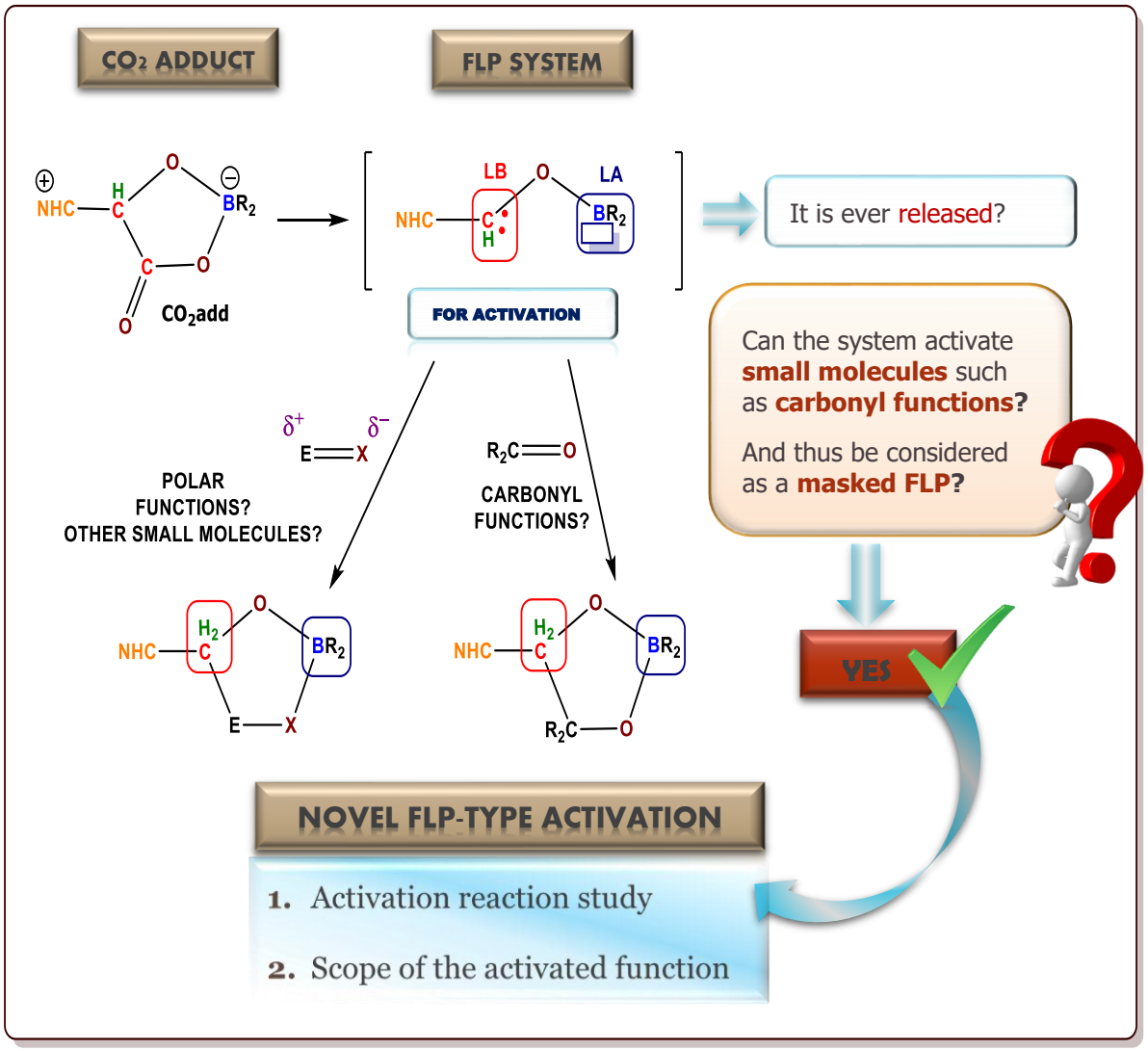

Figure 41. Question to address in the chapter.

II. REACTIVITY WITH SMALL MOLECULES

1. STARTING MATERIAL SYNTHESIS

CO2add was prepared following the protocol[9] mentioned in the previous chapter. Nevertheless, adjustments in reaction time were necessary to scale up the starting material from 318 mg to 3 grams and obtaining the same yield. In the reduction step, the time was increased from 45 min to 60 min. In the C-C coupling step, the time was changed from 60 min to 120 min. The Enders carbene necessary to prepare **CO2add** was produced in the laboratory. It will be explained in the following part (Figure 42).

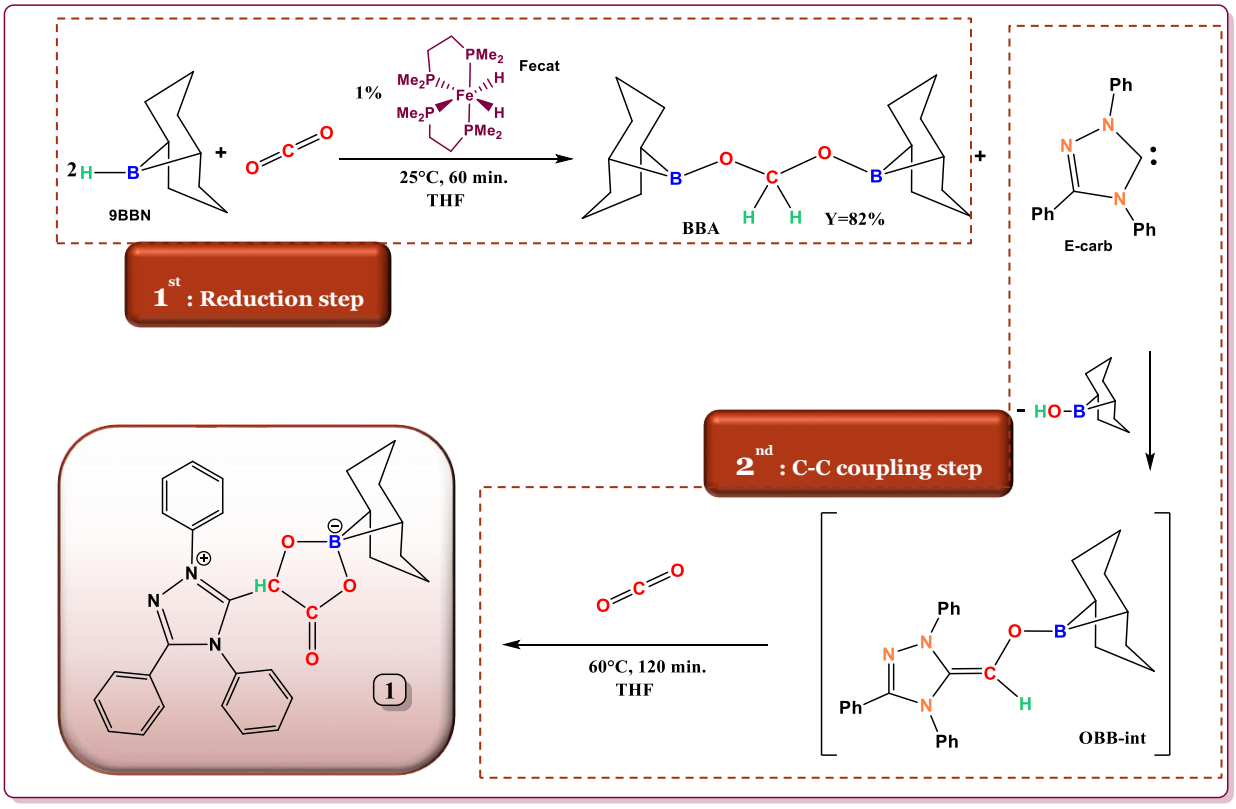

Figure 42. Synthesis product 1. The protocol used in the present work.

2. ENDERS CARBENE SYNTHESIS

N-heterocyclic carbenes (**NHC**s) have developed rapidly among organocatalysts since the first isolation and characterization of a stable NHC by Arduengo and coworkers in 1991[49]. Its capacity to be used as ligands during metal-based catalysis and its efficiency in nucleophilic catalysts in many synthetically organocatalytic transformations has encouraged the fast development of new types of stable carbenes[45].

In 1995, Enders, Teles, and coworkers[46] studied the reactivity and isolated 1 3 4-triphenyl-4 5-dihydro-1h-1 2 4-triazol-5-ylidene, better known as Enders Carbene (Figure 43). This particular carbene presents a high Lewis basicity and moderate nucleophilicity[90], stable enough for product **1** and still be reactive as Lewis base or the present potential masked FLP system.

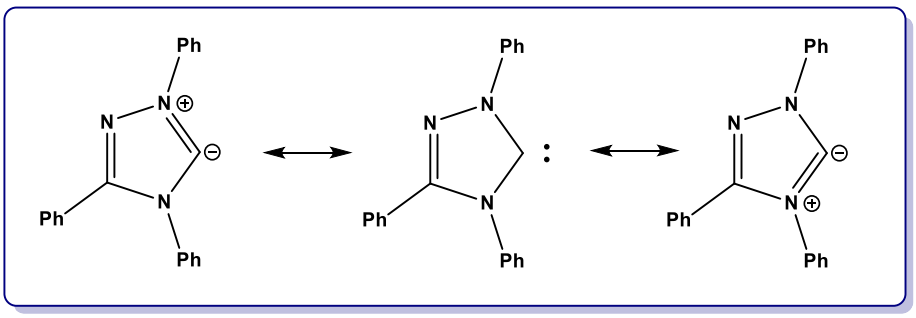

Figure 43. Triazolin-5-ylidene and its resonance structures

The Enders Carbene synthesis was prepared up to 10g. It was divided into three synthetic steps with two intermediates, following the main protocols[46,91] (Figure 44). The detailed process is in the experimental chapter.

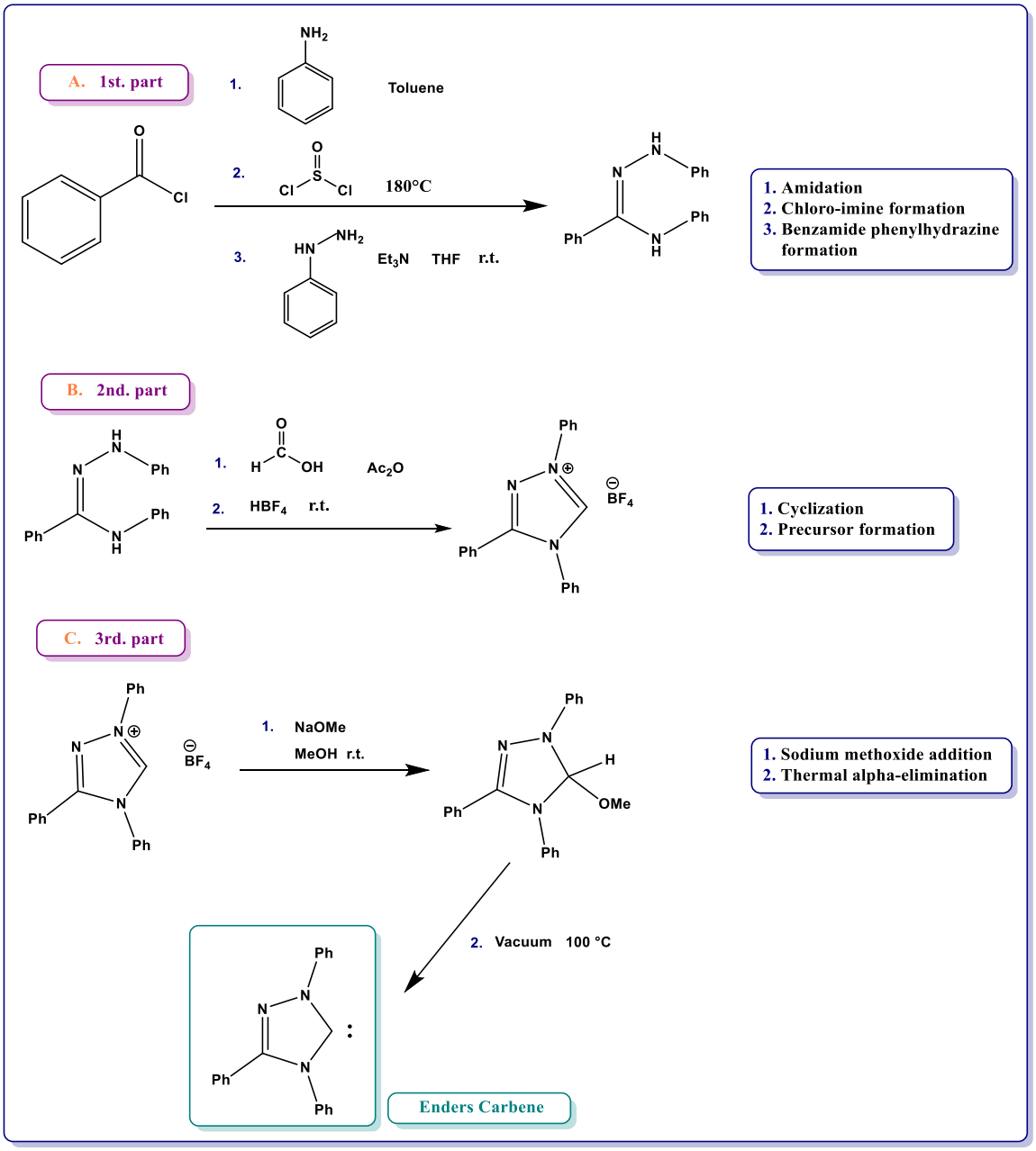

Figure 44. Synthesis of Enders Carbene[91].

3. PRODUCT 1 AS A FLP TYPE ACTIVATION OF SMALL MOLECULES

As discussed in chapter one, in 2019, Bontemps and coworkers[9] suggested that **CO2add**, possibly formed via transient formation of the O-borylated Breslow intermediate due to its ambiphilic nature, traps the carbon dioxide. With the carbon-based as a Lewis base and the boron as a Lewis acid (Figure 45).

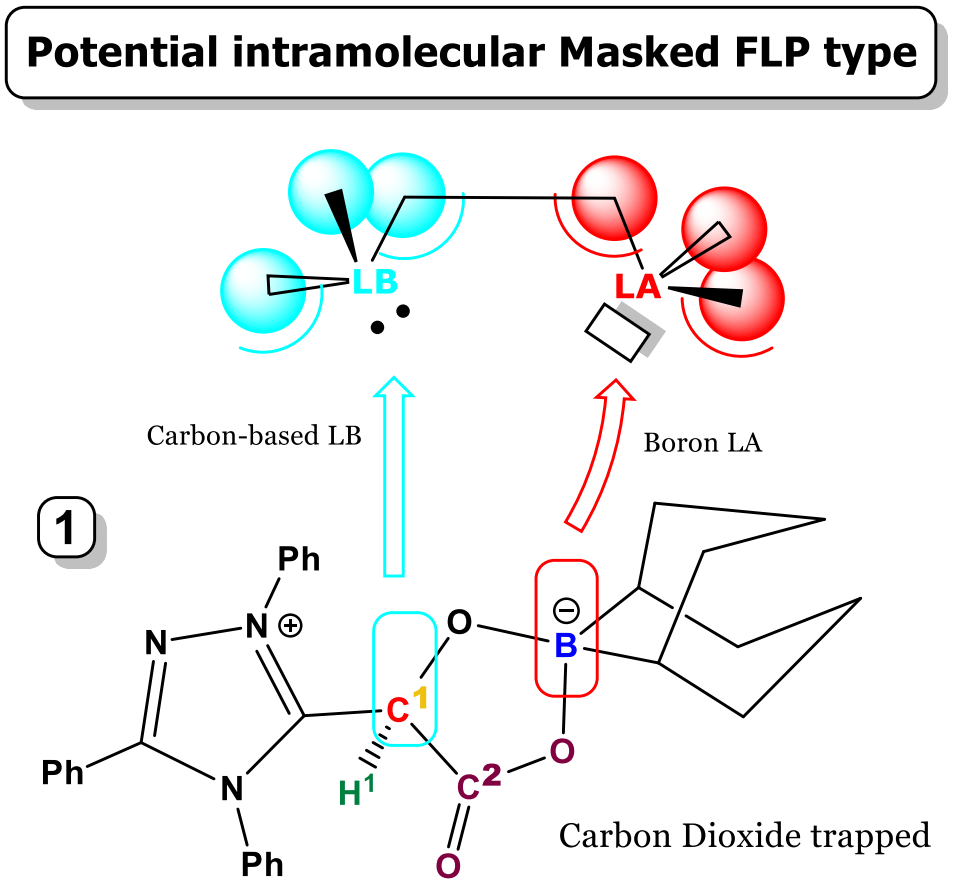

Figure 45. Potential intramolecular FLP system. Blue: Carbon-based Lewis base; red: boron Lewis acid.

With the purpose of corroborating this hypothesis, different small molecules such as alkynes, ketones, aldehydes, olefins, and other small molecules were used for the activation test.

Alkynes

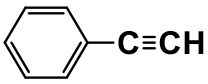

Olefins

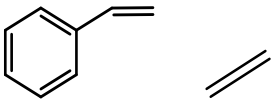

Ketones

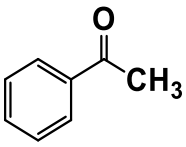

Aldehydes

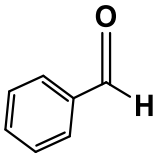

Other Small Molecules

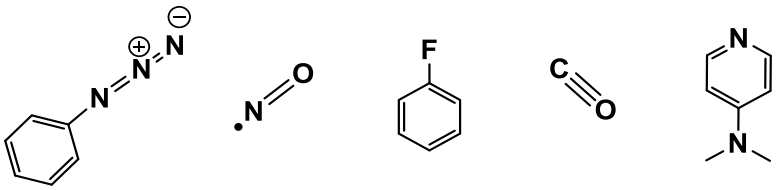

To test the molecules' reactivity with **CO2add**, each molecule was initially added in excess (5 and 10 eq) in a J. Young NMR tube, at room temperature, with C_6D_6 and THF-d_8 as solvents. The reactions were monitored for two weeks. After this time, if the reactions do not occur, an increase in temperature was applied. First 50°C and 80° if it was necessary. As a result, the aldehydes benzaldehyde and cyanobenzaldehyde reacted with **CO2add**.

4. REACTIVITY WITH ALDEHYDES

In Figure 46, it is possible to observe the formation of a new product. The reaction between **CO2add** and benzaldehyde (**Benz**) reveals the appearance of two new doublets at δ 4.44 and δ 4.67 with a coupling constant of $^3J_{HH}$ 8.2 Hz.

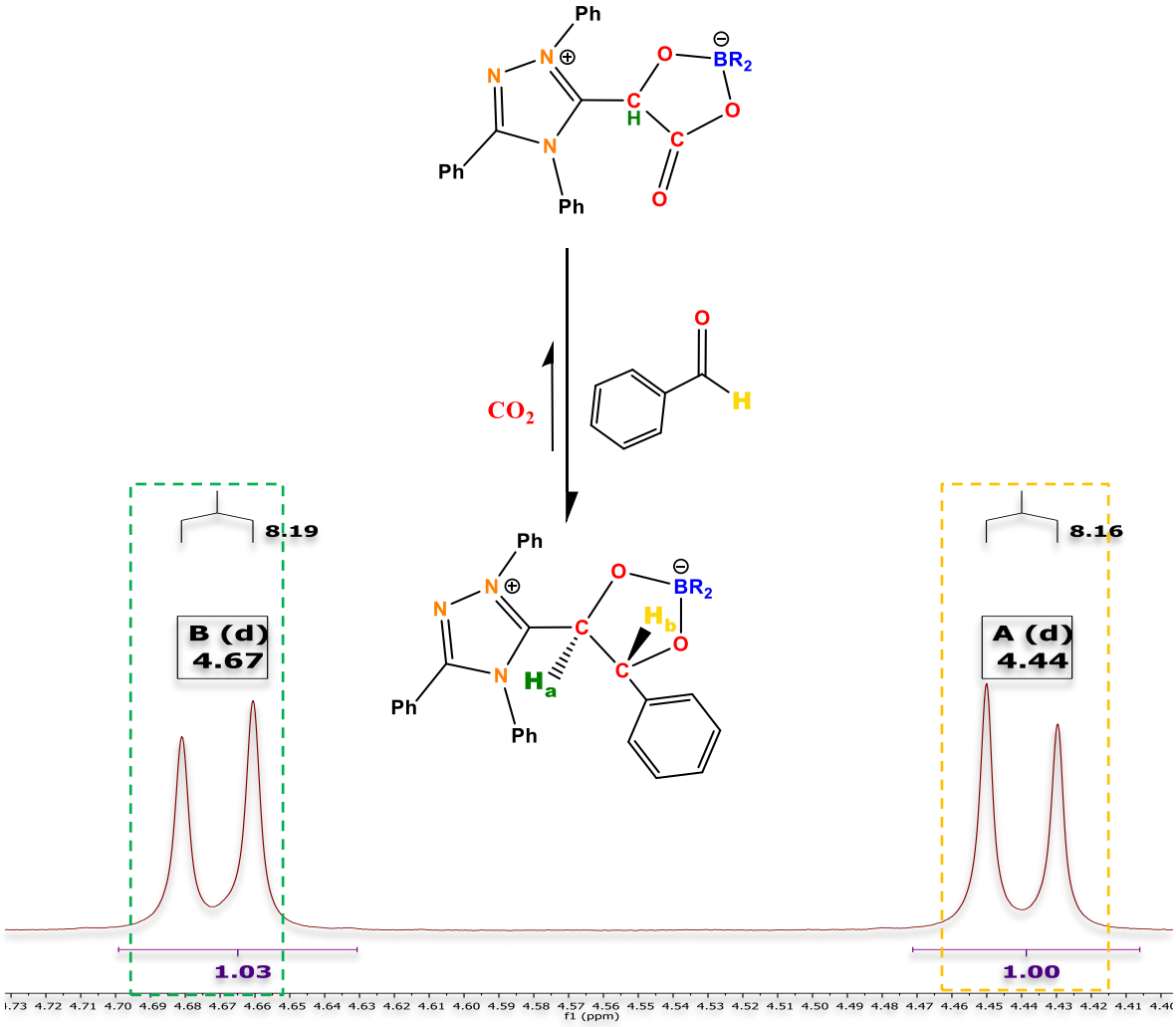

Figure 46. Reaction and spectrometric detection of 1 with benzaldehyde.

In summary, after the previous set of functional groups were tried, the carbonyl functional group -CHO, corresponding to aldehydes (Figure 47), is successfully activated. The system is trapping the aldehyde and releasing the carbon dioxide previously trapped. This substitution reaction, specifically in benzaldehyde, confirms that **CO2add** could be considered **a new unstable FLP type activation chemoselective for aldehydes.**

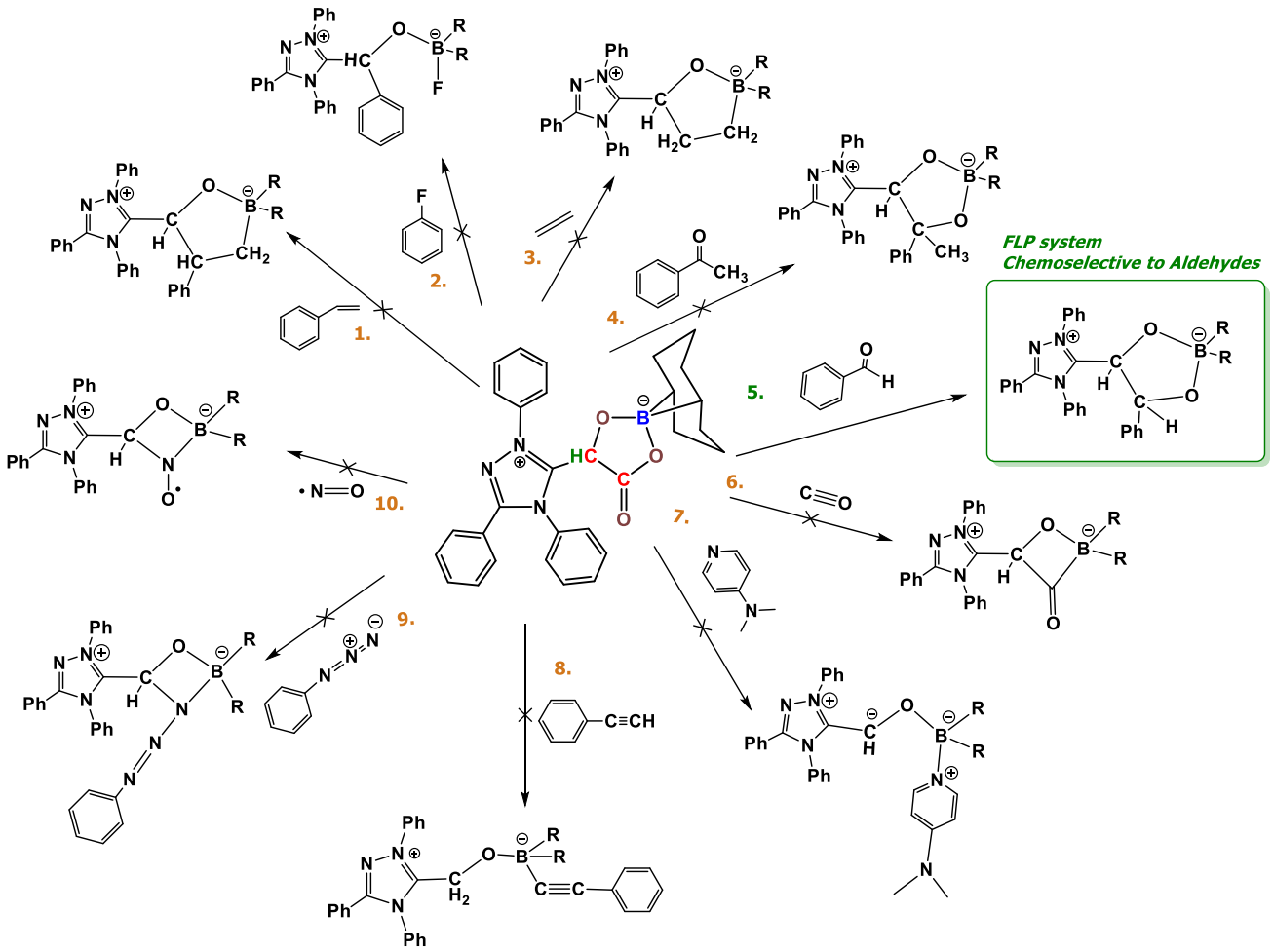

Figure 47. Small molecules tried with the FLP system. Chemoselectivity to aldehydes.

III. FLP SYSTEM: BENZALDEHYDE REACTION

1. SYNTHESIS AND CHARACTERIZATION

Once it validates **CO2add** reactivity with the two aldehydes in excess, the benzaldehyde reaction was chosen to go further in the analysis due to its complete formation without by-products, facilitating the study of the new FLP system. The reaction is performed in a stoichiometric ratio at 25°C with THF as a solvent (Figure 48).

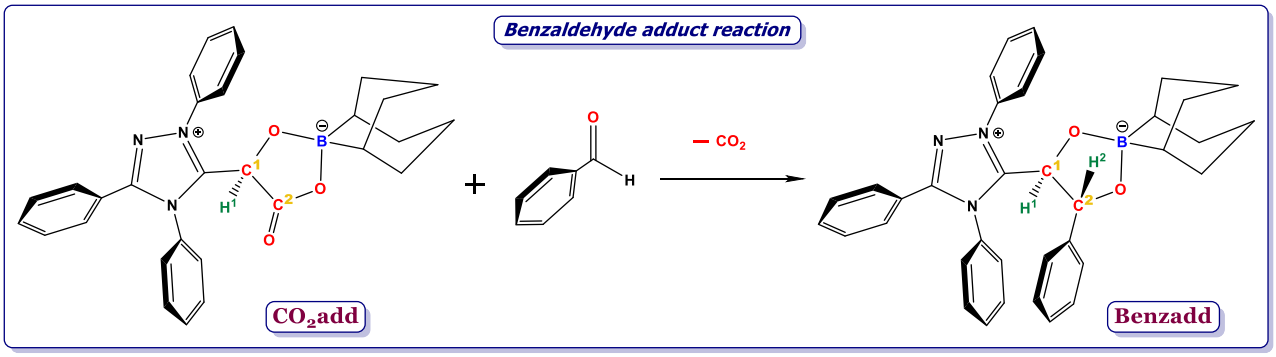

Figure 48. Benzaldehyde adduct reaction. Products: benzaldehyde adduct (**3**) and carbon dioxide (**CO_2**).

The reaction was followed by proton nuclear magnetic resonance (^{1}H NMR) spectrometry analysis until conversion. The disappearance of **CO2add** was monitored by ^{1}H NMR, the CH proton of the OBB moiety at δ 5.34 ppm (Figure 49). A new product corresponding to the benzaldehyde adduct (**Benzadd**) was observed with the appearance of two new doublets at δ 4.67 (H^1) and δ 4.44 ppm (H^2), corresponding to the protons of the new C-C bond with the aldehyde trapped (Benzadd, Figure 51). Benzaldehyde was followed by the disappearance of the aldehydic proton at δ 9.98 ppm. After 29 hours, the formation of **Benzadd** reach 71 %, and after 79 hours, the reaction evidenced a quantitative conversion of the reactants into the benzaldehyde

adduct. The 2 protons monitored in the product formation **Benzadd** shows a spin-spin coupling constant through the bonds of $^{3}J_{HH}$ = 8.2 Hz (Figure 49), also observed in the 2D $^{1}H/^{1}H$ NMR COSY (Figure 50.a). $^{11}B\{^{1}H\}$ analysis indicates the replacement of the signal at δ 13.9 ppm for **CO2add** to a close signal at δ 11.5 ppm **Benzadd** (Figure 50.b).

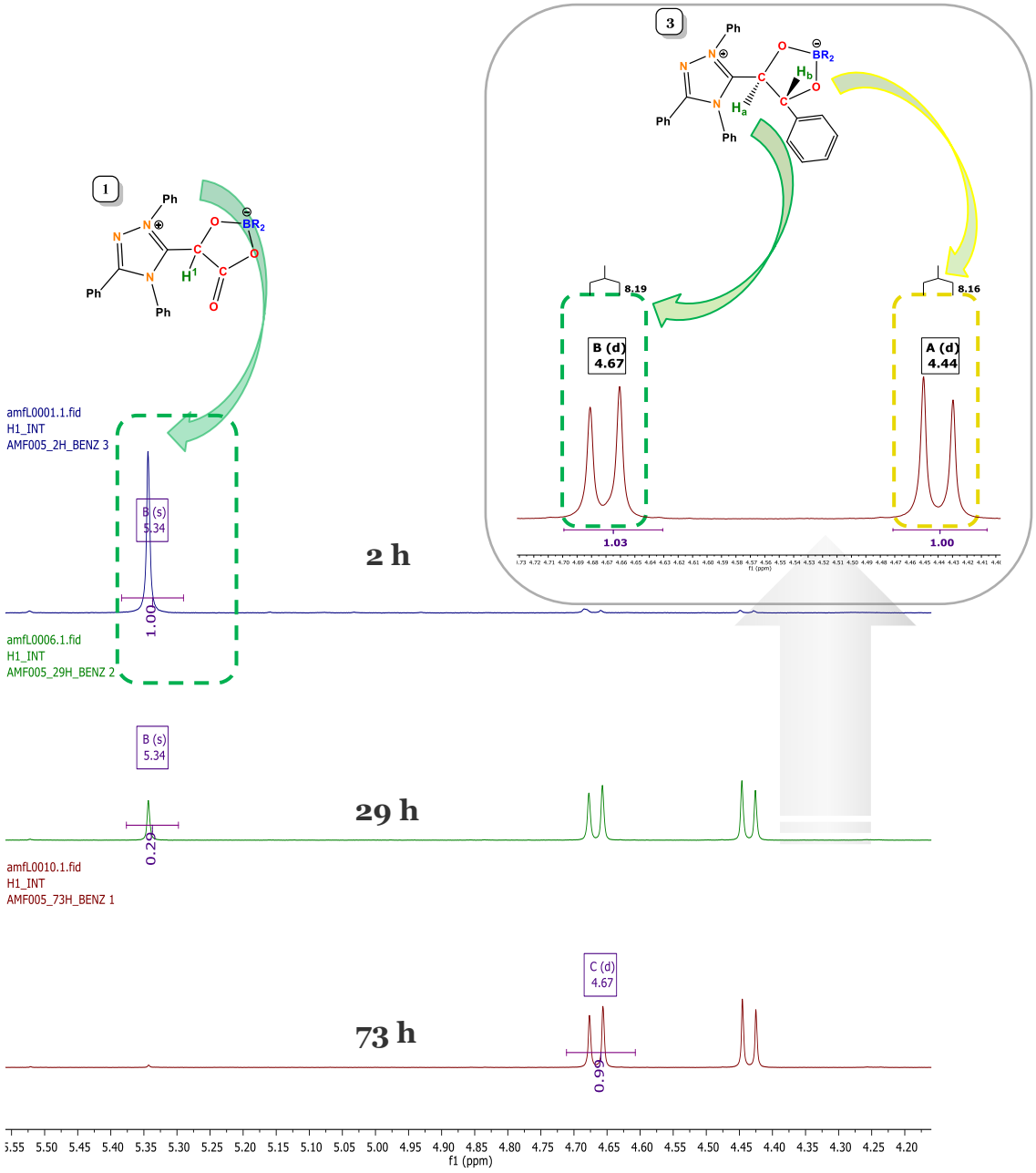

Figure 49. ^{1}H NMR formation of the benzaldehyde adduct.

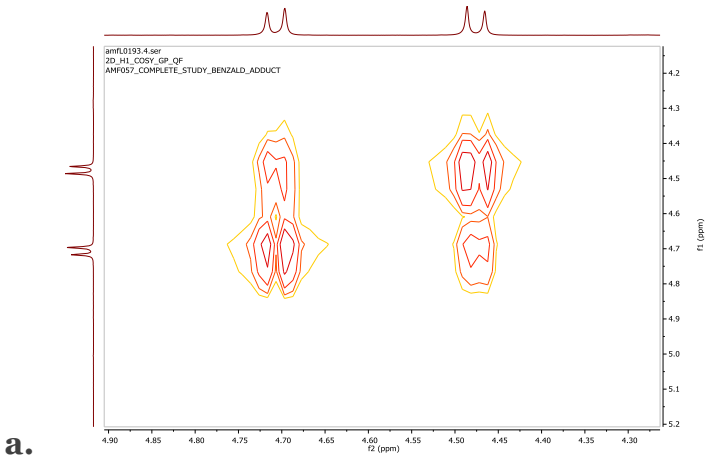

a.

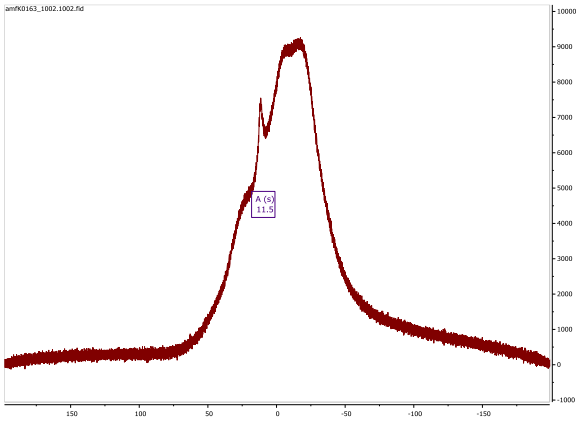

b.

Figure 50. a. ^{1}H / ^{1}H NMR COSY experiment at 298 K for compound 3 in THF-d8. Zoom on the 4.3 to 4.9 ppm area. b. $^{11}B\{^{1}H\}$ NMR spectrum of 3 at 298 K in THF-d8.

For the product's isolation and characterization, it was necessary to set the compound's optimal conditions. Parameters like sensitivity to air, water, temperature, and purity of the reactants were tested to standardized the conditions.

CO2add is sensitive to water and air. It was necessary to manipulate under argon with all the reactants and solvents carefully dry and pure. The reaction parameters were optimized in the following reactions, for which a complete conversion was observed after one hour at 80ºC in stoichiometric conditions. Subsequently, **Benzadd** was washed with pentane affording a yellow residue in a 50% yield. For the

isolation process, **Benzadd** was crystallized in a concentrated THF solution at -20°C for a week.

The crystals were suitable for X-ray diffraction (Figure 51). The magnitude of these coupling constant ($^3J_{HH}$ = 8.2 Hz) is indicative of an trans-vicinal configuration and the exclusive formation of rac-(R,R) enantiomers for compounds.

In solution state NMR analysis, shows the clean and quantitative formation of a single pair of enantiomers (Figure 49). No intermediate nor other diastereoisomer is observed *in-situ*. The protons shift of H^1 and H^2 in the NMR spectrum are in a no interference area with other peaks, providing a pretty good reading for the conversion. As expected in the crystal unit cell (Figure 52), it was also possible to observe the two enantiomers RR-SS (Figure 52.a). As a remark, this compound revealed noteworthy evidence of diastereomeric control. In the figure 52.b is possible to observe the enantiomers arrangement with THF in the unitary cell.

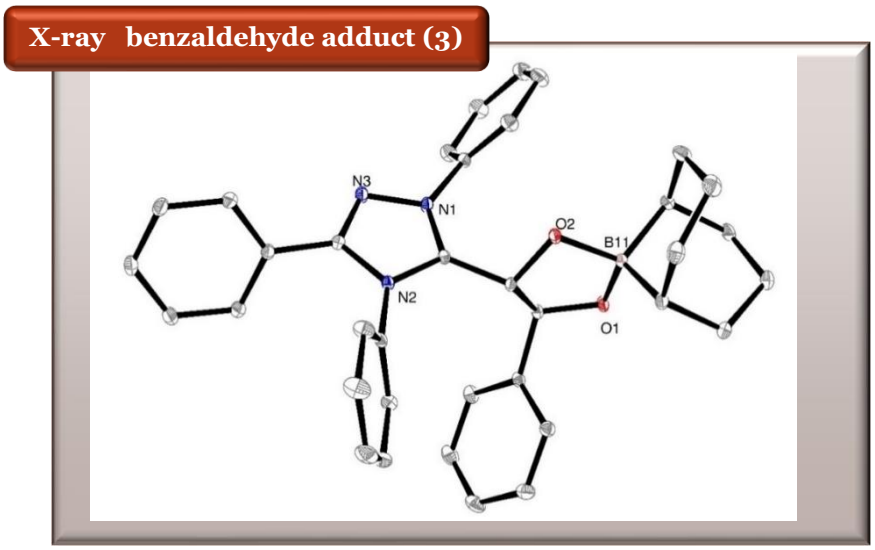

Figure 51. X-ray Benzaldehyde adduct, 3.

a.

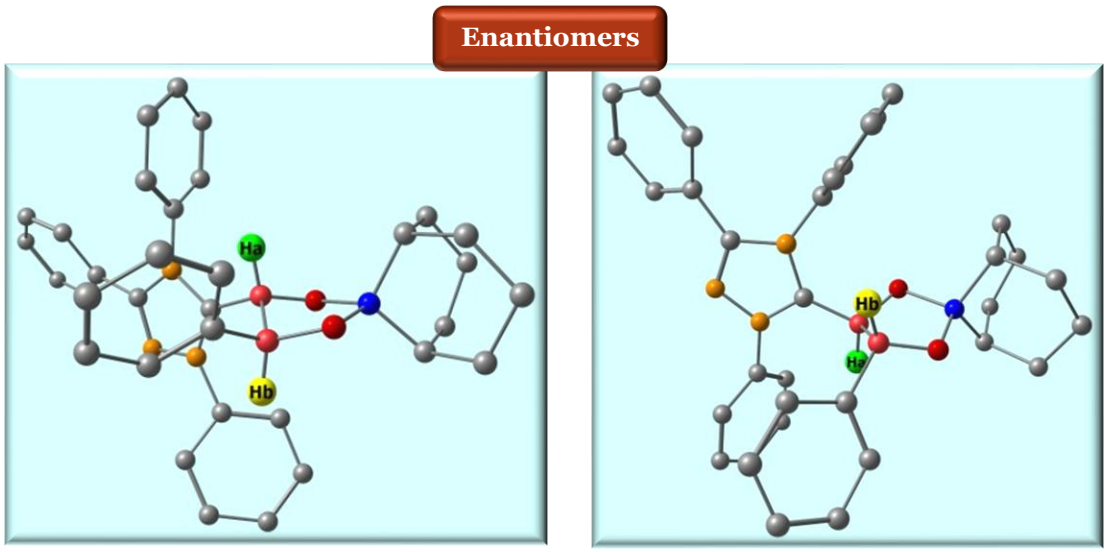

b.

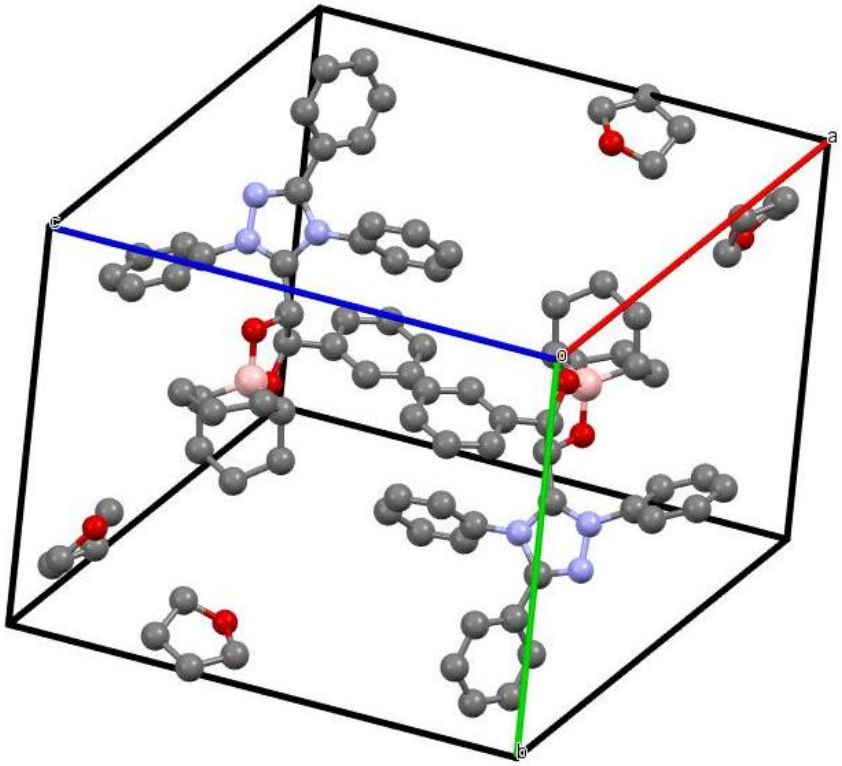

Figure 52. a. X-ray Benzaldehyde adduct, 3. Enantiomers RR and SS. b. Packing unitary cell.

The bond distance between the carbon-based Lewis base masked FLP C10-C19, and the central carbon from the aldehyde is 1.5149 (17) Å. The bond distance O1-B11 between the boron Lewis acid masked FLP, and the aldehyde's oxygen is 1.5685 (17) Å (Figure 53). Compared with the distances of **CO2add**, these values denote that the C-C bond in **Benzadd** is shorter and presumably stronger than **CO2add**. In both cases, the B-O bond is close to 1.57 Å, indicating the longest bonds and presumably weaker than the C-C bonds in **CO2add** and **Benzadd** (Figure 53).

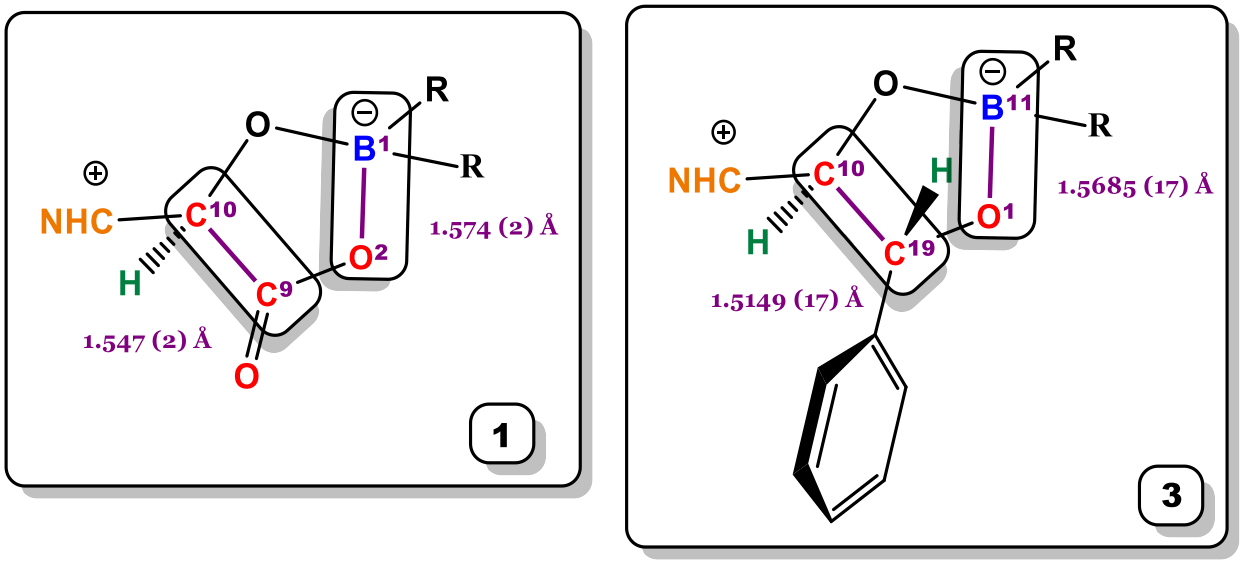

Figure 53. Bond distances for compounds CO2add (1) and Benzadd (3).

2. REVERSIBILITY REACTION OF BENZALDEHYDE ADDUCT

A reversibility study was performed to comprehend what could be carbon dioxide's effect on the system. Is this condition change could provide the system with a new equilibrium? What insights are obtained in terms of the stability and thermodynamics of compounds **CO2add** and **Benzadd**?

Benzadd was formed at room temperature in a stoichiometric ratio. Once it was completed, 1 atm of carbon dioxide was added three times (lapse of one second each time) to the closed system solution (Figure 54). The reaction was followed by ^{1}H NMR spectrometry for two weeks. After 96 hours, the reaction reaches the equilibrium at 15.5% formation of **1** (Figure 55). The reaction does not show any by-products.

This indicates that even in the presence of CO_2 excess, the reaction's equilibrium is still shifted towards **Benzadd**. However, it could be shifted to **CO2add** when CO_2 pressure increased (principle of Le Chatelier[92]), proving, more importantly, the reversibility of the system.

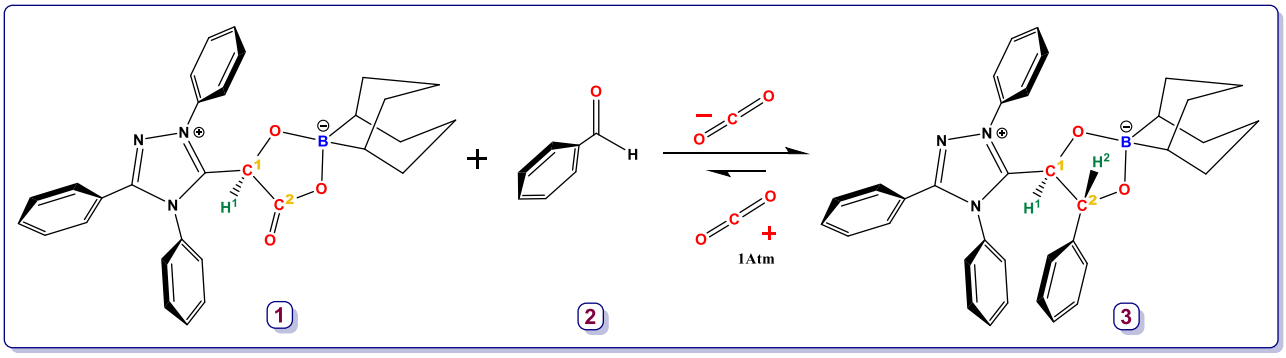

Figure 54. Reversibility reaction of Benzaldehyde adduct (3).

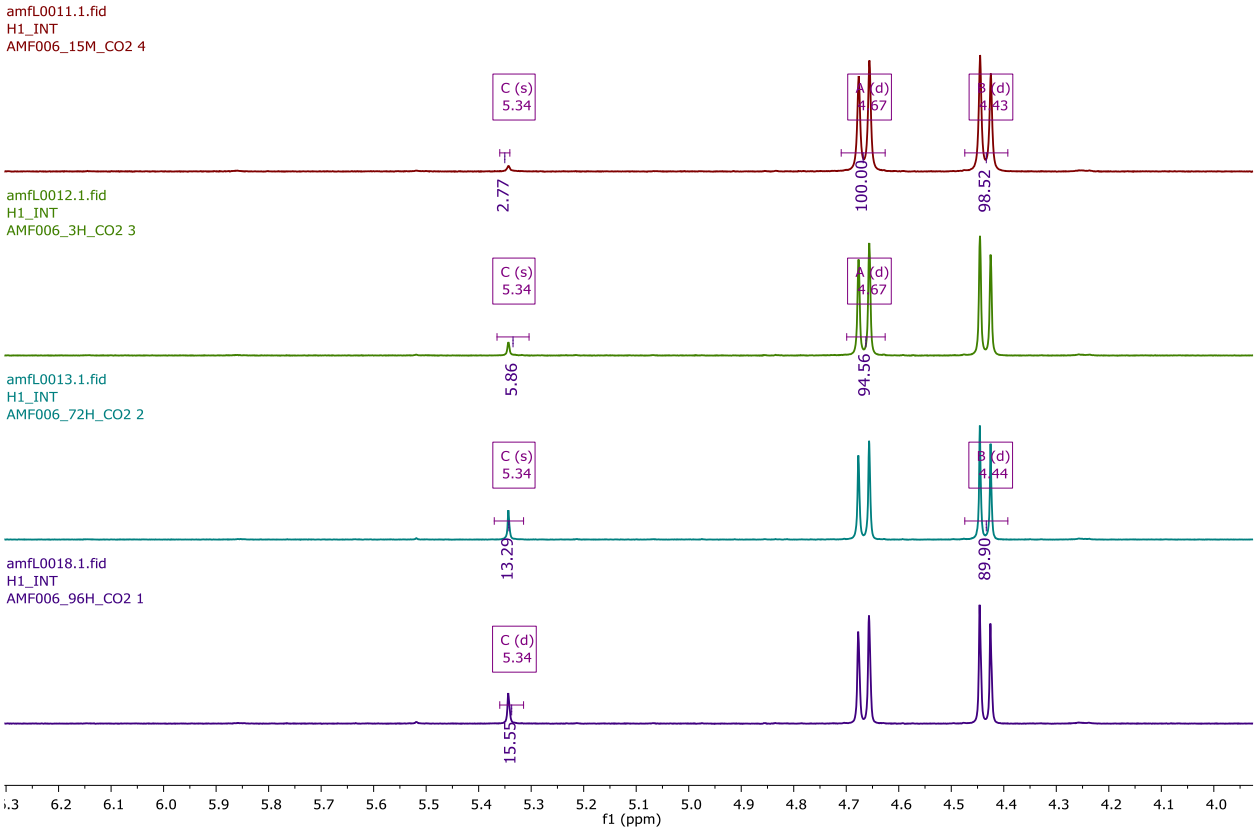

Figure 55. Stacked H1NMR from 15 min to 96 hours of the reversible reaction from 3 to 1.

IV. SCOPE OF ALDEHYDES

To understand the reactivity of the novel FLP-type, between the Lewis acid and base with CO_2 and aldehydes, benzaldehyde adduct reaction was taken as a reference (Figure 56) to develop a methodology that works as a model to be extended to other aldehydes.

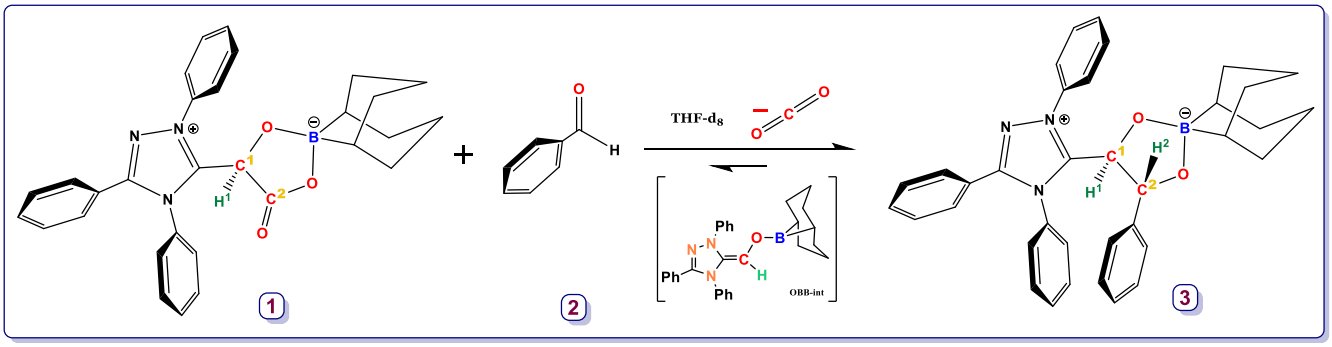

Figure 56. Reference reaction.

This section is dedicated to the aldehydes scope. All the experiments are being analyzed through a kinetic investigation, which can adequately study the electronic effect and the activation parameters. It is divided into three main parts: kinetics on the reference reaction, electronic study, and complementary studies.

The kinetic study on the reference reaction will provide the studies at room temperature at stoichiometric ratio and pseudo-order conditions and the studies at different temperatures to understand the temperature effect on the rate constant. This study would allow the calculation of the thermodynamic activation parameters $\Delta G^{\ddagger}$, $\Delta S^{\ddagger}$, and $\Delta H^{\ddagger}$.

The second part will study the electronic effect on the reference reaction, modifying the substituents on the benzaldehyde, providing a new set of reactions with their respective synthesis and characterizations. The reaction in pseudo-order conditions will deliver the Hammett Plot, which offers the understanding of the linear-free energy relationship of the reaction rate and the equilibrium constant.

The complementary studies were chosen to deepen into the possible insights of the reactivity and the mechanism.

CHAPTER II

1. KINETICS ON REFERENCE REACTION

In a chemical reaction study, it is essential to contemplate the reactants' chemical properties and the conditions under which the reaction occurs, the mechanism by which it takes place, the rate at which it occurs, and the equilibrium toward which it proceeds[93]. Concepts such as mass action law and rate law should be included in the analysis.

Mass action law indicates that a chemical reaction rate is proportional to the reacting substances' concentrations, whereas rate law implies the relationship between the chemical reaction rate and the reactant concentrations. Since a rate law can explain many systems, it is the first step to apply or discard if the reaction follows an integer order and not a fractional order[94].

For the kinetic investigation in this section, four parameters are fundamental to keep in account to obtain an accurate rate law:

i. System type: close or open
ii. Volume
iii. Temperature
iv. The phase of the reaction: homogeneous or heterogeneous

Thus, as a general equation for the general rate law (Eq. 1):

[Eq. 1]

Rate law = $k[\mathbf{A}]^n [\mathbf{B}]^m$ applied to the reaction is;

Rate law = $k[\mathbf{react\ 1}]^n [\mathbf{react\ 2}]^m$

According to the parameters mentioned before, the kinetic experiments were performed in a closed system (J. Young NMR tube) with a fixed volume of 600µL, with 9,10-dihydroanthracene as an internal standard and THF-d_8. Concentration and temperature conditions were changed, as table 2 shows below.

Table 2. Parameters to be changed in the kinetic study.

Ratio	CO2add	Benzadd	Experiment Temp °C/K
Stoichiometric	1	1	25°C / 298K
Excess	2	1	
Pseudo-order conditions excess	10	1	
	20	1	
	1	10	
	1	20	
	1	40	
	1	60	
	1	20	10°C / 283K
	1	20	40°C / 313K
	1	20	50°C / 323K
	1	20	60°C / 333K

1.1. At Room Temperature 298 K

Stoichiometric Ratio

The first reaction was performed under stoichiometric conditions to corroborate that reactant's consumption is equal to the formation of the product, as we observed in the synthesis and characterization of **Benzadd**. Once this is evaluated, speed, half-live calculation, and the formation and consumption curves' tendency were analyzed until the product was formed.

Figure 57 illustrates that indeed the product's formation is equal to the consumption, meaning that there is no by-product, being ideal as a reference reaction to understand the FLP system due to the minimization of variables.

One of the first analyses to observe the order of the reaction is the half-life. The first half-life of the reaction is at 21 hours of the 118 hours, where it can be observed that the consecutive half-lives are the same length of time (Figure 57), meaning that having only in account this analysis it could correspond to a first-order reaction, where the reaction is independent of the starting concentration (reactants). Another way to see it is that the intersection between product formation and substrate consumption is located in the middle, indicating that after half of the substrate has been consumed, it has been formed half of the product. The model is explained in a 99% linear fit for a first-order reaction, supporting the half-lives data (Figure 58).

In the trend lines, the speed of the formation product between 40 and 83 hours seems slower, as it could be observed in the graphic where the slope is less steep

(Figure 57). This change in the product formation speed could signify that one reactant (1 or 2) changes the concentration and affects the rate.

This preliminary analysis could imply that there may be more than one elementary step in the product formation in stoichiometric conditions. However, having in mind that during the 118 hours is not possible to maintain the experiment inside of the NMR machine, the slightly change of a temperature in the transit to take the measurement could affect the result.

It is necessary to analyze the reactant 1 (**CO2add**) and 2 (benzaldehyde, **PhCHO**) in pseudo-order conditions to isolate each reactant, ensuring that the reactant's concentration in excess remains effectively constant. For these experiments the reactions are recorded inside the NMR to assure an stable temperature (see experimental chapter).

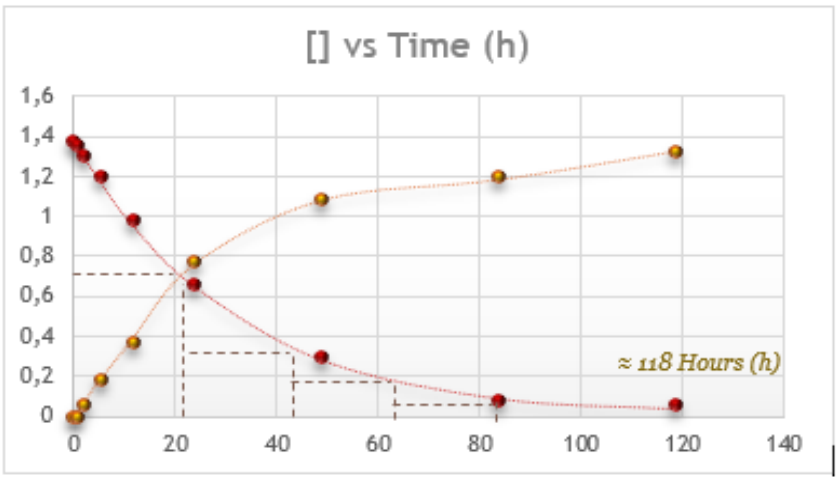

Figure 57. Reaction reference in stoichiometric ratio 1:1. The red line represents the consumption of reactant **1 CO2add** , and the yellow line the conversion of product **Benzadd**.

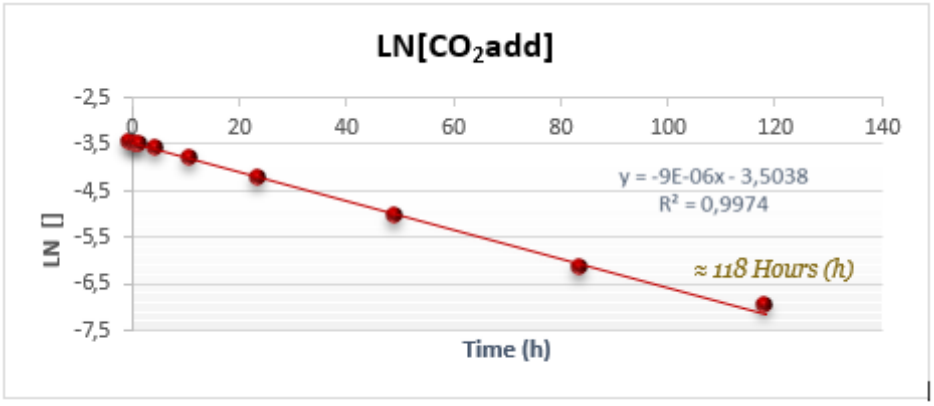

Figure 58. Linear fit LN [CO2add]. Model first order.

Pseudo-Order Conditions

In this segment, pseudo order conditions are going to be imposed in reactant 1, **CO2add** and reactant 2, **PhCHO** separately ([**CO2add**]≫[**PhCHO**] and [**PhCHO**]≫[**CO2add**]) to obtain the partial orders and identify which one presents a fractional-order, affecting the rate law. An excess of 10 and 20 equivalents was used for these experiments, as previously mentioned at the beginning of the section.

The equation applied to the system was:

If any of the reactants is in large excess, in this case, per example [**PhCHO**], it becomes a constant [**PhCHO**]$_0$, giving rise to the simplified equation 2, as explained in the introduction chapter.

[Eq. 2]

$$k = \frac{k_1 obs}{[\mathbf{PhCHO}]_0^n}$$

Excess in reactant 2 PhCHO

If **PhCHO** is in excess (10 and 20 equivalents), the consumption and formation tendency is constant (Figure 59). The reaction follows a pseudo-first-order in **CO2add** (*e.g.*, Figure 60 at 20 eq). Linear fit explains 99.7% of the model (Table 3). At 298K the rate k of the reaction oscillated between $4,65x10^{-5}$ (10 equivalents) and $5,99x10^{-5}$ (20 equivalents) (Table 3).

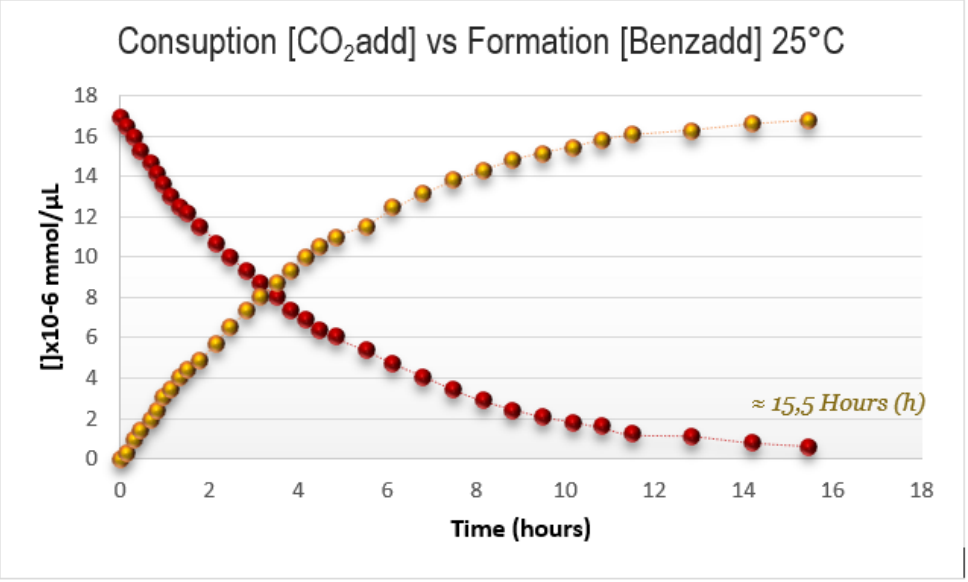

Figure 59. Red: Consumption of [CO2add] when [PhCHO] is in excess in 2O equivalents. Yellow: Formation of the product **Benzadd**.

Table 3. Rate k, Room temperature (25°C), an excess of PhCHO.

T° K	Equiv PhCHO	[CO_2add] mmol/µL	k_{obs} (s^{-1})	Exp Fit 1^{srt} Order
298	10	$1,7x10^{-4}$	$4,64x10^{-5}$	99.7%

298	20	$3,4 \times 10^{-4}$	$5,99 \times 10^{-5}$	99.8%

The data was taken to measure an initial blank test (starting compound and internal standard) and inside the NMR machine during reaction time. The points were taken exponentially, starting every 10 min.

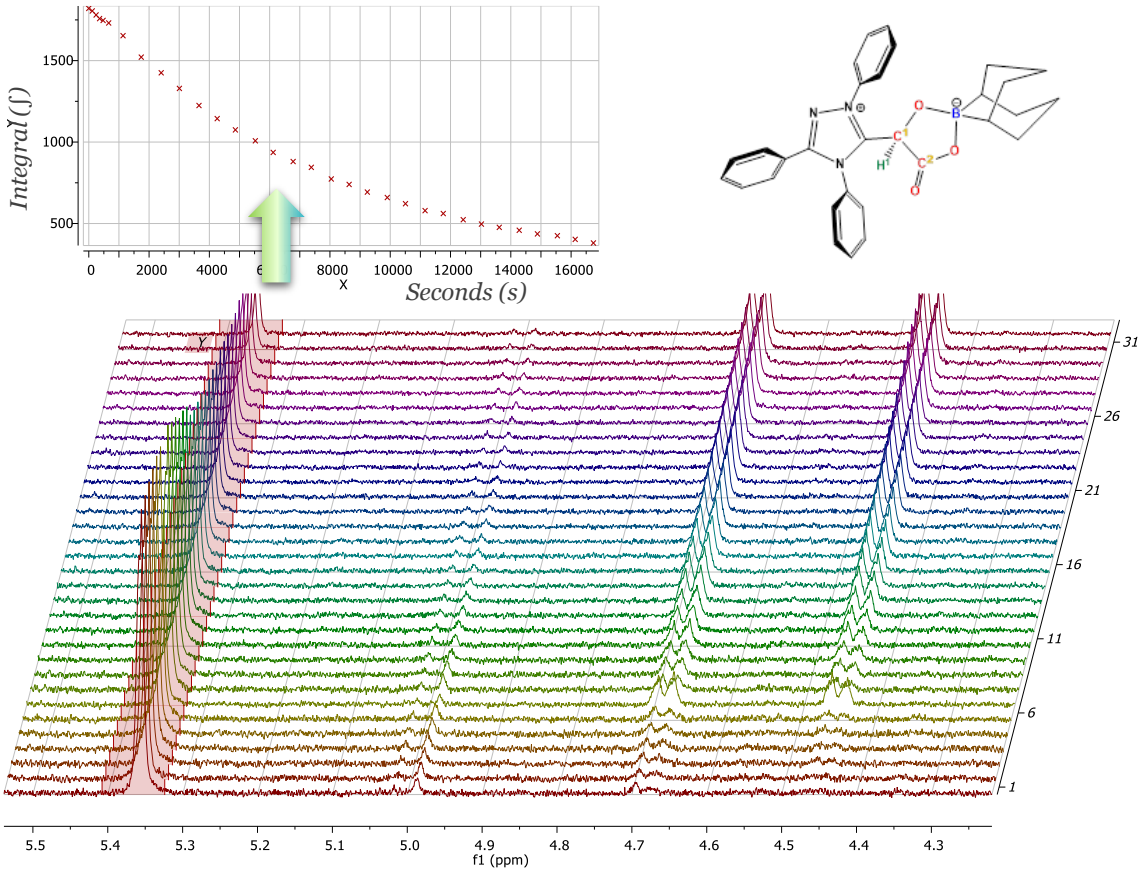

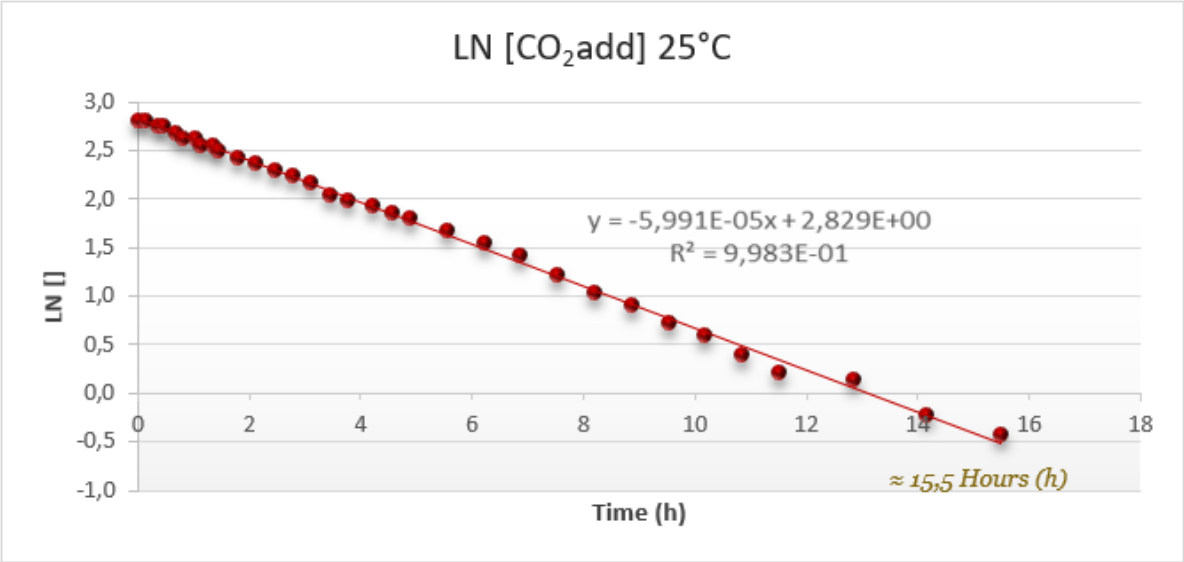

Figure 60. Experiment AMF081, excess in react 2 = 20 EQ. Reaction reference at room temperature. Superior: H^1NMR and conversion graphic. Inferior: LN [CO_2add] vs. time in hours.

As shown by Table 3, the rate constant was higher at 20 equivalents than 10, which shows a dependency on the concentration. However, when higher concentrations were applied (Table 4), the saturation reaction rate was observed after 20 equivalents (Figure 61).

Table 4. Saturation kinetics. [react 2] vs. Kobs.

Experiment	Equivalents	[PhCHO]mmol/µL	k_{obs} (s^{-1})
AMF332	60	$1,0x^{-03}$	$5,64x^{-05}$
AMF330	40	$6,8x^{-04}$	$5,86x^{-05}$
AMF081	20	$3,4x^{-04}$	$5,99x^{-05}$
AMF096	10	$1,7x^{-04}$	$4,64x^{-05}$
AMF050	1	$1,7x^{-05}$	$9,00x^{-06}$

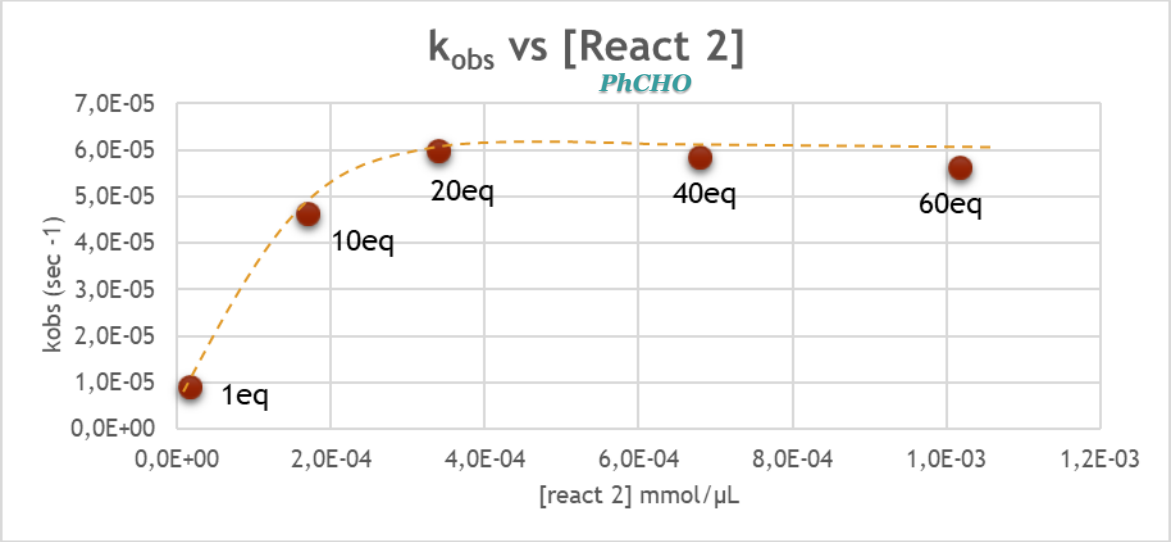

Figure 61. kobs vs. the concentration of reactant 2 (PhCHO).

As a summary in this section, partial order in **CO2add** follows a pseudo-first-order, and it could be included in the rate law like this (eq. 3).

$$r = k_1\,obs\,[\mathbf{CO2add}]^x \;;\; \text{where } x=1 \text{ and } k1_{obs} \qquad \text{[Eq. 3]}$$

Excess in reactant (CO_2 adduct)

When the excess is applied in **CO2add** (10 and 20 eq), the consumption tendency curve of **PhCHO** is subtle, almost with a pseudo linear decay (Figure 62). The linear fit corresponds to 95% of the model's explanation, given the possibility of a 0 (zero) order reaction. However, when LN linear correlation is performed for the first-order reaction, the curve presents a slight concave downwards shape, explaining 88 % of the system (Figure 62.b). Since these models are not conclusive to determine the

reaction's pseudo-order, it is necessary to study other models before discarding a non-integer pseudo-order.

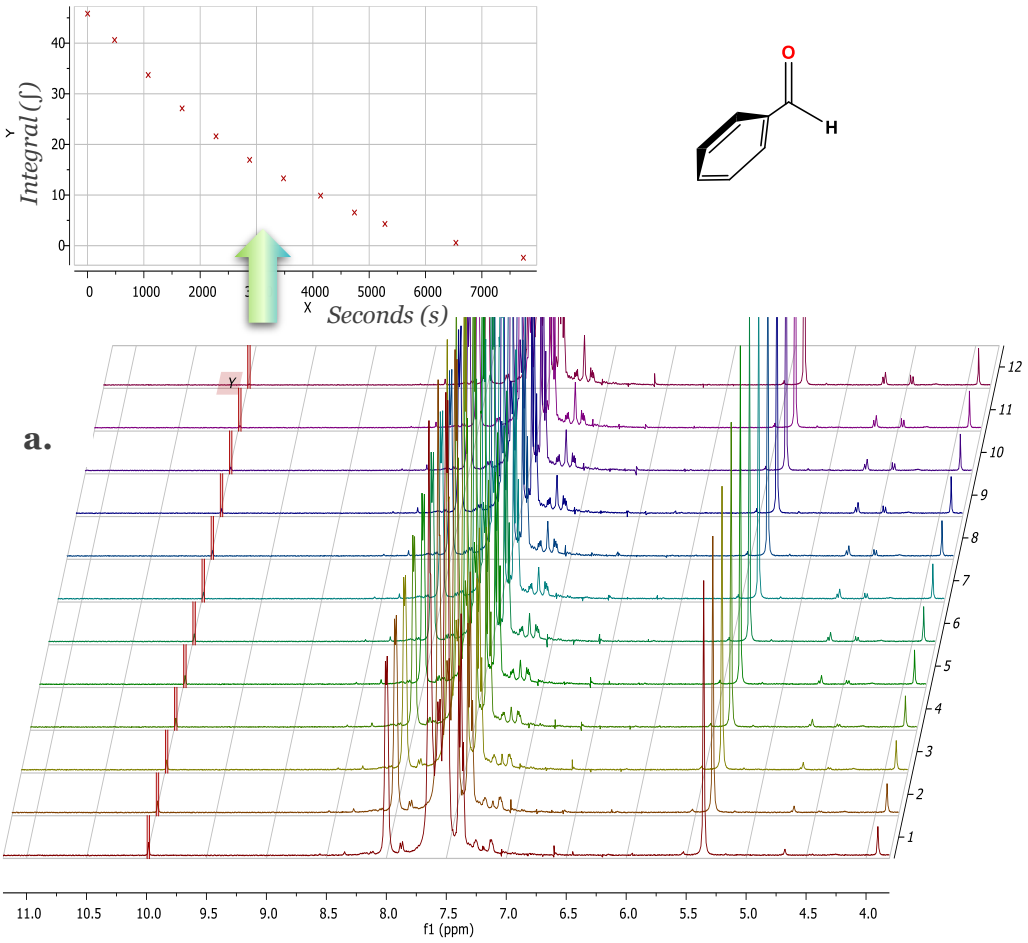

a.

b.

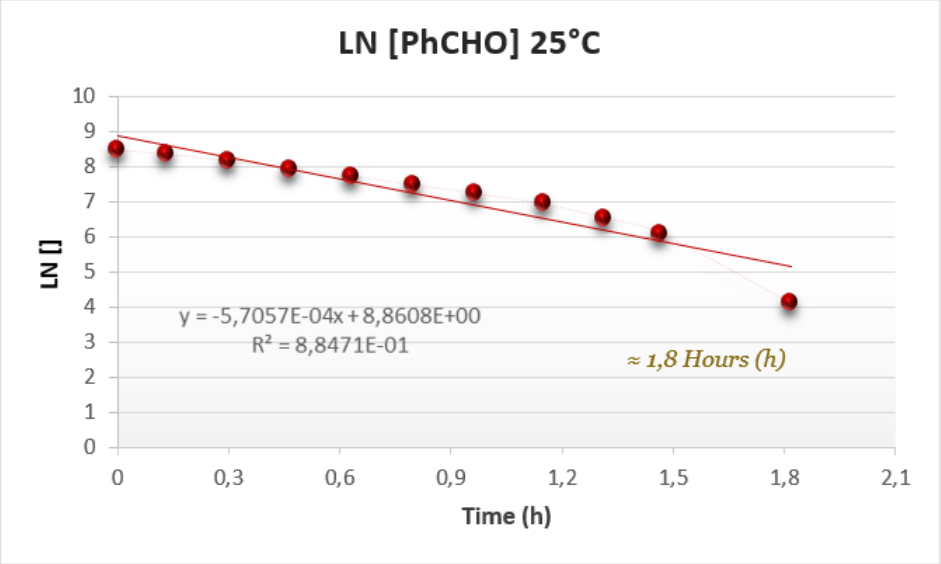

Figure 62. a. Experiment AMF117, excess in reactant 1 = 20 EQ. Reaction reference at room temperature. b. Ln [react 2] vs. time in hours.

The classical linear-squares method is not always the best fit in regressions to evaluate the rate constant. In fact, there is a systematic change in the spread of the residual error over the range of measured values (heteroskedasticity o heteroscedasticity). In this specific experiment, it could be the reason for the slight curve at the end of the points when the error in Ln[B] increases as [B] decreases (Figure 62.b). Therefore, a non-linear least squares with an exponential model decay is selected. This method reduces the error giving a more accurate rate constant *k*,[95] if the model explains the data.

Monoexponential decay with one iteration is applied to the data in order to prove pseudo-first-order in benzaldehyde following the equation 4:

[Eq. 4]

$$y = A_1 e^{-x/t_1} + y_0$$

The model (Figure 63) for pseudo-first-order explained 99.9 % of 2 (benzaldehyde) kinetic data in pseudo-order conditions. This result indicates that the two reactants present a pseudo-first-order for an overall reaction of order 2. Taking up the equation 1:

$$\text{Rate law} = k[\textbf{react 1}]^n\,[\textbf{react 2}]^m$$

Where n=1 ; m= 1

$$\text{Rate law} = k_r[\textbf{react 1}]^1\,[\textbf{react 2}]^1$$

Overall reaction order= n+m = 2

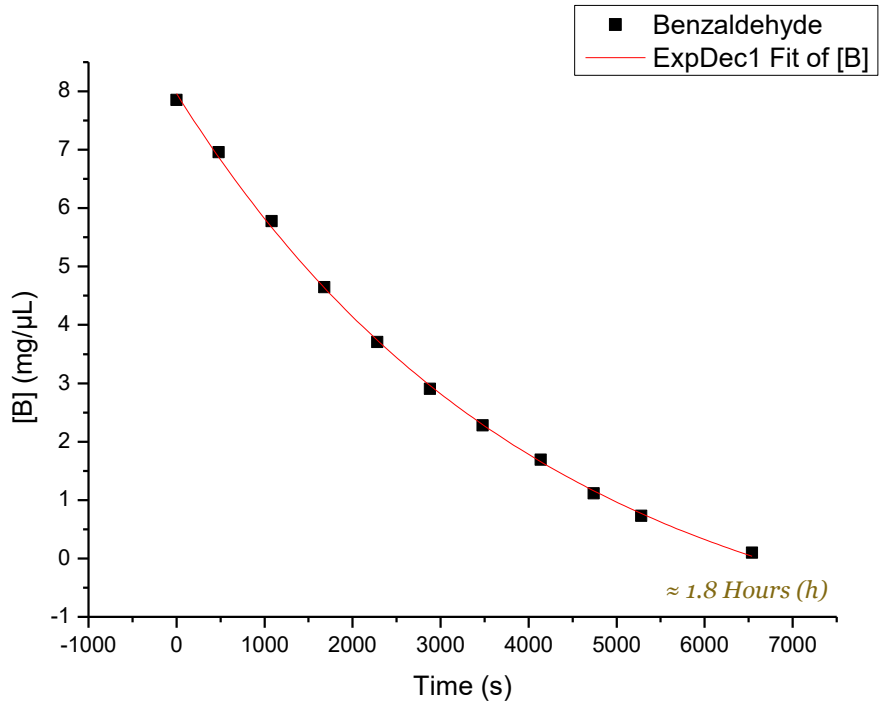

Equation	y = A1*exp(-x/t1) + y0		
Adj. R-Square	0,9992		
		Value	Standard Error
[B]	y0	-2,0327	0,232
[B]	A1	9,99284	0,21022
[B]	t1	4153,41852	184,50033

Figure 63. Nonlinear least-squares fitting monoexponential analysis with the equation proposed. The Redline indicates the theoretical model with one iteration and the black points to the real data.

This dependency in the result suggests that the rate-determining step (rds) involves one molecule of **CO2add** and one molecule of reactant **PhCHO**, being one elementary step. However, it is not possible to know if there are more elementary steps involved in the mechanism. Since there is an intermediate in this reaction, it is possible that it is a fast step and cannot be observed.

Moreover, the fact that the reaction is performed under a closed system, and the reaction is reversible. When the masked FLP is released, **PhCHO** is reacting, but

carbon dioxide molecules that are now free in the system can generate competition, slowing down the reaction. This could be the fast step that is not observed.

1.2. Temperature dependence of the rate constant

Rate constants for chemical reactions in the vast majority depend strongly on the thermal activation. One well known empirical relationship expressing this dependence is the Arrhenius equation (4):

[Eq. 4]

$$k = A \exp(-Ea/RT)$$

This association's essential parameters are the activation energy Ea (kJ/mol or kcal/mol units) and the preexponential factor-A. The latter is given in the same units as the rate constant itself ([s^{-1}] for a first-order reaction and [l mol^{-1} s^{-1}] for a second-order reaction).

A second expression used to describe the temperature dependence of reaction rate constants is the Eyring equation (5) that results from transition state theory :

[Eq. 5]

$$k = (k_B T/h) (1/c^n) \exp(-dG^{\neq}/RT)$$

k_B= Boltzmann's constant

h= Planck's constant

This section will study the temperature dependence of reaction rates on the reference reaction, studying the Eyring equation and activation parameters mentioned before.

For the experiments conducted in this section, the analysis on **CO2add** was chosen (excess of **PhCHO**), pondering that the partial order in **CO2add** is first order and not fractional.

Eyring Plot and Activation Energy

Eyring plot was obtained (Figure 64) from the range of temperatures mentioned above to understand the temperature effect on the rate constant and allowing the activation parameters $\Delta G^{\ddagger}$, $\Delta S^{\ddagger}$, and $\Delta H^{\ddagger}$.

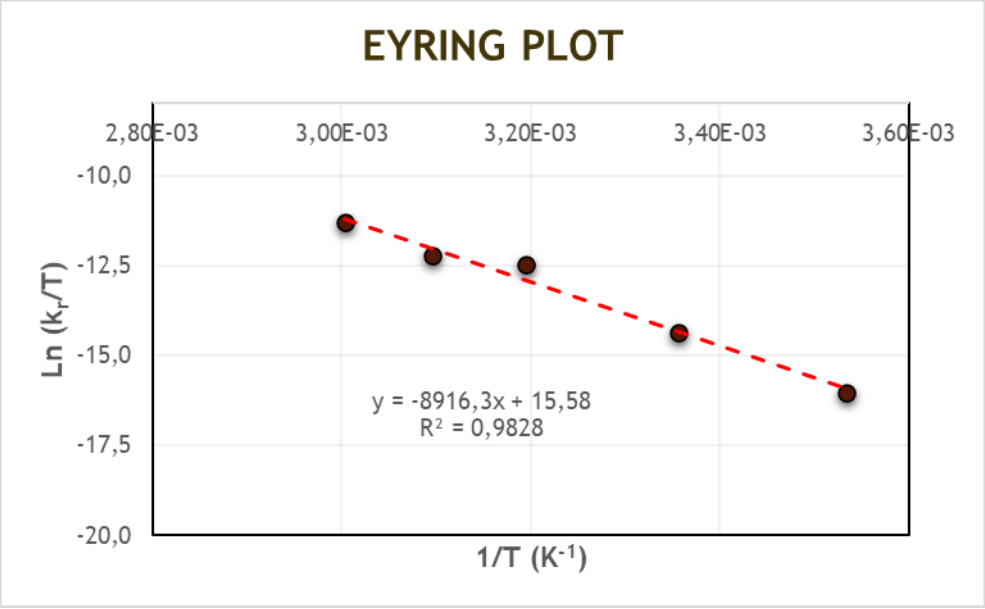

Figure 64 Eyring plot for the reaction **3**. k_r/T

The Gibbs free energy of activation (ΔG‡) for the benzaldehyde adduct **3** is 22.6 kcal/mol K at 25°C (298 K). This result is consistent with the present kinetic study that proves the complete product formation at room temperature; however, since the barrier is high, it takes 72h for completion. As expected, ΔG‡ increases with the temperature reaching at 60°C (333 K) 27.7 kcal/mol.

The enthalpy, which refers to the reaction's heat, is 17,7 kcal/mol, being in accordance with the reactivity at mild temperatures. The entropy associated with the state of disorder for the benzaldehyde adduct is noticeably negative (-16,2 kcal/mol) as expected with a formation of the product and suggesting an associative rate-determining step.

With the same data provided, it was also possible to obtain the activation plot (Figure 65) (Table 5) that affords the activation energy Ea. The plot explains a linear correlation of 98%, providing the parameter Ea=-m*R (Figure 65). Replacing into the equation, where m is the slope and R = 8,314 J/mol K, the activation barrier is 18.3 Kcal/mol, which explains why at 20°C, it starts to be accessible. In the benzaldehyde adduct case, the high value for the activation energy is consistent with Gibss the free energy, indicating the reaction rate's temperature dependence.

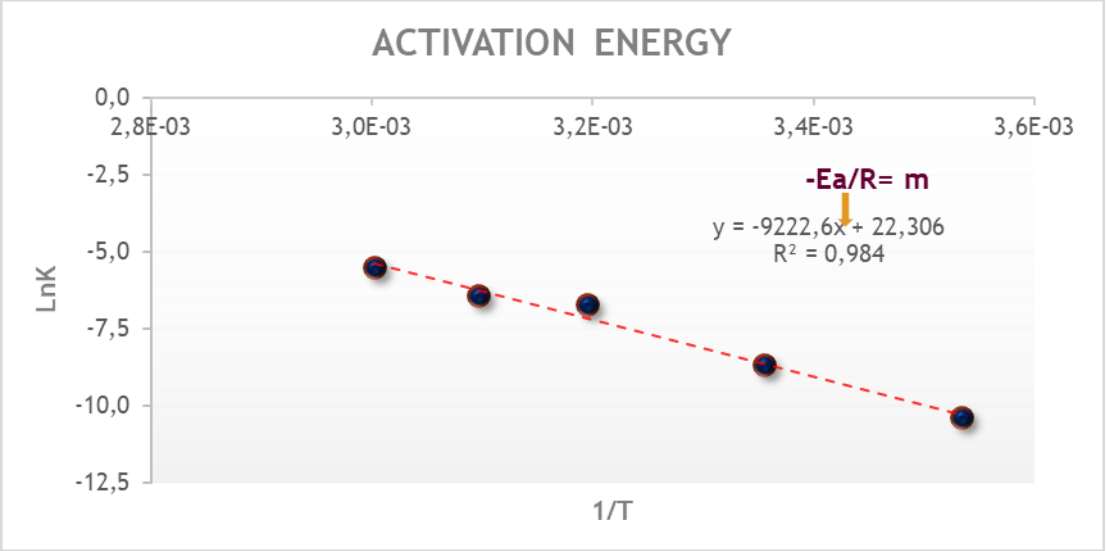

Figure 65. Activation Energy plot for the reaction 3.

Table 5. Reaction rates (k's) at different temperatures. Parameters for the energy of activation.

Excess	Temp K	1/T	k_{obs} (s^{-1})	k_r ($M^{-1}.s^{-1}$)	Ln k	Ln (K/T)
20	*283*	*3,53E-03*	*$1,0x10^{-5}$*	*$3,1x10^{-5}$*	*-10,38*	*-16,027*
20	*298*	*3,36E-03*	*$5,9x10^{-5}$*	*$1,7x10^{-4}$*	*-8,68*	*-14,377*
20	*313*	*3,19E-03*	*$4,4x10^{-4}$*	*$1,2x10^{-3}$*	*-6,73*	*-12,472*
20	*323*	*3,10E-03*	*$5,6x10^{-4}$*	*$1,6x10^{-3}$*	*-6,44*	*-12,215*
20	*333*	*3,00E-03*	*$1,410^{-4}$*	*$4,1x10^{-3}$*	*-5,50*	*-11,305*

2. ELECTRONIC STUDY

In order to study the electronic effect on the reference reaction, it was necessary to modify the substituents of the benzaldehyde to obtain the free-energy relationship meaning the relating reaction rates on the electronic characteristics through the Hammett plot. It was selected 6 different substituents: tBu, MeO, F, Cl, Br, and CN (Figure 66).

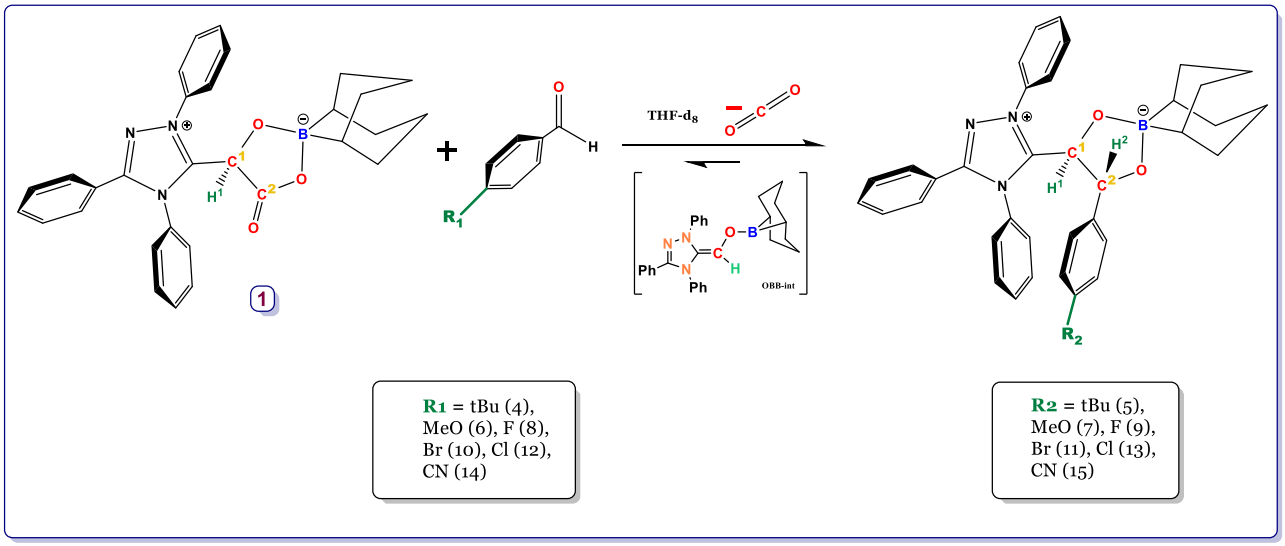

Figure 66. Reference reaction with substituents modification in the phenyl for electronic study.

2.1. Synthesis and characterization of the adducts from benzaldehyde derivatives

All the following reactions were performed in stoichiometric ratio and pseudo-order conditions with 20 equivalents of excess at room temperature.

4-tButylbenzaldehyde adduct reaction (5)

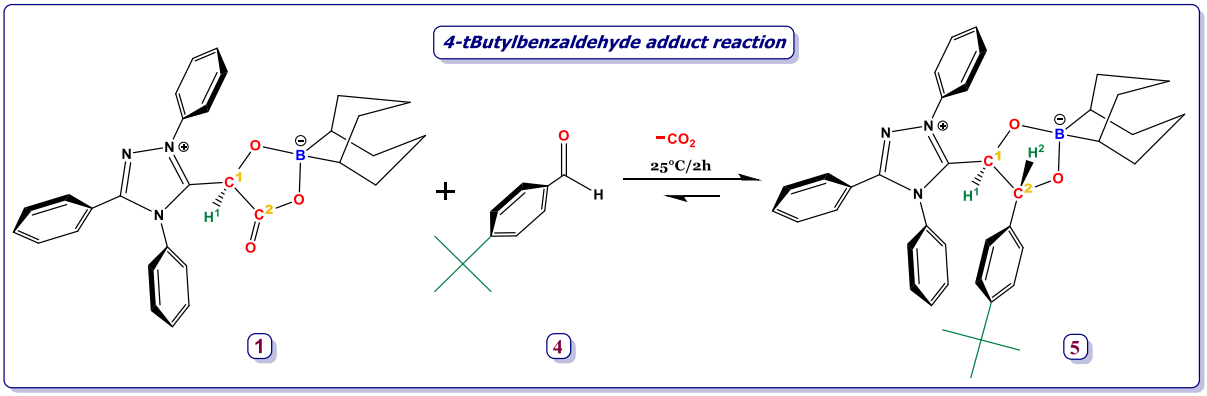

Figure 67. Reference reaction with tBu substituent in the benzaldehyde phenyl. THF-d8, Fisher porter 100mg.

The reaction of **1** with **4** trapped the aldehyde forming adduct **5** (Figure 67). ^{1}H NMR Analysis shows the pair of doublets that corresponds to H1 and H2 (Figure 68, δ4.66-δ4.45) in the adduct **5**. With a coupling constant between them of $^{3}J_{HH}$ = 8.2 Hz. Product 5 was isolated with an 85% yield, and monocrystals were obtained from the reaction (Figure 68).

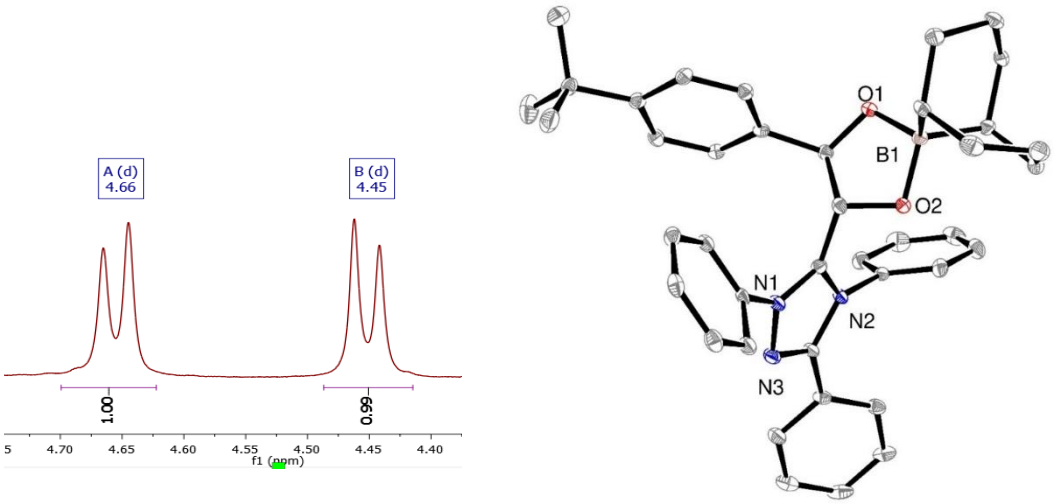

Figure 68. ^{1}H NMR and X-ray structure of product 5.

4-anisaldehyde adduct (7)

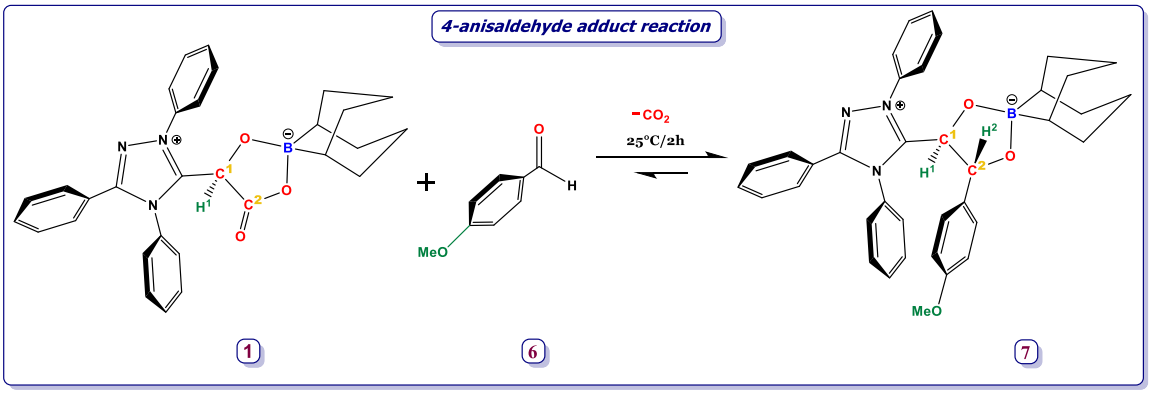

Figure 69. Reference reaction with MeO substituent in the benzaldehyde phenyl. THF-d8, Fisher porter 100mg.

Adduct 7 (Figure 69) was characterized in situ with a yield of 89%. The characteristic doublet that identifies the product's presence was found at δ 5.06 and δ4.86, corresponding to H1 and H2 with a coupling constant of $^{3}J_{HH}$ = 8.1 Hz. Monocrystals were obtained by pentane diffusion into THF (Figure 70).

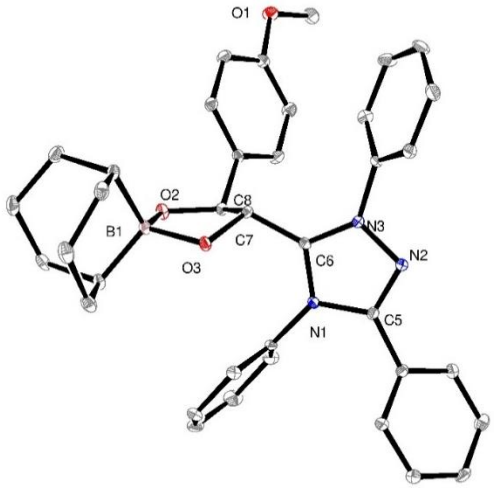

Figure 70. Right: X-ray structure of product 5.

4-fluorobenzaldehyde adduct (9)

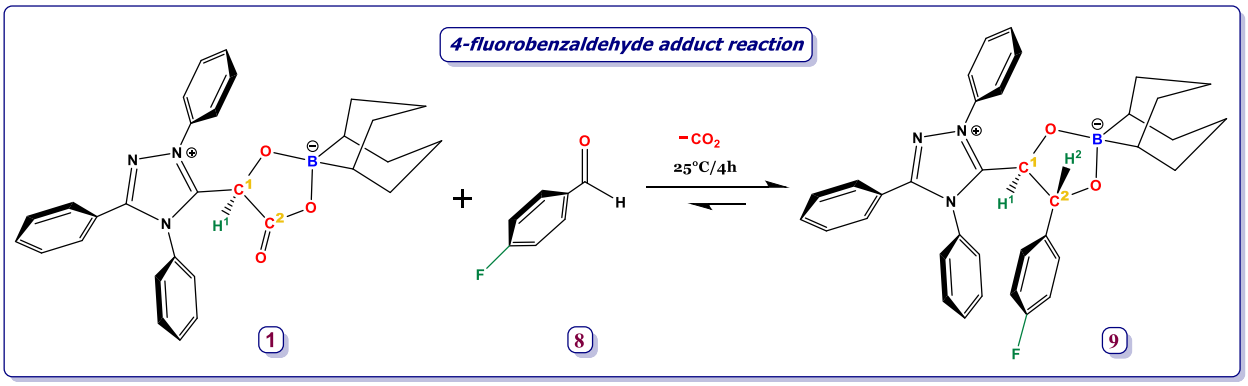

Figure 71. Reference reaction with F substituent in the benzaldehyde phenyl. THF-d8, Fisher porter 100mg.

Product **9** (Figure 71) was fully characterized by NMR spectroscopy analysis. In the proton NMR, it is possible to observe the doublets at δ 4.51 (H2) and δ4.71 (H1) ppm with a coupling constant of $^{3}J_{HH}$ = 8.0 Hz. The in situ yield was 90%.

4-bromobenzaldehyde adduct (11)

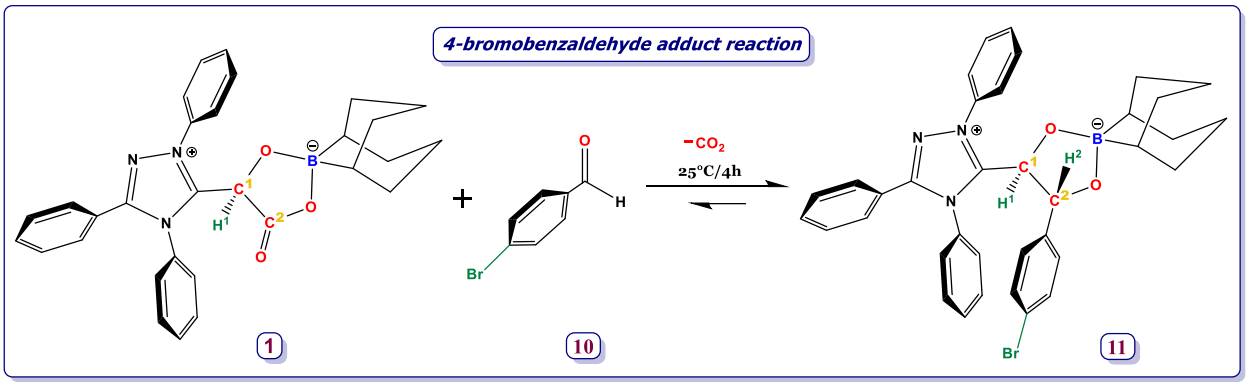

Figure 72. Reference reaction with Br substituent in the benzaldehyde phenyl. THF-d8, Fisher porter 100mg.

Reference reaction with the bromo substituent **10** affords the product **11** with a 97% yield (Figure 72). NMR shows the pair of doublets at δ 4.44 and δ 4.62 ppm corresponding to H2 and H1 with a coupling constant of $^{3}J_{HH}$ = 8.0 Hz., in the adduct **11**.

4-chlorobenzaldehyde adduct (13)

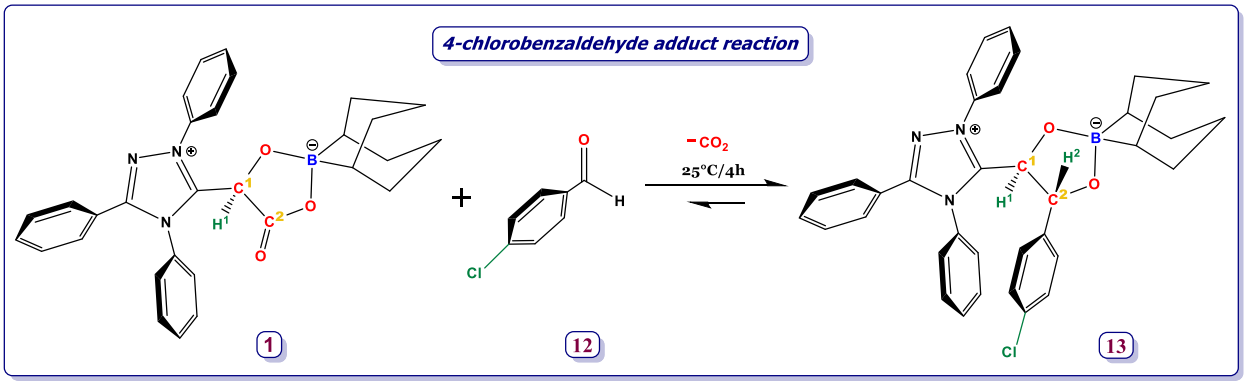

Figure 73. Reference reaction with Cl substituent in the benzaldehyde phenyl. THF-d8, Fisher porter 100mg.

Product **13** (Figure 73) was characterized in situ with a yield of 96%. In the proton NMR, the doublets at δ 4.47 and δ4.66 ppm corresponding to H2 and H1 ($^3J_{HH}$ = 8.0 Hz) corroborate the appearance of the desired product (Figure 74).

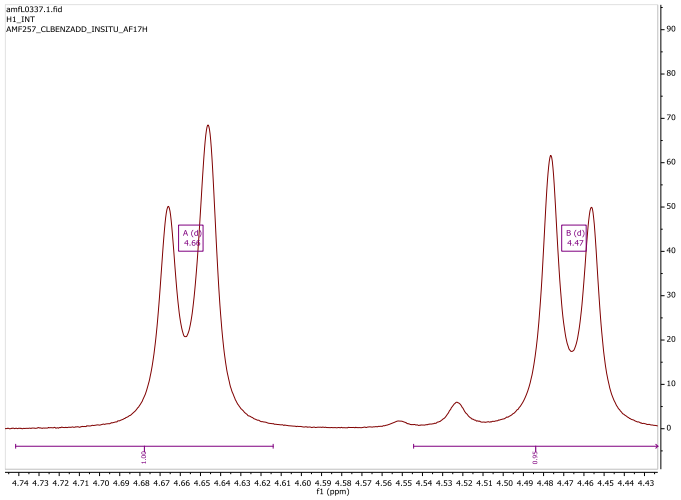

Figure 74. Spectrometric detection of product 13: 4-chlorobenzaldehyde adduct.

4-cyanobenzaldehyde adduct (15)

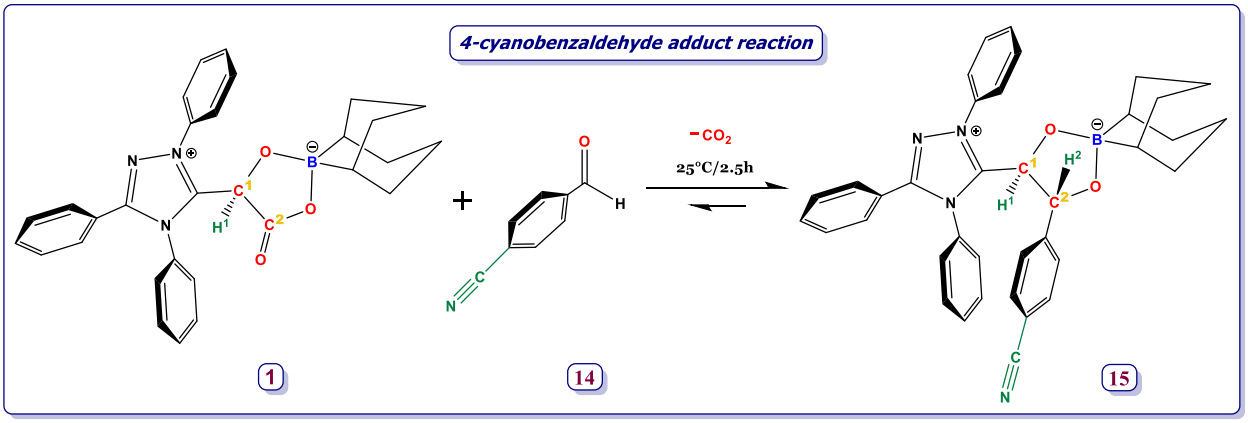

Figure 75. Reference reaction with CN substituent in the benzaldehyde phenyl. THF-d8, Fisher porter 100mg.

Product **15** (Figure 75) was identified by proton NMR spectrometry with the pair of doublets' appearance at δ 4.47 and δ4.70 ppm ($^3J_{HH}$ = 8.1 Hz). It was characterized and isolated with a 95% yield.

Comparative analysis

Electron withdrawing groups (EWG) took a longer time for the reaction to be completed and are less stable for isolation. All the products present the trans-diastereoisomers selectivity with coupling constants between $^{3}J_{HH}$ 8.0 and 8.2 Hz, a narrow range of +/- 0.2 Hz (Table 6).

Table 6. Comparative table of the aldehydes substituents.

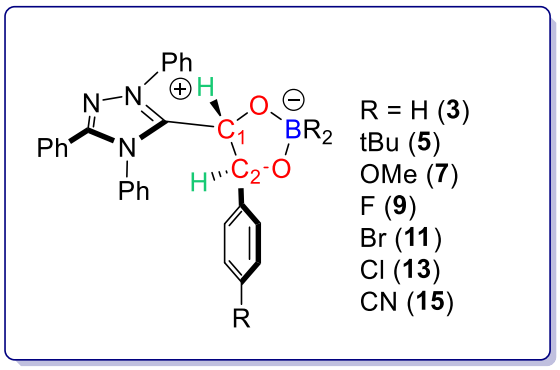

	Yield (in-situ/isolated)	Temp °C	Time(h) 1:1 In fisher porter (stirring) 100mg	Time(h) 1:20 *In situ*	δH C1 and C2	$^{3}J_{HH}$ (Hz)
H (3)	83% yield	25	1h	15.6	δ 4.66 δ 4.40	$^{3}J_{H\text{-}H}$ = 8.2 Hz
tBu (5)	85% yield	25	2 h	5	δ 4.66 δ 4.45	$^{3}J_{H\text{-}H}$ = 8.2 Hz
MeO (7)	89 (*in situ*)	25	2 h	1.5	δ 4.37 δ 4.19	$^{3}J_{H\text{-}H}$ = 8.1 Hz
F (9)	90% (*in situ*)	25	4h	11.9	δ 4.66 δ 4.46	$^{3}J_{H\text{-}H}$ = 8.0 Hz
Br (11)	97% (*in situ*)	25	4h	6	δ 4.62 δ 4.44	$^{3}J_{H\text{-}H}$ = 8.0 Hz
Cl (13)	96 % (*in situ*)	25	4h	14.5	δ 4.66 δ 4.47	$^{3}J_{H\text{-}H}$ = 8.0 Hz
CN (15)	95% yield	25	2.5h	9.3	δ 4.71 δ 4.47	$^{3}J_{H\text{-}H}$ = 8.1 Hz

Crystal comparisons

In a general manner, the O-B bonds in the aldehydes adducts are stronger (shorter distances) than in **1**, the adduct with the CO_2 trapped. In contrast to the C-C bonds that are weaker (longer)in aldehydes than in adduct **1**. The C-C bond distances are in the regular distances for a single bond (Table 7).

Table 7. Comparative table of the Crystal distances.

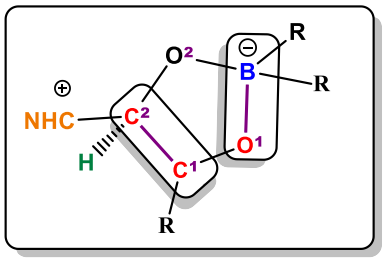

	COMP 1	COMP 3	COMP 5	COMP 7
BOND LENGTHS (Å)				
C1-C2	1.5464(18)	1.5681(15)	1.561(6)	1.578(3)
C2-O2	1.2907(17)	1.3928(13)	1.398(5)	1.399(3)
O2-B	1.5737(18)	1.5150(15)	1.511(6)	1.512(3)
O1-B	1.5233(17)	1.5213(14)	1.525(5)	1.527(3)
C1-O1	1.3774(16)	1.3849(13)	1.390(5)	1.390(3)
BOND ANGLES (°)				
C1C2O2	108.77(10)	103.41(8)	105.3(3)	103.60(16)
C2O2B	111.34(10)	110.96(8)	104.4(3)	111.40(16)
O2BO1	100.5(10)	102.35(8)	102.4(3)	102.15(16)
BO1C1	109.02(10)	105.96(8)	110.8(3)	106.59(16)
O1C1C2	107.45(10)	105.50(8)	102.5(3)	105.30(16)
ΣB	334.5	330.57	332.5	329.17
Σ5-membered ring	537.12	528.18	525.4	529.04

Σ= sum of the interior bond angles (ring specified).

2.2. Mechanistic Investigation: Calculation of the rate constant with the benzaldehyde derivatives

The impact of para-substituted benzaldehydes on the kinetics was performed. With the information provided by the variation of the rate constants logarithm as a function of the Hammett σ parameters[96] of the selected benzaldehydes (Table 8), it was possible to draw the Hammett plot at 20 equivalents (Figure 76).

Table 8. K, log K, and σp for the different devitatives at 10 and 20 equivalents.

EQ	SUBS	σp	[B]mM/µL	$K_r(M^{-1}.s^{-1})$
20	*Cl*	*0,232*	*3,39 x 10 $^{-4}$*	*1,3 x 10 $^{-4}$*
20	*tBu*	*-0,197*	*3,39 x 10 $^{-4}$*	*5,8 x 10 $^{-4}$*
20	*OMe*	*-0,268*	*3,39 x 10 $^{-4}$*	*7,8 x 10 $^{-4}$*
20	*CN*	*0,66*	*3,39 x 10 $^{-4}$*	*1,8 x 10 $^{-4}$*
20	*H*	*0*	*3,39 x 10 $^{-4}$*	*1,7 x 10 $^{-4}$*

The electronics in this reaction follow a linear tendency with a negative slope for the substituents OMe, tBu, H, and Cl, indicating that the Electron Donating Groups (EDG) in the para-position of the benzaldehyde speed up the reaction by decreasing the kinetic barrier of the rds (Figure 76).

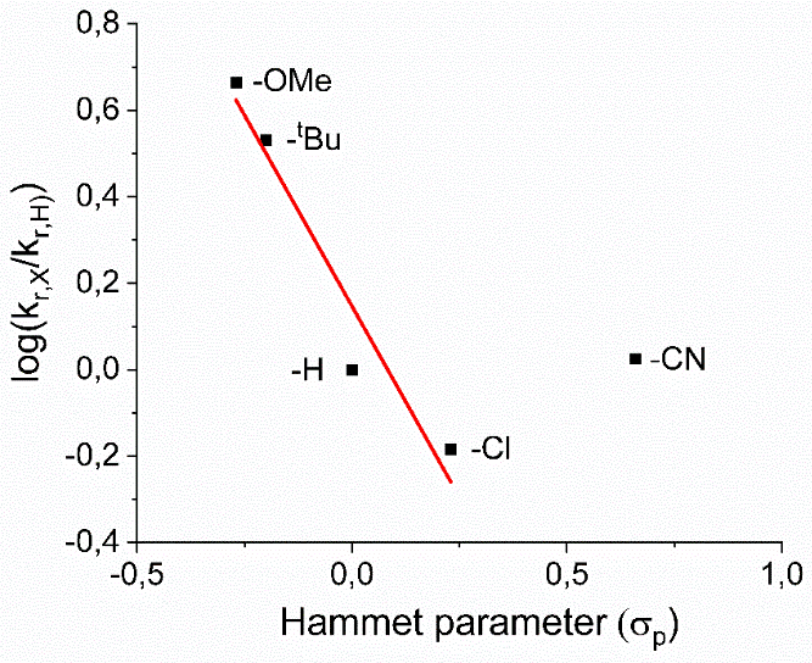

Figure 76. Hammett Plot for the benzaldehyde adducts derivatives at 20 equivalents.

The results explain that the inductive effect changed the rate of the reaction. When there is an EWG such as Cl, the electrons are going to be withdrawn. That means the carbon will be more electrophile and, due to that, will withdraw some electrons from the oxygen. In this case, the reaction is slower, which means that an EDG will be faster, providing stronger nucleophilic oxygen. This behavior gives us an intriguing clue about the importance of oxygen, which seems to be the element that propitiates the initial nucleophilic attack.

However, the cyano-derivative leading to compound **15** significantly differs from the observed trend. This feature could arise from a change in the rate-determining step with this EWG or the CN moiety involvement in the reaction. The cyano group is indeed a Lewis basic function. With this in mind, we tested the influence of the addition of a Lewis base on the kinetic parameters of the reaction. When 20 and 70

equivalents of DMAP (DMAP = 4-dimethylaminopyridine) are added to a mixture of **CO2add** and 4-tBu-benzaldehyde, an increase of the k_{obs} value is observed (from 1.9 x 10^{-4} s^{-1} in the absence of DMAP to 3.3 x10^{-4} s^{-1} in its presence) (Figure 77). Such a result suggests that the presence of Lewis bases could kinetically assist the rate-determining step. The reaction rate with the 4-CN-benzaldehyde would then be influenced by opposite effects: rate decrease due to the electron-withdrawing nature of CN and rate increase due to its Lewis basic property. It is valuable to mention that no reactivity of **3** towards DMAP was observed.

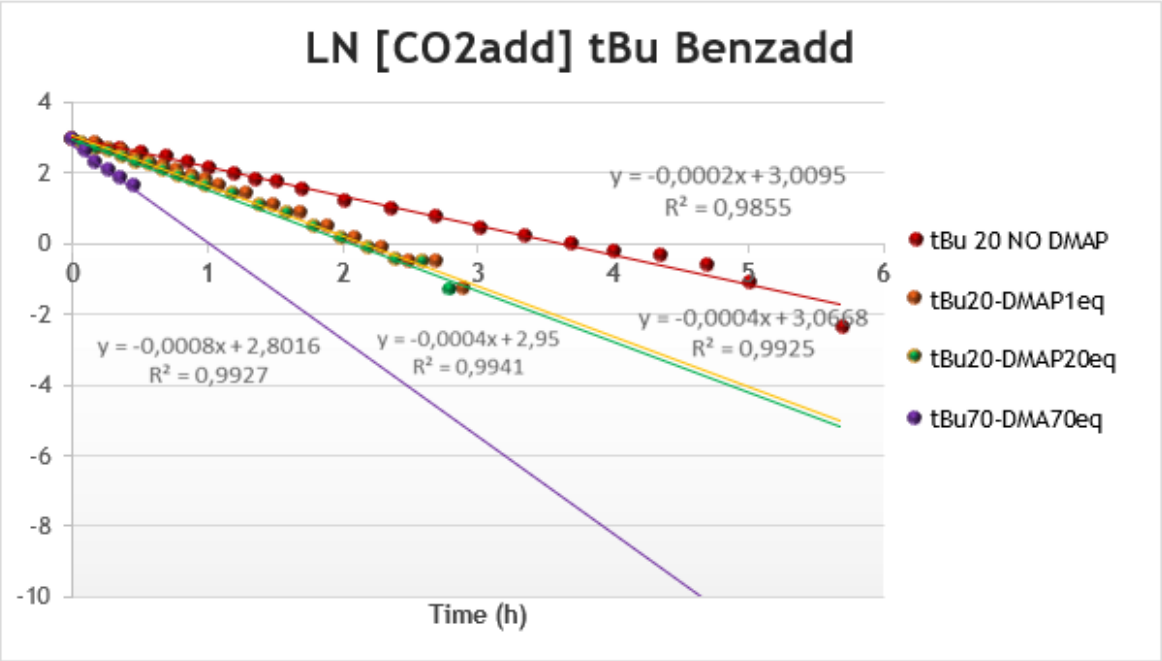

Figure 77. LN [CO2add] vs tBu Benzadd 20 equivaments under DMAP and no DMAP.

Additional kinetic measurements were carried out under 3 atmospheres of CO_2 as it follows (Figure 77).

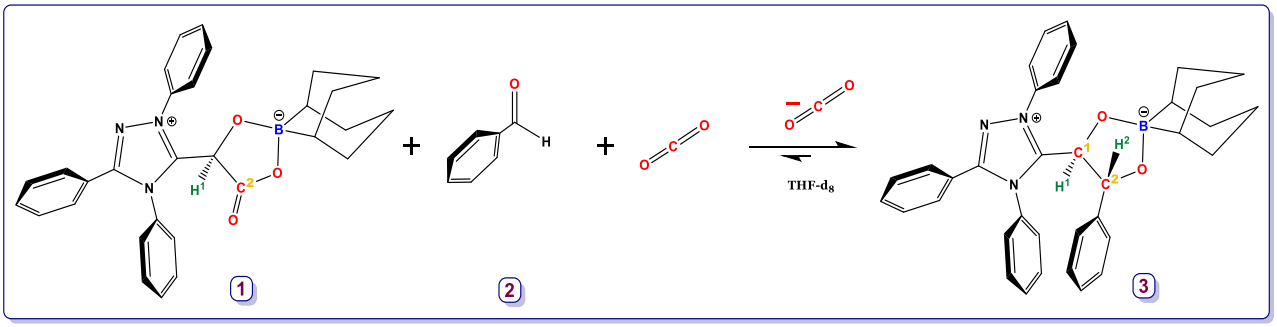

Figure 77. Reference reaction under 3 atmospheres of CO_2. Conditions: 5 mg of CO2 adduct ($10{,}3x10^{-3}$ mmol) and 20 equivalents of benzaldehyde, 41 µL ($407x10^{-3}$ mmol) and 3 atmospheres of CO_2 at 25°C. Solvent THF-d8, internal standard 9,10-dihydroanthracene, volume 600 µL.

Under these conditions, a significant lengthening of the required time was necessary to reach 80% conversion at 25°C, from 7.5 h in the absence of CO_2 to 11.8 h under a pressure of 3 atm. A kinetic rate constant $k_{r,obsCO2}$ = 1.7 $x10^{-5}$ s^{-1} could be determined, but great care must be taken in its analysis. Indeed, such an excess of CO_2 is likely to modify the rate-determining step's nature, thus preventing any fair comparison with the previously determined kinetic parameters. Without pressure CO_2: $k_{r,obsCO2}$ = 5.9 $x10^{-5}$ s^{-1}. The reactant consumption and product formation (Figure 78) show a linear trend supporting a possible modification of RDS, being closer to a zero pseudo-order reaction.

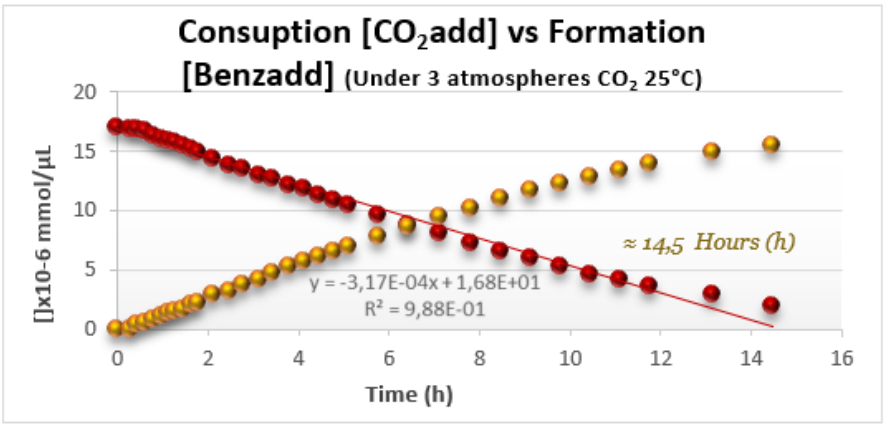

Figure 78. CO2add consumption and formation of the product in hours. Reaction performs under three atmospheres of CO2.

V. INSIGHTS INTO THE MECHANISM

The following insights have been hypothesized based on the obtained experimental results in this work and preliminary theoretical studies with Laboratoire de Physique et Chimie des Nano-Objets (LPCNO).

As hypothesis, we can say that molecule 1a exists in another more reactive form 1b, where the oxygen of the CO_2 takes back the electron engaged with the boron (Figure 79). This unstable form is elucidated from the reversibility of the reaction. The oxygen in the benzaldehyde (**2**) triggers the reaction, and **1b** reacts with **2**, as suggested in the electronic study. A hydrogen bond appears between the oxygen of **1b** and the hydrogen of the aldehyde, allowing an optimal geometry leading to decarboxylation. The oxygen of the aldehyde donates its electron pair to make the O-B bond. The generated carbanion attacks the aldehyde's electrophilic carbon, leading to product **3**, and carbon dioxide is released from the system (Figure 79). The OBB intermediate is never released completely, and it could explain why it has not been observed or isolated the **ts**. Finally, **Benzadd** is formed in a complete diastereoselective fashion, giving rise to the trans-diastereoisomer of **3**.

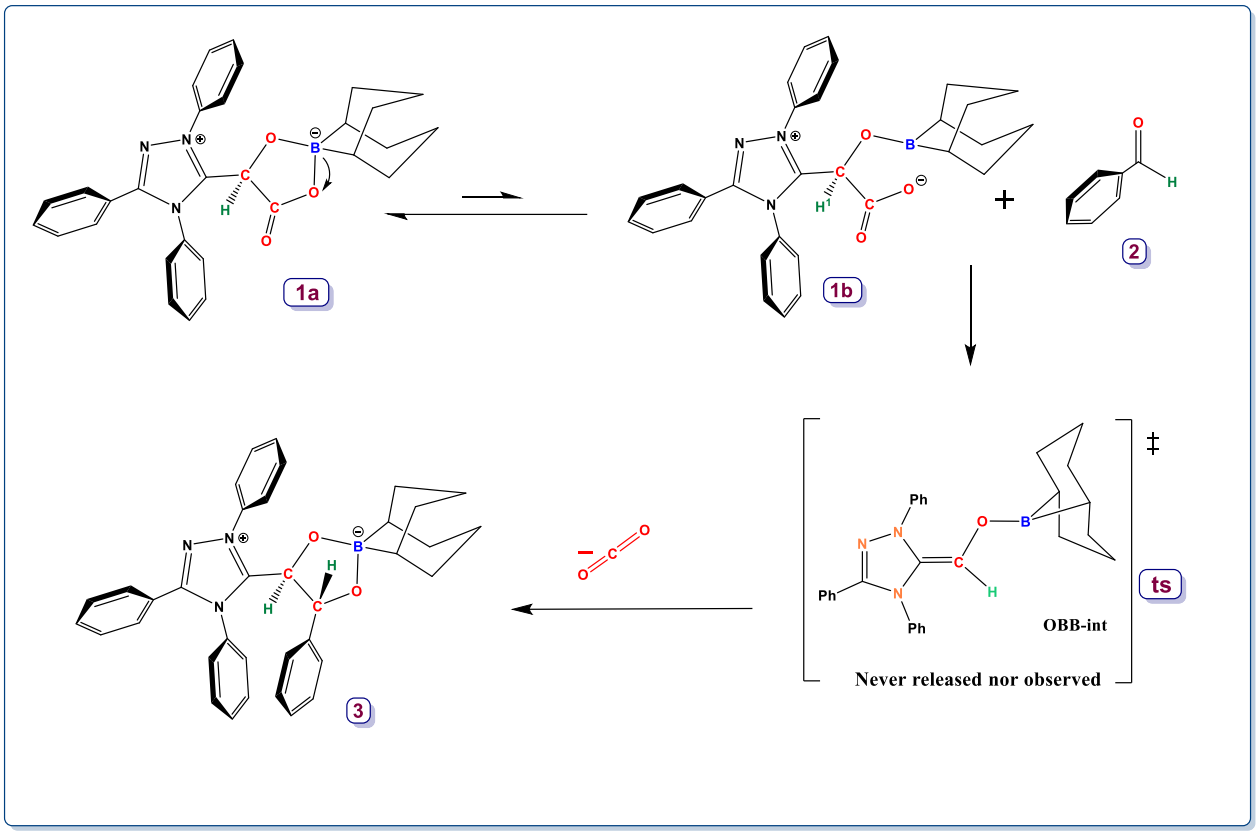

Figure 79. The mechanism proposed for the FLP system for activation of aldehydes.

From the statement, *a kinetic product is the product that is formed faster, and a thermodynamic product is the more stable one*, and taking into consideration that during the present kinetic and mechanistic investigation, the cis-diastereoisomer was nor-observed at any moment. The diastereoselectivity of the system could be led by both, thermodynamic and kinetic control. This system behavior enables a complete diastereocontrol for the trans-disposition configuration experimentally observed, suggesting that the rate-determining-step is associated with the activation barrier and consequently avoiding the cis structural feature formation.

VI. CONCLUSIONS

A new intramolecular FLP-type with complete diastereoselectivity specific for aldehydes has been revealed. This chemoselective FLP-type expands the use of Lewis base carbon-based studies that are not coming directly from a carbene, opening new options for activation of small molecules in green chemistry.

The use of **CO2add** (1) enabled access to an O-Bolylated Breslow intermediate as an FLP system in mild conditions. This new OBB intermediate is made from a new synthetic pathway, the acetal BBA, instead of the aldehyde in the classical benzoin condensation reaction.

The kinetic studies provide original insights about how the OBB is never released to activate the aldehydes. The rate-determining step includes a molecule of **1** and a molecule of **2** (Figure 80). EDG aldehydes favor the system, reducing the kinetic barrier.

GENERAL CONCLUSION

GENERAL CONCLUSION

This young field of FLP systems has proliferated fast, finding remarkable discoveries in small molecule activation. We probed that modern FLP chemistry goes beyond dihydrogen activation and hydrogenation catalysis. This FLP-type expands the use of Lewis base carbon-based studies that are not coming directly from a carbene, a unique feature in this system, opening new options for activation of small molecules in green chemistry.

We have studied the reactivity of various small molecule types on the system, including polar and non-polar molecules, finding that the system is chemoselective to aldehydes. This new intramolecular FLP-type with complete unprecedented diastereoselectivity has been revealed, lead by kinetic and thermodynamic control for the trans-diastereoisomer product. Additionally, we isolate and fully characterized seven new compounds from the Novel FLP-type system.

The use of **CO2add** enabled access to an O-Borylated Breslow intermediate as an FLP system in mild conditions. This new OBB intermediate is made from a new synthetic pathway. The mechanism proposed for this reaction is a result of the experimental and preliminary theoretical studies performed in this work; for which we know that the OBB intermediate is never released during the activation, answering why it is not possible to observe it in the system.

The Hammett plot indicates that the reaction rate is first order in both reactants, demonstrating that the rate-determining step includes a molecule of **1** and a molecule of **2** (Figure 80). EDG aldehydes favor the system, reducing the kinetic barrier, and

EWG destabilizes the system. However, the reaction rate is affected by the possible assistance of an external lewis base (as in the cyano group case or the DMAP). The rate law equation = k_r[**CO2Add**]^1 [**PhCHO**]^1 provides the overall order reaction 2.

This study came with its encounters in the synthetic paths. Working with this FLP that includes an Enders carbene makes the compound highly sensitive to air and water, challenging isolation and crystallization processes. Nevertheless, it was possible to fully characterize all the products and obtain three X-ray structures. Solubility was also a challenge, being THF the only solvent that provided stability enough time to complete the reactions. For example, under other solvents like benzene, some reactions were soluble but rapidly lost stability leading to decomposition.

As the main conclusion of this work, we proved the hypothesis that **CO2add**: is a novel intramolecular masked FLP system with original features as a carbon-based Lewis base; is chemoselective to activate aldehydes; has unprecedented diastereoselectivity, and include original insights about the kinetics and its mechanism (Figure 80).

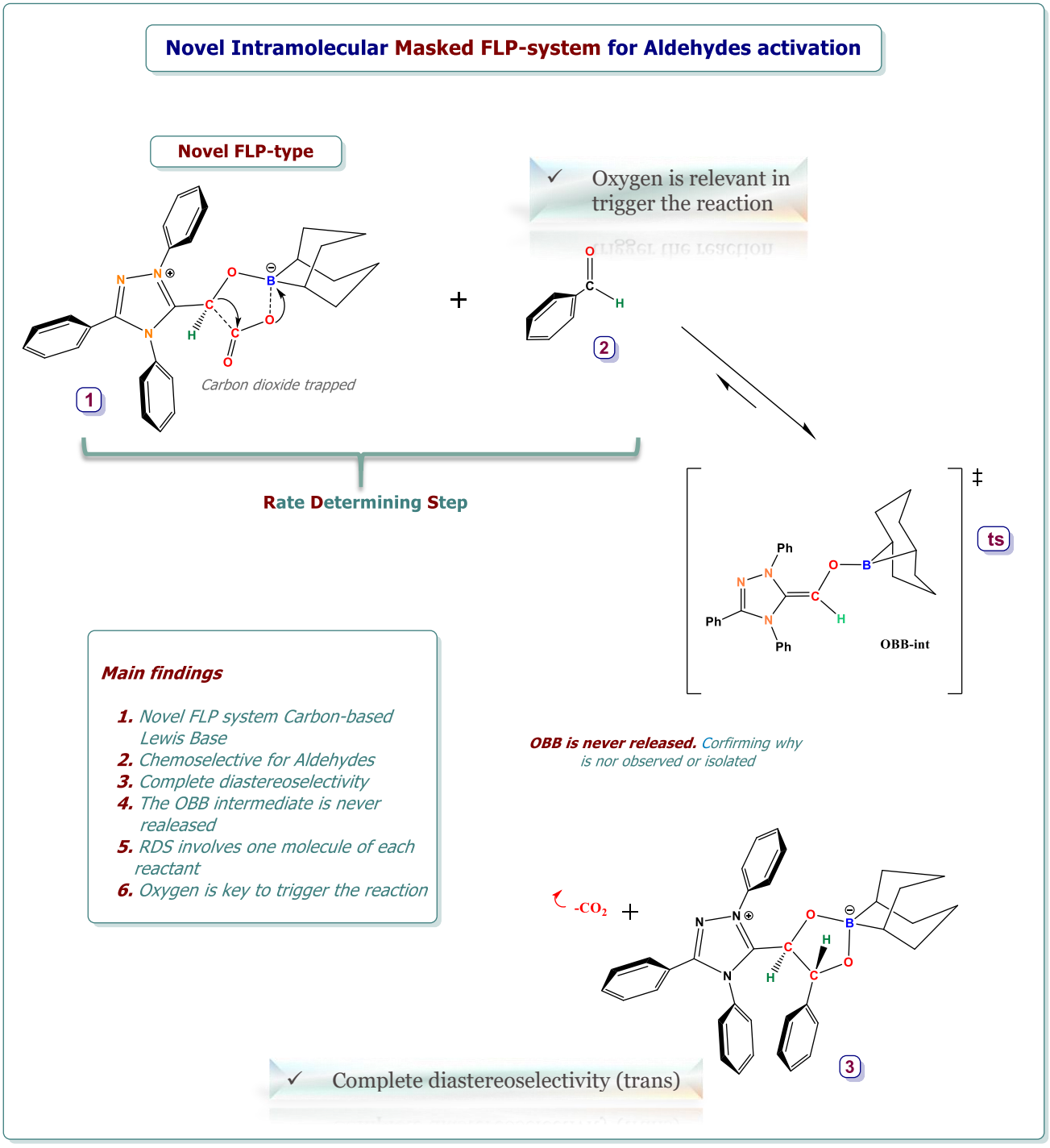

Figure 80. Main findings for the novel intramolecular Masked FLP type for activation of aldehydes.

Perspectives

- ✓ The theoretical study is in progress to complement the experimental results obtained.
- ✓ Try to obtain the cis-diastereoisomer.
- ✓ Try aliphatic aldehydes to observe the FLP reactivity and stability.
- ✓ Create a new FLP system (**CO2add**) to activate aldehydes, changing the Enders carbene for other carbenes and the boron moiety for other Lewis acid donors.

EXPERIMENTAL CHAPTER

EXPERIMENTAL DETAILS

I. GENERAL CONSIDERATIONS

All the experiments were performed under an argon atmosphere in a glove box or using standard Schlenk techniques. Likewise, the dry solvents were used to avoid water or oxygen under the reactions. The compounds were degassed by three freeze-pump-thaw cycles and stored with molecular sieves in the glove box before use. All the NMR data were collected with a Bruker AV400 NMR spectrometer. All chemical shifts for ^{1}H and ^{13}C are relative to TMS. ^{11}B spectra were referenced relative to $F_3B.Et_2O$. Chemical shifts are reported in ppm (δ) and coupling constants in Hertz (Hz). The following abbreviations were used, s – singlet, d – doublet, t – triplet, quart – quartet, sept – septet, br-broad and m – multiplet. ESI-MS mass spectra were measured on a TSQ 7000 Thermo Electron mass instrument at ICT "Institut de Chimie de Toulouse" (website: ict.ups-tlse.fr). Elemental analyses were performed in the facility available in Laboratoire de Chimie de Coordination du CNRS using PerkinElmer 2400 Series Analyzer, Toulouse. Single crystals were diffracted in Bruker Kappa APEX II diffractometer at 100 – 115 K using Mo Kα radiation (λ = 0.71073 Å) filtered through graphite monochromator.

$Fe(H)_2(dmpe)_2$, and Enders' carbene (1,3,4-triphenyl-4*H*-1,2,4-triazol-l-ium-5-ide), have been prepared according to literature procedures. 9-BBN and aldehydes were purchased from commercial sources and used without further purification.

1. COMPOUNDS

1.1. Benzaldehyde adduct (3)

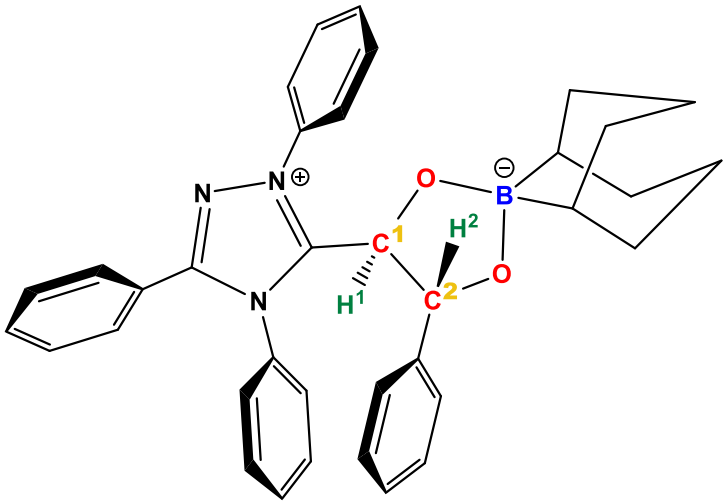

In a schlenk, CO_2 adduct **1** (200 mg, 0.41 mmol) and benzaldehyde **2** (43.4 µL, 0.41 mmol) were dissolved in 5ml of THF. The resulting solution was placed at 80°C and stirred for 1 hour 30 minutes under argon. The volatiles was removed under reduced pressure. The residue was washed with pentane (4x10 ml). Finally, the excess of benzaldehyde and solvents were removed under vacuum overnight. The product was washed with pentane to afford the desired product **3** as a yellow powder (188 mg, 0.34 mmol, Yield = 83%). Crystals were obtained from 200 mg of the benzaldehyde in a solution of 0.7 mL of THF at -20°C within four days.

^{1}H NMR (THF-*d*$_8$, 298 K, 400.0 MHz): : δ 7.82 (d, 2H, J_{HH} = 7.7 Hz, CHar), 7.61-7.46 (m, 7H, CH_{ar}), 7.46-7.40 (m, 3H, CH_{ar}), 7.39-7.33 (m, 3H, CH_{ar}), 7.21-7.16 (m, 5H, CH_{ar}), 4.66 (d, 1H, $^{3}J_{HH}$ = 8.1 Hz, CH-NHC), 4.43 (d, 1H, $^{3}J_{HH}$ = 8.1 Hz, CHPhO), 2.06-1.91 (m, 3H, CH_2), 1.90- 1.81 (m, 3H, CH_2), 1.67-1.61 (m, 1H, CH_2), 1.67-1.50 (m, 2H, CH_2), 1.48-1.43 (m, 1H, CH_2), 1.41-1.36 (m, 1H, CH_2), 1.34-1.28 (m, 1H, CH_2), 0.23 (br. s, 1H, BCH), 0.13 (br. s, 1H, BCH).

^{13}C{^{1}H} (THF-*d*$_8$, 298 K, 400.0 MHz): δ 158.4 (s, N=CN), 154.5 (s, N=CPh), 145.9 (s, C_{ipso}PhCHO), 137.3 (s, C_{ipso}Ph), 133.0 (s, C_{ipso}Ph), 132.8 (s, CH_{ar}), 132.1 (s,

CH_{ar}), 131.8 (s, CH_{ar}), 130.7 (s, CH_{ar}), 130.2 (s, 3C, CH_{ar}), 130.1 (s, 3C, CH_{ar}), 129.8 (s, 3C, CH_{ar}), 128.8 (s, 2C, CH_{ar}), 127.6 (s, CH_{ar}), 127.3 (s, 2C, CH_{ar}), 127.2 (s, 2C, CH_{ar}), 124.3 (s, $C_{ipso}Ph$), 81.0 (s, CHPhO), 77.7 (s, CH-NHC), 34.7 (s, CH_2), 34.5 (s, CH_2), 34.4 (s, CH2), 33.9 (s, CH_2), 27.8 (br. s, 2C, BCH), 27.2 (s, 2C, CH_2).

$^{11}B\{^1H\}$ NMR (THF-d_8, 298 K, 128.4 MHz): δ 11.5

IR (solid, cm^{-1}): 1494 (stretch, HCO).

Anal. cald. for $C_{36}H_{36}BN_3O_2$ + 0.55 THF: C, 77.21; **H**, 7.04; **N**, 7.07. **Found: C,** 77.05; **H,** 6.92; **N,** 7.19. Remark: the isolated sample contains THF. This product is sensitive to prolonged drying under a vacuum. Therefore, the product was only dried for 2 hours (70 mTorr) at 25°C to avoid decomposition. Considering the exact amount of these solvents determined by NMR - C36H36BN3O2 + 0.55 THF.

T. Decomp: 120°C

Mass DCI-CH_4 [M^+]: Calc: 553.2901. Found: 553.2927 mDa: 2.6 ppm: 4.7

1.2. 4-tertbutylbenzaldehyde adduct (5)

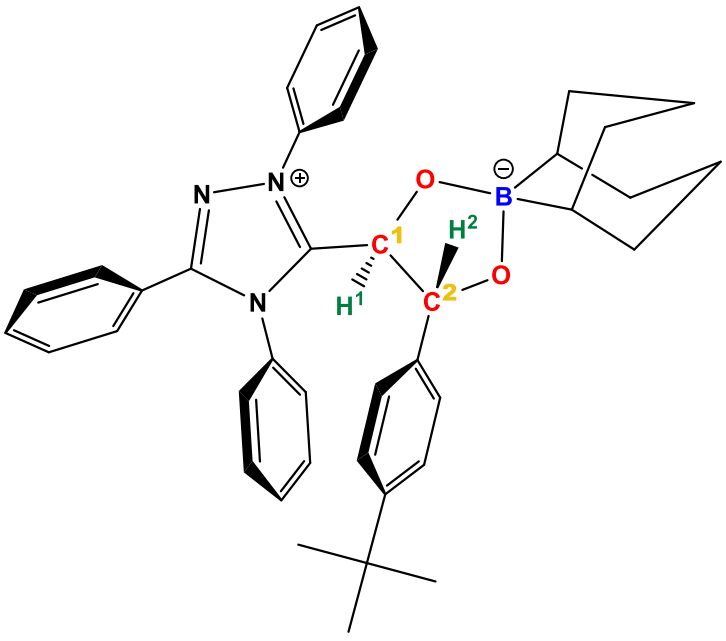

In a Schlenk, compound **1** (200 mg, 0.41 mmol) and 4-tertbutylbenzaldehyde (68 µL, 0.41 mmol) are dissolved in **5** ml of THF. The resulting solution is placed at 50°C and stirred

for 1.5 h under argon. The volatiles was removed under reduced pressure overnight. The residue is washed with pentane (4x10 ml) to afford the desired product 5 as a yellow powder (212 mg, 0.35 mmol, Yield = 85 %). Crystals were obtained from 200 mg of 5 in a solution of 0.7 mL of THF at - 37°C within two weeks. Pentane despite overnight vacuum at rt. At higher temp lead to decomp.

^{1}H NMR (THF-*d*$_8$, 298 K, 400.0 MHz): : δ 7.72 (d, 2H, $^{3}J_{HH}$ = 7.9 Hz, CH_{ar}), 7.61-7.30 (m, 13H, CH_{ar}), 7.27 (d, 2H, $^{3}J_{HH}$ = 7.9 Hz, CH_{ar}), 7.12 (d, 2H, $^{3}J_{HH}$ = 7.9 Hz, CH_{ar}), 4.66 (d, 1H, $^{3}J_{HH}$ = 8.2 Hz, CH-NHC), 4.45 (d, 1H, $^{3}J_{HH}$ = 8.2 Hz, CHPhO), 2.07-1.90 (m, 2H, CH_2), 1.89-1.66 (m, 4H, CH_2), 1.66-1.37 (m, 6H, CH_2), 1.34 (s, 9H, CH_3), 0.23 (br. s, 1H, BC*H*), 0.11 (br. s, 1H, BC*H*).

^{13}C{^{1}H} (THF-*d*$_8$, 273 K, 125.7 MHz): δ 158.63 (s, N=*C*N), 154.67 (s, N=*C*Ph), 150.71 (s, C_{ipso} para-Ph*C*HO), 142.97 (s, C_{ipso} Ph*C*HO), 137.35 (s, C_{ipso}), 133.22 (s, C_{ipso}), 132.89 (s, *C*H_{ar}), 132.21 (s, *C*H_{ar}), 131.93 (s, *C*H_{ar}), 130.77 (s, 2C, *C*H_{ar}), 130.28 (s, 2C, *C*H_{ar}), 130.17 (s, 3C, *C*H_{ar}), 129.88 (s, 3C, *C*H_{ar}), 127.41 (s, 2C, *C*H_{ar}), 127.24 (s, 2C, *C*H_{ar}), 127.75 (s, 2C, *C*H_{ar}), 124.45 (s, C_{ipso}), 81.10 (s, H*C*PH), 77.84 (s, H*C*C), 34.82 (s, *C*H_2), 34.69 (s, *C*H_2), 34.58 (s, *C*H_2), 34.08 (s, *C*H_2), 27.95 (br. s, 2C, B*C*H), 27.16 (s, 2C, *C*H_2).

^{11}B{^{1}H} NMR (THF-d$_8$, 298 K, 128.3 MHz): δ 11.5

IR (solid, cm^{-1}): 1494 (stretch, HCO).

T. Decomp: 109-112°C

Mass DCI-CH_4 [M]$^{+}$: Calc: 609.3542 Found: 609.3567 mDa: -2.5 ppm:-4.1

1.3. 4-anisaldehyde adduct (7)

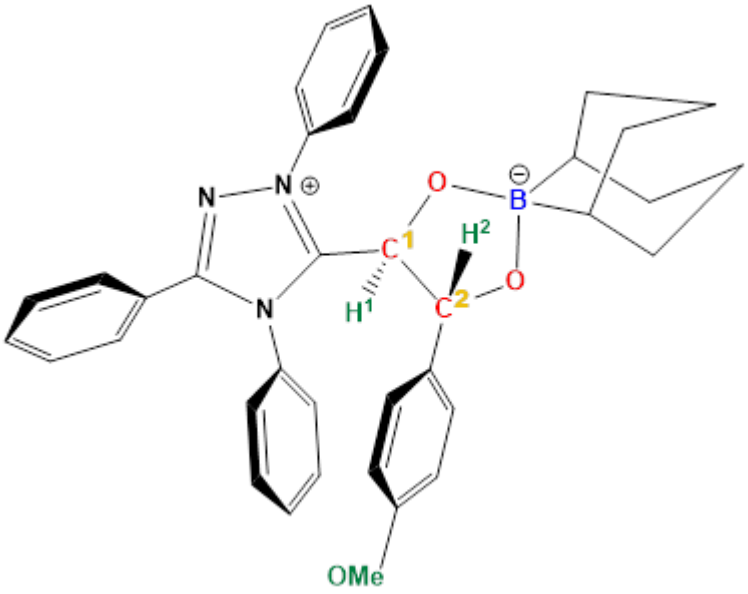

In a schlenk, CO_2 adduct **1** (200 mg, 0.41 mmol) and 7 (49,47 μL, 0.41 mmol) were dissolved in 5ml of THF. The resulting solution was placed at 25°C and stirred for eight inside the glove box. The volatiles are removed under reduced pressure for two hours. In stoichiometric conditions, the product reached the equilibrium at 89% conversion. The product is sensitive to vacuum for more than two hours, and it is detrimental if pentane is applied to wash. A monocrystal for the anisaldehyde adduct powder mix was obtained by diffusion with a THF/EtO2. In a Schlenk, compound 1 (200 mg, 0.41 mmol) and 4-anisaldehyde (49 µL, 0.41 mmol) are dissolved in 5 ml of THF. The resulting solution is placed at 25°C and stirred for 8 h under argon. The volatiles are removed under reduced pressure. The residue are washed with pentane (4x10 ml) to afford the desired product as a yellow powder (196 mg, 0.40 mmol, Yield = 98 %). Crystals were obtained from 200 mg of 5 in a solution of 0.7 mL of THF at -37°C within two weeks. Equilibrated to 92% conv max.

^{1}H NMR (C_6D_6, 298 K, 400.0 MHz): δ 7.25-7.66 (d, 2H, C*H*$_{ar}$), 7.33-7.26 (d, 2H, C*H*$_{ar}$), 7.13-7.06 (m, 2H, C*H*$_{ar}$), 7.05-7.96 (m, 4H, C*H*$_{ar}$), 6.91-6.80 (m, 4H, C*H*$_{ar}$), 6.79-6.65 (m, 5H, C*H*$_{ar}$), 5.06 (d, 1H, $^3J_{HH}$ = 8.1 Hz, CC*H*CO), 4.86 (d, 1H, $^3J_{HH}$

= 8.1 Hz, CC*H*PhO), 3.31 (s, 3H, CH_3), 2.98-2.89 (m, 1H, CH_2), 2.83-2.72 (m, 2H, CH_2), 2.70-2.58 (m, 2H, CH_2), 2.50-2.42 (m, 3H, CH_2), 2.41-2.33 (m, 1H, CH_2), 2.27-2.20 (m, 1H, CH_2), 2.18 -2.10 (m, 1H, CH_2), 1.16 (br. s, 1H, BC*H*), 0.87 (br. s, 1H, BC*H*).

$^{13}C\{^1H\}$ (C_6D_6, 298 K, 400.0 MHz): δ 159.6 (s, N=*C*N), 158.5 (s, N=*C*Ph), 153.5 (s, *C*ipso), 136.9 (s, *C*ipso), 136.1 (s, *C*ipso), 132,1 (s, *C*Har), 131.64(s, *C*ipso), 131.38 (s, *C*Har), 131.34 (s, *C*Har), 130.1 (s, 2C, *C*Har), 129.7 (s, 3C, *C*Har), 129.1 (s, 2C, *C*Har), 129.0 (s, 2C, *C*Har), 128.1 (s, 3C, *C*Har), 126.3 (s, 2C, *C*Har), 122.9 (s, *C*ipso), 114.2 (s, 2C, *C*Har), 81.6 (s, H*C*PH), 77.6 (s, H*C*C), 54.9 (s, *C*H_3), 34.9 (s, *C*H_2), 34.7 (s, *C*H_2), 34.6 (s, *C*H_2), 34.1 (s, *C*H_2), 28.2 (br. s, B*C*H), 27.7 (br. s, B*C*H), 27.1 (s, *C*H_2), 26.9 (s, *C*H_2).

$^{11}B\{^1H\}$ NMR (C_6D_6, 298 K, 128.3 MHz): δ 11.8

IR (solid, cm^{-1}): 1662 and 1499 (stretch, H-C-O and C-O).

T. Decomp: 104°C

Mass DCI-CH_4 $[M]^+$: Calc: 583.30 Found: 529.2992 ppm: 5.0

1.4. 4-fluorobenaldehyde adduct (9)

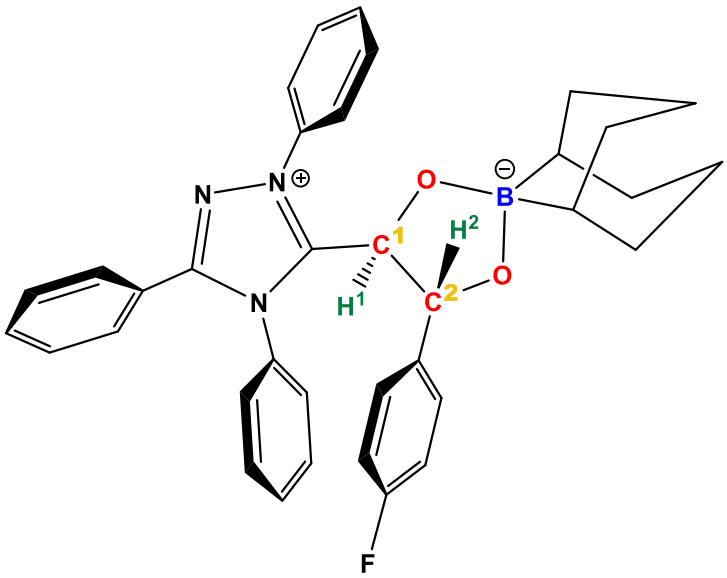

In a schlenk, CO_2 adduct **1** (200 mg, 0.41 mmol) and 4-fluorobenzaldehyde 8 (43,95µL, 0.41 mmol) were dissolved in 5ml of THF. The resulting solution was placed at 25°C and stirred for five hours under argon. The volatiles was removed under reduced pressure. The product reaches the equilibrium at 90% conversion as a yellow powder.

^{1}H NMR (THF-d_8, 298 K, 400.0 MHz): δ 8.05-7.76 (d, 2H, C*H*$_{ar}$), 7.74-7.46 (m, 7H, C*H*$_{ar}$), 7.46-7.40 (m, 3H, C*H*$_{ar}$), 7.40-7.29 (m, 3H, C*H*$_{ar}$), 7.23-7.09 (m, 2H, C*H*$_{ar}$), 6.97-6.85 (m, 2H, C*H*$_{ar}$), 4.66 (d, 1H, $^{3}J_{HH}$ = 8.0 Hz, CC*H*CO), 4.46 (d, 1H, $^{3}J_{HH}$ = 8.0 Hz, CC*H*PhO), 2.04-1.75 (m, 5H, C*H*$_2$), 1.69-1.20 (m, 7H, C*H*$_2$), 0.24 (br. s, 1H, BC*H*), 0.13 (br. s, 1H, BC*H*).

^{13}C{^{1}H} (THF-d_8, 298 K, 400.0 MHz): δ 165.5 (s, N=*C*N), 163.1 (s, N=*C*Ph), 159.3 (s, *C*$_{ipso}$ FPh*C*HO), 155.8 (s, *C*$_{ipso}$), 142.9 (s, *C*$_{ipso}$), 138.4 (s, *C*$_{ipso}$), 134.1 (s, *C*H$_{ar}$), 133.5 (s, *C*H$_{ar}$), 133.2 (s, *C*H$_{ar}$), 132.0 (s, *C*H$_{ar}$), 131.5 (s, 3C, *C*H$_{ar}$), 131.3 (s, 3C, *C*H$_{ar}$), 131.0 (s, 3C, *C*H$_{ar}$), 130.2 (s, *C*H$_{ar}$), 130.1 (s, *C*H$_{ar}$), 128.4 (s, 2C, *C*H$_{ar}$), 125.4 (s, *C*$_{ipso}$), 116.8 (s, *C*H$_{ar}$), 116.6 (s, *C*H$_{ar}$), 81.5 (s, H*C*PH), 78.9 (s, H*C*C), 35.9 (s, *C*H$_2$), 35.7 (s, *C*H$_2$), 35.6 (s, *C*H$_2$), 35.2 (s, *C*H$_2$), 29.1 (br. s, 2C, B*C*H), 28.2 (s, *C*H$_2$), 28.2 (s, *C*H$_2$).

^{11}B{^{1}H} NMR (THF-d$_8$, 298 K, 128.3 MHz): δ 12.5

IR (solid, cm^{-1}): 1660 and 1497 (stretch, H-C-O and C-O).

T. Decomp: 109° C

Mass DCI-CH_4 [M]$^+$: Calc: 572.2815 Found: 572.2806 mDa: 0.9 ppm: 1.6

1.5. 4-bromobenzaldehyde adduct (11)

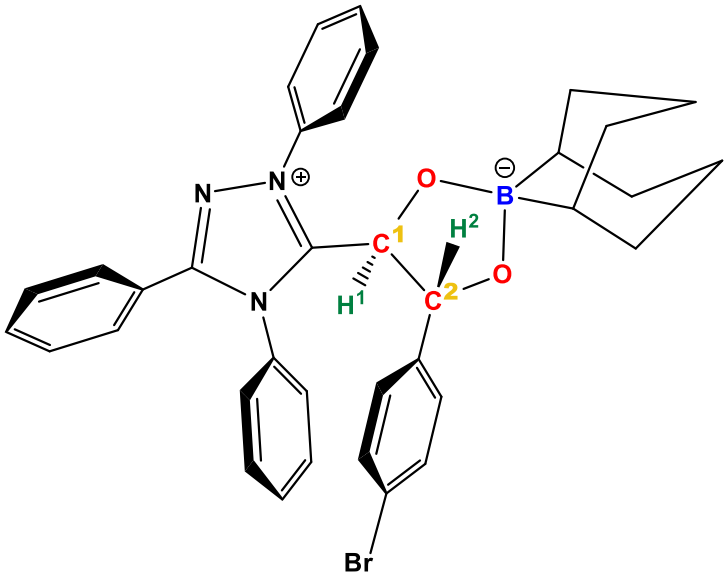

In a schlenk, CO_2 adduct **1** (200 mg, 0.407 mmol) and 4-bromobenzaldehyde **10** (75.38 mg, 0.407 mmol) were dissolved in 5ml of THF. The resulting solution was placed at 60°C and stirred for 1 hour 30 minutes under argon. The volatiles was removed under reduced pressure. Product **11** afford the desired product as a yellow powder (198.4 mg, 0.407 mmol, Yield = 99%).

^{1}H NMR (THF-d_8, 298 K, 400.0 MHz): δ 7.88-7.82 (d, 2H, C*H*$_{ar}$), 7.62-7.47 (m, 7H, C*H*$_{ar}$), 7.46-7.42 (m, 3H, C*H*$_{ar}$), 7.39-7.34 (m, 3H, C*H*$_{ar}$), 7.33-7.28 (m, 3H, C*H*$_{ar}$), 7.11-704 (d, 2H, C*H*$_{ar}$), 4.62 (d, 1H, $^3J_{HH}$ = 8.0 Hz, CC*H*CO), 4.44 (d, 1H, $^3J_{HH}$ = 8.04 Hz, CC*H*PhO), 2.0-1.76 (m, 5H, C*H*$_2$), 1.66-1.26 (m, 7H, C*H*$_2$), 0.21 (br. s, 1H, BC*H*), 0.11 (br. s, 1H, BC*H*).

^{13}C{^{1}H} (THF-d_8, 298 K, 400.0 MHz): δ 158.2 (s, N=*C*N), 154.7 (s, N=*C*Ph), 145.4 (s, *C*$_{ipso}$ BrPh*C*HO), 137.3 (s, *C*$_{ipso}$), 133.1 (s, *C*$_{ipso}$), 132,9 (s, *C*H$_{ar}$), 132.4 (s, *C*H$_{ar}$), 132.1 (s, *C*H$_{ar}$), 132.0 (s, 2C, *C*H$_{ar}$), 130.9 (s, *C*H$_{ar}$), 130.4 (s, 3C, *C*H$_{ar}$), 130.2

(s, 3C, *C*Har), 129.9 (s, 3C, *C*Har), 128.4 (s, 2C, *C*Har), 127.3 (s, 2C, *C*Har), 124.4 (s, *C*ipso), 121.2 (*C*ipso *paraCHO*Br), 80.5 (s, H*C*PH), 77.7 (s, H*C*C), 34.8 (s, *C*H2), 34.6 (s, *C*H2), 34.5 (s, *C*H2), 34.0 (s, *C*H2), 27.9 (br. s, 2C, B*C*H), 27.1 (s, *C*H2), 26.1 (s, *C*H2).

$^{11}B\{^{1}H\}$ NMR (THF-d8, 298 K, 128.3 MHz): δ 12.05

IR (solid, cm^{-1}): 1496 (stretch H-C-O)

T. Decomp: 115°C

Mass DCI-CH_4 $[M]^+$: Calc: 631.1995 Found: 631.2019

1.6. 4-chlorobenzaldehyde adduct (13)

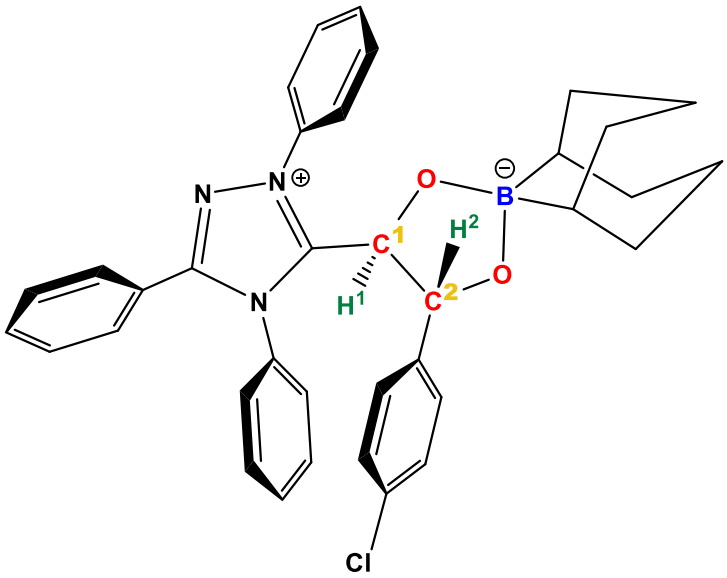

In a schlenk, CO_2 adduct **1** (200 mg, 0.41 mmol) and 4-chlorobenzaldehyde **13** (57,21 mg, 0.41 mmol) were dissolved in 5ml of THF. The resulting solution was placed at 25°C and stirred for five hours under argon. The volatiles was removed under reduced pressure. The product reaches the equilibrium at 98% conversion as a yellow powder. The powder was unstable under solution pentane, and it was not possible to eliminate the 2% of the reactants.

^{1}H NMR (THF-*d*8, 298 K, 400.0 MHz): δ 7.88-7.82 (d, 2H, C*H*ar), 7.69-7.48 (m, 6H, C*H*ar), 7.47-7.41 (m, 3H, C*H*ar), 7.40-7.33 (m, 3H, C*H*ar), 7.20-7.12 (m, 5H, C*H*ar), 4.66 (d, 1H, $^{3}J_{HH}$ = 8.0 Hz, CC*H*CO), 4.47 (d, 1H, $^{3}J_{HH}$ = 8.0 Hz, CC*H*PhO),

2.04-1.74 (m, 5H, C*H*$_2$), 1.70-1.23 (m, 7H, C*H*$_2$), 0.24 (br. s, 1H, BC*H*), 0.13 (br. s, 1H, BC*H*).

^{13}C{^{1}H} (THF-*d*$_8$, 298 K, 400.0 MHz): δ 158.09 (s, N=*C*N), 154.70 (s, N=*C*Ph), 144.84 (s, *C*$_{ipso}$ ClPh*C*HO), 137.28 (s, *C*$_{ipso}$), 133.20 (s, *C*$_{ipso}$), 133,06 (s, *C*$_{ipso}$), 132.97 (s, *C*H$_{ar}$), 132.34 (s, *C*H$_{ar}$), 132.04 (s, *C*H$_{ar}$), 130.90 (s, 2C, *C*H$_{ar}$), 130.37 (s, 3C, *C*H$_{ar}$), 130.18 (s, 3C, *C*H$_{ar}$), 129.90 (s, 3C, *C*H$_{ar}$), 128.02 (s, 3C, *C*H$_{ar}$), 127.26 (s, 2C, *C*H$_{ar}$), 124.28 (s, *C*$_{ipso}$), 80.45 (s, H*C*PH), 77.70 (s, H*C*C), 34.82 (s, *C*H$_2$), 34.62 (s, *C*H$_2$), 34.50 (s, *C*H$_2$), 34.03 (s, *C*H$_2$), 27.92 (br. s, 2C, B*C*H), 27.08 (s, *C*H$_2$), 27.05 (s, *C*H$_2$).

^{11}B{^{1}H} NMR (THF-d$_8$, 298 K, 128.3 MHz): δ 12.1.

IR (solid, cm^{-1}): 1593 (stretch H-C-O).

T. Decomp: 106°C

Mass DCI-CH$_4$ [M]$^+$ Calc: 587.2496 Found: 587.2511 mDa: -1.5 ppm:-2.6

1.7. 4-cyanobenzaldehyde adduct (15)

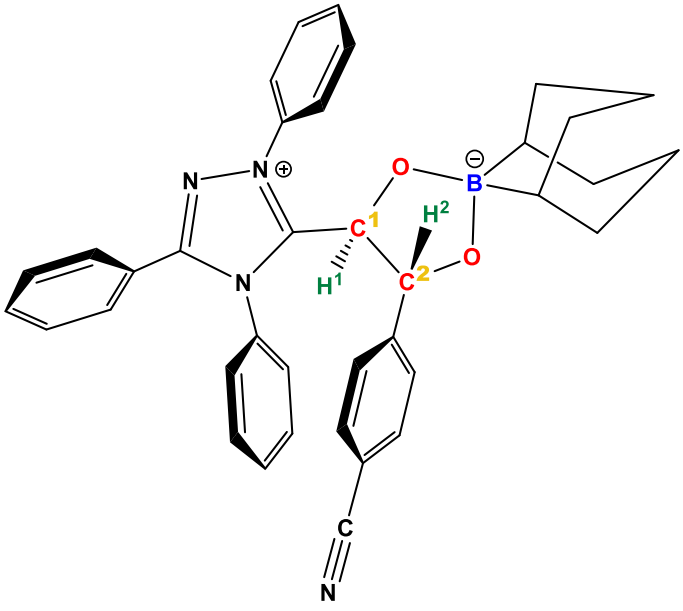

In a schlenk, CO_2 adduct **1** (200 mg, 0.407 mmol) and 4-cyanobenzaldehyde **14** (53.37mg, 0.427 mmol) were dissolved in 5ml of THF. The resulting solution was placed at 60°C and stirred for 1 hour 30 minutes under argon. The

volatiles was removed under reduced pressure. The product was washed with pentane, 3x5 mL, to afford the desired product **15** as a dark green powder (195.3 mg, 0.39 mmol, Yield = 97%).

^{1}H NMR (THF-*d*$_8$, 298 K, 400.0 MHz): δ 7.93-7.87 (m, 2H, C*H*$_{ar}$), 7.64-7.53 (m, 6H, C*H*$_{ar}$), 7.52-7.48 (m, 3H, C*H*$_{ar}$), 7.47-7.43 (m, 3H, C*H*$_{ar}$), 7.41-7.34 (m, 3H, C*H*$_{ar}$), 7.32-7.29 (m, 2H, C*H*$_{ar}$), 4.71 (d, 1H, $^{3}J_{HH}$ = 8.1 Hz, CC*H*CO), 4.47 (d, 1H, $^{3}J_{HH}$ = 8.04 Hz, CC*H*PhO), 2.01-1.76 (m, 6H, C*H*$_2$), 1.66-1.28 (m, 8H, C*H*$_2$), 0.22 (br. s, 1H, BC*H*), 0.15 (br. s, 1H, BC*H*).

^{13}C{^{1}H} (THF-*d*$_8$, 298 K, 400.0 MHz): δ 157.7 (s, N=*C*N), 154.8 (s, N=*C*Ph), 151.8 (s, *C*$_{ipso}$ tBuPh*C*HO), 137.2 (s, *C*$_{ipso}$), 133.1 (s, *C*H$_{ar}$), 133.0 (s, *C*$_{ipso}$) 132.8 (s, 2C, *C*H$_{ar}$), 132.5 (s, *C*H$_{ar}$), 132.2 (s, *C*H$_{ar}$), 131.0 (s, *C*H$_{ar}$), 130.5 (s, 3C, *C*H$_{ar}$), 130.2 (s, 3C, *C*H$_{ar}$), 129.9 (s, 3C, *C*H$_{ar}$), 128.2 (s, 2C, *C*H$_{ar}$), 127.2 (s, 2C, *C*H$_{ar}$), 124.3 (s, *C*$_{ipso}$), 119.5 (*C*$_{ipso}$ *paraCHO*CN), 111.9 (s, *C*$_{ipso}$ Aliphatic *PhCHO*CN), 80.54 (s, H*C*PH), 77.4 (s, H*C*C), 34.8 (s, *C*H$_2$), 34.6 (s, *C*H$_2$), 34.5 (s, *C*H$_2$), 34.0 (s, *C*H$_2$), 27.8 (br. s, 2C, B*C*H), 27.0 (s, *C*H$_2$), 26.9 (s, *C*H$_2$).

^{11}B{^{1}H} NMR (THF-d8, 298 K, 128.3 MHz): δ 11.58

IR (solid, cm^{-1}): 1497 (stretch H-C-O).

T. Decomp: 118-122°C

Mass DCI-CH$_4$ [M+H]$^{+}$: Calc: 579.2947 Found: 579.2972 mDa: -2.5 ppm: 4.3

II. GENERAL PROCEDURE FOR KINETIC STUDIES

The reactions were followed under pseudo-first-order conditions by keeping a large excess (×20) of the benzaldehyde over the CO_2 adduct. In an NMR J. young tube into the glove box, a sample was prepared with $10.2x10^{-3}$ mmol of CO_2 adduct, $20,4x10^{-2}$ of benzaldehyde, 9,10-dihydroanthracene as internal standard, and THF-d_8 to complete 0.6 mL in total volume. The reactions were followed by monitoring the concentration's decrease and the product's formation in the AV400 NMR. The reactions at room temperature (298 K) were taken with eight scans (30 seconds relaxation time). Meanwhile, for the other temperatures, 283 K, 313 K, 323 K, and 333 K integrals, one scan was chosen. The t_0 was taken into account from the moment the benzaldehyde addition inside an argon glove box. The time until the sample reaches the NMR machine is between 3-5 min, a time where the temperature sample is not controlled. Thus, for the linear fit calculations, t_0 is not taken into account. Once the tube is inside, it was kept constant to ±0.1 K until the reaction is finished or when it passes the reaction's half-life.

1. Equations for the activation parameters

[Eq. 1]

$$-Ea/R = -9222,6$$

Where R = 8,314 J/mol K

$$Ea /8,314 = -9222,6$$

$$Ea = 9222,6* 8,314$$

Ea (J/mol)	*76676,69*
Ea (kcal/mol)	***18,3***

[Eq. 2]

R = 8,314 J/mol K

Plank's constant ***h*** =6.62607004x10^{-34} m^2 kg s^{-1}

Boltzmann constant ***k'*** = 1.38064852x10^{-23} m^2 kg s^{-2} K^{-1}

If y = mx+b (m=Eyring plot)

$\mathbf{\Delta S^{\neq}}$ = R (b –Ln (k'/h))

[Eq. 3]

$\mathbf{\Delta H^{\neq}}$= -m * R

[Eq. 4]

$\mathbf{\Delta G^{\neq}}$ = $\Delta H^{\neq}$ - T ($\Delta S^{\neq}$)

Temp K	ΔG≠	ΔS≠	ΔH≠
298	*94396,6*	*-68,008333*	*74130,1182*
283	*93376,5*		
313	*95416,7*		
323	*96096,8*		
333	*96776,9*		

2. Eyring plot

With the aim of understanding the Gibbs free energy of activation, kinetic data was studied in the range of 283-333 K to understand the temperature effect on the rate constant and allowing the activation parameters $\Delta G^{\ddagger}$, $\Delta S^{\ddagger}$, and $\Delta H^{\ddagger}$.

The Eyring plot for benzaldehyde adduct was measured from the following conditions:

- ✓ From the substrate's consumption, CO_2 adduct (A), in pseudo-order conditions at 20 equivalents.
- ✓ Rate constants at five different temperatures, 283, 298, 313, 323, and 333 K.

Pseudo first order in A. Proven in the LN [A] linear fit and the concentrations plot for consumption substrate and formation product. In this last case, the half-life depends exclusively on the reaction rate constant, k. Visually, it is possible on the graph for first-order reactions when the amount of time between one half-life and the next are the same. Another way to see it is that the intersection between the formation of the product and the substrate's consumption is located in the middle, indicating that after half of the amount of the substrate has been consumed, it has been formed the half of the product. In this case, the half-life of a first-order reaction is independent of its initial concentration, and it takes the same amount of time for the concentration to decrease from one point to another point.

In this analysis, five temperatures were chosen, 283K, 298K, 313K, 323K, and 333K. As expected, the reaction goes faster with the temperature increased (Figure 81, Figure 82).

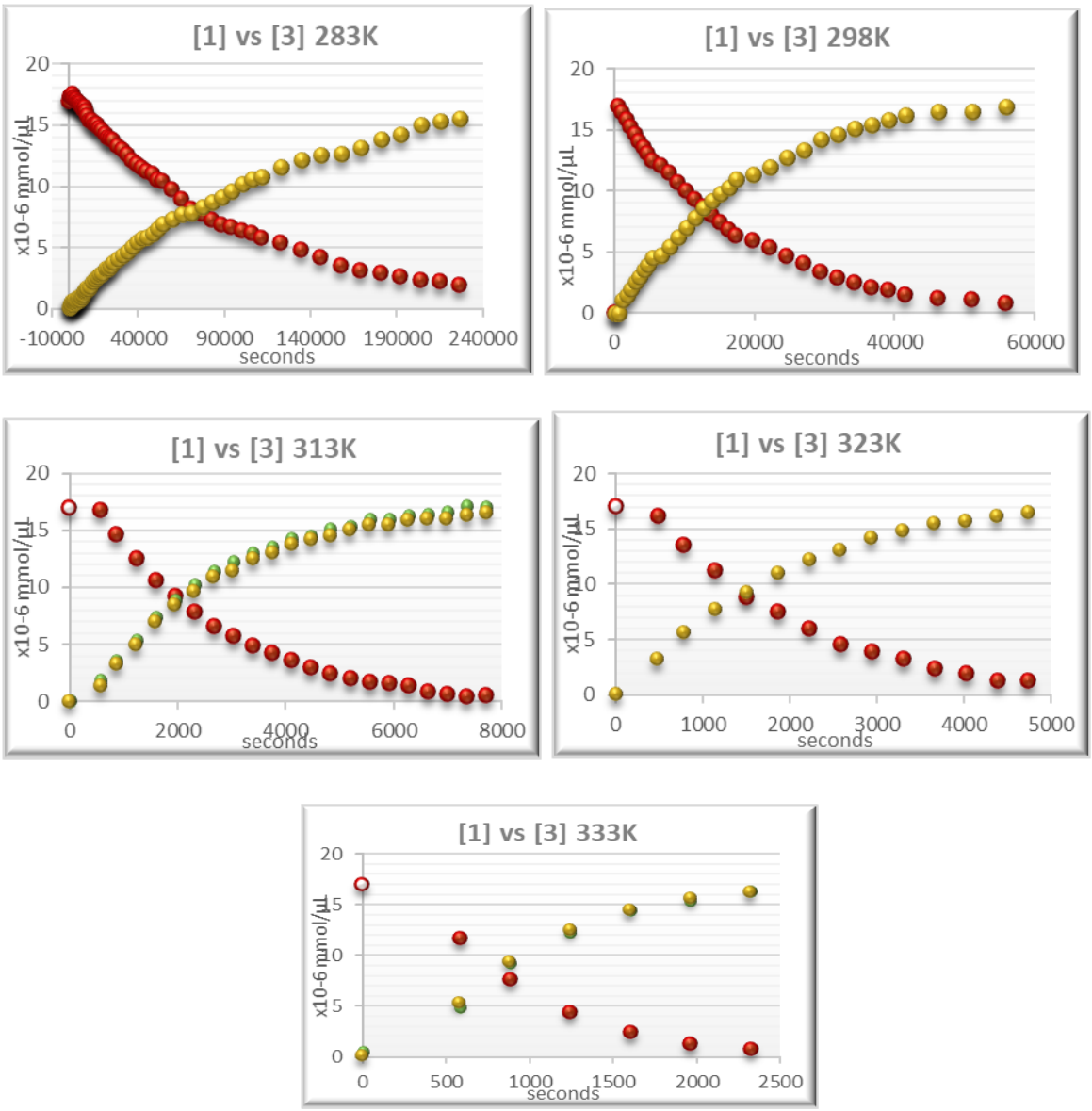

Figure 81. Concentration of CO2 adduct [react 1] vs. benzaldehyde adduct [3] at 283 K, 298 K, 313 K, 323 K, and 333K. Because temperature can not be controlled in the first point, it is not considered in the kinetic analysis. It is used to control the initial concentration.

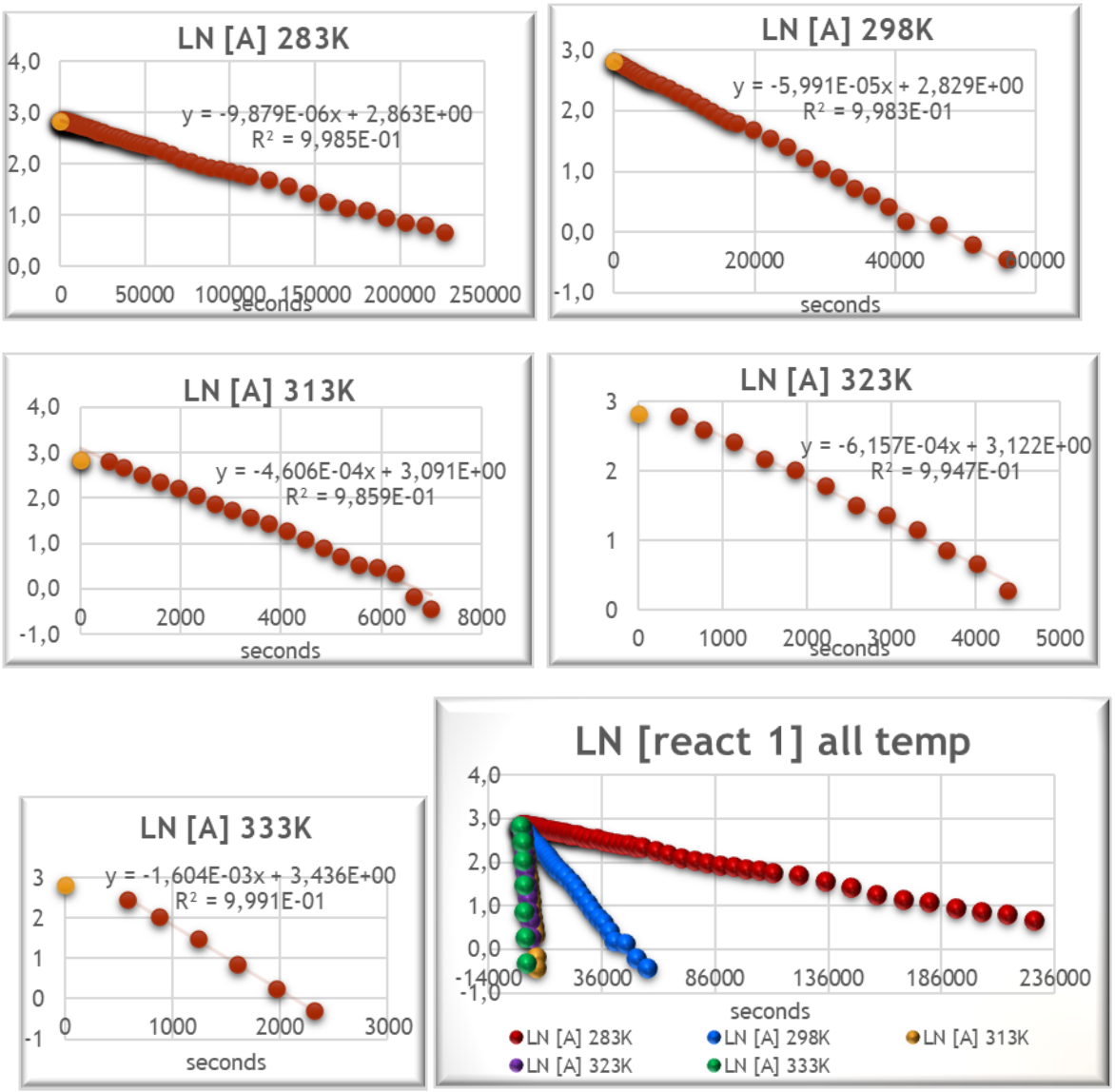

Figure 82. Linear fit LN [react 1] vs. time (seconds) at 283K, 298 K, 313 K, 323 K. Because temperature can not be controlled in the first point, it is not considered in the kinetic analysis. It is used to control the initial concentration.

III. HAMMETT PLOT

Experimental conditions: All the experiments were conducted following the instructions below

Samples: The reactions were prepared in excess of B (Derivatives aldehydes) in pseudo-order conditions (Figure 83).

Two different methods were applied for the measurements.

1. Continuing measurement in the NMR machine at room temperature (RT) (298K) controlled by the NMR AV400, 8 scans and 30 seconds of relaxation time.

2. Interrupted measurement in the NMR AV400 machine (8 scans, 30s relaxation time) at RT and temperature control outside during the intervals.

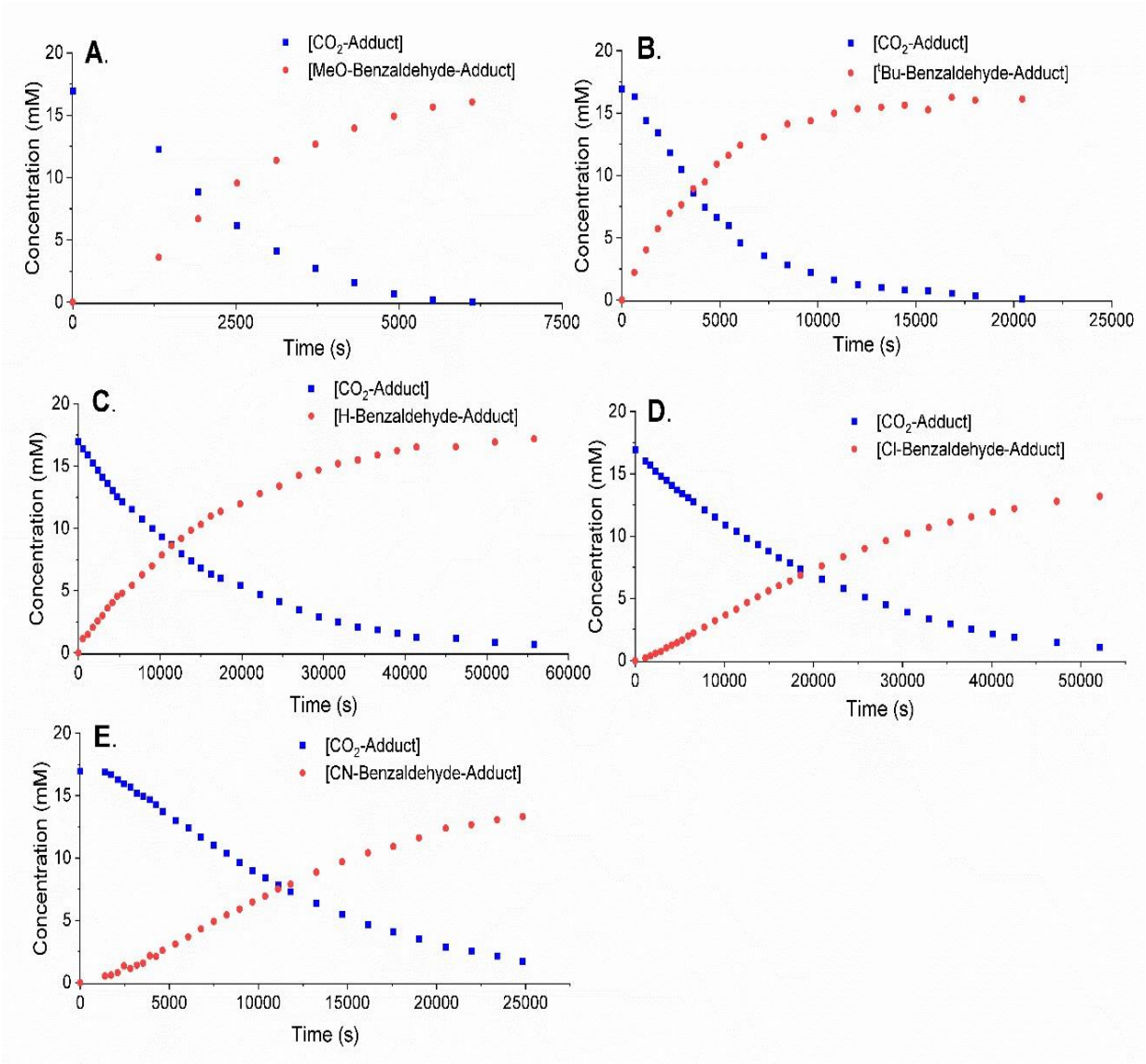

Figure 83. Derivatives aldehydes in pseudo order conditions.

IV. ENDERS CARBENE SYNTHESIS

The Enders Carbene synthesis is divided into three parts, following the main protocol (Figure 84 and Figure 87), as it is detailed in this chapter.

The first part (Figure 84) starts from the amidation process were placed in a round flask, then from 16,5 mL of Benzoyl chloride (20g - 0,142 mol) and 140 mL of Toluene, one equivalent of Aniline was added dropwide to the reaction in a cold bath. Then thionyl chloride is added in excess (4 eq) for the chloro-imidation formation, and 24 hours later, $SOCl_2$ and Toluene are removed by trap by trap at 50C under vacuum. The residue is dissolved in 140mL of THF, 28,79 mL of triethylamine (1,5eq) and 13,86mL (1eq) of phenylhydrazine are added drop by drop. The reaction is left at RT overnight. The reaction is then evaporated trap by trap under vacuum (Figure 85).

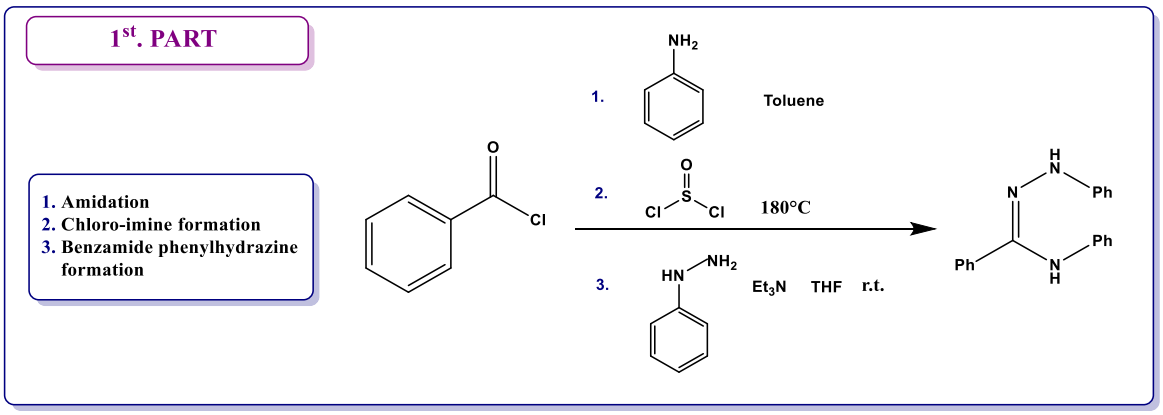

Figure 84. First part of the Enders Carbene reaction.

Figure 85. Evaporation step trap by trap.

A solution of 240 mL of acetic acid at 4% is added to the solid residue and left under the ultrasound at 70°C for the benzamide phenylhydrazine formation. When the solid start to present cracks, it is washed with water (once), methanol (three times), and then filtrated in the Büchner until it is almost white (86). The product is dried for following measurements of weight and yield.

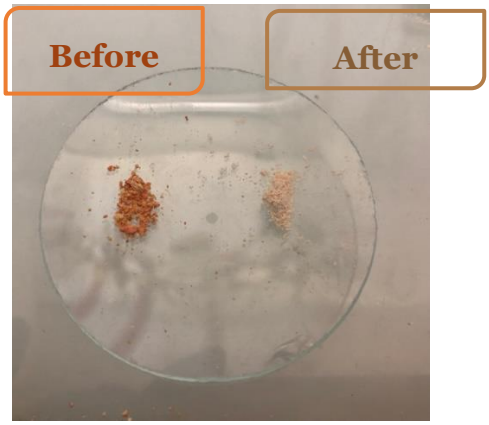

Figure 86. Powder before and after being washed.

For the second part (Figure 87), the process of cyclization, 15 eq of Acetic Anhydride, and 15eq of formic acid are stirred for 20 min. The product obtained previously from the first part is added to the solution using a cold bath to avoid overflowing. The reaction is left at RT under stirring for 48 hours. Then, the acetic acid of the reaction is removed with a rotary evaporator (Figure 88).

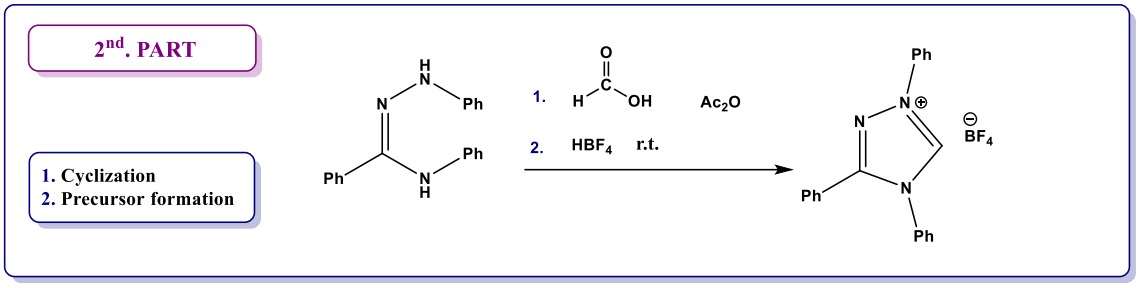

Figure 87. Second part of Enders Carbene reaction.

Figure 88. Acetic acid is being removed with a rotary evaporator.

For the precursor formation, a solution containing 3 eq of HBF_4 + Et_2O and 50 mL of water is poured and stirred for two hours. Then, 100 mL more of water is

added, and the reaction is stirred for an extra 15min. The product is washed with water (once), methanol (three times), and filtrated in the Büchner (Figure 89). The Enders Carbene precursor ECP (product) is dried under vacuum for following weight and yield measurements.

Figure 89. Washing and filtration process with Büchner.

In order to obtain the Ender's Carbene, there are two steps to complete in the third part: the sodium methoxide addition and the thermal alpha elimination (Figure 90). For the first part, a solution is prepared with 1.5 eq of metallic sodium and 110mL of MeOH which are stir until the metallic sodium is dissolved. Meanwhile, in a round flask, the ECP is added with 600 mL of methanol. Once the NaOMe solution is ready, it is poured to the solution with the product and stirred for 2 hours at RT. Then, the

reaction is washed with methanol (three times) and filtrated in the Büchner. The solid is solubilized in methanol and then the solvent is reduced with a rotary evaporator for a crystallization process. The solution is placed at -20°C in the freezer for 24 hours.

In the second step, the crystals are collected and crushed to facilitate methanol alpha-elimination (Figure 91). This process is carried out under vacuum (30 mTorr) at 100°C for 72 hours (Figure 92). After this step, the Ender's carbene is ready, and it should be stored in the glove box.

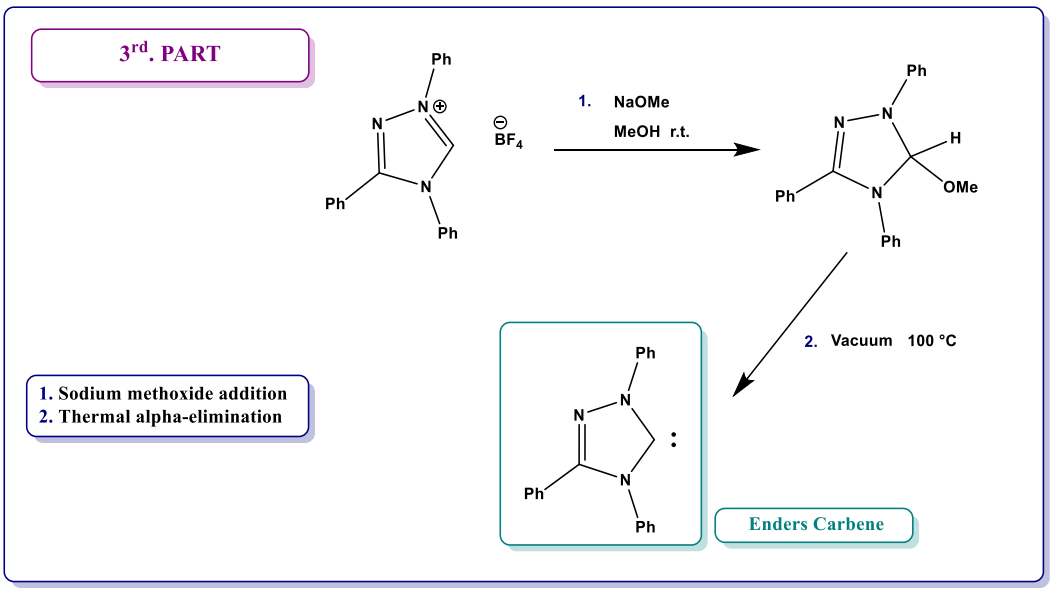

Figure 90. Third part of Enders Carbene reaction.

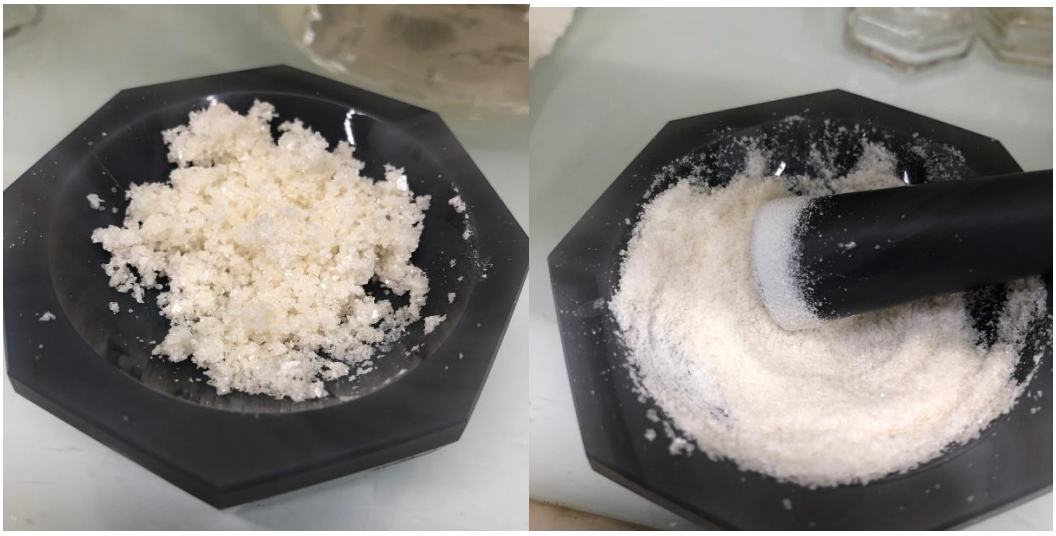

Figure 91. Collected and crushed crystals.

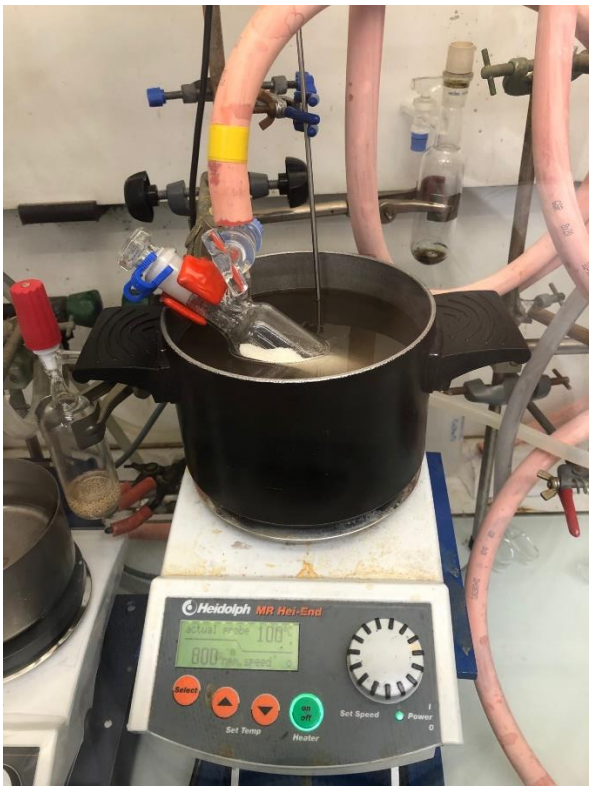

Figure 92. Methanol alpha elimination process under vacuum and 30 mTorr.

REFERENCES

(1) Appel, A. M.; Bercaw, J. E.; Bocarsly, A. B.; Dobbek, H.; DuBois, D. L.; Dupuis, M.; Ferry, J. G.; Fujita, E.; Hille, R.; Kenis, P. J. A.; Kerfeld, C. A.; Morris, R. H.; Peden, C. H. F.; Portis, A. R.; Ragsdale, S. W.; Rauchfuss, T. B.; Reek, J. N. H.; Seefeldt, L. C.; Thauer, R. K.; Waldrop, G. L. Frontiers, Opportunities, and Challenges in Biochemical and Chemical Catalysis of CO 2 Fixation . *Chem. Rev.* **2013**, *113* (8), 6621–6658. https://doi.org/10.1021/cr300463y.

(2) UNFCCC. *Framework Convention on Climate Change Adoption of the Paris Agreement, 21st Conference of the Parties, Paris: United Nations. Official Publication*; 2015.

(3) D'Alessandro, D. M.; Smit, B.; Long, J. R. Carbon Dioxide Capture: Prospects for New Materials. *Angew. Chem. Int. Ed.* **2010**, *49* (35), 6058–6082. https://doi.org/10.1002/anie.201000431.

(4) IPCC. *IPCC Special Report on CCS*; 2011; Vol. 45. https://doi.org/10.1021/es200619j.

(5) Anastas, P.; Warner, J. *12 Principles of Green Chemistry - American Chemical Society*; 1998.

(6) Lapkin, A.; Constable, D. J. C. *Green Chemistry Metrics: Measuring and Monitoring Sustainable Processes*; John Wiley and Sons, 2009. https://doi.org/10.1002/9781444305432.

(7) lei, L. Mini – Review Reaction Mechanism of Hydrogen Activation by Frustrated Lewis Pairs.

(8) Stephan, D. W.; Erker, G. Frustrated Lewis Pair Chemistry: Development and Perspectives. *Angew. Chem. Int. Ed.* **2015**, *54* (22), 6400–6441. https://doi.org/10.1002/anie.201409800.

(9) Béthegnies, A.; Escudié, Y.; Nuñez-Dallos, N.; Vendier, L.; Hurtado, J.; del Rosal, I.; Maron, L.; Bontemps, S. Reductive CO_2 Homocoupling: Synthesis of a Borylated C_3 Carbohydrate. *ChemCatChem* **2018**, *11* (2), cctc.201801875. https://doi.org/10.1002/cctc.201801875.

(10) Stephan, D. W.; Erker, G. Frustrated Lewis Pair Chemistry of Carbon, Nitrogen and Sulfur Oxides. *Chemical Science*. Royal Society of Chemistry June 3, 2014, pp 2625–2641. https://doi.org/10.1039/c4sc00395k.

(11) Chemistry, O. *Jonathan Clayden_ Nick Greeves_ Stuart G Warren-Organic Chemistry-Oxford University Press (2012).Pdf*.

(12) Vollhardt, K. P. C.; Schore, N. E. *Organic Chemistry : Structure and Function*; W.H. Freeman, 2007.

(13) Yurkanis Bruice, P. *Essential Organic Chemistry*; 2016.

(14) Yurkanis Bruice, P. *Organic Chemistry*, Eight.; Pearson, 2015.

(15) Giacometti, G. Hybrid π Orbitals and Partial Double Bond Character in

Covalent Complexes. *J. Chem. Phys.* **1955**, *23* (11), 2068–2073. https://doi.org/10.1063/1.1740667.

(16) Ouellette J., R.; Rawn J., D. *Principles of Organic Chemistry*; Academic Press, 2015.

(17) Brown, W.; Foote, C.; Brent, I.; Eric, A. *Organic Chemistry*, 6th ed.; CEngage Learning, 2011.

(18) Osterheld, K. Bonding and Structure: A Review of Fundamental Chemistry. *J. Chem. Educ.* **1969**. https://doi.org/10.1021/ed046p259.2.

(19) Therien, M. *Reaction Mechanisms, Kinetics, Spectroscopy, Electrochemical and Theoretical ... - Michael J. Therien - Google Books*; University of California, San Diego, 1987.

(20) Brown, T. *Chemistry: The Central Science*, 14th ed.; Pearson: New York, 2018.

(21) Solomons, T. W. G.; Fryhle, C. B.; Snyder, S. A. (Scott A. . *Organic Chemistry*.

(22) Mondal, P.; Kr Hazarika, K.; Ch Deka, R. Paper Reactivity of a,b-Unsaturated Carbonyl Compounds towards Nucleophilic Addition Reaction: A Local Hard-Soft Acid-Base Approach. https://doi.org/10.1039/b301675g.

(23) Biirgi, H. B.; Dunitz, J. D.; Shefter, E. Geometrical Reaction Coordinates. II. Nucleophilic Addition to a Carbonyl Group. *Journal of the American Chemical Society*. American Chemical Society July 1, 1973, pp 5065–5067.

https://doi.org/10.1021/ja00796a058.

(24) Liu, Y. L.; Lin, X. T. Recent Advances in Catalytic Asymmetric Synthesis of Tertiary Alcohols via Nucleophilic Addition to Ketones. *Advanced Synthesis and Catalysis*. Wiley-VCH Verlag March 5, 2019, pp 876–918. https://doi.org/10.1002/adsc.201801023.

(25) Chattaraj, P. K.; Roy, D. R. Update 1 of: Electrophilicity Index. *Chemical Reviews*. American Chemical Society 2007, pp PR46–PR74. https://doi.org/10.1021/cr078014b.

(26) Vollhardt, K. P. C.; Schore, N. E. *Organic Chemistry : Structure and Function*; W.H. Freeman, 2011.

(27) Bruice, P. Y. Organic Chemistry. In *Organic chemistry*; Pearson, 2014; p 1263.

(28) Bell, R. P.; McDougall, A. O. Hydration Equilibria of Some Aldehydes and Ketones. *Trans. Faraday Soc.* **1960**, *56* (0), 1281. https://doi.org/10.1039/tf9605601281.

(29) Lewis, C. A.; Wolfenden, R. Influence of Pressure on the Equilibrium of Hydration of Aliphatic Aldehydes. *J. Am. Chem. Soc.* **1973**, *95* (20), 6685–6688. https://doi.org/10.1021/ja00801a026.

(30) Krow, G. R. The Baeyer-VilligerOxidation of Ketones and Aldehydes. In *Organic Reactions*; John Wiley & Sons, Inc.: Hoboken, NJ, USA, 1993; pp 251–798. https://doi.org/10.1002/0471264180.or043.03.

(31) Tojo, G.; Fernandez, M. *Oxidation of Alcohols to Aldehydes and Ketones: A Guide to Current Common Practice (Basic Reactions in Organic Synthesis)*; Springer US, 2010.

(32) Erker, G.; Stephan, D. W. *Frustrated Lewis Pairs II: Expanding the Scope*; 2013; Vol. 334. https://doi.org/10.1007/978-3-642-37759-4.

(33) Elmer, L.-M.; Kehr, G.; Daniliuc, C. G.; Siedow, M.; Eckert, H.; Tesch, M.; Studer, A.; Williams, K.; Warren, T. H.; Erker, G. The Chemistry of a Non-Interacting Vicinal Frustrated Phosphane/Borane Lewis Pair. *Chem. - Eur. J.* **2017**, *23* (25), 6056–6068. https://doi.org/10.1002/chem.201603954.

(34) Mömming, C. M.; Otten, E.; Kehr, G.; Fröhlich, R.; Grimme, S.; Stephan, D. W.; Erker, G. Reversible Metal-Free Carbon Dioxide Binding by Frustrated Lewis Pairs. *Angew. Chem. Int. Ed.* **2009**, *48* (36), 6643–6646. https://doi.org/10.1002/anie.200901636.

(35) Carey, F. A.; Sundberg, R. J. *Advanced Organic Chemistry Part A: Structure and Mechanisms*; 2007. https://doi.org/10.1021/ed065pA139.2.

(36) Wolf, C. *Dynamic Stereochemistry of Chiral Compounds: Principles and Applications*¤¶; Royal Society of Chemistry, 2008.

(37) Nasipuri, D. *Stereochemistry of Organic Compounds: Principles and Applications*; 2013.

(38) He, Y.; Wang, B.; Dukor, R. K.; Nafie, L. A. Determination of Absolute

Configuration of Chiral Molecules Using Vibrational Optical Activity: A Review. *Appl. Spectrosc.* **2011**, *65* (7), 699–723. https://doi.org/10.1366/11-06321.

(39) Lin, J.; Tsang, C.; Lieu, R.; Zhang, K. Method Screening Strategies of Stereoisomers of Compounds with Multiple Chiral Centers and a Single Chiral Center. *J. Chromatogr. A* **2020**, *1624*. https://doi.org/10.1016/j.chroma.2020.461244.

(40) Clayden, J. Transmission of Stereochemical Information over Nanometre Distances in Chemical Reactions. *Chem. Soc. Rev.* **2009**, *38* (3), 817–829. https://doi.org/10.1039/b801639a.

(41) Kim, Y.; Kim, S. T.; Kang, D.; Sohn, T. I.; Jang, E.; Baik, M. H.; Hong, S. Stereoselective Construction of Sterically Hindered Oxaspirocycles: Via Chiral Bidentate Directing Group-Mediated C(Sp3)-O Bond Formation. *Chem. Sci.* **2018**, *9* (6), 1473–1480. https://doi.org/10.1039/c7sc04691j.

(42) Peng, Q.; Duarte, F.; Paton, R. S. Computing Organic Stereoselectivity-from Concepts to Quantitative Calculations and Predictions. *Chem. Soc. Rev.* **2016**, *45* (22), 6093–6107. https://doi.org/10.1039/c6cs00573j.

(43) Ceballos, B. M.; Yang, J. Y. Highly Selective Electrocatalytic CO2 Reduction by [Pt(Dmpe)2]2+ through Kinetic and Thermodynamic Control. *Organometallics* **2020**, *39* (9), 1491–1496. https://doi.org/10.1021/acs.organomet.9b00720.

(44) Alharis, R. A.; McMullin, C. L.; Davies, D. L.; Singh, K.; Macgregor, S. A. The

Importance of Kinetic and Thermodynamic Control When Assessing Mechanisms of Carboxylate-Assisted C-H Activation. *J. Am. Chem. Soc.* **2019**, *141* (22), 8896–8906. https://doi.org/10.1021/jacs.9b02073.

(45) Enders, D.; Niemeier, O.; Henseler, A. Organocatalysis by N-Heterocyclic Carbenes. *Chemical Reviews*. American Chemical Society December 2007, pp 5606–5655. https://doi.org/10.1021/cr068372z.

(46) Enders, D.; Breuer, K.; Raabe, G.; Runsink, J.; Teles, J. H.; Melder, J. -P; Ebel, K.; Brode, S. Preparation, Structure, and Reactivity of 1,3,4-Triphenyl-4,5-dihydro-1H-1,2,4-triazol-5-ylidene, a New Stable Carbene. *Angew. Chem. Int. Ed.* **1995**, *34* (9), 1021–1023. https://doi.org/10.1002/anie.199510211.

(47) Breslow, R. On the Mechanism of Thiamine Action. IV. Evidence from Studies on Model Systems. *J. Am. Chem. Soc.* **1958**, *80* (14), 3719–3726. https://doi.org/10.1021/ja01547a064.

(48) Stetter, H. Catalyzed Addition of Aldehydes to Activated Double Bonds—A New Synthetic Approach. *Angew. Chem. Int. Ed.* **1976**, *15* (11), 639–647. https://doi.org/10.1002/anie.197606391.

(49) Arduengo, A. J.; Harlow, R. L.; Kline, M. A Stable Crystalline Carbene. *J. Am. Chem. Soc.* **1991**, *113* (1), 361–363. https://doi.org/10.1021/ja00001a054.

(50) Maji, B.; Mayr, H. Structures and Reactivities of O-Methylated Breslow Intermediates. *Angew. Chem. Int. Ed.* **2012**, *51* (41), 10408–10412.

https://doi.org/10.1002/anie.201204524.

(51) Berkessel, A.; Yatham, V. R.; Elfert, S.; Neudörfl, J.-M. Characterization of the Key Intermediates of Carbene-Catalyzed Umpolung by NMR Spectroscopy and X-Ray Diffraction: Breslow Intermediates, Homoenolates, and Azolium Enolates. *Angew. Chem. Int. Ed.* **2013**, *52* (42), 11158–11162. https://doi.org/10.1002/anie.201303107.

(52) Yatham, V. R.; Neudörfl, J. M.; Schlörer, N. E.; Berkessel, A. Carbene Catalyzed Umpolung of α,β-Enals: A Reactivity Study of Diamino Dienols vs. Azolium Enolates, and the Characterization of Advanced Reaction Intermediates. *Chem. Sci.* **2015**, *6* (7), 3706–3711. https://doi.org/10.1039/c5sc01027f.

(53) Lewis, G. N.; Pitzer, K. S. *Valence and the Structure of Atoms and Molecules*; Dover Publications, 1966.

(54) Brown, H. C.; Schlesinger, H. I.; Cardon, S. Z. Studies in Stereochemistry. I. Steric Strains as a Factor in the Relative Stability of Some Coördination Compounds of Boron. *J. Am. Chem. Soc.* **1942**, *64* (2), 325–329. https://doi.org/10.1021/ja01254a031.

(55) Liu, L.; Lukose, B.; Jaque, P.; Ensing, B. Reaction Mechanism of Hydrogen Activation by Frustrated Lewis Pairs. *Green Energy and Environment*. KeAi Publishing Communications Ltd. January 1, 2019, pp 20–28. https://doi.org/10.1016/j.gee.2018.06.001.

(56) Suga, H.; Lshimoto, D.; Higuchi, S.; Ohtsuka, M.; Arikawa, T.; Tsuchida, T.;

Kakehi, A.; Baba, T. Dipole-LUMO/Dipolarophile-HOMO Controlled Asymmetrie Cycloadditions of Carbonyl Ylides Catalyzed by Chiral Lewis Acids. *Org. Lett.* **2007**, *9* (21), 4359–4362. https://doi.org/10.1021/ol701936b.

(57) Dupré, J.; Gaumont, A. C.; Lakhdar, S. Mechanistic Investigations of Reactions of the Frustrated Lewis Pairs (Triarylphosphines/B(C6F5)3) with Michael Acceptors. *Org. Lett.* **2017**, *19* (3), 694–697. https://doi.org/10.1021/acs.orglett.6b03868.

(58) Welch, G. C.; San Juan, R. R.; Masuda, J. D.; Stephan, D. W. Reversible, Metal-Free Hydrogen Activation. *Science (80-.).* **2006**, *314* (5802), 1124–1126. https://doi.org/10.1126/science.1134230.

(59) SciFinder; Chemical Abstracts Service: Columbus, OH; Frustrated Lewis Pairs; Https://Scifinder.Cas.Org (Accessed June 10, 2021). **2021**.

(60) Li, N.; Zhang, W. X. Frustrated Lewis Pairs: Discovery and Overviews in Catalysis. *Chinese Journal of Chemistry*. Shanghai Institute of Organic Chemistry November 1, 2020, pp 1360–1370. https://doi.org/10.1002/cjoc.202000027.

(61) Stephan, D. W.; Erker, G. *Frustrated Lewis Pairs I: Uncovering and Understanding*; 2013; Vol. 332. https://doi.org/10.1007/978-3-642-36697-0.

(62) Stephan, D. W.; Erker, G. Frustrated Lewis Pair Chemistry: Development and Perspectives. *Angew. Chem. Int. Ed.* **2015**, *54* (22), 6400–6441. https://doi.org/10.1002/anie.201409800.

(63) Stephan, D. W. Frustrated Lewis Pairs. *J. Am. Chem. Soc.* **2015**, *137* (32), 10018–10032. https://doi.org/10.1021/jacs.5b06794.

(64) Lam, J.; Szkop, K. M.; Mosaferi, E.; Stephan, D. W. FLP Catalysis: Main Group Hydrogenations of Organic Unsaturated Substrates. *Chem. Soc. Rev.* **2018**. https://doi.org/10.1039/c8cs00277k.

(65) Stephan, D. W. The Broadening Reach of Frustrated Lewis Pair Chemistry. *Science (80-.).* **2016**, *354* (6317). https://doi.org/10.1126/science.aaf7229.

(66) Sapsford, J. S.; Scott, D. J.; Allcock, N. J.; Fuchter, M. J.; Tighe, C. J.; Ashley, A. E. Direct Reductive Amination of Carbonyl Compounds Catalyzed by a Moisture Tolerant Tin(IV) Lewis Acid. *Adv. Synth. Catal.* **2018**, *360* (6), 1066–1071. https://doi.org/10.1002/adsc.201701418.

(67) Mahdi, T.; Stephan, D. W. Facile Protocol for Catalytic Frustrated Lewis Pair Hydrogenation and Reductive Deoxygenation of Ketones and Aldehydes. *Angew. Chem. Int. Ed.* **2015**, *54* (29), 8511–8514. https://doi.org/10.1002/anie.201503087.

(68) Roy, L.; Ghosh, B.; Paul, A. Lewis Acid Promoted Hydrogenation of CO2 and HCOO- by Amine Boranes: Mechanistic Insight from a Computational Approach. *J. Phys. Chem. A* **2017**. https://doi.org/10.1021/acs.jpca.7b03843.

(69) Jupp, A. R.; Stephan, D. W. New Directions for Frustrated Lewis Pair Chemistry. *Trends in Chemistry*. Cell Press April 1, 2019, pp 35–48. https://doi.org/10.1016/j.trechm.2019.01.006.

(70) Liu, L.; Lukose, B. A Free Energy Landscape of the Capture of CO 2 by Frustrated Lewis Pairs. 1–17.

(71) Peuser, I.; Neu, R. C.; Zhao, X.; Ulrich, M.; Schirmer, B.; Tannert, J. A.; Kehr, G.; Fröhlich, R.; Grimme, S.; Erker, G.; Stephan, D. W. CO2 and Formate Complexes of Phosphine/Borane Frustrated Lewis Pairs. *Chem. - Eur. J.* **2011**, *17* (35), 9640–9650. https://doi.org/10.1002/chem.201100286.

(72) Neu, R. C.; Ménard, G.; Stephan, D. W. Exchange Chemistry of TBu3P(CO2)B(C6F5)2Cl. *Dalton Trans.* **2012**, *41* (30), 9016. https://doi.org/10.1039/c2dt30206c.

(73) Ashley, A. E.; Thompson, A. L.; O'Hare, D. Non-Metal-Mediated Homogeneous Hydrogénation of CO2 to CH3OH. *Angew. Chem. Int. Ed.* **2009**, *48* (52), 9839–9843. https://doi.org/10.1002/anie.200905466.

(74) Tran, S. D.; Tronic, T. A.; Kaminsky, W.; Michael Heinekey, D.; Mayer, J. M. Metal-Free Carbon Dioxide Reduction and Acidic C-H Activations Using a Frustrated Lewis Pair. *Inorganica Chim. Acta* **2011**, *369* (1), 126–132. https://doi.org/10.1016/j.ica.2010.12.022.

(75) Sgro, M. J.; Dömer, J.; Stephan, D. W. Stoichiometric CO2 Reductions Using a Bis-Borane-Based Frustrated Lewis Pair. *Chem. Commun.* **2012**, *48* (58), 7253. https://doi.org/10.1039/c2cc33301e.

(76) Ménard, G.; Stephan, D. W. Room Temperature Reduction of CO2 to Methanol by Al-Based Frustrated Lewis Pairs and Ammonia Borane. *J. Am. Chem. Soc.*

2010, *132* (6), 1796–1797. https://doi.org/10.1021/ja9104792.

(77) Ménard, G.; Stephan, D. W. Stoichiometric Reduction of CO2 to CO by Aluminum-Based Frustrated Lewis Pairs. *Angew. Chem. Int. Ed.* **2011**, *50* (36), 8396–8399. https://doi.org/10.1002/anie.201103600.

(78) Mömming, C. M.; Frömel, S.; Kehr, G.; Fröhlich, R.; Grimme, S.; Erker, G. Reactions of an Intramolecular Frustrated Lewis Pair with Unsaturated Substrates: Evidence for a Concerted Olefin Addition Reaction. *J. Am. Chem. Soc.* **2009**, *131* (34), 12280–12289. https://doi.org/10.1021/ja903511s.

(79) Möricke, J.; Wibbeling, B.; Daniliuc, C. G.; Kehr, G.; Erker, G. Design and Reactions of a Carbon Lewis Base/Boron Lewis Acid Frustrated Lewis Pair. *Philos. Trans. R. Soc. A Math. Phys. Eng. Sci.* **2017**, *375* (2101). https://doi.org/10.1098/rsta.2017.0015.

(80) Dureen, M. A.; Stephan, D. W. Reactions of Boron Amidinates with CO2 and CO and Other Small Molecules. *J. Am. Chem. Soc.* **2010**, *132* (38), 13559–13568. https://doi.org/10.1021/ja1064153.

(81) Runyon, J. W.; Steinhof, O.; Dias, H. V. R.; Calabrese, J. C.; Marshall, W. J.; Arduengo, A. J. Carbene-Based Lewis Pairs for Hydrogen Activation. *Aust. J. Chem.* **2011**, *64* (8), 1165–1172. https://doi.org/10.1071/CH11246.

(82) Chase, P. A.; Stephan, D. W. Hydrogen and Amine Activation by a Frustrated Lewis Pair of a Bulky N-Heterocyclic Carbene and B(C_6F_5)$_3$. *Angew. Chem. Int. Ed.* **2008**, *47* (39), 7433–7437. https://doi.org/10.1002/anie.200802596.

(83) Chase, P. A.; Gille, A. L.; Gilbert, T. M.; Stephan, D. W. Frustrated Lewis Pairs Derived from N-Heterocyclic Carbenes and Lewis Acids. *Dalton Trans.* **2009**, *0* (35), 7179. https://doi.org/10.1039/b908737k.

(84) Holschumacher, D.; Bannenberg, T.; Hrib, C. G.; Jones, P. G.; Tamm, M. Heterolytic Dihydrogen Activation by a Frustrated Carbene-Borane Lewis Pair. *Angew. Chem. Int. Ed.* **2008**, *47* (39), 7428–7432. https://doi.org/10.1002/anie.200802705.

(85) Bontemps, S. Boron-Mediated Activation of Carbon Dioxide. *Coord. Chem. Rev.* **2016**, *308*, 117–130. https://doi.org/10.1016/j.ccr.2015.06.003.

(86) Van Ausdall, B. R.; Glass, J. L.; Wiggins, K. M.; Aarif, A. M.; Louie, J. A Systematic Investigation of Factors Influencing the Decarboxylation of Imidazolium Carboxylates. *J. Org. Chem.* **2009**, *74* (20), 7935–7942. https://doi.org/10.1021/jo901791k.

(87) Kolychev, E. L.; Bannenberg, T.; Freytag, M.; Daniliuc, C. G.; Jones, P. G.; Tamm, M. Reactivity of a Frustrated Lewis Pair and Small-Molecule Activation by an Isolable Arduengo Carbene-B{3,5-(CF3)2C6H 3}3 Complex. *Chem. - Eur. J.* **2012**, *18* (52), 16938–16946. https://doi.org/10.1002/chem.201202840.

(88) Roters, S.; Appelt, C.; Westenberg, H.; Hepp, A.; Slootweg, J. C.; Lammertsma, K.; Uhl, W. Dimeric Aluminum-Phosphorus Compounds as Masked Frustrated Lewis Pairs for Small Molecule Activation. *Dalton Trans.* **2012**, *41* (30), 9033–

9045. https://doi.org/10.1039/c2dt30080j.

(89) Stephan, D. W. The Broadening Reach of Frustrated Lewis Pair Chemistry. *Science (80-.).* **2016**, *354* (6317), aaf7229–aaf7229. https://doi.org/10.1126/science.aaf7229.

(90) Maji, B.; Breugst, M.; Mayr, H. N-Heterocyclic Carbenes: Organocatalysts with Moderate Nucleophilicity but Extraordinarily High Lewis Basicity. *Angew. Chem. Int. Ed.* **2011**, *50* (30), 6915–6919. https://doi.org/10.1002/anie.201102435.

(91) Enders, D.; Breuer, K.; Kallfass, U.; Balensiefer, T. Preparation and Application Of1,3,4-Triphenyl-4,5-Dihydro-1 *H* -1,2,4-Triazol-5-Ylidene,A Stable Carbene. *Synthesis (Stuttg).* **2003**, *2003* (08), 1292–1295. https://doi.org/10.1055/s-2003-39409.

(92) Ihde, J. Le Chatelier and Chemical Equilibrium. *Journal of Chemical Education*. Division of Chemical Education 1989, pp 238–239. https://doi.org/10.1021/ed066p238.

(93) Blackmond, D. G. Reaction Progress Kinetic Analysis: A Powerful Methodology for Mechanistic Studies of Complex Catalytic Reactions. *Angew. Chem. Int. Ed.* **2005**, *44* (28), 4302–4320. https://doi.org/10.1002/anie.200462544.

(94) Gurdeep Raj. *Chemical Kinetics*; Krishna Prakashan Media, 2010.

(95) Perrin, C. L. Linear or Nonlinear Least-Squares Analysis of Kinetic Data? *J.*

Chem. Educ. **2017**, *94* (6), 669–672. https://doi.org/10.1021/acs.jchemed.6b00629.

(96) Hansch, C.; Leo, A.; Taft, R. W. A Survey of Hammett Substituent Constants and Resonance and Field Parameters. *Chem. Rev.* **1991**, *91* (2), 165–195. https://doi.org/10.1021/cr00002a004.

1. BENZALDEHYDE ADDUCT

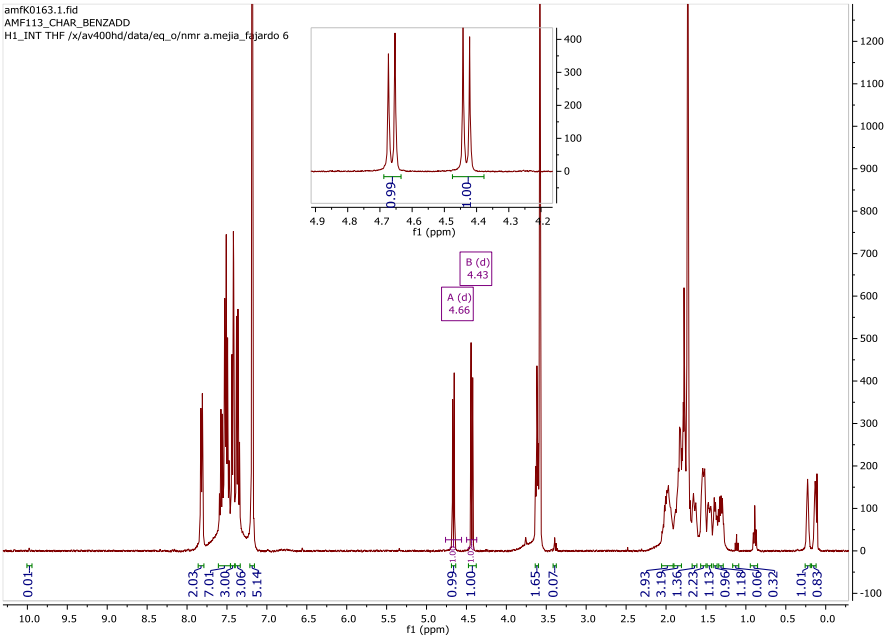

Figure 93. ^{1}H NMR spectrum observed for 3.

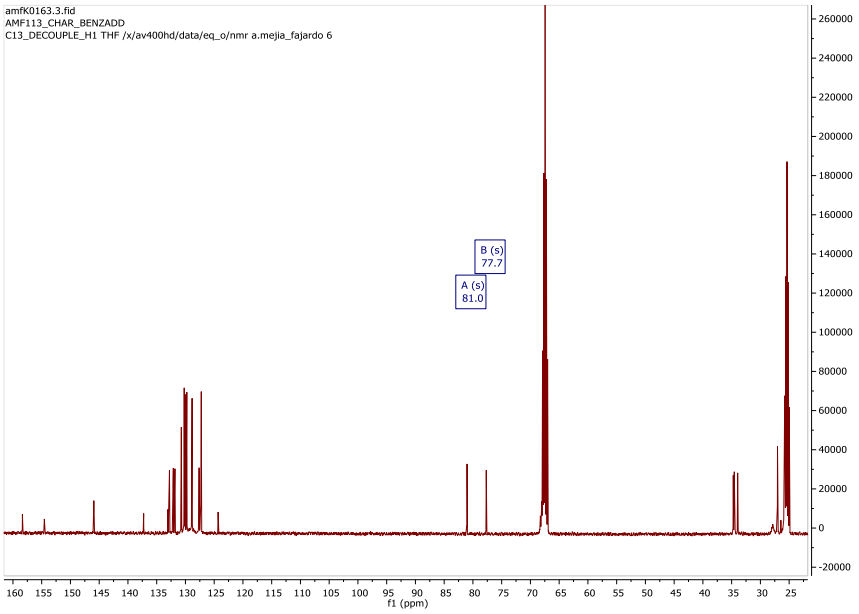

Figure 94. ^{13}C{1H} NMR spectrum observed for 3. Zoom on the 25 to 160 ppm area.

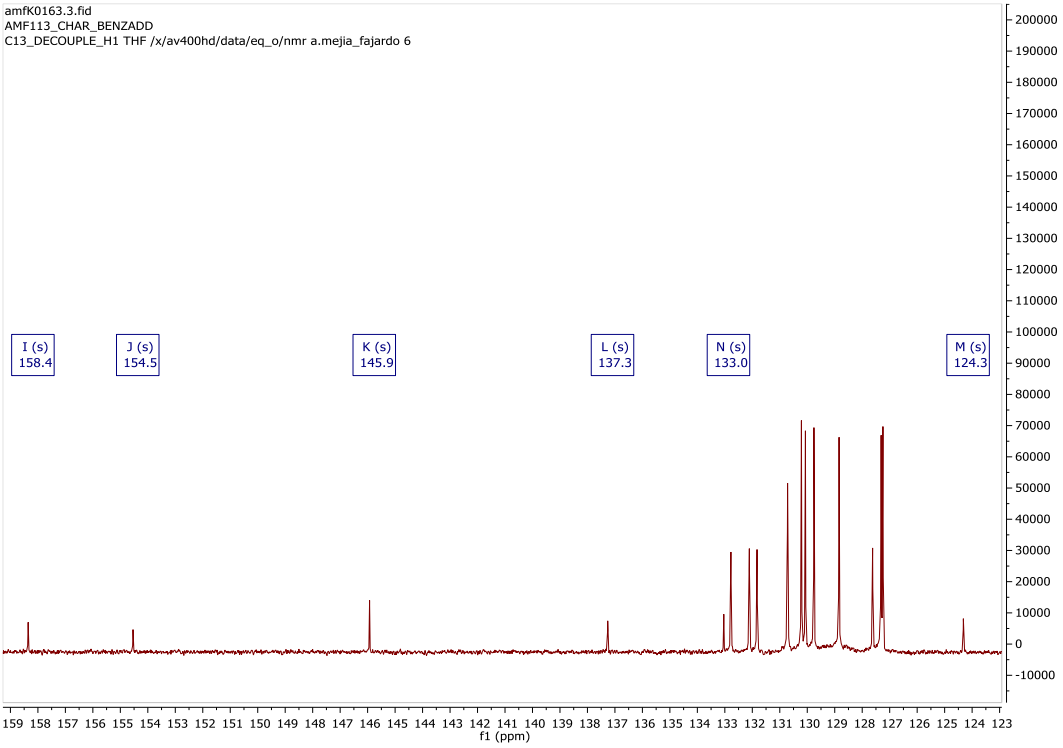

Figure 95. $^{13}C\{^{1}H\}$ NMR spectrum observed for 3. Zoom on the 123 to 159 ppm area.

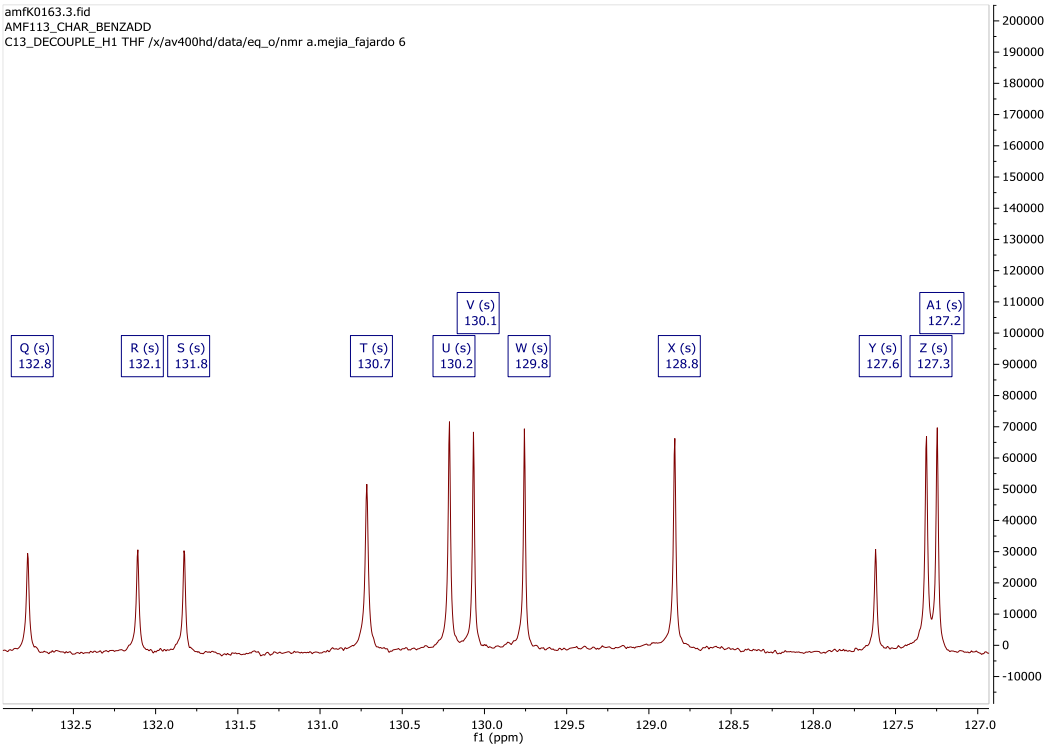

Figure 96. $^{13}C\{^{1}H\}$ NMR spectrum observed for 3. Zoom on the 127 to 133 ppm area.

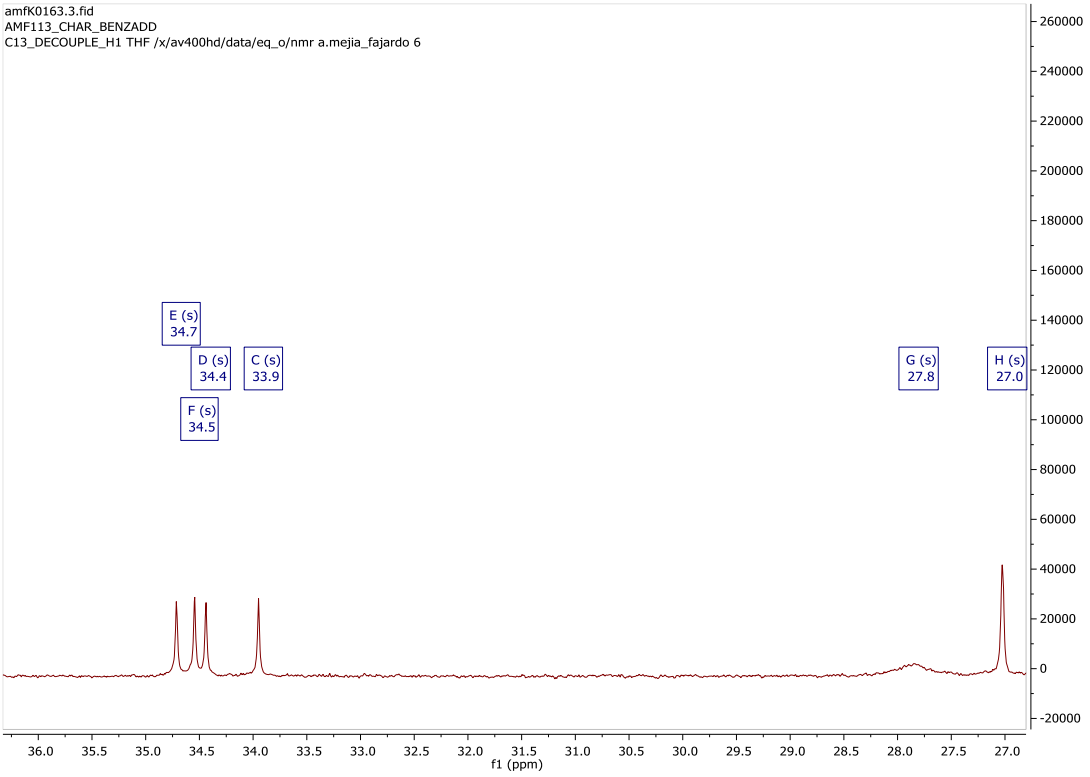

Figure 97. $^{13}C\{^{1}H\}$ NMR spectrum observed for 3. Zoom on the 27 to 36 ppm area.

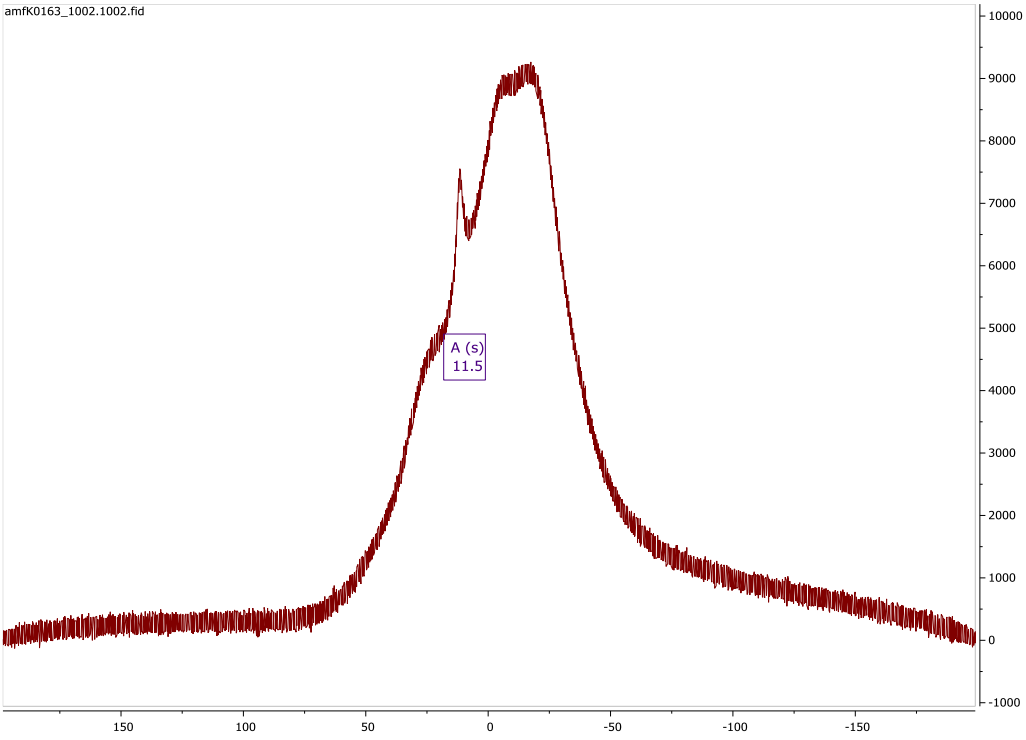

Figure 98. $^{11}B\{^{1}H\}$ NMR spectrum of 3 at 298 K in THF-d8.

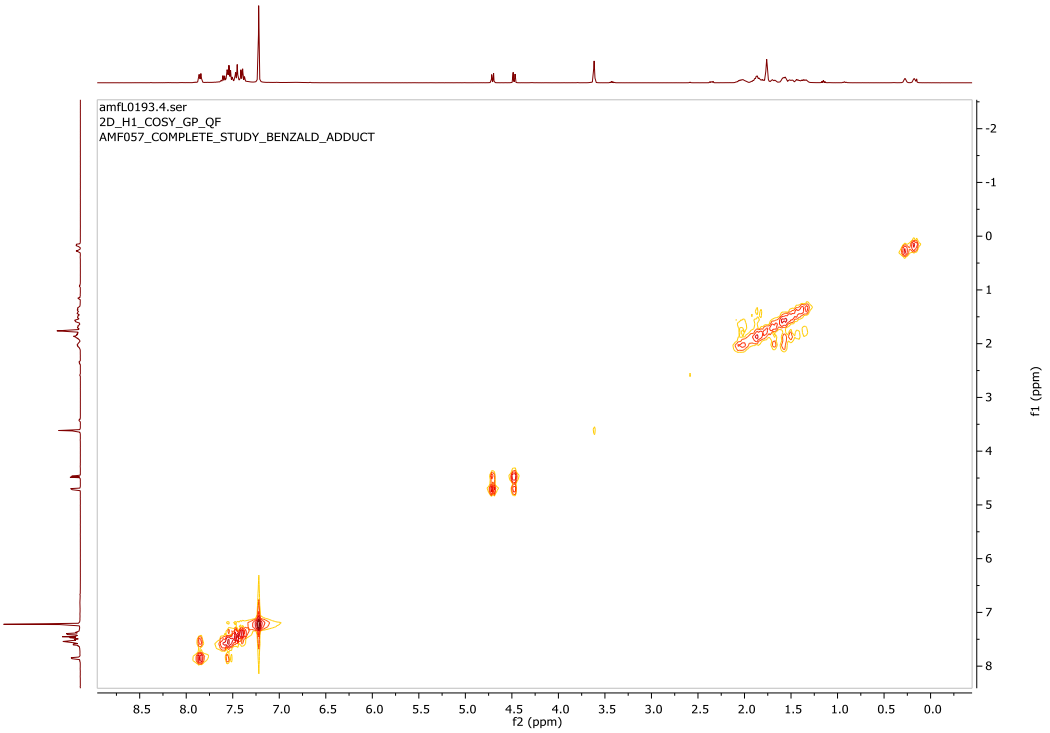

Figure 99. ^{1}H / ^{1}H NMR COSY experiment at 298 K for compound 3 in THF-d8.

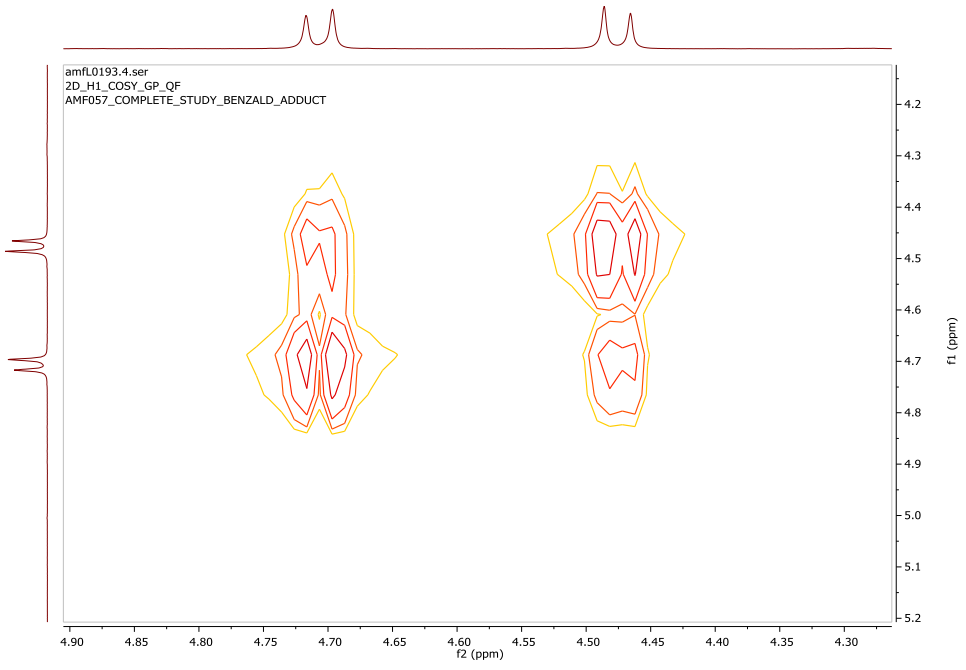

Figure 100. ^{1}H / ^{1}H NMR COSY experiment at 298 K for compound 3 in THF-d8. Zoom on the 4.3 to 4.9 ppm area.

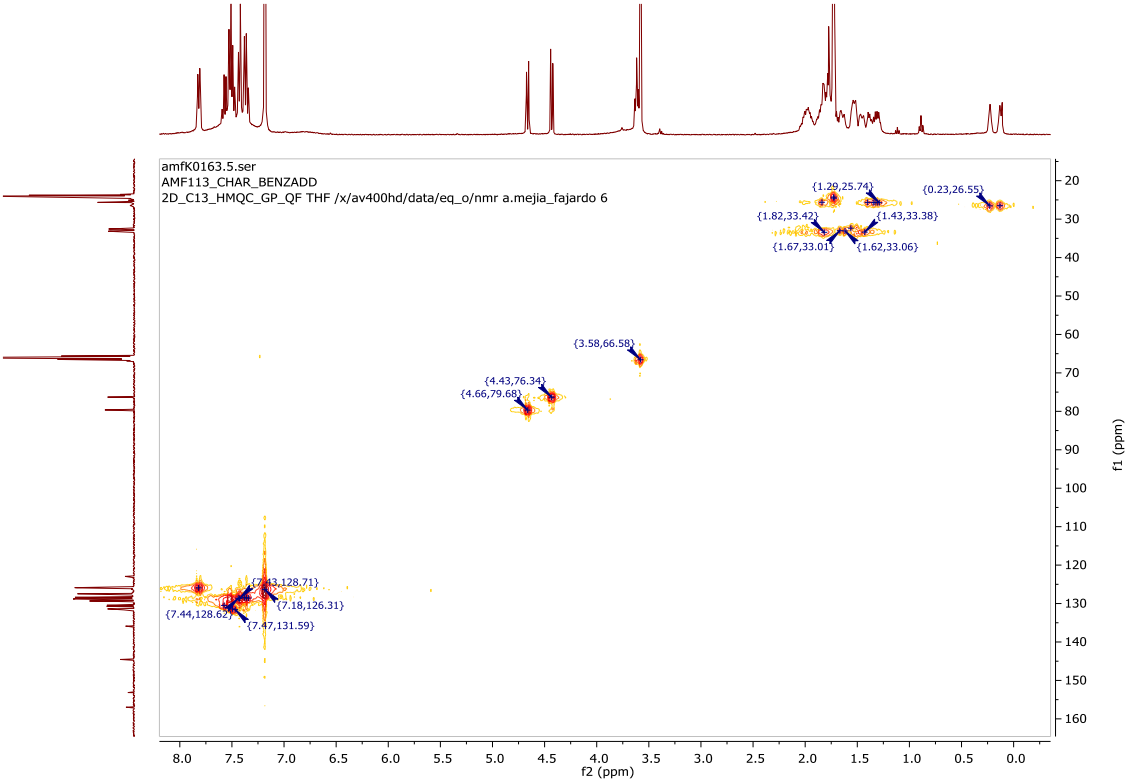

Figure 101. HMQC $^{13}C\{^{1}H\}/^{1}H$ NMR spectrum of 3 at 298 K in THF-d8.

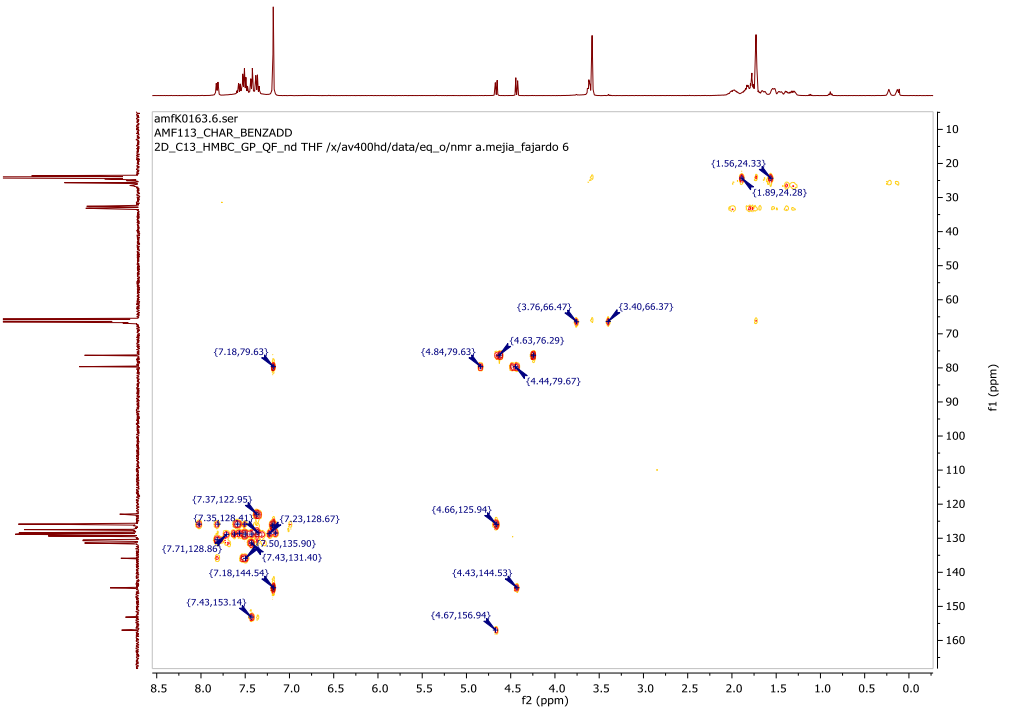

Figure 102. HMBC: long-range $^{13}C\{^{1}H\}/^{1}H$ NMR spectrum for 3 at 298 K in THF-d8

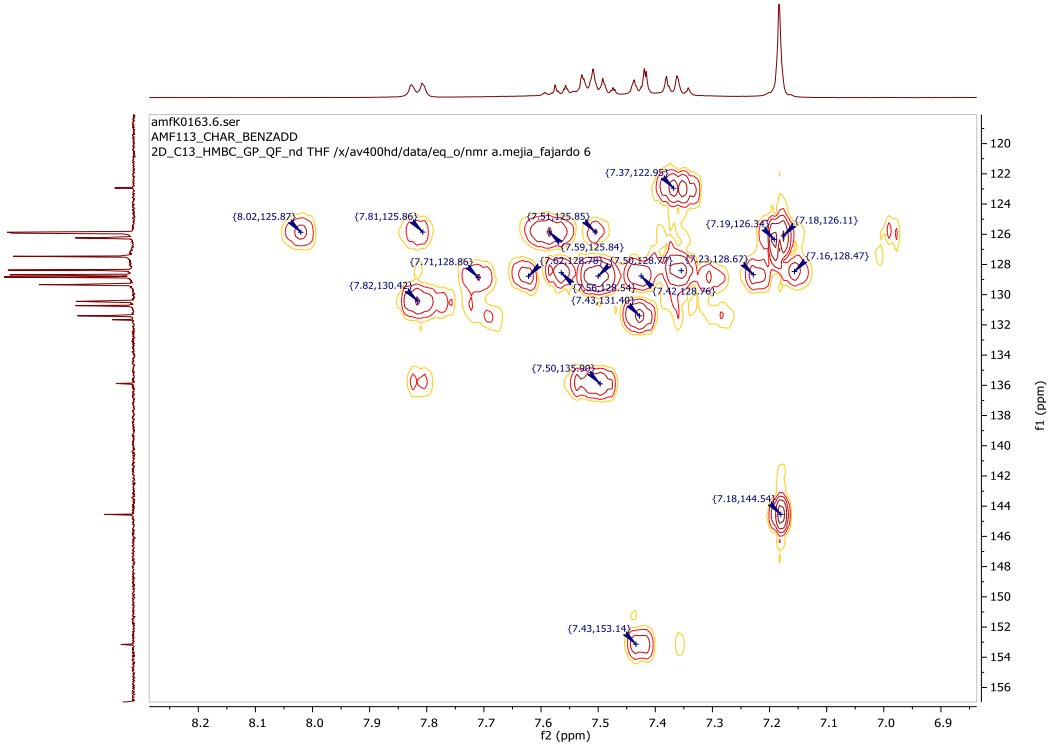

Figure 103. HMBC: long range $^{13}C\{^1H\}/^1H$ NMR spectrum for 3 at 298 K in THF-d8. Zoom on aromatics.

Mass spectra

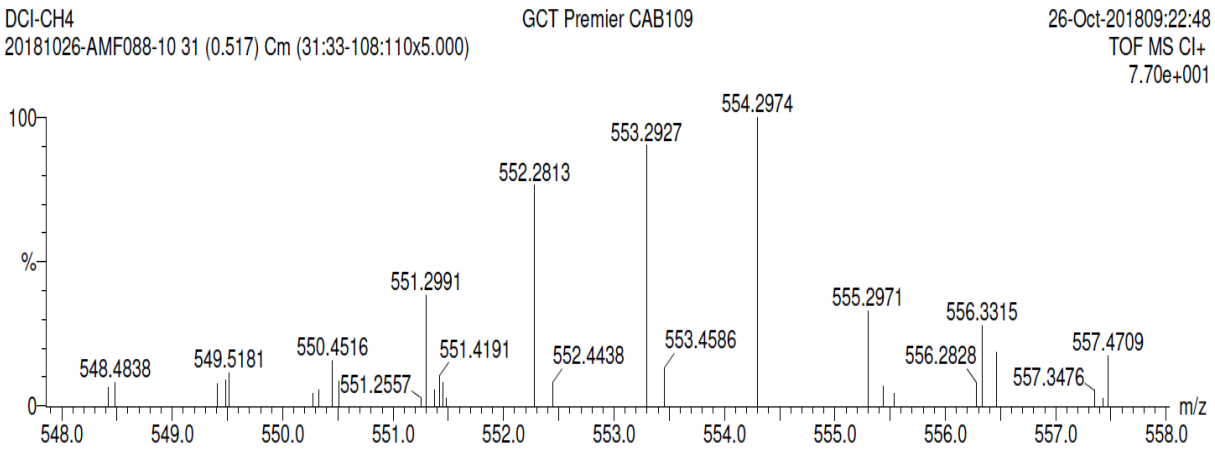

Figure 104. ESI DCI-CH4 mass spectrum for compound 3.

X-ray crystal structure

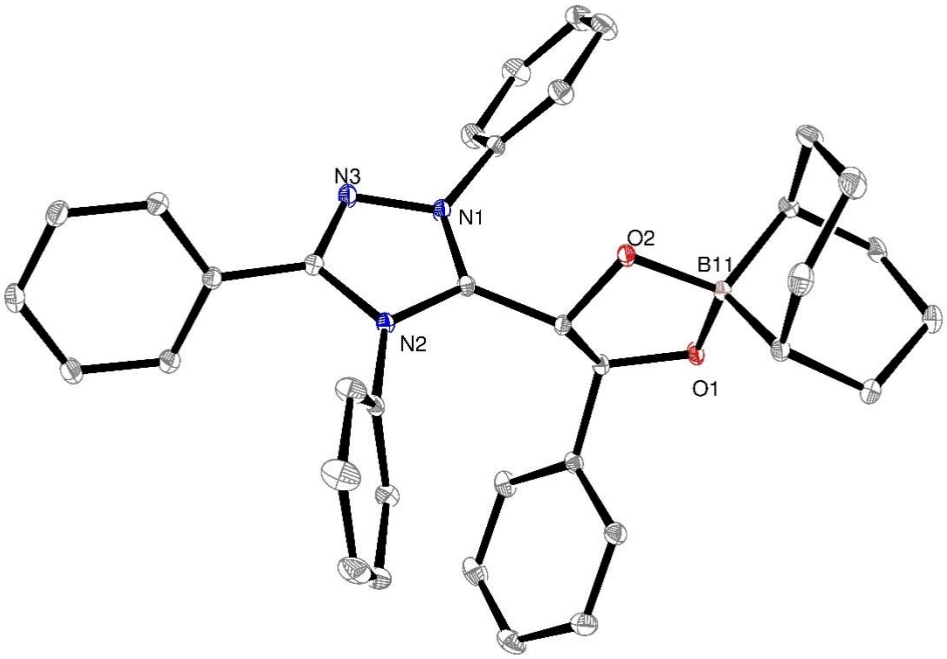

Figure 105. Molecular structure of 3.

General information

$C_{44}H_{52}BN_3O_4$	$F(000)$ = 748
M_r = 697.72	
Triclinic, *P*-1	D_x = 1.166 Mg m^{-3}
Hall symbol: -P 1	
a = 11.7592 (4) Å	Mo $K\alpha$ radiation, λ = 0.71073 Å
b = 12.2491 (5) Å	Cell parameters from 9996 reflections
c = 16.5600 (6) Å	θ = 2–25°
α = 92.091 (1)°	μ = 0.07 mm^{-1}
β = 107.675 (1)°	T = 100 K

γ = 116.744 (1)°	Block, colourless
V = 1987.13 (13) Å^3	0.20 × 0.12 × 0.05 mm
Z = 2	

Refinement

Refinement on F	
Least-squares matrix: full	Hydrogen site location: difference Fourier map
$R[F^2 > 2\sigma(F^2)]$ = 0.060	H-atom parameters not refined
$wR(F^2)$ = 0.062	Method, part 1, Chebychev polynomial, (Watkin, 1994, *P*rince, 1982) [*w*eight] = 1.0/[A_0*T_0(x) + A_1*T_1(x) ⋯ + A_{n-1}]*T_{n-1}(x)] where A_i are the Chebychev coefficients listed below and x = F /Fmax Method = Robust Weighting (*P*rince, 1982) W = [*w*eight] * [1-(delta$F$/6*sigma$F$)^2]^2 A_i are: 0.649 0.853 0.527 0.231 0.731E-01
S = 1.03	$(\Delta/\sigma)_{max}$ = 0.001
8253 reflections	$\Delta\rho_{max}$ = 0.57 e Å^{-3}
469 parameters	$\Delta\rho_{min}$ = −0.63 e Å^{-3}
0 restraints	Extinction correction: None

Geometric parameters (Å, º)

O3—C45	1.434 (2)	C17—H172	0.989
O3—C3	1.420 (2)	C17—C18	1.5441 (19)
O2—C10	1.3840 (15)	C18—H181	0.999
O2—B11	1.5211 (16)	C18—C40	1.536 (2)
O1—B11	1.5149 (17)	C19—H191	1.001
O1—C19	1.3934 (15)	C19—C20	1.5089 (18)

O4—C41	1.403 (3)	C20—C21	1.3945 (18)
O4—C44	1.421 (3)	C20—C25	1.3944 (19)
C1—H11	0.976	C21—H211	0.953
C1—H12	0.996	C21—C22	1.394 (2)
C1—C45	1.514 (3)	C22—H221	0.954
C1—C2	1.480 (5)	C22—C23	1.382 (2)
N2—C8	1.3819 (16)	C23—H231	0.949
N2—C9	1.3477 (16)	C23—C24	1.393 (2)
N2—C26	1.4477 (16)	C24—H241	0.957
N3—N1	1.3763 (15)	C24—C25	1.3879 (19)
N3—C8	1.3058 (17)	C25—H251	0.949
N1—C9	1.3302 (16)	C26—C27	1.3830 (19)
N1—C32	1.4463 (16)	C26—C31	1.3832 (19)
C45—H451	0.989	C27—H271	0.950
C45—H452	0.990	C27—C28	1.3886 (19)
C2—H22	0.994	C28—H281	0.951
C2—H21	0.992	C28—C29	1.383 (2)
C2—C3	1.520 (2)	C29—H291	0.951
C3—H31	0.994	C29—C30	1.389 (2)
C3—H32	0.993	C30—H301	0.946
C4—H41	0.949	C30—C31	1.389 (2)
C4—C5	1.390 (2)	C31—H311	0.953
C4—C38	1.389 (2)	C32—C33	1.3800 (19)
C5—H51	0.953	C32—C37	1.3880 (19)
C5—C6	1.3875 (19)	C33—H331	0.950

C6—H61	0.950	C33—C34	1.391 (2)
C6—C7	1.3921 (19)	C34—H341	0.950
C7—C8	1.4667 (17)	C34—C35	1.381 (2)
C7—C39	1.3987 (18)	C35—H351	0.951
C9—C10	1.4976 (17)	C35—C36	1.388 (2)
C10—H101	1.001	C36—H361	0.952
C10—C19	1.5685 (17)	C36—C37	1.388 (2)
B11—C12	1.6210 (19)	C37—H371	0.948
B11—C18	1.6110 (19)	C38—H381	0.948
C12—H121	1.004	C38—C39	1.3887 (19)
C12—C13	1.5399 (19)	C39—H391	0.952
C12—C16	1.540 (2)	C40—H401	0.989
C13—H131	0.988	C40—H402	0.991
C13—H132	0.990	C41—H411	0.988
C13—C14	1.537 (2)	C41—H412	1.002
C14—H141	0.985	C41—C42	1.482 (5)
C14—H142	0.991	C42—H422	0.999
C14—C17	1.536 (2)	C42—H421	0.988
C15—H152	0.987	C42—C43	1.503 (5)
C15—H151	0.994	C43—H431	0.995
C15—C16	1.534 (2)	C43—H432	1.000
C15—C40	1.541 (2)	C43—C44	1.486 (4)
C16—H161	0.990	C44—H441	0.988
C16—H162	0.997	C44—H442	0.978
C17—H171	0.988		

C45—O3—C3	107.56 (15)	C17—C18—H181	108.3
C10—O2—B11	106.00 (9)	B11—C18—H181	108.3
B11—O1—C19	110.98 (9)	C17—C18—C40	114.07 (12)
C41—O4—C44	109.6 (2)	B11—C18—C40	109.47 (11)
H11—C1—H12	109.2	H181—C18—C40	108.5
H11—C1—C45	110.9	C10—C19—O1	103.34 (10)
H12—C1—C45	109.6	C10—C19—H191	109.9
H11—C1—C2	110.7	O1—C19—H191	109.4
H12—C1—C2	109.6	C10—C19—C20	111.59 (10)
C45—C1—C2	106.87 (19)	O1—C19—C20	112.75 (10)
C8—N2—C9	107.21 (10)	H191—C19—C20	109.7
C8—N2—C26	125.72 (11)	C19—C20—C21	121.33 (12)
C9—N2—C26	126.59 (11)	C19—C20—C25	119.69 (11)
N1—N3—C8	104.41 (10)	C21—C20—C25	118.83 (12)
N3—N1—C9	111.88 (10)	C20—C21—H211	119.4
N3—N1—C32	116.89 (10)	C20—C21—C22	120.40 (14)
C9—N1—C32	131.23 (11)	H211—C21—C22	120.2
C1—C45—O3	106.1 (2)	C21—C22—H221	119.4
C1—C45—H451	110.7	C21—C22—C23	120.22 (13)
O3—C45—H451	110.8	H221—C22—C23	120.4
C1—C45—H452	109.9	C22—C23—H231	120.2
O3—C45—H452	110.6	C22—C23—C24	119.78 (14)
H451—C45—H452	108.8	H231—C23—C24	120.0
C1—C2—H22	111.5	C23—C24—H241	120.1

C1—C2—H21	110.8	C23—C24—C25	119.96 (14)
H22—C2—H21	108.6	H241—C24—C25	119.9
C1—C2—C3	103.88 (19)	C20—C25—C24	120.68 (13)
H22—C2—C3	110.9	C20—C25—H251	119.8
H21—C2—C3	111.2	C24—C25—H251	119.6
C2—C3—O3	105.93 (16)	N2—C26—C27	119.32 (12)
C2—C3—H31	110.7	N2—C26—C31	118.41 (12)
O3—C3—H31	110.5	C27—C26—C31	122.26 (12)
C2—C3—H32	110.9	C26—C27—H271	120.6
O3—C3—H32	110.6	C26—C27—C28	118.71 (13)
H31—C3—H32	108.2	H271—C27—C28	120.6
H41—C4—C5	120.0	C27—C28—H281	119.3
H41—C4—C38	119.6	C27—C28—C29	120.13 (14)
C5—C4—C38	120.40 (13)	H281—C28—C29	120.6
C4—C5—H51	119.9	C28—C29—H291	119.3
C4—C5—C6	120.24 (13)	C28—C29—C30	120.23 (14)
H51—C5—C6	119.9	H291—C29—C30	120.5
C5—C6—H61	120.0	C29—C30—H301	120.0
C5—C6—C7	119.58 (13)	C29—C30—C31	120.40 (14)
H61—C6—C7	120.4	H301—C30—C31	119.5
C6—C7—C8	120.37 (12)	C30—C31—C26	118.26 (14)
C6—C7—C39	120.12 (12)	C30—C31—H311	120.3
C8—C7—C39	119.45 (12)	C26—C31—H311	121.4
C7—C8—N2	125.55 (11)	N1—C32—C33	119.54 (12)
C7—C8—N3	123.79 (11)	N1—C32—C37	117.86 (12)

N2—C8—N3	110.65 (11)	C33—C32—C37	122.37 (12)
N2—C9—N1	105.82 (11)	C32—C33—H331	120.9
N2—C9—C10	125.70 (11)	C32—C33—C34	118.24 (13)
N1—C9—C10	128.48 (11)	H331—C33—C34	120.9
C9—C10—O2	111.05 (10)	C33—C34—H341	119.8
C9—C10—H101	109.3	C33—C34—C35	120.37 (14)
O2—C10—H101	109.4	H341—C34—C35	119.9
C9—C10—C19	112.31 (10)	C34—C35—H351	119.7
O2—C10—C19	105.55 (10)	C34—C35—C36	120.60 (13)
H101—C10—C19	109.1	H351—C35—C36	119.6
O2—B11—O1	102.35 (9)	C35—C36—H361	120.0
O2—B11—C12	111.84 (11)	C35—C36—C37	119.87 (14)
O1—B11—C12	111.76 (11)	H361—C36—C37	120.1
O2—B11—C18	112.00 (10)	C36—C37—C32	118.54 (13)
O1—B11—C18	112.27 (11)	C36—C37—H371	120.6
C12—B11—C18	106.73 (10)	C32—C37—H371	120.8
B11—C12—H121	108.2	C4—C38—H381	119.7
B11—C12—C13	108.32 (11)	C4—C38—C39	119.65 (13)
H121—C12—C13	108.3	H381—C38—C39	120.7
B11—C12—C16	108.87 (11)	C7—C39—C38	119.98 (13)
H121—C12—C16	108.2	C7—C39—H391	120.4
C13—C12—C16	114.79 (11)	C38—C39—H391	119.6
C12—C13—H131	108.3	C15—C40—C18	115.21 (12)
C12—C13—H132	108.3	C15—C40—H401	108.7
H131—C13—H132	107.7	C18—C40—H401	108.5

C12—C13—C14	114.85 (12)	C15—C40—H402	108.3
H131—C13—C14	109.0	C18—C40—H402	108.4
H132—C13—C14	108.5	H401—C40—H402	107.5
C13—C14—H141	109.3	O4—C41—H411	109.5
C13—C14—H142	108.7	O4—C41—H412	109.2
H141—C14—H142	107.9	H411—C41—H412	107.9
C13—C14—C17	114.38 (11)	O4—C41—C42	107.0 (3)
H141—C14—C17	108.4	H411—C41—C42	111.8
H142—C14—C17	108.0	H412—C41—C42	111.5
H152—C15—H151	107.5	C41—C42—H422	111.7
H152—C15—C16	108.5	C41—C42—H421	112.0
H151—C15—C16	108.5	H422—C42—H421	108.3
H152—C15—C40	109.2	C41—C42—C43	105.3 (2)
H151—C15—C40	108.7	H422—C42—C43	109.4
C16—C15—C40	114.29 (12)	H421—C42—C43	110.2
C12—C16—C15	115.15 (13)	C42—C43—H431	113.1
C12—C16—H161	108.6	C42—C43—H432	112.8
C15—C16—H161	109.0	H431—C43—H432	108.2
C12—C16—H162	108.3	C42—C43—C44	101.4 (2)
C15—C16—H162	108.6	H431—C43—C44	111.3
H161—C16—H162	106.9	H432—C43—C44	110.1
C14—C17—H171	108.5	C43—C44—O4	106.7 (2)
C14—C17—H172	108.4	C43—C44—H441	110.8

H171—C17—H172	107.7	O4—C44—H441	109.4
C14—C17—C18	115.25 (12)	C43—C44—H442	111.0
H171—C17—C18	108.4	O4—C44—H442	109.4
H172—C17—C18	108.3	H441—C44—H442	109.5
C17—C18—B11	108.05 (11)		

2. TERTBUTYL BENZALDEHYDE ADDUCT

NMR Spectra

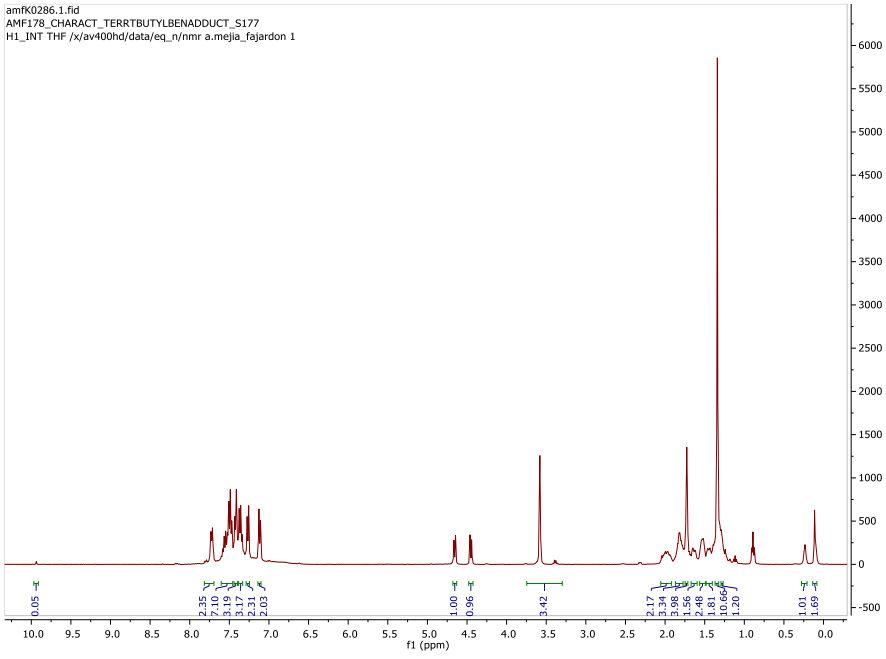

Figure 106. ^{1}H NMR spectrum observed for 5.

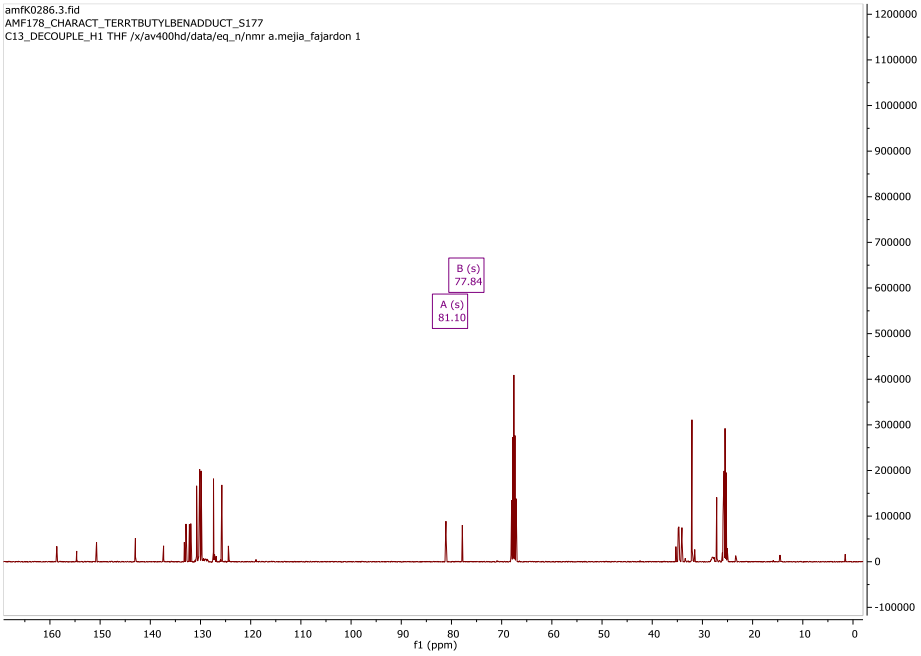

Figure 107. $^{13}C\{^{1}H\}$ NMR spectrum observed for 5. Zoom on the 0 to 160 ppm area.

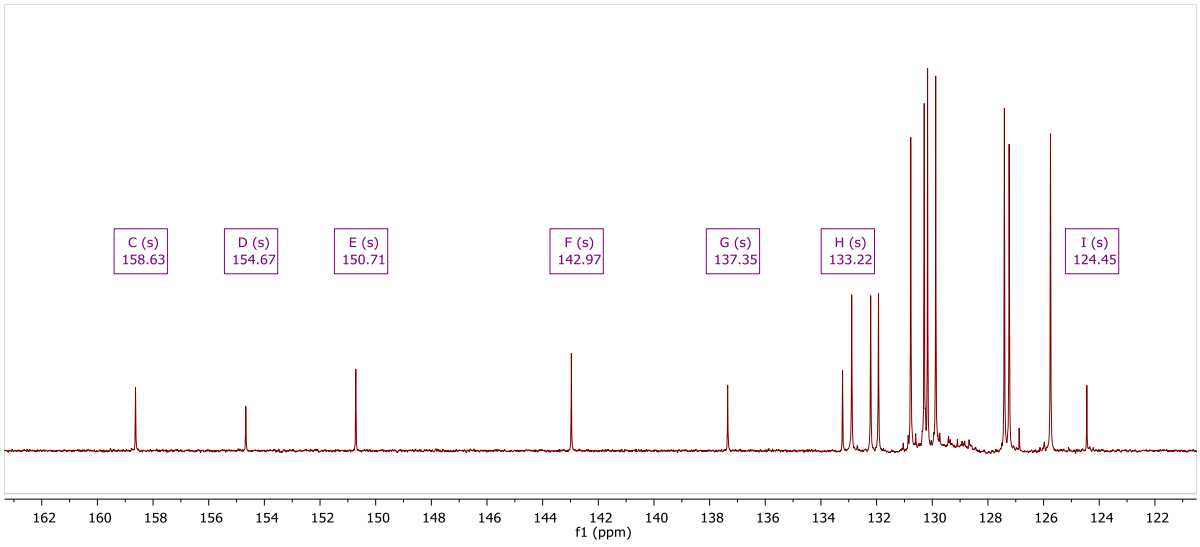

Figure 108. $^{13}C\{^{1}H\}$ NMR spectrum observed for 5. Zoom on the 122 to 162 ppm area.

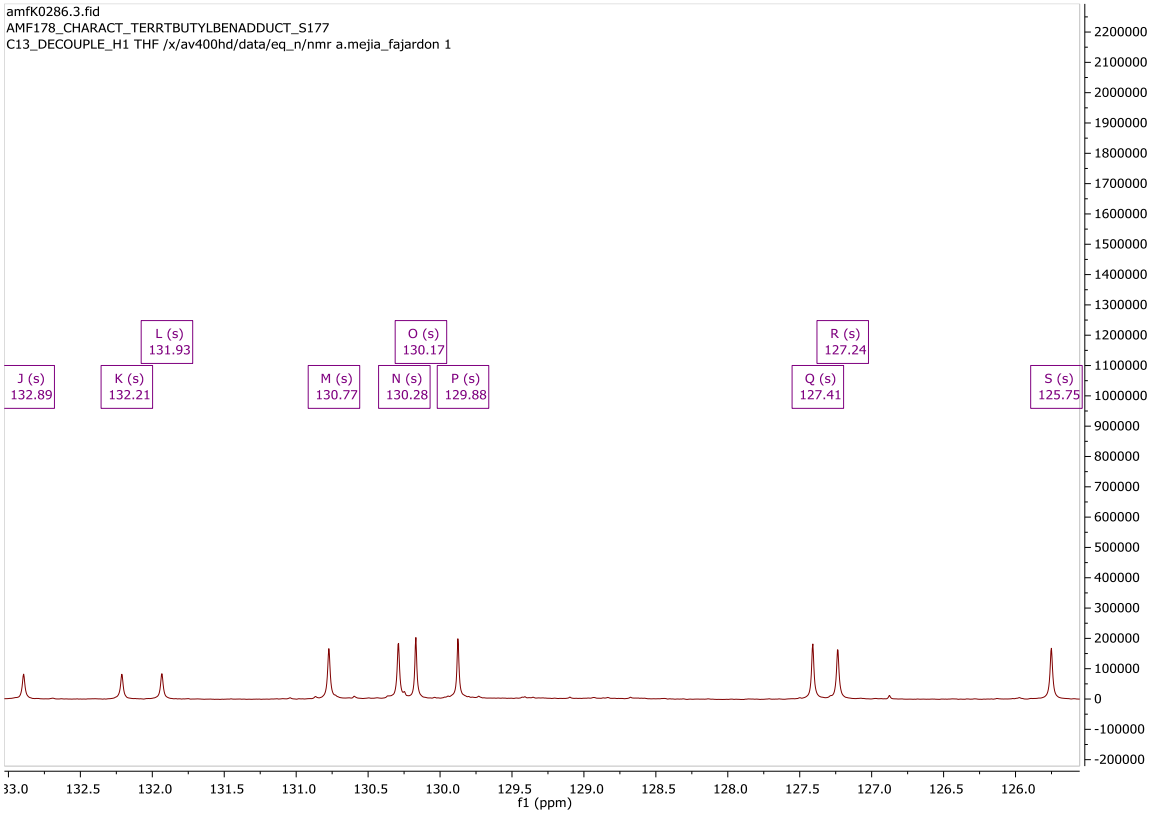

Figure 109. $^{13}C\{^{1}H\}$ NMR spectrum observed for 5. Zoom on the 125 to 133 ppm area.

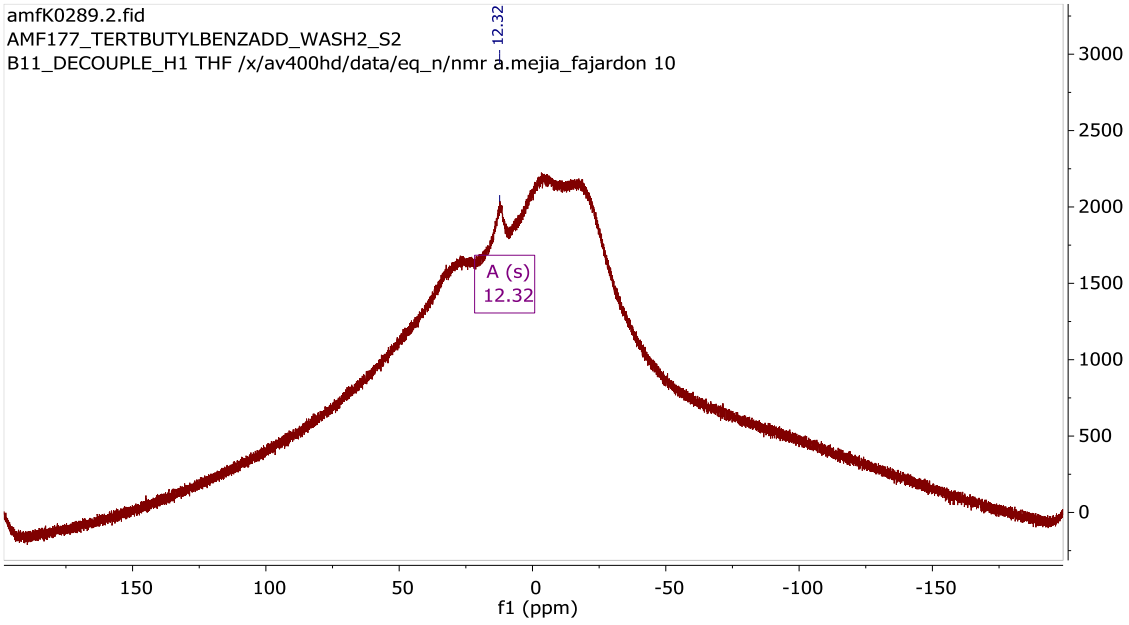

Figure 110. $^{11}B\{^{1}H\}$ NMR spectrum of 5 at 298 K in THF-d8.

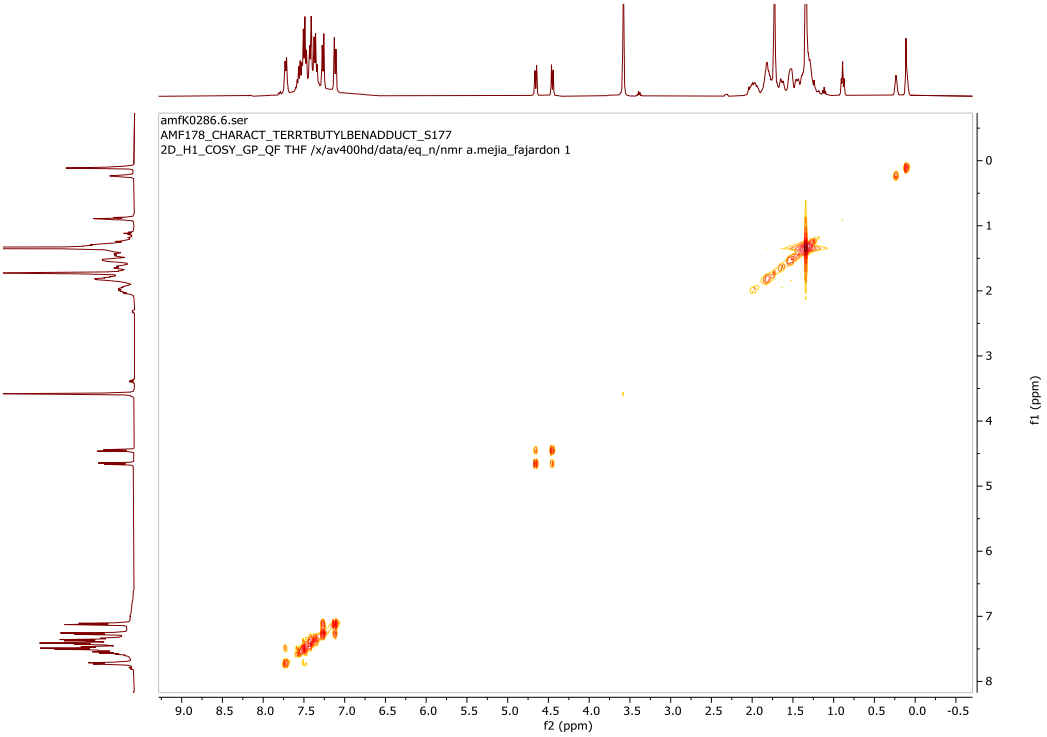

Figure 111. ^{1}H / ^{1}H NMR COSY experiment at 298 K for compound 5 in THF-d8.

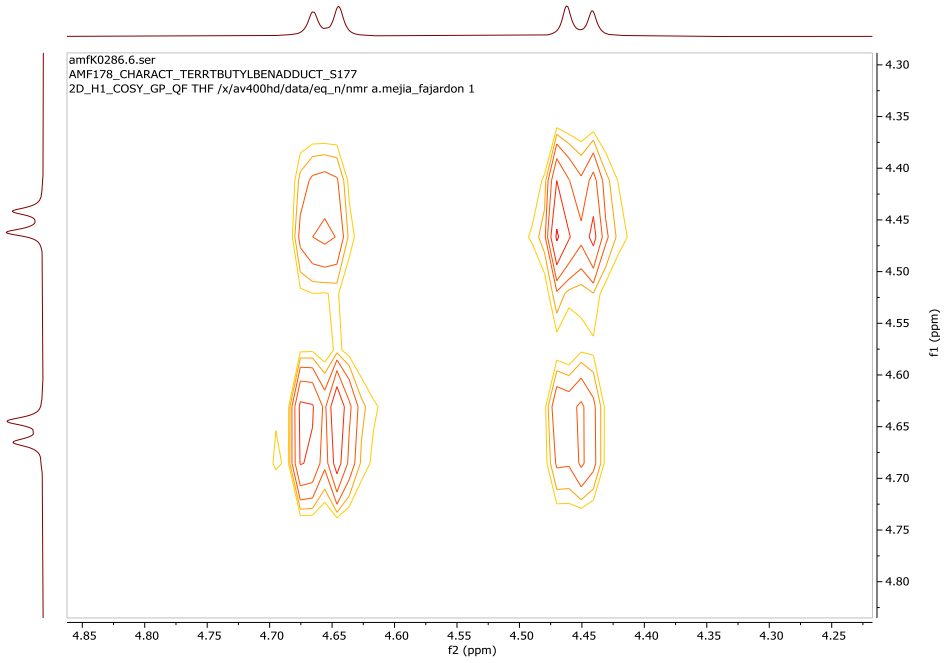

Figure 112. ^{1}H / ^{1}H NMR COSY experiment at 298 K for compound 5 in THF-d8. Zoom on the 4.2 to 4.9 ppm area.

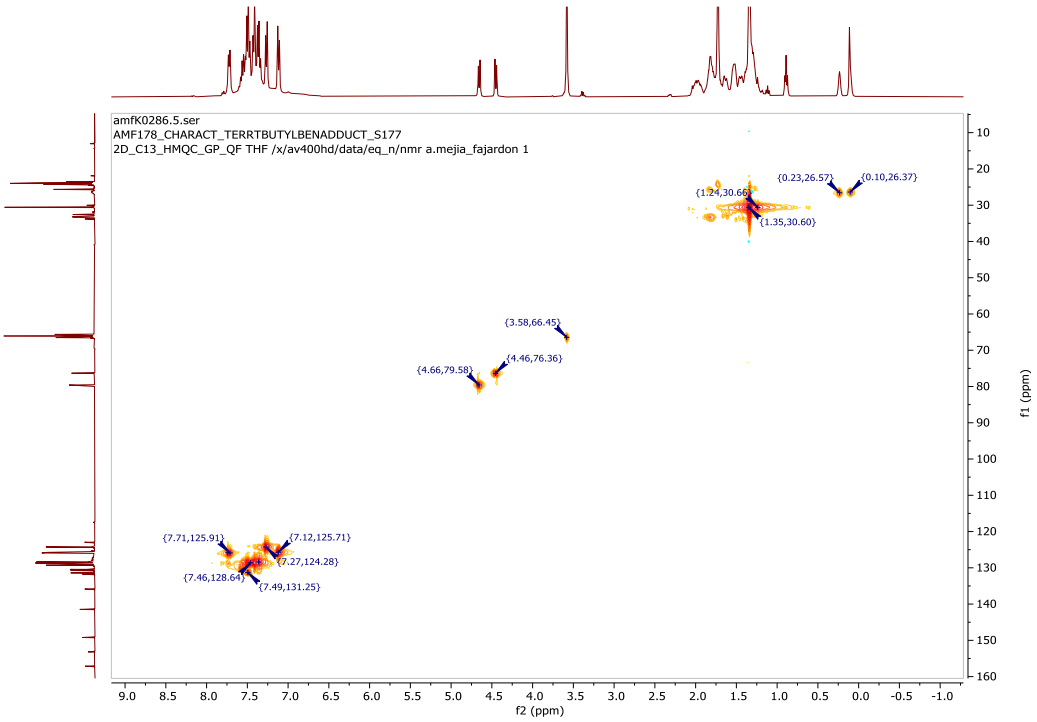

Figure 113. HMQC $^{13}C\{^{1}H\}/^{1}H$ NMR spectrum of 5 at 298 K in THF-d8.

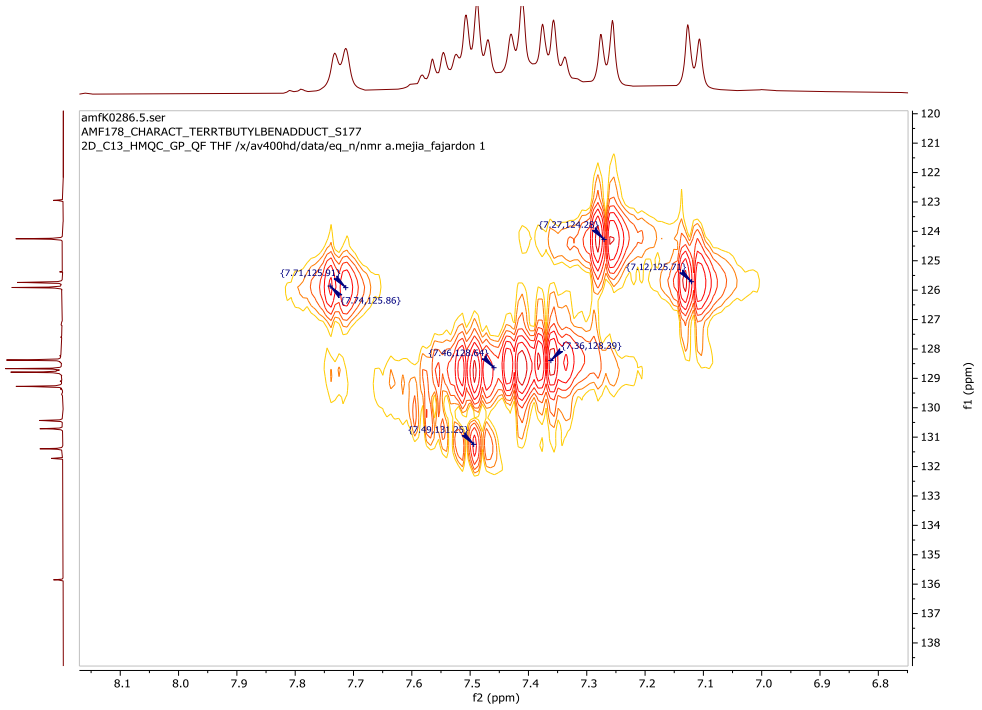

Figure 114. HMQC $^{13}C\{^{1}H\}/^{1}H$ NMR spectrum of 5 at 298 K in THF-d8. Zoom on the aromatic area

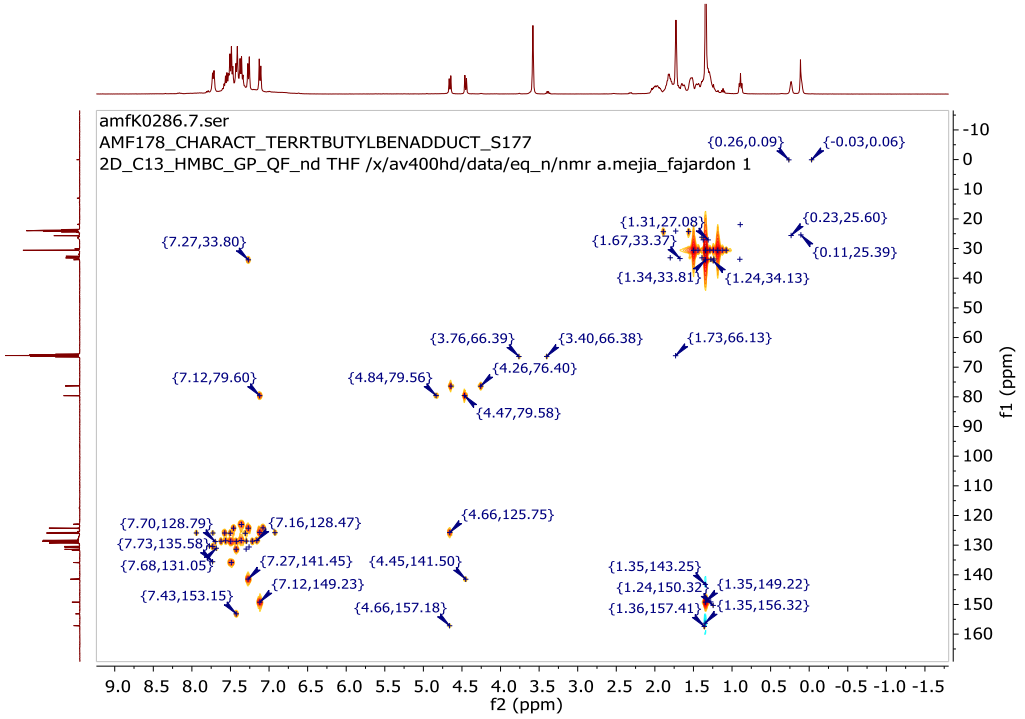

Figure 115. HMBC: long-range $^{13}C\{^{1}H\}/^{1}H$ NMR spectrum for 5 at 298 K in THF-d8.

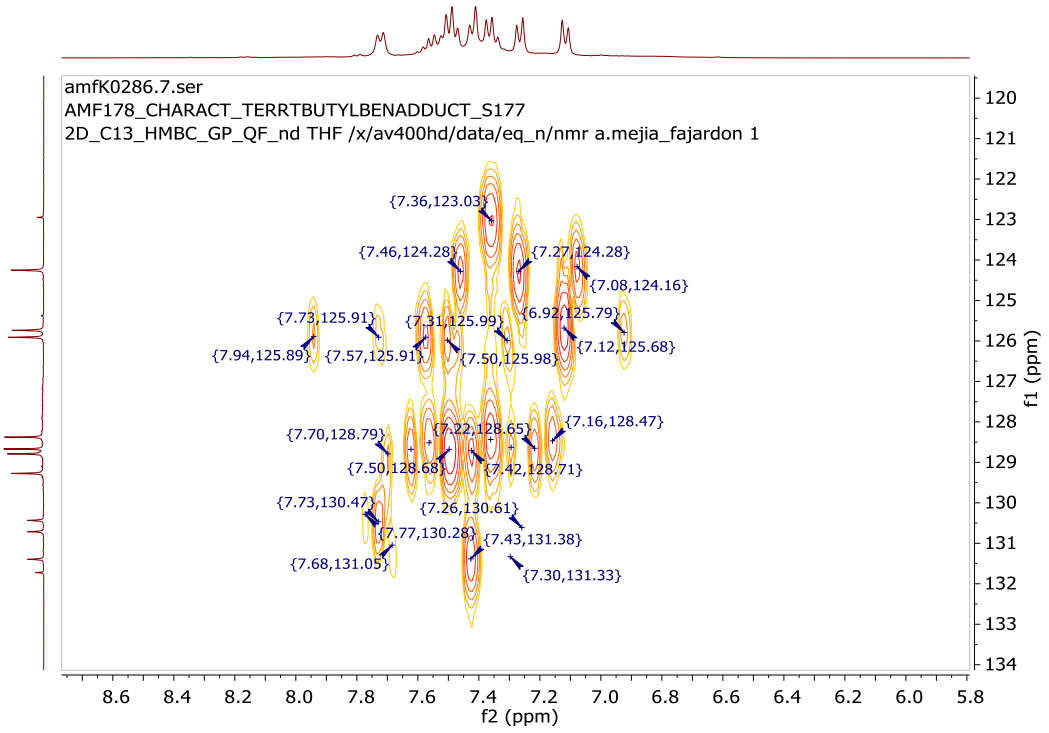

Figure 116. HMBC: long-range $^{13}C\{^{1}H\}/^{1}H$ NMR spectrum for 5 at 298 K in THF-d8. Zoom on aromatics.

Mass Spectra

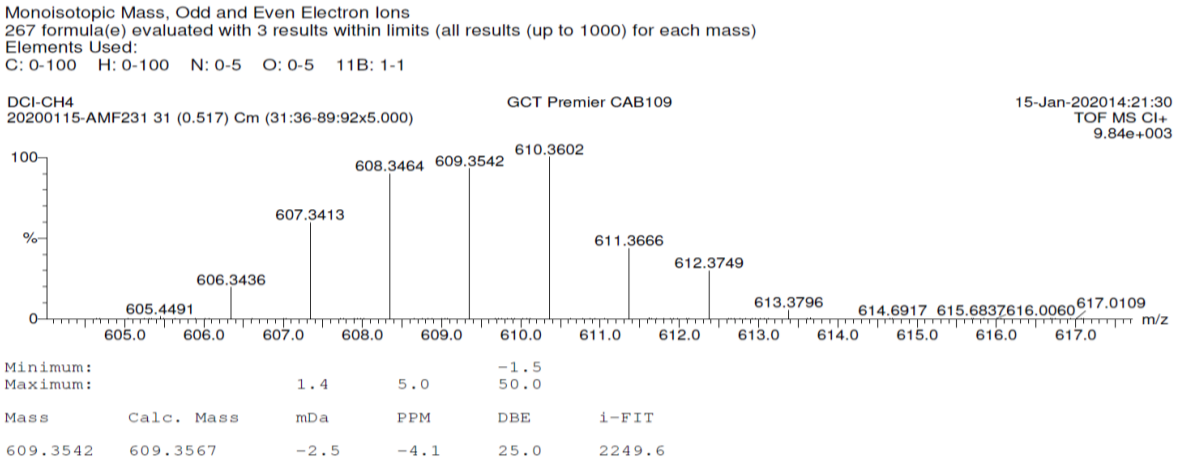

Figure 117. ESI DCI-CH4 mass spectrum for compound 5.

X-ray crystal structure

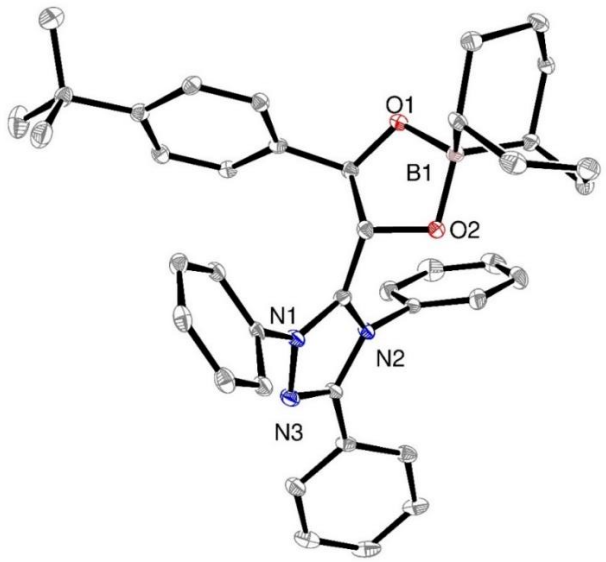

Figure 118. Molecular structure of 5.

General information

Crystal data

$C_{44}H_{52}BN_3O_3$	
M_r = 681.73	D_x = 1.150 Mg m^{-3}
Orthorhombic, *Fdd*2	
Hall symbol: F 2 -2d	Mo *K*α radiation, λ = 0.71073 Å
a = 22.332 (12) Å	Cell parameters from 8259 reflections
b = 67.090 (4) Å	θ = 2–21°
c = 10.411 (6) Å	μ = 0.07 mm^{-1}
V = 15598 (12) Å^3	*T* = 100 K
Z = 16	Needle, colourless
F(000) = 5856	0.12 × 0.03 × 0.02 mm

Refinement

Refinement on F^2	Hydrogen site location: difference Fourier map
Least-squares matrix: full	H-atom parameters not refined
$R[F^2 > 2\sigma(F^2)]$ = 0.063	Method = Modified Sheldrick *w* = $1/[\sigma^2(F^2) + (0.1P)^2 + 28.13P]$, where $P = (\max(F_o^2,0) + 2F_c^2)/3$
$wR(F^2)$ = 0.159	$(\Delta/\sigma)_{max}$ = 0.006
S = 1.02	$\Delta\rho_{max}$ = 0.42 e Å^{-3}
3683 reflections	$\Delta\rho_{min}$ = −0.27 e Å^{-3}
460 parameters	Extinction correction: None
1 restraint	

Geometry parameters (Å, °)

O1—C12	1.398 (5)	C25—C26	1.559 (8)
O1—B1	1.511 (6)	C26—H261	0.992
O2—C13	1.390 (5)	C26—H262	0.987
O2—B1	1.525 (5)	C26—C27	1.522 (7)
N3—N1	1.360 (5)	C27—H27	0.999
N3—C15	1.314 (5)	C27—C28	1.538 (6)
O4—C51	1.430 (7)	C27—B1	1.624 (6)
O4—C52	1.376 (8)	C28—H281	0.989
C5—C11	1.384 (6)	C28—H282	0.990
C5—C12	1.516 (6)	C28—C29	1.529 (6)
C5—C21	1.386 (6)	C29—H291	0.989
N2—C14	1.355 (5)	C29—H292	0.991
N2—C15	1.381 (5)	C29—C30	1.538 (7)
N2—C31	1.453 (5)	C30—H301	0.991
N1—C14	1.327 (5)	C30—H302	0.984
N1—C39	1.450 (5)	C31—C32	1.379 (6)
C8—H81	0.983	C31—C36	1.376 (6)
C8—H82	0.976	C32—H32	0.948
C8—H83	0.979	C32—C33	1.393 (7)
C8—C53	1.523 (8)	C33—H33	0.948
C9—C10	1.401 (6)	C33—C34	1.367 (8)
C9—C22	1.403 (7)	C34—H34	0.944

C9—C53	1.535 (6)	C34—C35	1.389 (8)
C10—H10	0.951	C35—H35	0.950
C10—C11	1.395 (6)	C35—C36	1.378 (7)
C11—H11	0.949	C36—H36	0.952
C12—H12	1.000	C37—H37	0.952
C12—C13	1.561 (6)	C37—C38	1.369 (7)
C13—H13	1.001	C38—H38	0.952
C13—C14	1.495 (6)	C39—C40	1.379 (6)
C15—C16	1.466 (6)	C39—C44	1.389 (6)
C16—C17	1.389 (6)	C40—H40	0.951
C16—C37	1.399 (7)	C40—C41	1.402 (6)
C17—H17	0.947	C41—H41	0.946
C17—C18	1.373 (6)	C41—C42	1.382 (6)
C18—H18	0.952	C42—H42	0.953
C18—C19	1.394 (7)	C42—C43	1.381 (7)
C19—H19	0.953	C43—H43	0.946
C19—C38	1.367 (7)	C43—C44	1.381 (6)
C20—H201	0.982	C44—H44	0.948
C20—H202	0.979	C45—H451	0.980
C20—H203	0.977	C45—H452	0.973
C20—C53	1.530 (7)	C45—H453	0.984
C21—H21	0.950	C45—C53	1.537 (7)
C21—C22	1.380 (6)	C49—H491	0.991

C22—H22	0.950	C49—H492	0.983
C23—H23	0.999	C49—C50	1.511 (18)
C23—C24	1.535 (7)	C49—C52	1.354 (12)
C23—C30	1.549 (6)	C50—H501	0.993
C23—B1	1.607 (6)	C50—H502	0.984
C24—H241	0.990	C50—C51	1.541 (15)
C24—H242	0.990	C51—H511	0.986
C24—C25	1.532 (8)	C51—H512	0.988
C25—H251	0.991	C52—H521	0.986
C25—H252	0.990	C52—H522	0.986
C12—O1—B1	110.8 (3)	C27—C28—H282	108.7
C13—O2—B1	104.4 (3)	H281—C28—H282	107.7
N1—N3—C15	104.7 (3)	C27—C28—C29	114.3 (3)
C51—O4—C52	110.6 (5)	H281—C28—C29	108.7
C11—C5—C12	121.8 (4)	H282—C28—C29	108.5
C11—C5—C21	118.0 (4)	C28—C29—H291	108.9
C12—C5—C21	119.8 (4)	C28—C29—H292	108.7
C14—N2—C15	107.0 (3)	H291—C29—H292	107.6
C14—N2—C31	126.5 (3)	C28—C29—C30	114.4 (4)
C15—N2—C31	126.4 (3)	H291—C29—C30	108.8
N3—N1—C14	112.4 (3)	H292—C29—C30	108.3
N3—N1—C39	118.7 (3)	C29—C30—C23	115.6 (4)

C14—N1—C39	128.3 (3)	C29—C30—H301	108.1
H81—C8—H82	109.6	C23—C30—H301	108.1
H81—C8—H83	109.4	C29—C30—H302	108.6
H82—C8—H83	109.9	C23—C30—H302	108.4
H81—C8—C53	109.1	H301—C30—H302	107.8
H82—C8—C53	109.4	N2—C31—C32	118.2 (4)
H83—C8—C53	109.4	N2—C31—C36	119.8 (4)
C10—C9—C22	117.1 (4)	C32—C31—C36	122.0 (4)
C10—C9—C53	123.1 (4)	C31—C32—H32	120.9
C22—C9—C53	119.8 (4)	C31—C32—C33	118.2 (4)
C9—C10—H10	119.5	H32—C32—C33	120.9
C9—C10—C11	121.0 (4)	C32—C33—H33	119.2
H10—C10—C11	119.5	C32—C33—C34	120.8 (5)
C10—C11—C5	121.1 (4)	H33—C33—C34	120.0
C10—C11—H11	119.3	C33—C34—H34	120.1
C5—C11—H11	119.5	C33—C34—C35	119.8 (4)
C5—C12—O1	114.0 (3)	H34—C34—C35	120.1
C5—C12—H12	109.9	C34—C35—H35	119.7
O1—C12—H12	110.0	C34—C35—C36	120.5 (5)
C5—C12—C13	110.2 (3)	H35—C35—C36	119.8
O1—C12—C13	102.5 (3)	C35—C36—C31	118.7 (4)
H12—C12—C13	110.0	C35—C36—H36	120.6
C12—C13—O2	105.3 (3)	C31—C36—H36	120.7

C12—C13—H13	108.7	C16—C37—H37	120.0
O2—C13—H13	109.0	C16—C37—C38	119.8 (4)
C12—C13—C14	115.0 (4)	H37—C37—C38	120.3
O2—C13—C14	109.9 (3)	C37—C38—C19	120.9 (5)
H13—C13—C14	108.8	C37—C38—H38	119.6
C13—C14—N2	127.7 (4)	C19—C38—H38	119.6
C13—C14—N1	126.6 (4)	N1—C39—C40	120.2 (4)
N2—C14—N1	105.7 (3)	N1—C39—C44	117.3 (4)
N2—C15—N3	110.2 (3)	C40—C39—C44	122.6 (4)
N2—C15—C16	127.5 (4)	C39—C40—H40	121.2
N3—C15—C16	122.1 (4)	C39—C40—C41	117.8 (4)
C15—C16—C17	122.9 (4)	H40—C40—C41	120.9
C15—C16—C37	117.6 (4)	C40—C41—H41	119.8
C17—C16—C37	119.2 (4)	C40—C41—C42	120.4 (4)
C16—C17—H17	119.9	H41—C41—C42	119.8
C16—C17—C18	120.3 (4)	C41—C42—H42	120.0
H17—C17—C18	119.8	C41—C42—C43	120.2 (4)
C17—C18—H18	119.9	H42—C42—C43	119.8
C17—C18—C19	119.7 (4)	C42—C43—H43	119.7
H18—C18—C19	120.3	C42—C43—C44	120.7 (4)
C18—C19—H19	119.9	H43—C43—C44	119.6
C18—C19—C38	120.0 (4)	C39—C44—C43	118.3 (4)
H19—C19—C38	120.1	C39—C44—H44	120.8

H201—C20—H202	109.4	C43—C44—H44	120.9
H201—C20—H203	109.5	H451—C45—H452	110.0
H202—C20—H203	109.8	H451—C45—H453	109.2
H201—C20—C53	109.2	H452—C45—H453	109.7
H202—C20—C53	109.4	H451—C45—C53	109.3
H203—C20—C53	109.6	H452—C45—C53	109.7
C5—C21—H21	119.3	H453—C45—C53	108.9
C5—C21—C22	121.6 (4)	H491—C49—H492	109.4
H21—C21—C22	119.0	H491—C49—C50	110.5
C9—C22—C21	121.1 (4)	H492—C49—C50	110.6
C9—C22—H22	119.5	H491—C49—C52	110.5
C21—C22—H22	119.4	H492—C49—C52	111.0
H23—C23—C24	108.1	C50—C49—C52	104.8 (9)
H23—C23—C30	108.0	C49—C50—H501	110.6
C24—C23—C30	113.5 (4)	C49—C50—H502	110.9
H23—C23—B1	108.3	H501—C50—H502	109.0
C24—C23—B1	109.8 (4)	C49—C50—C51	106.1 (7)
C30—C23—B1	109.1 (3)	H501—C50—C51	109.9
C23—C24—H241	108.7	H502—C50—C51	110.5
C23—C24—H242	108.8	C50—C51—O4	100.8 (7)

H241—C24—H242	107.7	C50—C51—H511	111.5
C23—C24—C25	114.1 (4)	O4—C51—H511	111.4
H241—C24—C25	108.7	C50—C51—H512	111.7
H242—C24—C25	108.8	O4—C51—H512	111.4
C24—C25—H251	108.4	H511—C51—H512	109.8
C24—C25—H252	108.4	O4—C52—C49	113.1 (7)
H251—C25—H252	107.5	O4—C52—H521	108.9
C24—C25—C26	115.2 (4)	C49—C52—H521	108.5
H251—C25—C26	108.5	O4—C52—H522	109.0
H252—C25—C26	108.6	C49—C52—H522	108.9
C25—C26—H261	108.6	H521—C52—H522	108.3
C25—C26—H262	108.9	C45—C53—C9	111.0 (4)
H261—C26—H262	107.6	C45—C53—C20	108.7 (4)
C25—C26—C27	114.9 (4)	C9—C53—C20	107.7 (4)
H261—C26—C27	108.2	C45—C53—C8	108.9 (4)
H262—C26—C27	108.4	C9—C53—C8	112.2 (4)
C26—C27—H27	107.9	C20—C53—C8	108.1 (4)
C26—C27—C28	114.3 (4)	C27—B1—C23	106.0 (4)
H27—C27—C28	107.9	C27—B1—O2	111.5 (3)
C26—C27—B1	110.1 (4)	C23—B1—O2	110.7 (3)
H27—C27—B1	107.9	C27—B1—O1	111.9 (3)

C28—C27—B1	108.5 (3)	C23—B1—O1	114.6 (3)
C27—C28—H281	108.7	O2—B1—O1	102.4 (3)

3. ANISALDEHYDE ADDUCT

NMR Spectra

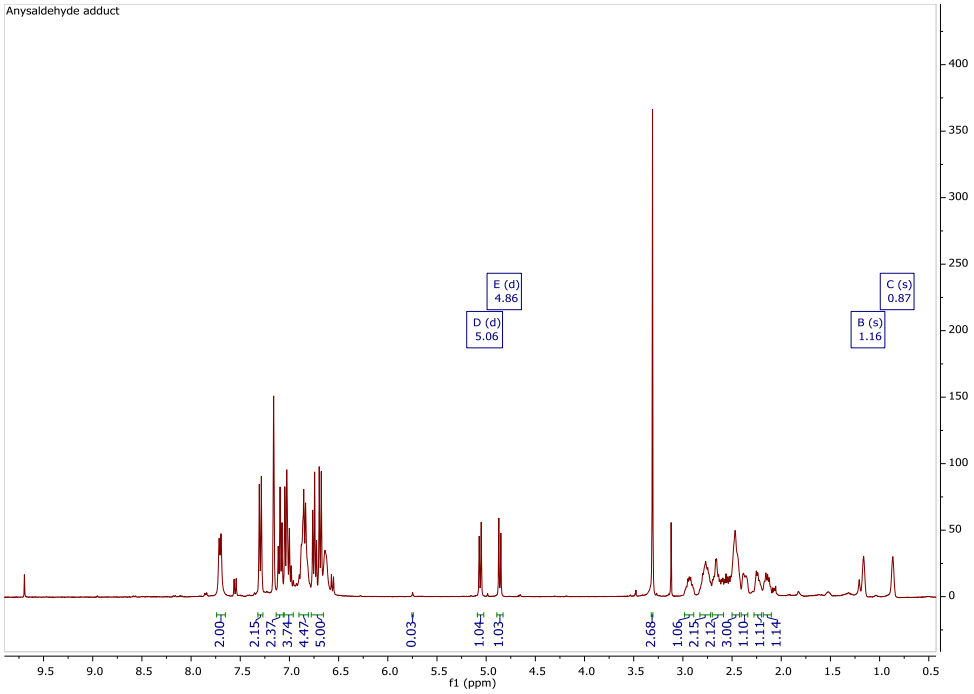

Figure 119. ^{1}H NMR spectrum observed for 7.

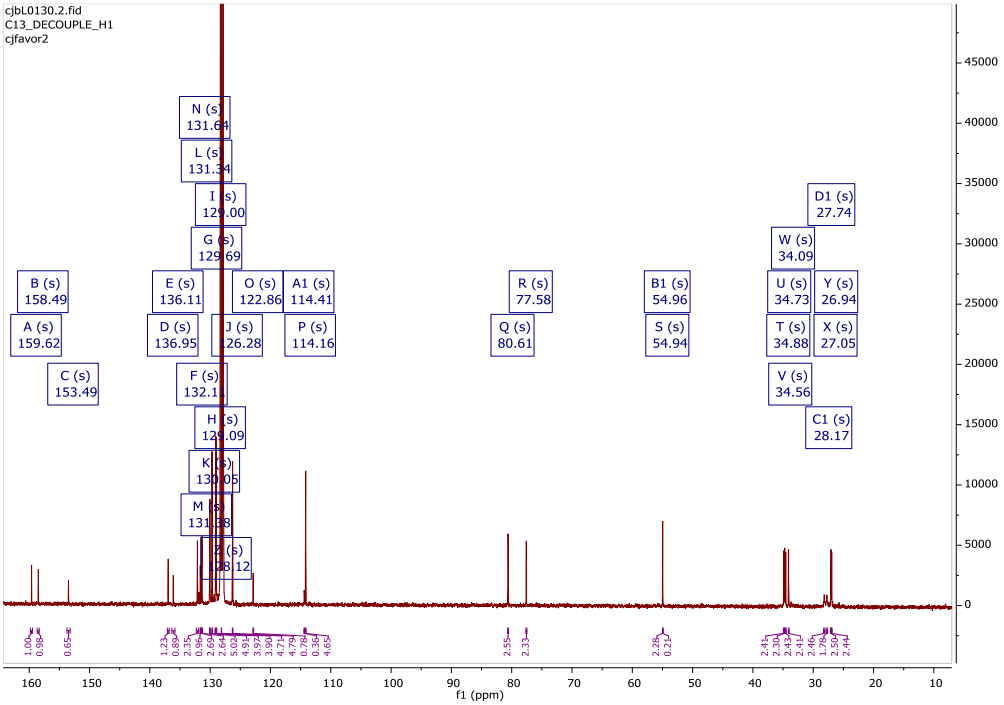

Figure 120. $^{13}C\{^{1}H\}$ NMR spectrum observed for 7. Zoom on the 0 to 160 ppm area.

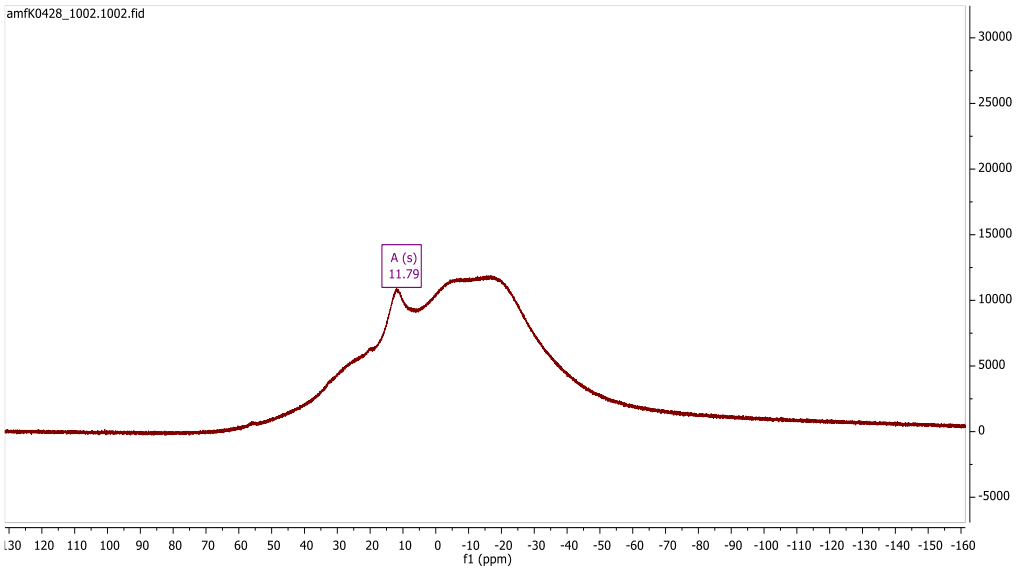

Figure 121. $^{11}B\{^{1}H\}$ NMR spectrum of 7 at 298 K in C_6D_6.

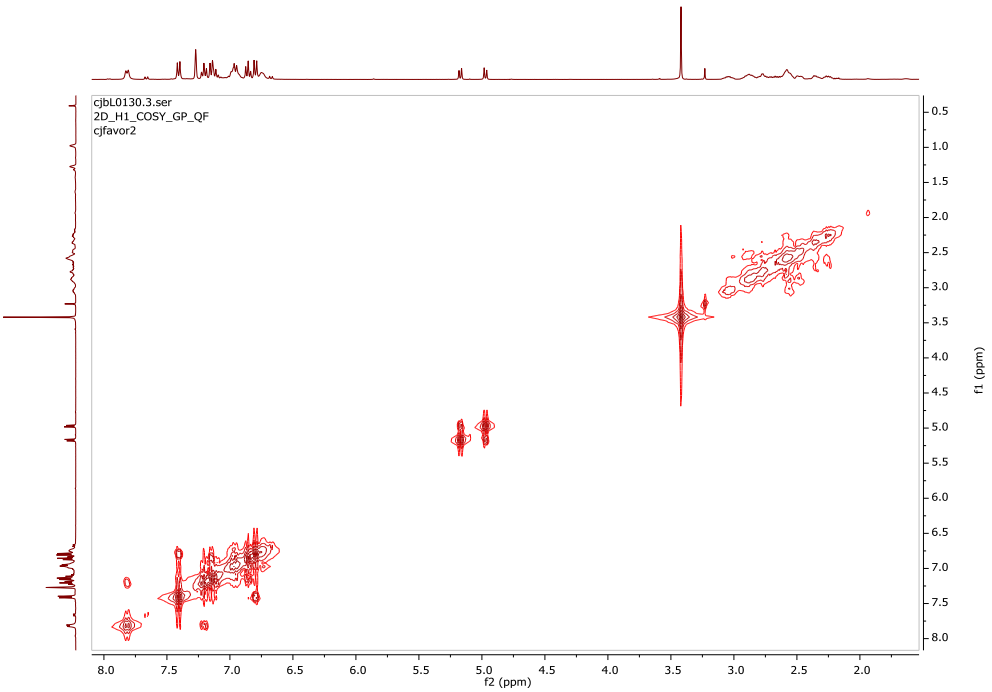

Figure 122. ^{1}H / ^{1}H NMR COSY experiment at 298 K for compound 7 in C_6D_6.

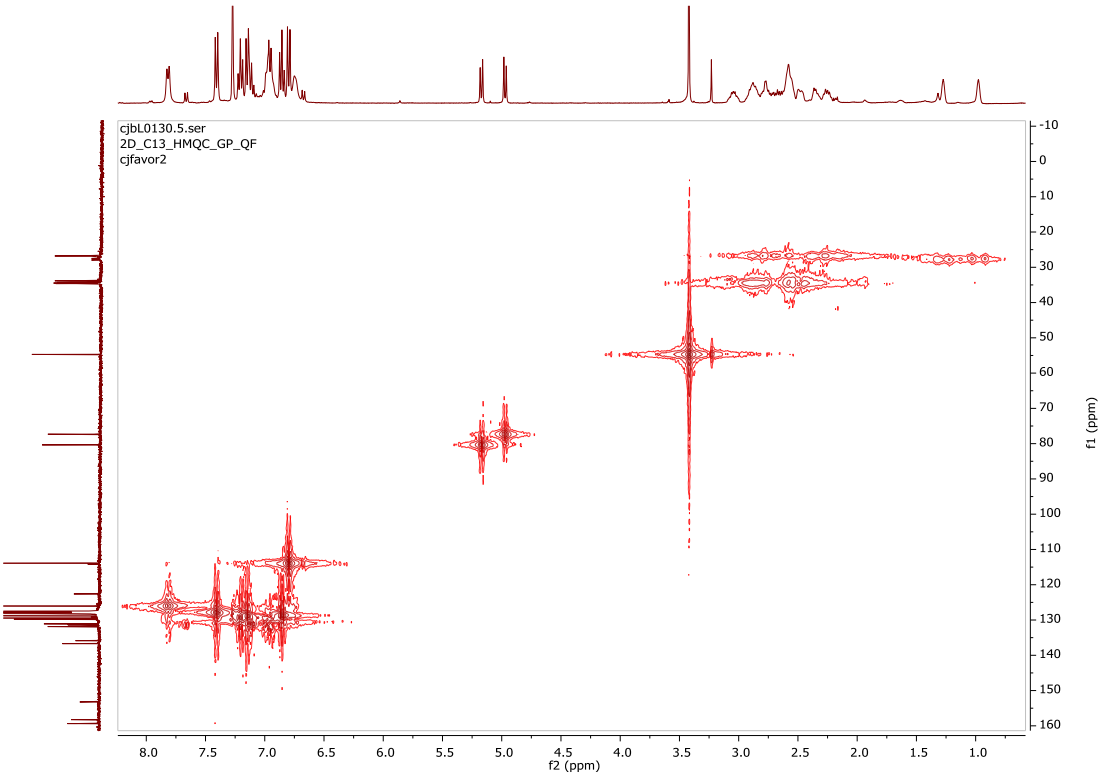

Figure 123. HMQC $^{13}C\{^{1}H\}/^{1}H$ NMR spectrum of 7 at 298 K in C_6D_6.

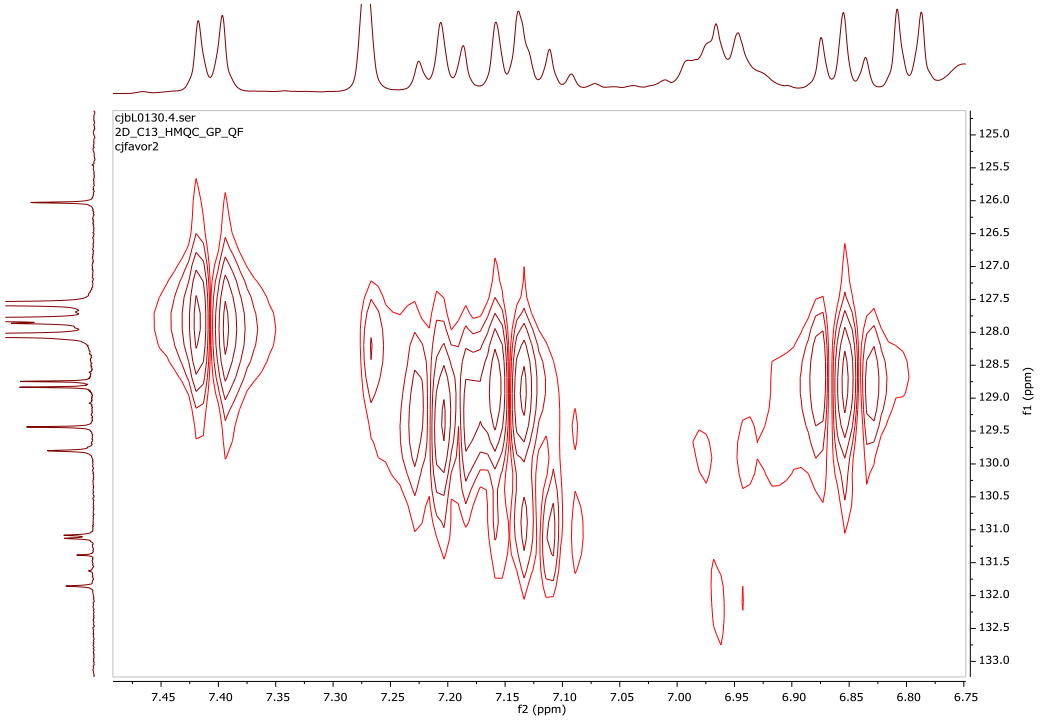

Figure 124. HMQC $^{13}C\{^{1}H\}/^{1}H$ NMR spectrum of 7 at 298 K in THF-d8. Zoom on the aromatic area

Mass Spectra

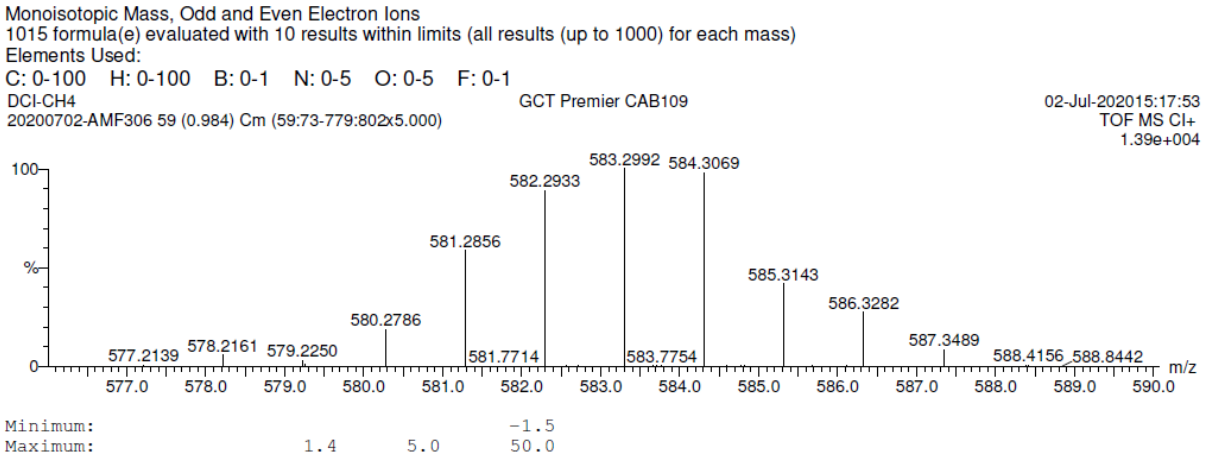

Figure 125. ESI DCI-CH4 mass spectrum for compound 7.

X-ray crystal structure

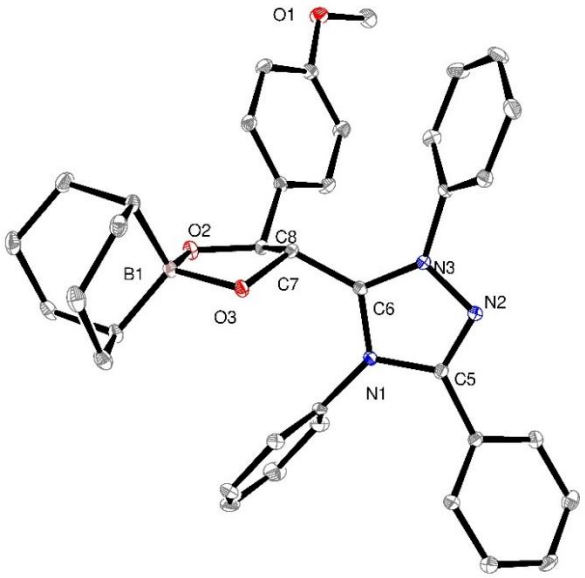

Figure 126. Molecular structure of 7.

General information

$C_{41}H_{46}BN_3O_4$	
M_r = 655.64	D_x = 1.116 Mg m^{-3}
Monoclinic, $P2_1/n$	
Hall symbol: -P 2yn	Mo $K\alpha$ radiation, λ = 0.71073 Å
a = 11.94690 (6) Å	Cell parameters from 7052 reflections
b = 20.51380 (8) Å	θ = 3–22°
c = 15.93370 (7) Å	μ = 0.07 mm^{-1}
β = 91.887 (5)°	T = 103 K
V = 3902.85 (3) Å^3	Platelet, colourless
Z = 4	0.15 × 0.12 × 0.02 mm
F(000) = 1400	

Refinement

Refinement on *F*	
Least-squares matrix: full	Hydrogen site location: difference Fourier map
$R[F^2 > 2\sigma(F^2)]$ = 0.058	H-atom parameters not refined
$wR(F^2)$ = 0.063	Method, part 1, Chebychev polynomial, (Watkin, 1994, *P*rince, 1982) [*w*eight] = 1.0/[A_0*T_0(x) + A_1*T_1(x) ⋯ + A_{n-1}]*T_{n-1}(x)] where A_i are the Chebychev coefficients listed below and x = *F* /*F*max Method = Robust Weighting (*P*rince, 1982) W = [*w*eight] * [1-(delta*F*/6*sigma*F*)^2]^2 A_i are: 1.43 0.307 0.976 0.505E-01
S = 1.15	$(\Delta/\sigma)_{max}$ = 0.0003
5380 reflections	$\Delta\rho_{max}$ = 0.32 e Å^{-3}
442 parameters	$\Delta\rho_{min}$ = −0.35 e Å^{-3}
0 restraints	Extinction correction: None

Geometry parameters (Å, °)

O1—C12	1.377 (3)	C19—H7	0.973
O1—C13	1.428 (3)	C19—C20	1.532 (4)
O2—C8	1.402 (3)	C20—H10	0.968
O2—B1	1.514 (3)	C20—H9	0.965
O3—C7	1.389 (3)	C20—C21	1.548 (4)
O3—B1	1.527 (3)	C21—H17	0.975
O4—C45	1.431 (4)	C21—C22	1.543 (4)
O4—C46	1.415 (4)	C22—H16	0.966

N1—C5	1.384 (3)	C22—H15	0.968
N1—C6	1.361 (3)	C22—C23	1.540 (4)
N1—C33	1.453 (3)	C23—H14	0.968
N2—N3	1.376 (3)	C23—H11	0.967
N2—C5	1.304 (3)	C23—C24	1.540 (4)
N3—C6	1.333 (3)	C24—H13	0.970
N3—C27	1.445 (3)	C24—H12	0.967
C1—H1	0.934	C25—H23	0.935
C1—C2	1.383 (4)	C25—C26	1.392 (4)
C1—C25	1.384 (4)	C26—H24	0.927
C2—H22	0.927	C27—C28	1.387 (3)
C2—C3	1.385 (4)	C27—C32	1.387 (3)
C3—H25	0.931	C28—H30	0.924
C3—C4	1.398 (3)	C28—C29	1.386 (4)
C4—C5	1.477 (3)	C29—H26	0.936
C4—C26	1.394 (3)	C29—C30	1.388 (4)
C6—C7	1.497 (3)	C30—H29	0.928
C7—H21	0.978	C30—C31	1.387 (4)
C7—C8	1.580 (3)	C31—H27	0.930
C8—H36	0.978	C31—C32	1.395 (4)
C8—C9	1.514 (3)	C32—H28	0.930
C9—C10	1.399 (3)	C33—C34	1.379 (4)
C9—C14	1.382 (3)	C33—C38	1.382 (4)
C10—H37	0.925	C34—H35	0.926
C10—C11	1.385 (3)	C34—C35	1.395 (4)

C11—H38	0.927	C35—H34	0.925
C11—C12	1.392 (4)	C35—C36	1.381 (5)
C12—C15	1.388 (4)	C36—H33	0.930
C13—H3	0.968	C36—C37	1.386 (4)
C13—H4	0.963	C37—H31	0.929
C13—H2	0.960	C37—C38	1.394 (4)
C14—H5	0.930	C38—H32	0.931
C14—C15	1.402 (4)	C45—H46	0.965
C15—H6	0.930	C45—H44	0.979
B1—C17	1.622 (4)	C45—C48	1.506 (5)
B1—C21	1.610 (4)	C46—H47	0.971
C17—H20	0.982	C46—H45	0.969
C17—C18	1.545 (4)	C46—C47	1.503 (5)
C17—C24	1.540 (4)	C47—H48	0.973
C18—H18	0.970	C47—H49	0.965
C18—H19	0.967	C47—C48	1.535 (5)
C18—C19	1.537 (4)	C48—H51	0.965
C19—H8	0.968	C48—H50	0.974
C12—O1—C13	116.6 (2)	H10—C20—C21	108.1
C8—O2—B1	111.35 (18)	H9—C20—C21	108.2
C7—O3—B1	106.58 (17)	C20—C21—B1	108.2 (2)
C45—O4—C46	106.1 (2)	C20—C21—H17	108.7
C5—N1—C6	107.01 (19)	B1—C21—H17	108.2

C5—N1—C33	125.43 (19)	C20—C21—C22	114.9 (2)
C6—N1—C33	127.35 (19)	B1—C21—C22	108.6 (2)
N3—N2—C5	103.96 (18)	H17—C21—C22	108.1
N2—N3—C6	112.73 (18)	C21—C22—H16	108.6
N2—N3—C27	116.99 (18)	C21—C22—H15	108.2
C6—N3—C27	130.2 (2)	H16—C22—H15	108.1
H1—C1—C2	119.6	C21—C22—C23	114.8 (2)
H1—C1—C25	119.9	H16—C22—C23	108.7
C2—C1—C25	120.5 (2)	H15—C22—C23	108.3
C1—C2—H22	119.9	C22—C23—H14	108.5
C1—C2—C3	119.8 (2)	C22—C23—H11	108.9
H22—C2—C3	120.3	H14—C23—H11	108.1
C2—C3—H25	119.7	C22—C23—C24	114.0 (2)
C2—C3—C4	120.1 (2)	H14—C23—C24	108.5
H25—C3—C4	120.2	H11—C23—C24	108.8
C3—C4—C5	117.6 (2)	C23—C24—C17	115.5 (2)
C3—C4—C26	120.0 (2)	C23—C24—H13	108.2
C5—C4—C26	122.3 (2)	C17—C24—H13	108.3
C4—C5—N1	125.4 (2)	C23—C24—H12	108.5
C4—C5—N2	123.3 (2)	C17—C24—H12	108.5
N1—C5—N2	111.2 (2)	H13—C24—H12	107.7
N1—C6—N3	105.05 (19)	C1—C25—H23	120.5

N1—C6—C7	126.1 (2)	C1—C25—C26	120.4 (2)
N3—C6—C7	128.7 (2)	H23—C25—C26	119.1
C6—C7—O3	108.14 (18)	C4—C26—C25	119.2 (2)
C6—C7—H21	109.5	C4—C26—H24	120.7
O3—C7—H21	109.8	C25—C26—H24	120.1
C6—C7—C8	114.55 (19)	N3—C27—C28	117.6 (2)
O3—C7—C8	105.42 (18)	N3—C27—C32	120.1 (2)
H21—C7—C8	109.4	C28—C27—C32	122.1 (2)
C7—C8—O2	103.46 (18)	C27—C28—H30	120.0
C7—C8—H36	109.3	C27—C28—C29	119.3 (2)
O2—C8—H36	109.7	H30—C28—C29	120.7
C7—C8—C9	114.15 (19)	C28—C29—H26	120.3
O2—C8—C9	110.60 (19)	C28—C29—C30	119.5 (3)
H36—C8—C9	109.5	H26—C29—C30	120.2
C8—C9—C10	119.3 (2)	C29—C30—H29	120.2
C8—C9—C14	122.2 (2)	C29—C30—C31	120.7 (2)
C10—C9—C14	118.4 (2)	H29—C30—C31	119.0
C9—C10—H37	119.1	C30—C31—H27	119.6
C9—C10—C11	120.8 (2)	C30—C31—C32	120.4 (3)
H37—C10—C11	120.1	H27—C31—C32	120.0
C10—C11—H38	119.9	C31—C32—C27	118.0 (3)
C10—C11—C12	120.0 (2)	C31—C32—H28	120.7

H38—C11—C12	120.0	C27—C32—H28	121.3
C11—C12—O1	115.3 (2)	N1—C33—C34	118.1 (2)
C11—C12—C15	120.2 (2)	N1—C33—C38	119.0 (2)
O1—C12—C15	124.5 (2)	C34—C33—C38	122.8 (2)
O1—C13—H3	109.9	C33—C34—H35	121.0
O1—C13—H4	110.0	C33—C34—C35	118.3 (3)
H3—C13—H4	108.6	H35—C34—C35	120.7
O1—C13—H2	110.2	C34—C35—H34	120.4
H3—C13—H2	108.8	C34—C35—C36	119.9 (3)
H4—C13—H2	109.3	H34—C35—C36	119.8
C9—C14—H5	119.4	C35—C36—H33	119.3
C9—C14—C15	121.6 (2)	C35—C36—C37	120.8 (2)
H5—C14—C15	119.0	H33—C36—C37	119.8
C14—C15—C12	118.9 (2)	C36—C37—H31	120.0
C14—C15—H6	120.3	C36—C37—C38	120.1 (3)
C12—C15—H6	120.7	H31—C37—C38	120.0
O3—B1—O2	102.23 (18)	C37—C38—C33	118.0 (3)
O3—B1—C17	111.0 (2)	C37—C38—H32	120.6
O2—B1—C17	113.4 (2)	C33—C38—H32	121.4
O3—B1—C21	111.9 (2)	O4—C45—H46	110.9
O2—B1—C21	112.1 (2)	O4—C45—H44	109.8
C17—B1—C21	106.3 (2)	H46—C45—H44	108.3
B1—C17—H20	108.3	O4—C45—C48	106.5 (3)
B1—C17—C18	109.8 (2)	H46—C45—C48	110.9

H20—C17—C18	108.2	H44—C45—C48	110.4
B1—C17—C24	108.9 (2)	O4—C46—H47	109.4
H20—C17—C24	107.9	O4—C46—H45	109.7
C18—C17—C24	113.7 (2)	H47—C46—H45	108.3
C17—C18—H18	108.6	O4—C46—C47	109.4 (3)
C17—C18—H19	108.7	H47—C46—C47	110.2
H18—C18—H19	107.8	H45—C46—C47	109.9
C17—C18—C19	114.2 (2)	C46—C47—H48	111.1
H18—C18—C19	108.6	C46—C47—H49	111.5
H19—C18—C19	108.9	H48—C47—H49	109.1
C18—C19—H8	108.9	C46—C47—C48	104.1 (3)
C18—C19—H7	108.4	H48—C47—C48	110.4
H8—C19—H7	107.6	H49—C47—C48	110.6
C18—C19—C20	114.2 (2)	C47—C48—C45	102.5 (3)
H8—C19—C20	109.0	C47—C48—H51	111.5
H7—C19—C20	108.5	C45—C48—H51	111.2
C19—C20—H10	108.2	C47—C48—H50	111.2
C19—C20—H9	108.2	C45—C48—H50	111.1
H10—C20—H9	108.0	H51—C48—H50	109.2
C19—C20—C21	115.9 (2)		

4. FLUOROBENZALDEHYDE ADDUCT

NMR Spectra

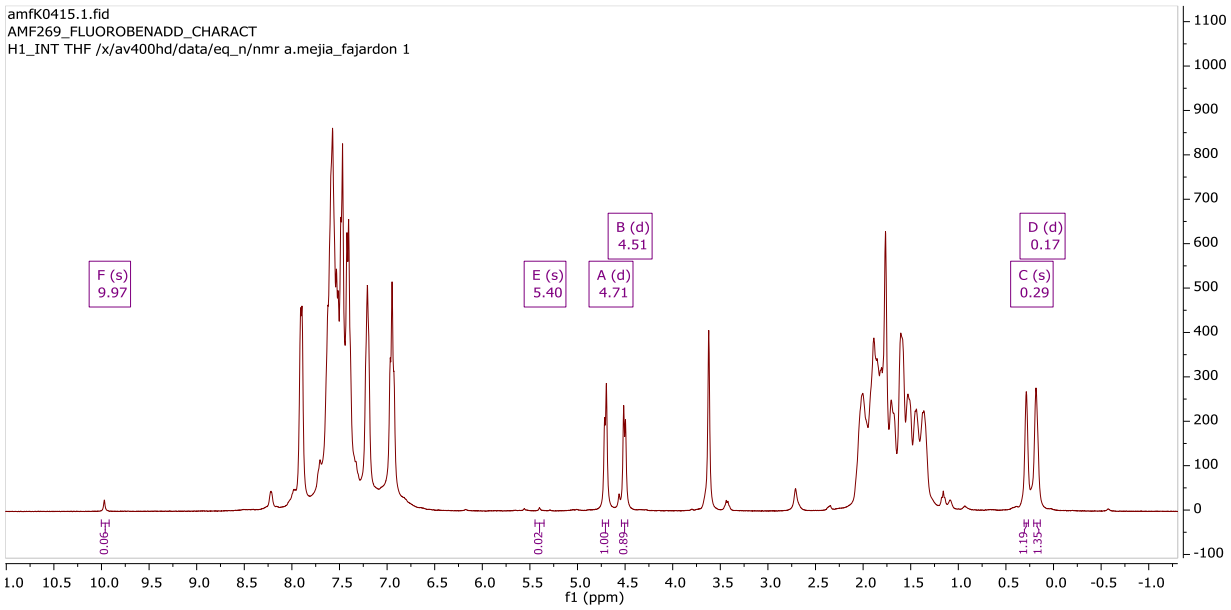

Figure 127. ^{1}H NMR spectrum observed for 9.

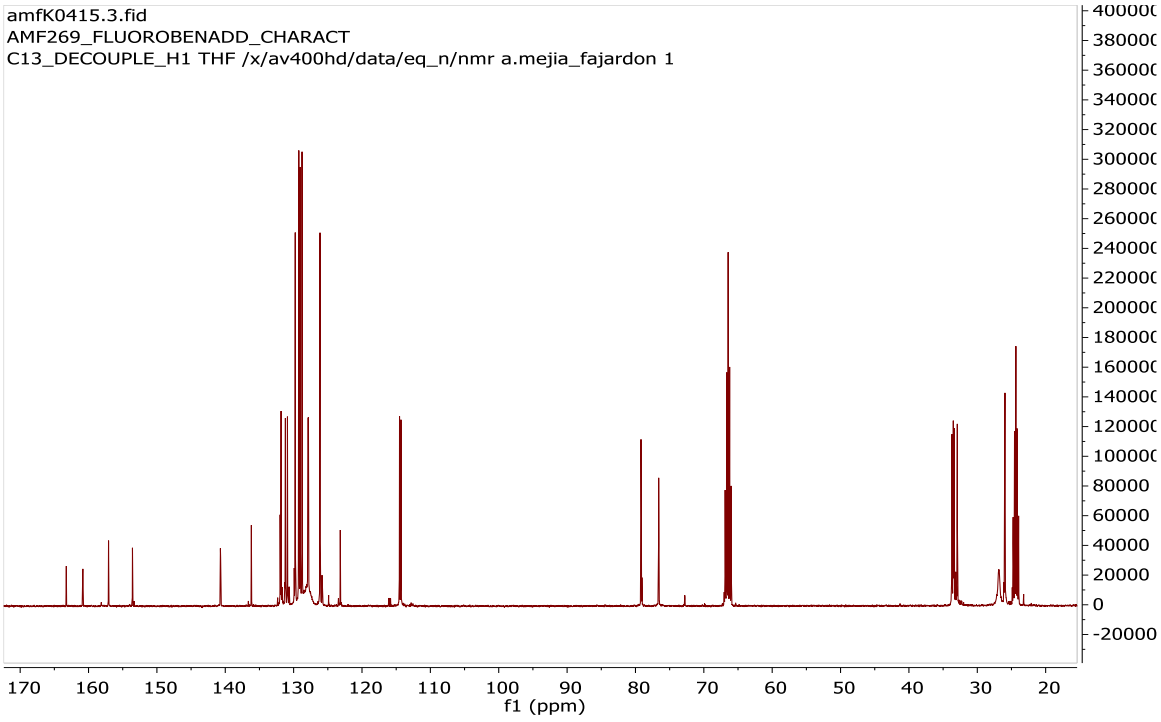

Figure 128. $^{13}C\{^{1}H\}$ NMR spectrum observed for 9. Zoom on the 0 to 160 ppm area.

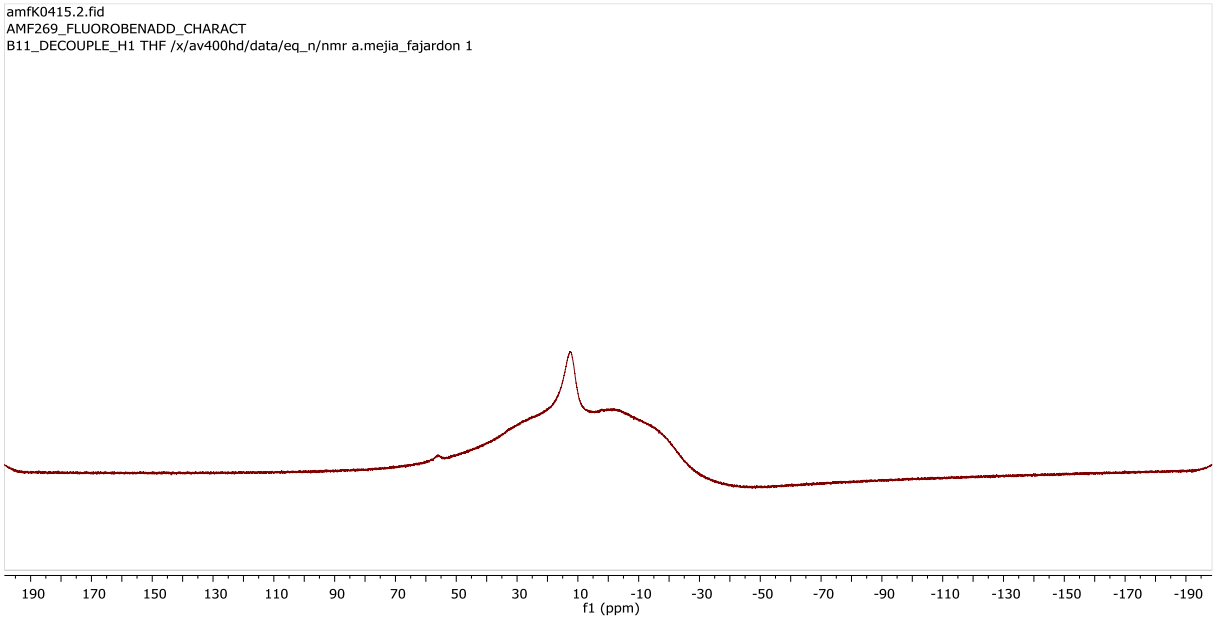

Figure 129. $^{11}B\{^{1}H\}$ NMR spectrum of 9 at 298 K in THF-d8.

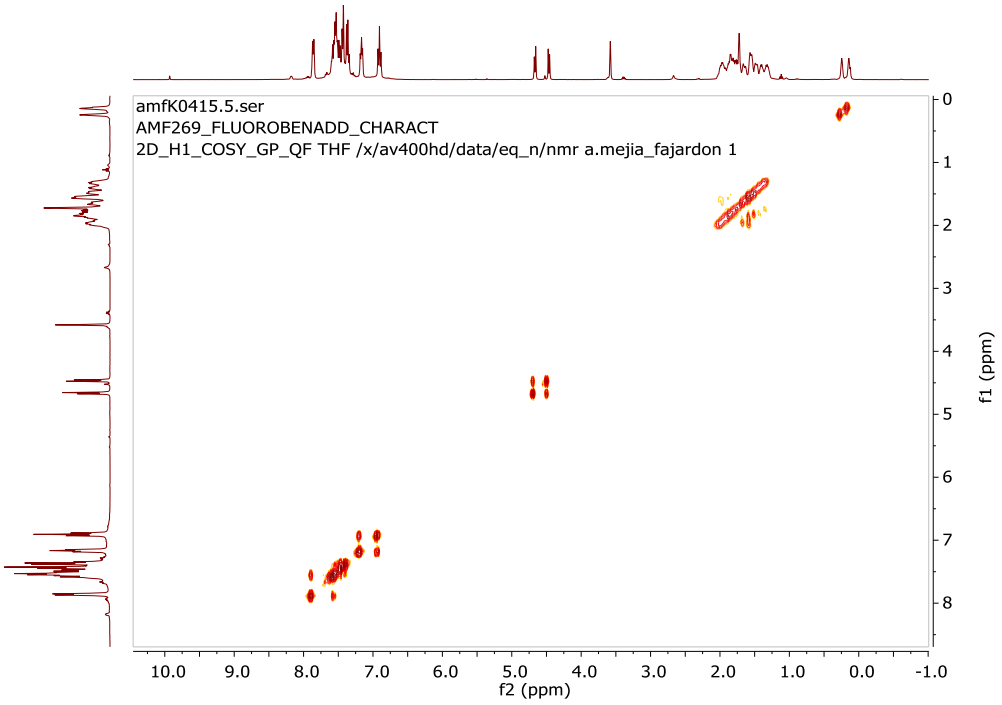

Figure 130. ^{1}H / ^{1}H NMR COSY experiment at 298 K for compound 9 in THF-d8.

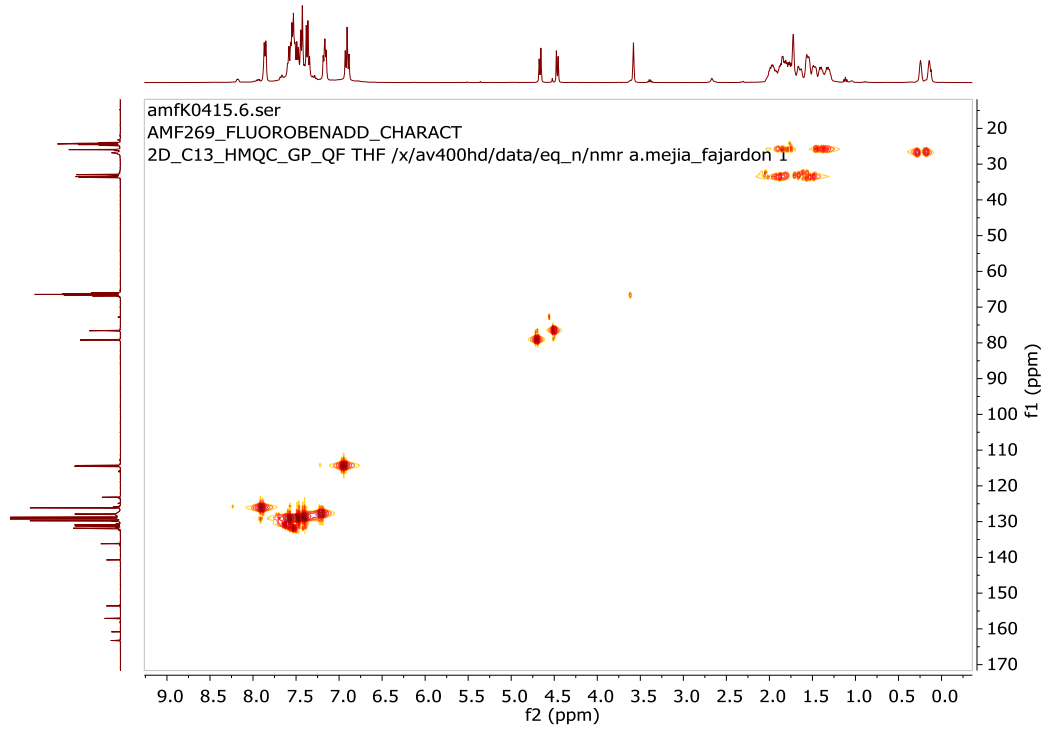

Figure 131. HMQC $^{13}C\{^{1}H\}/^{1}H$ NMR spectrum of 9 at 298 K in THF-d8.

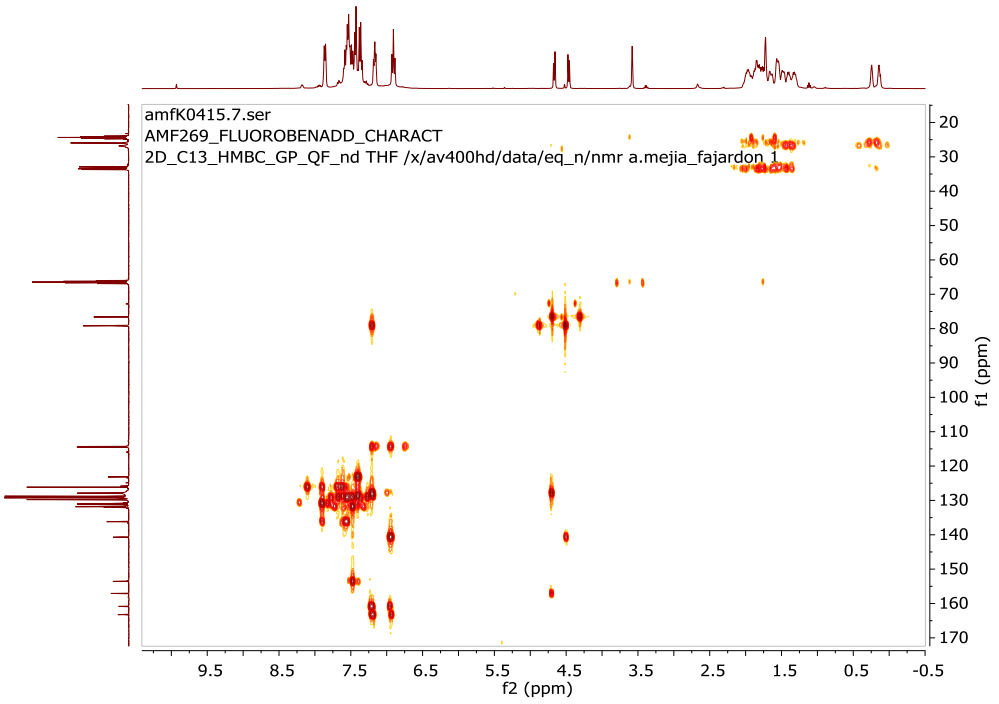

Figure 132. HMBC: long-range $^{13}C\{^{1}H\}/^{1}H$ NMR spectrum for 9 at 298 K in THF-d8.

Mass Spectra

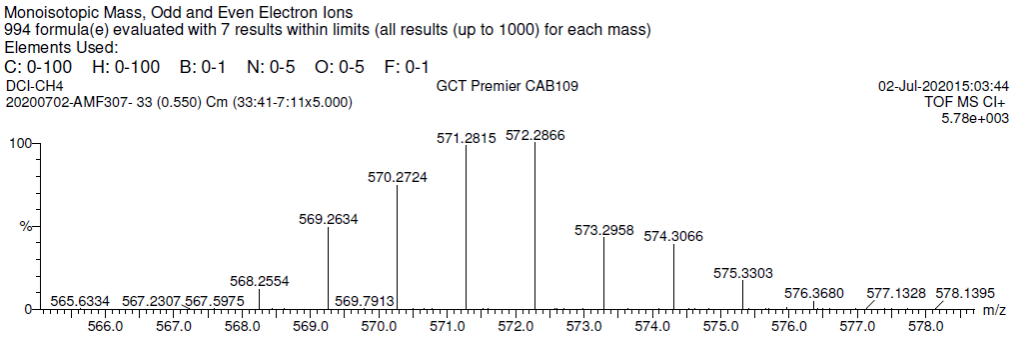

Minimum:				-1.5		
Maximum:		1.4	5.0	50.0		
Mass	Calc. Mass	mDa	PPM	DBE	i-FIT	Formula
571.2815	571.2801	1.4	2.5	25.5	1215.6	C43 H36 F
	571.2808	0.7	1.2	24.5	1419.0	C41 H36 B O2
	571.2835	-2.0	-3.5	21.0	1476.1	C37 H37 N3 O3
	571.2795	2.0	3.5	25.0	1492.6	C39 H34 B N3 O
	571.2820	-0.5	-0.9	20.5	1575.5	C38 H37 B O3 F
	571.2806	0.9	1.6	21.0	1651.3	C36 H35 B N3 O2 F
	571.2795	2.0	3.5	17.0	1728.0	C32 H37 N5 O5

Figure 133. ESI DCI-CH4 mass spectrum for compound 9.

5. BROMOBENZALDEHYDE ADDUCT

NMR spectra

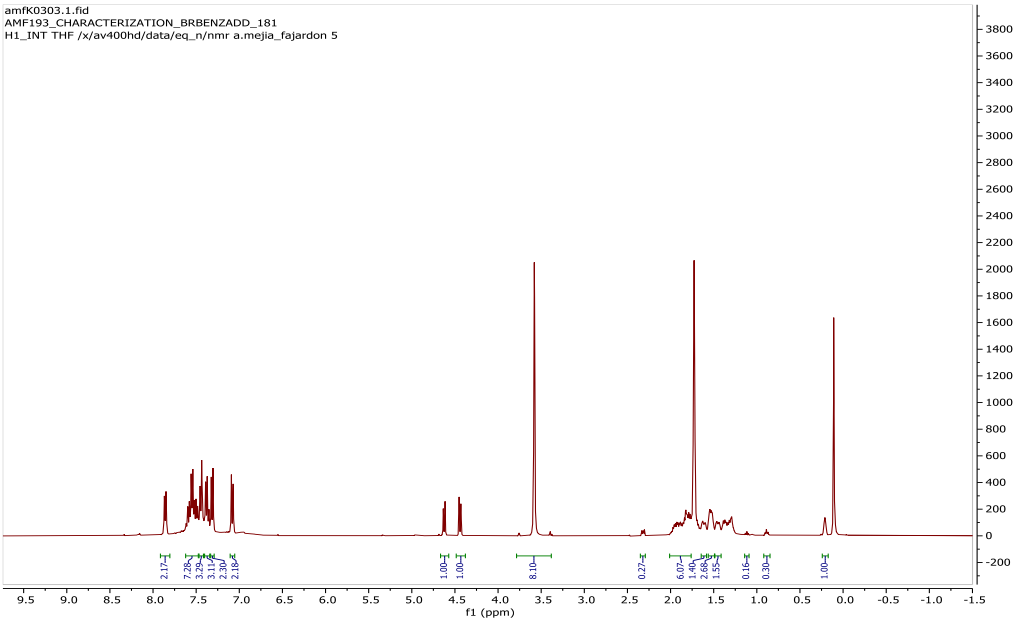

Figure 134. ^{1}H NMR spectrum observed for 11.

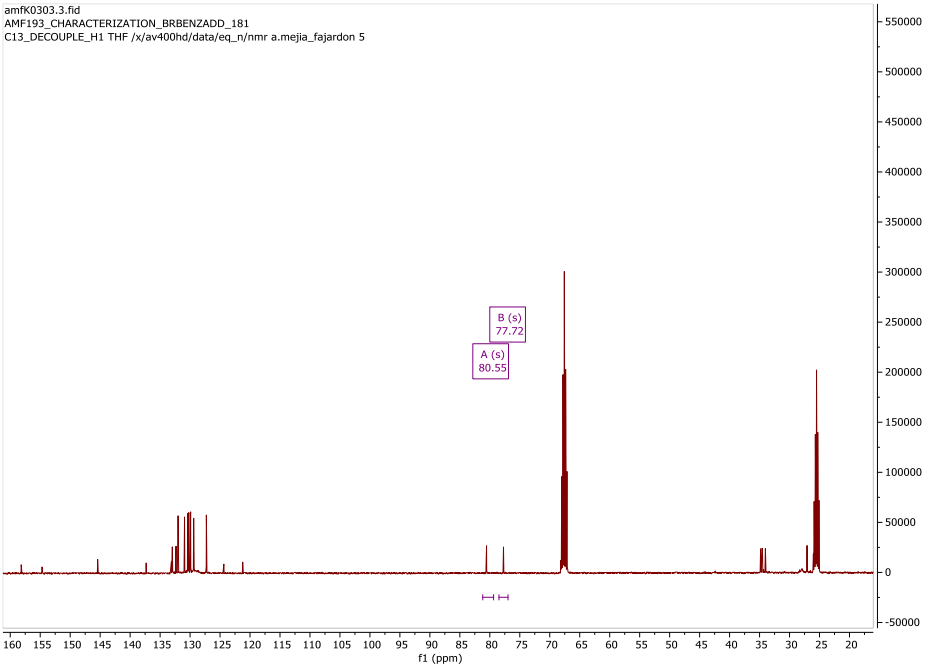

Figure 135. ^{13}C NMR spectrum observed for 11.

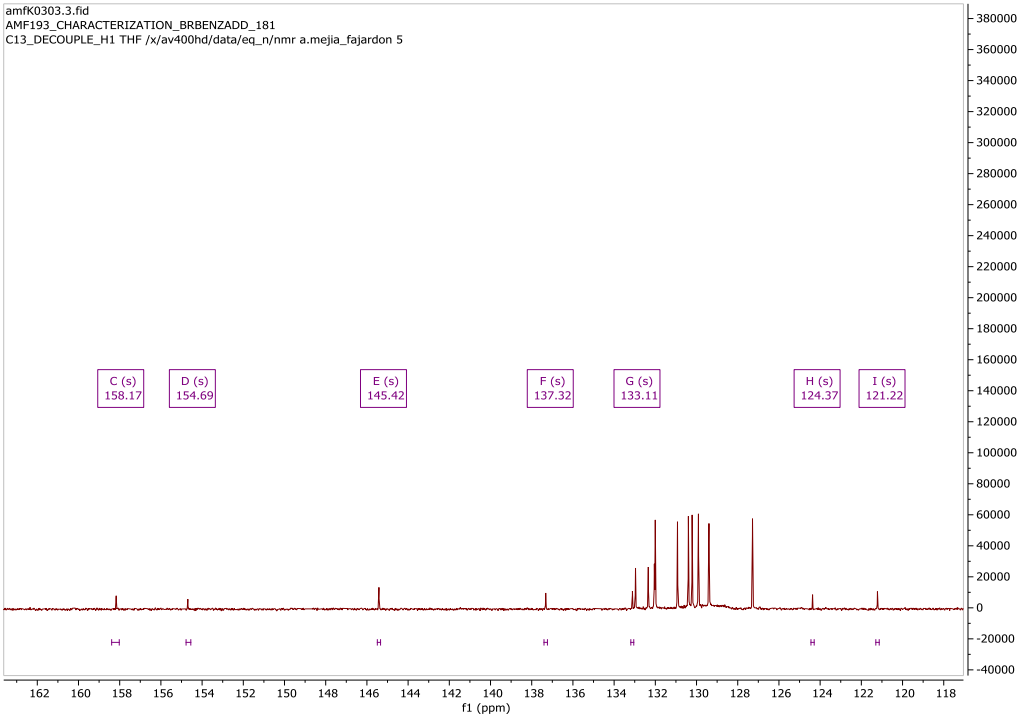

Figure 136.^{13}C NMR spectrum observed for 11. Zoom on the 118 to 1621 ppm area to emphasize the quaternary aromatics.

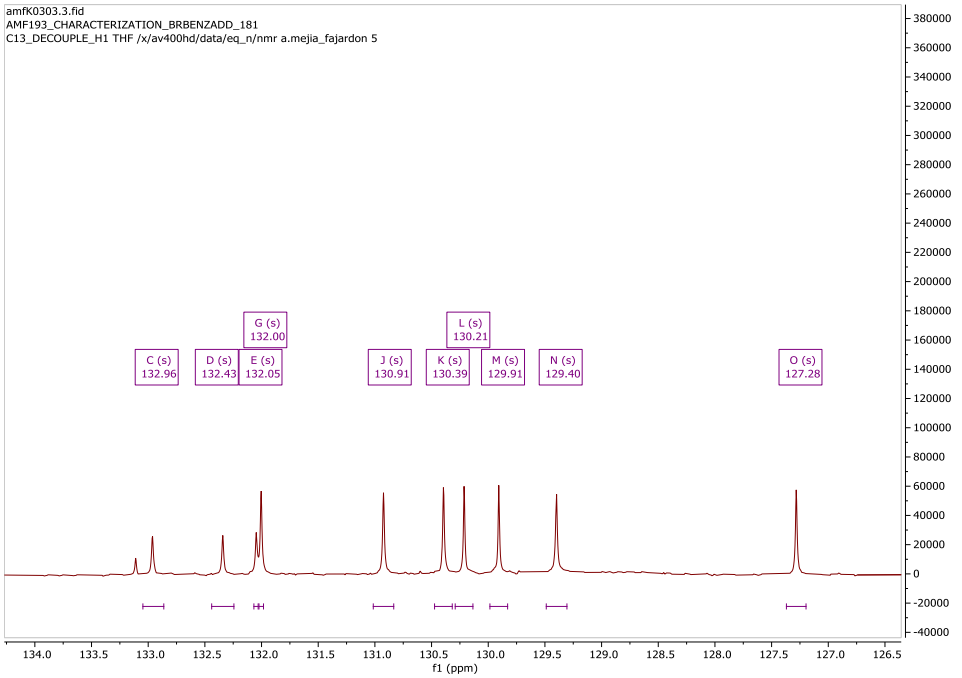

Figure 137. ^{13}C NMR spectrum observed for 11. Zoom on the 126 to 134 ppm area to emphasize the aromatic carbons.

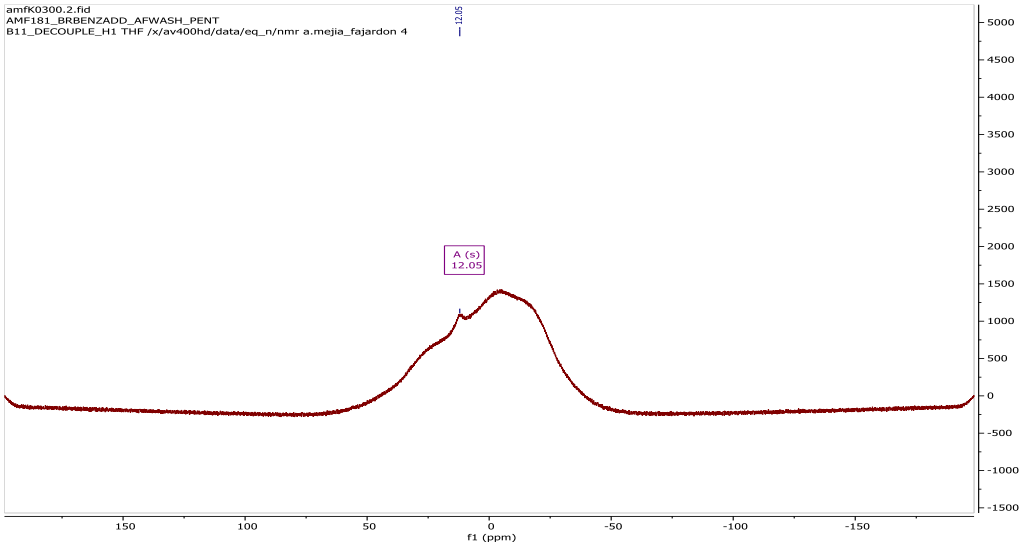

Figure 138. $^{11}B\{^{1}H\}$ NMR spectrum of 11 at 298 K in THF-d8.

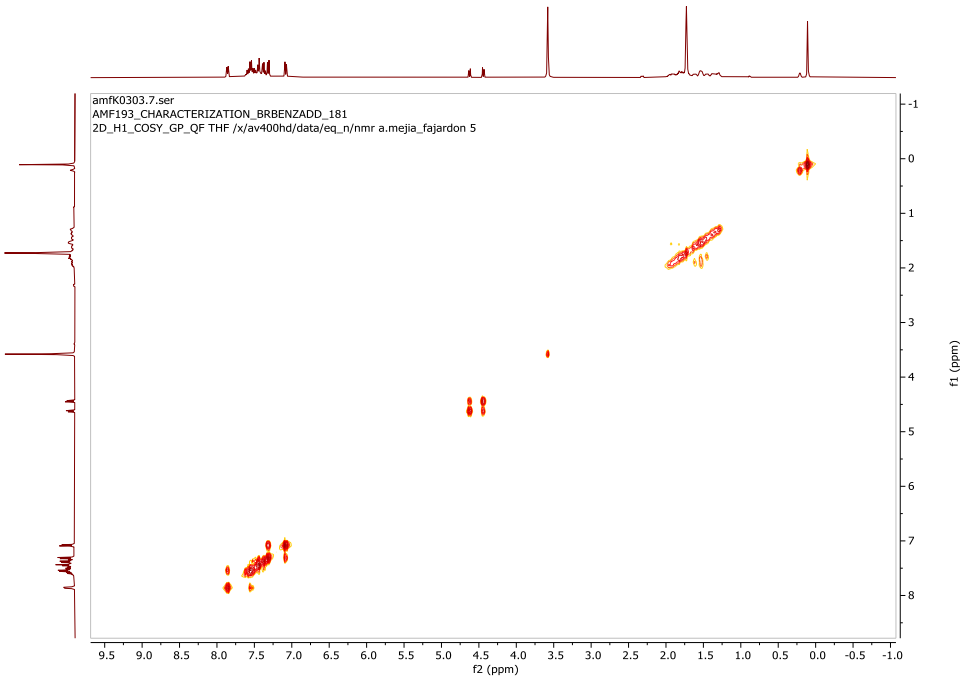

Figure 139. ^{1}H / ^{1}H NMR COSY experiment at 298 K for compound 11 in THF-d8.

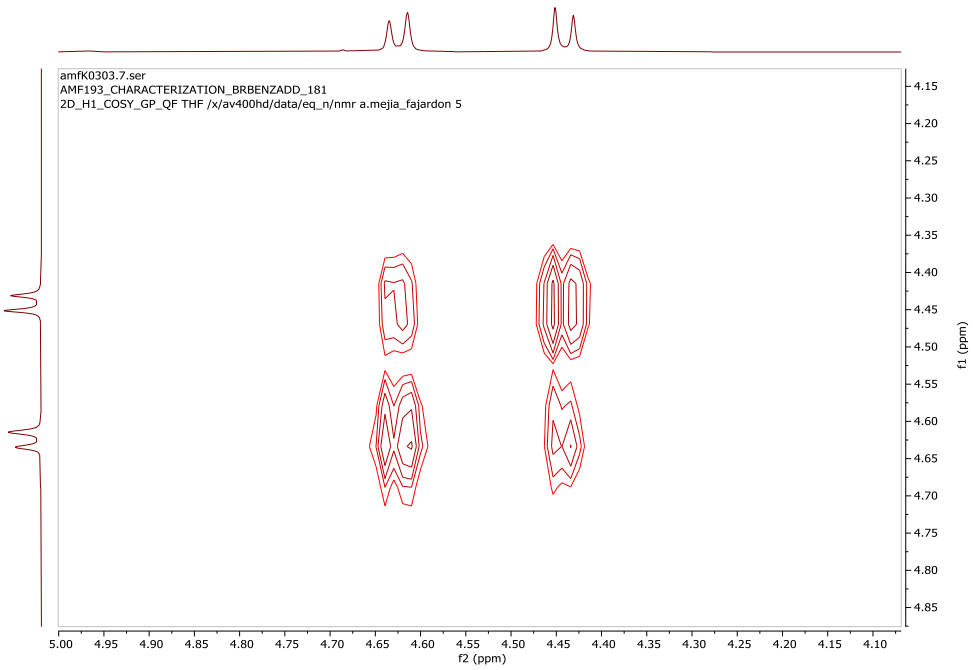

Figure 140. ^{1}H / ^{1}H NMR COSY experiment at 298 K for compound 11 in THF-d8. Zoom on the 4.3 to 4.9 ppm area.

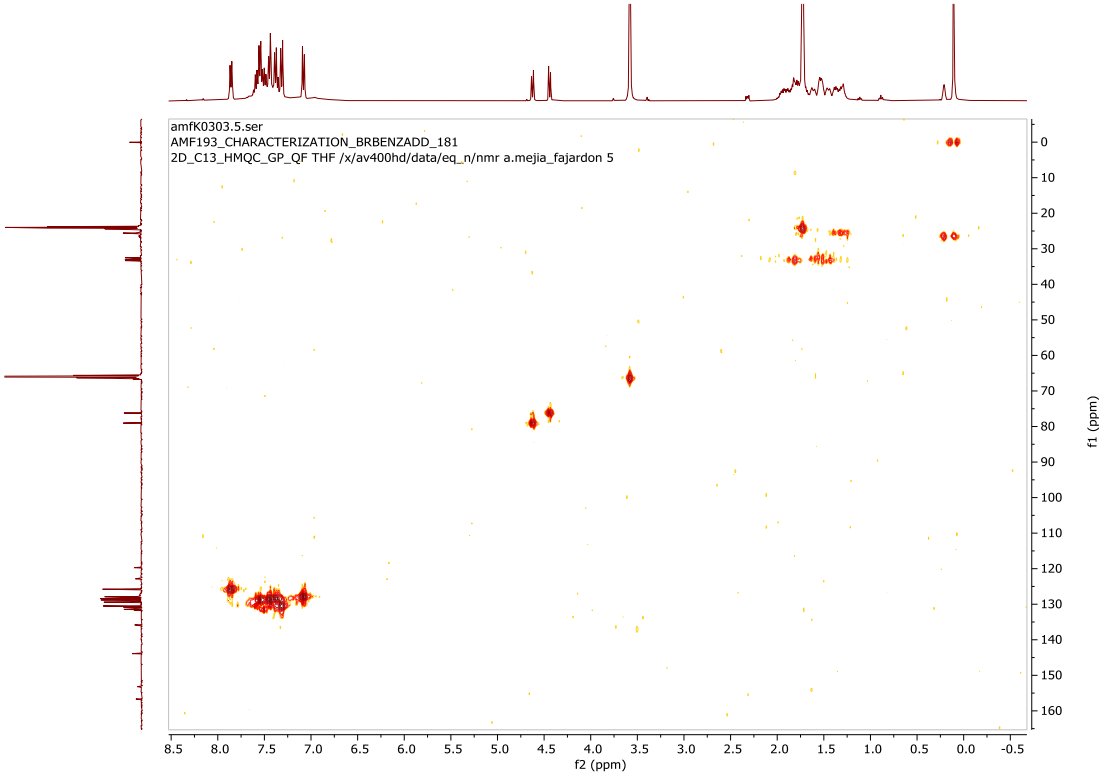

Figure 141. HMQC $^{13}C\{^1H\}/^1H$ NMR spectrum of 11 at 298 K in THF-d8.

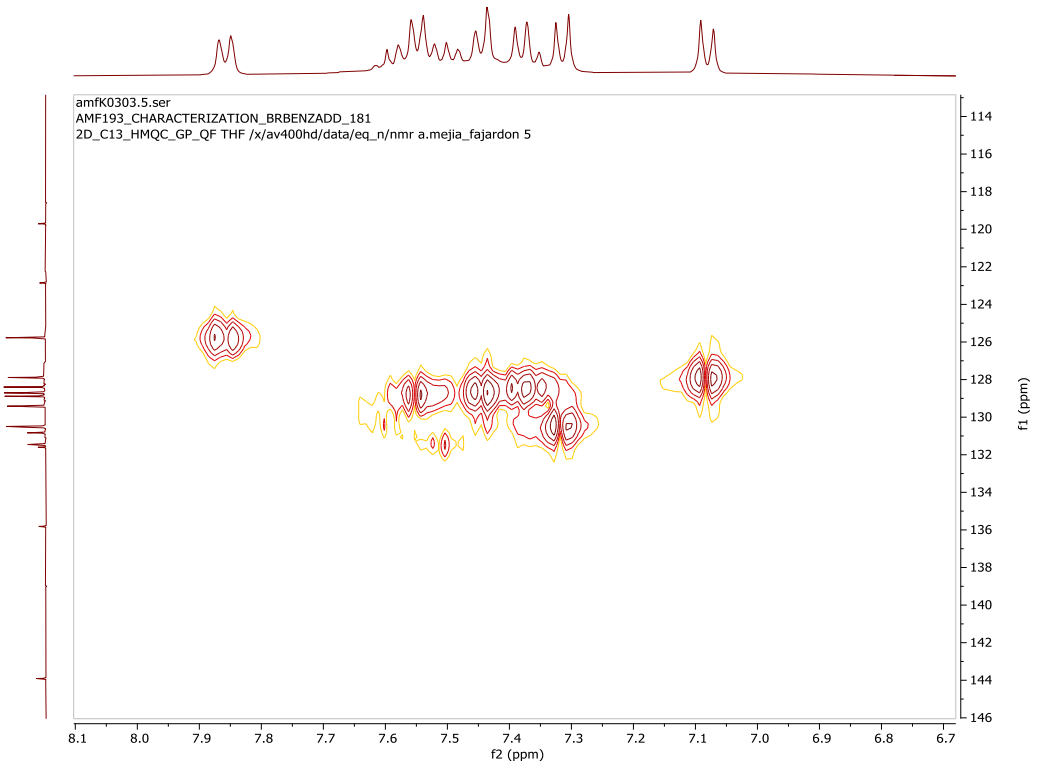

Figure 142. HMQC $^{13}C\{^1H\}/^1H$ NMR spectrum of 11 at 298 K in THF-d8. Zoom on the aromatic area

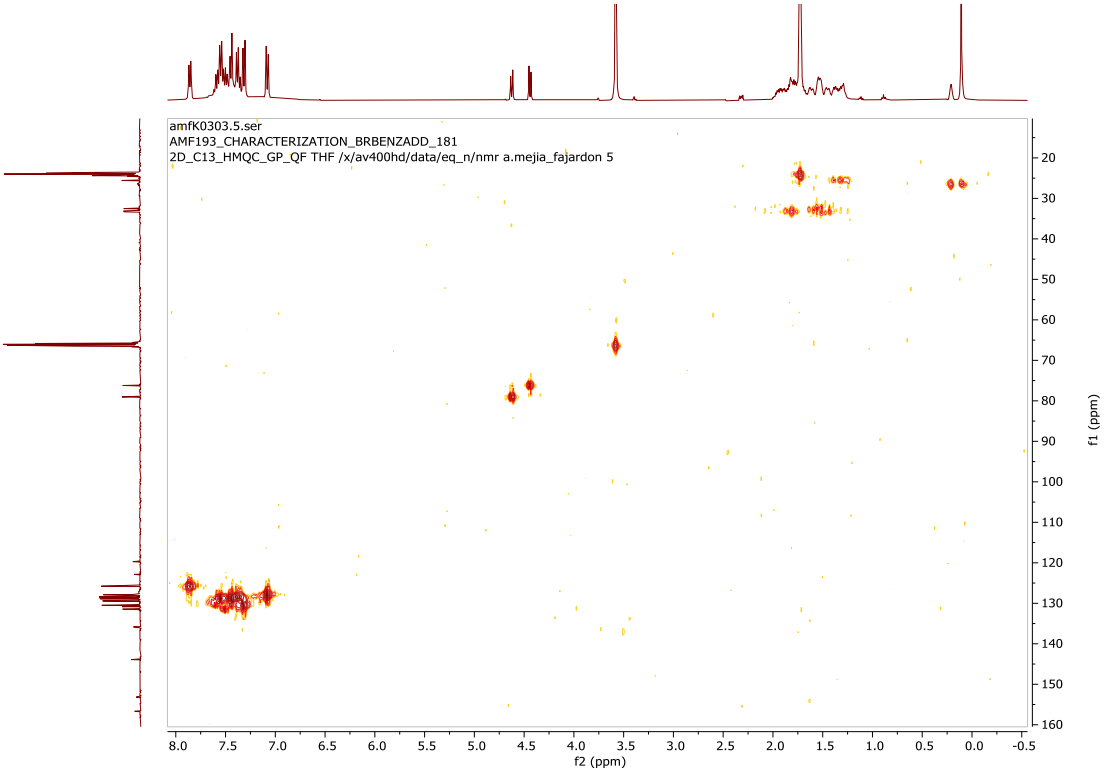

Figure 143. HMBC: long range $^{13}C\{^1H\}/^1H$ NMR spectrum for 11 at 298 K in THF-d8

Mass Spectra

Monoisotopic Mass, Odd and Even Electron Ions
243 formula(e) evaluated with 4 results within limits (all results (up to 1000) for each mass)
Elements Used:
C: 0-100 H: 0-100 N: 0-5 O: 0-5 Br: 1-1 11B: 1-1

DCI-CH4
20200115-AMF232- 43 (0.717) Cm (38:43-333:337x5.000)

GCT Premier CAB109

15-Jan-202014:37:09
TOF MS CI+
6.10e+003

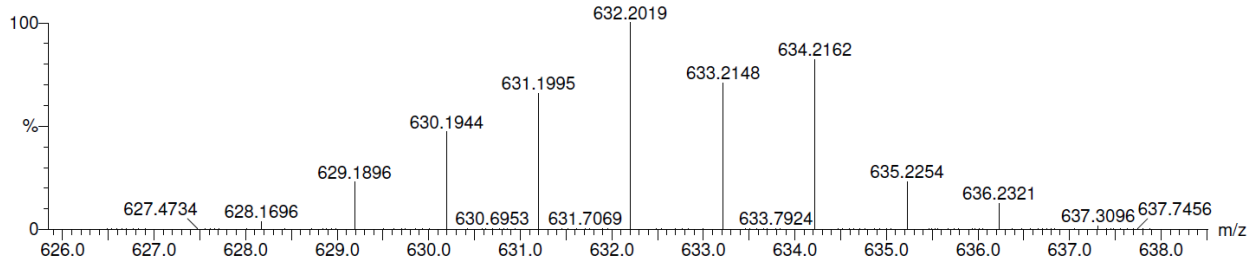

Minimum:				-1.5	
Maximum:		1.4	5.0	50.0	
Mass	Calc. Mass	mDa	PPM	DBE	i-FIT
631.1995	631.2019	-2.4	-3.8	20.5	928.3

6. CHLOROBENZALDEHYDE ADDUCT

NMR spectra

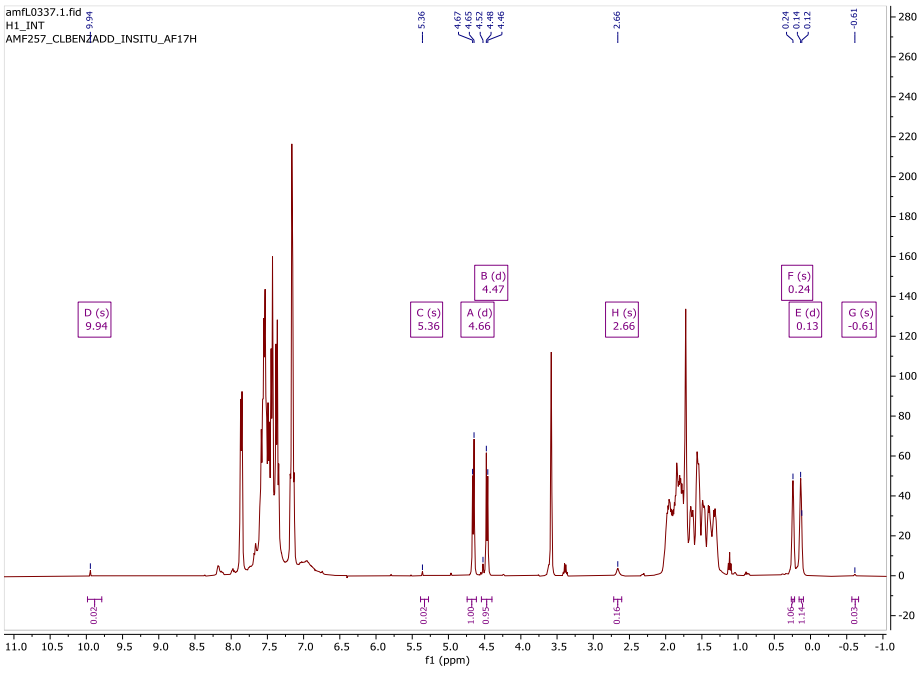

Figure 145. ^{1}H NMR spectrum observed for 13.

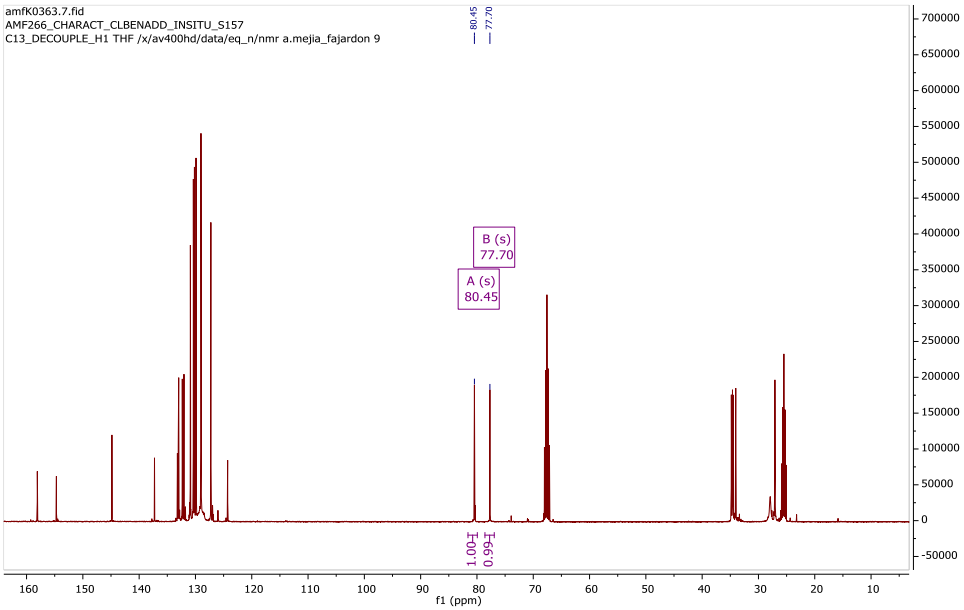

Figure 146. ^{13}C NMR spectrum observed for 13.

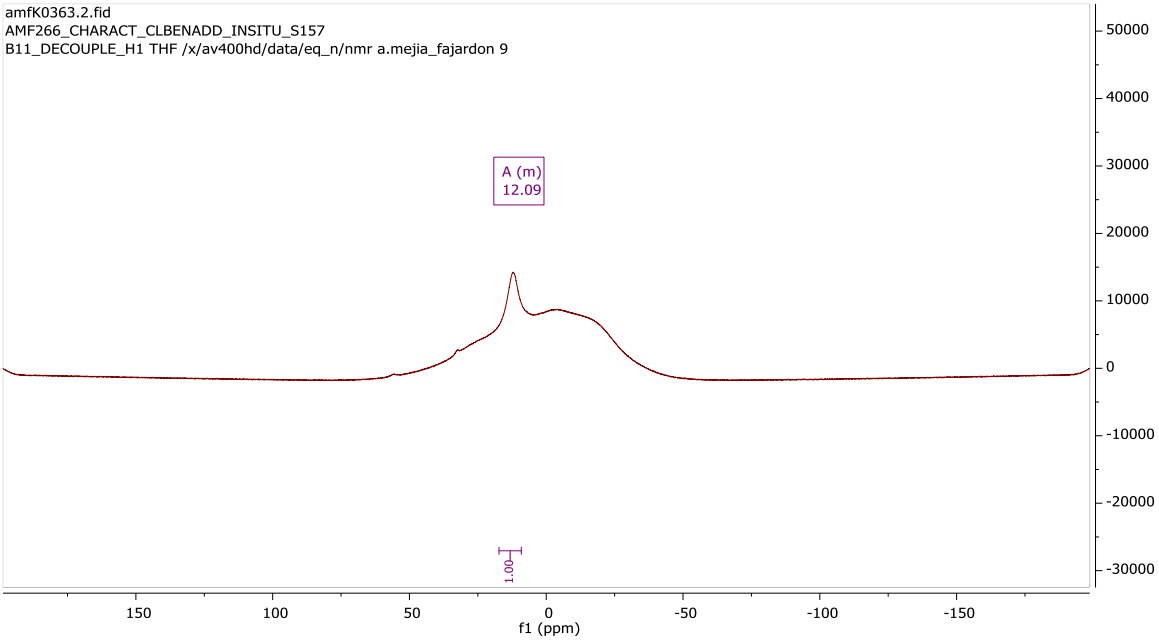

Figure 147. $^{11}B\{^{1}H\}$ NMR spectrum of 13 at 298 K in THF-d8.

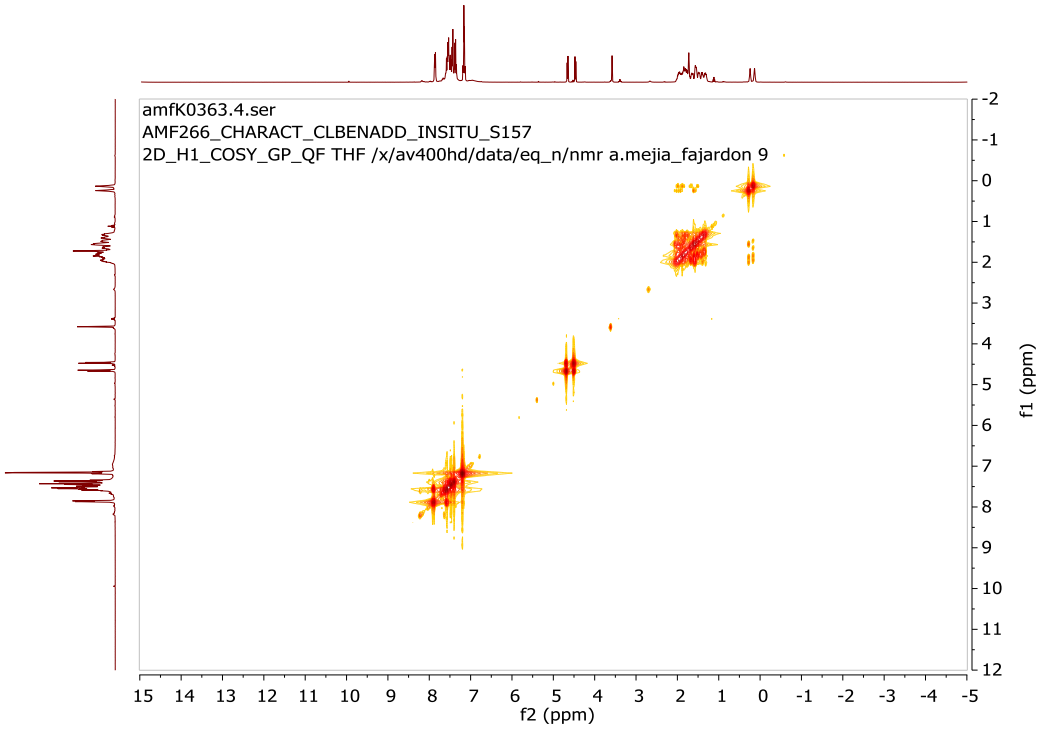

Figure 148. ^{1}H / ^{1}H NMR COSY experiment at 298 K for compound 13 in THF-d8.

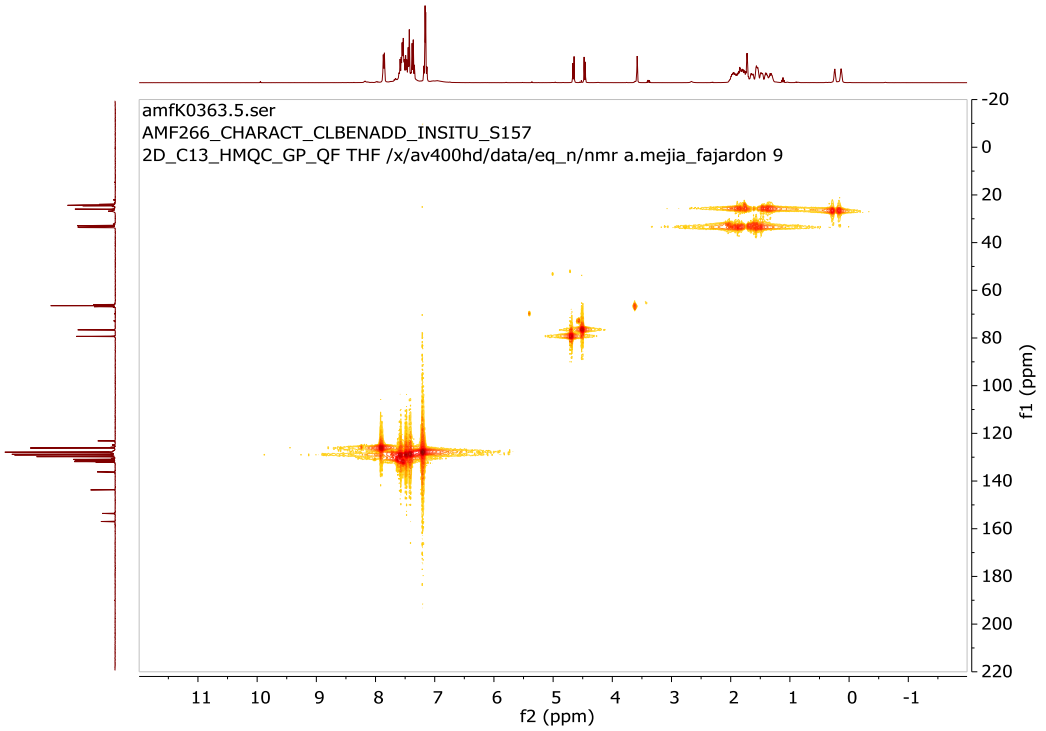

Figure 149. HMQC $^{13}C\{^1H\}/^1H$ NMR spectrum of 13 at 298 K in THF-d8.

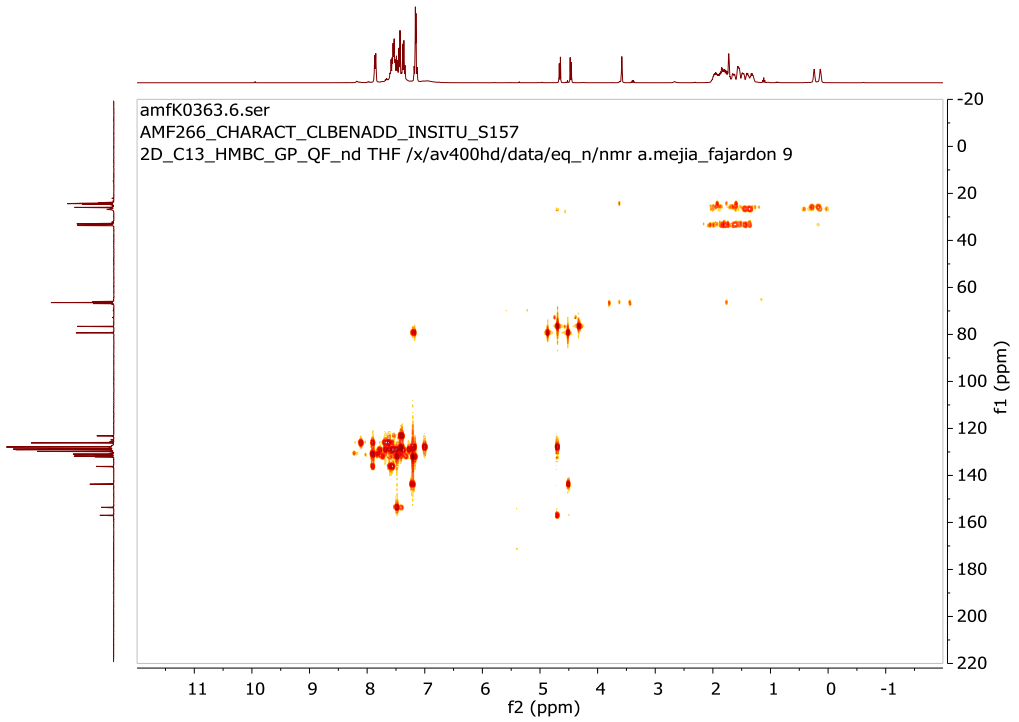

Figure 150. HMBC: long-range $^{13}C\{^1H\}/^1H$ NMR spectrum for 13 at 298 K in THF-d8

Mass spectra

Single Mass Analysis
Tolerance = 5.0 PPM / DBE: min = -1.5, max = 50.0
Element prediction: Off

Monoisotopic Mass, Odd and Even Electron Ions
486 formula(e) evaluated with 5 results within limits (all results (up to 1000) for each mass)
Elements Used:
C: 0-100 H: 0-100 B: 0-1 N: 0-5 O: 0-5 Cl: 1-1

DCI-CH4 GCT Premier CAB109 06-Jul-202016:51:14
20200706-AMF310- 30 (0.500) Cm (29:37-3:7x5.000) TOF MS CI+
1.13e+003

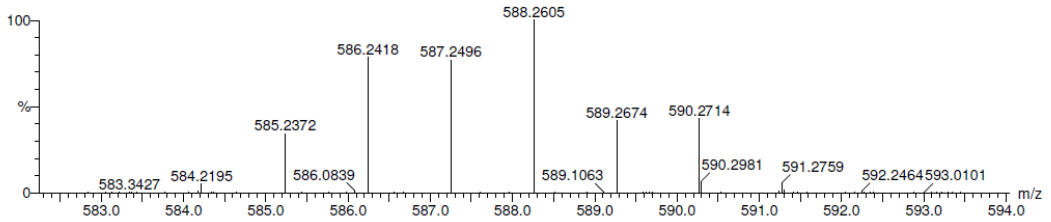

Minimum:				-1.5		
Maximum:		1.4	5.0	50.0		
Mass	Calc. Mass	mDa	PPM	DBE	i-FIT	Formula
587.2496	587.2506	-1.0	-1.7	25.5	190.0	C43 H36 Cl
	587.2524	-2.8	-4.8	20.5	191.5	C38 H37 B O3 Cl
	587.2511	-1.5	-2.6	21.0	198.7	C36 H35 B N3 O2 Cl
	587.2484	1.2	2.0	16.5	218.6	C33 H37 B N2 O5 Cl
	587.2471	2.5	4.3	17.0	226.6	C31 H35 B N5 O4 Cl

Figure 151. ESI DCI-CH4 mass spectrum for compound 13.

7. CYANOBENZALDEHYDE ADDUCT

NMR Spectra

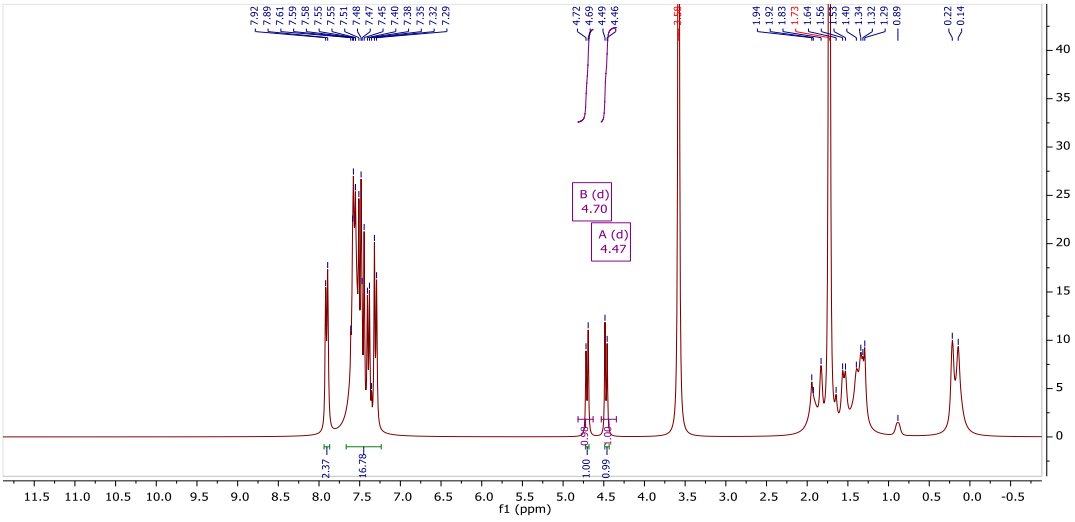

Figure 152. ^{1}H NMR spectrum observed for 15.

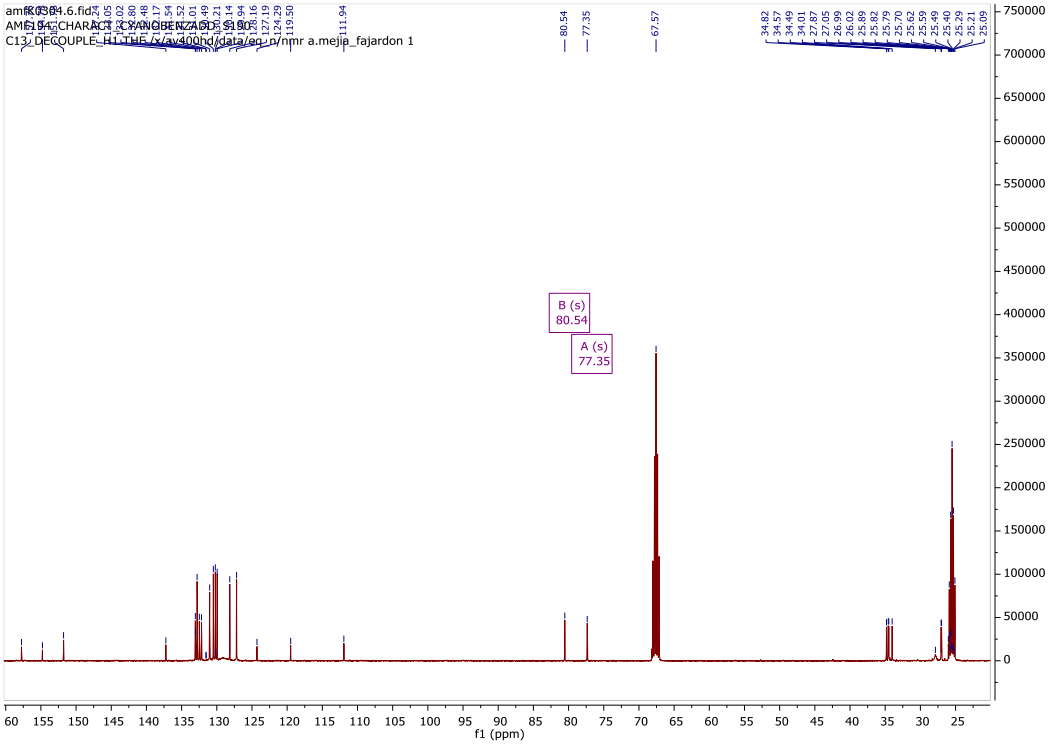

Figure 153. ^{13}C NMR spectrum observed for 15.

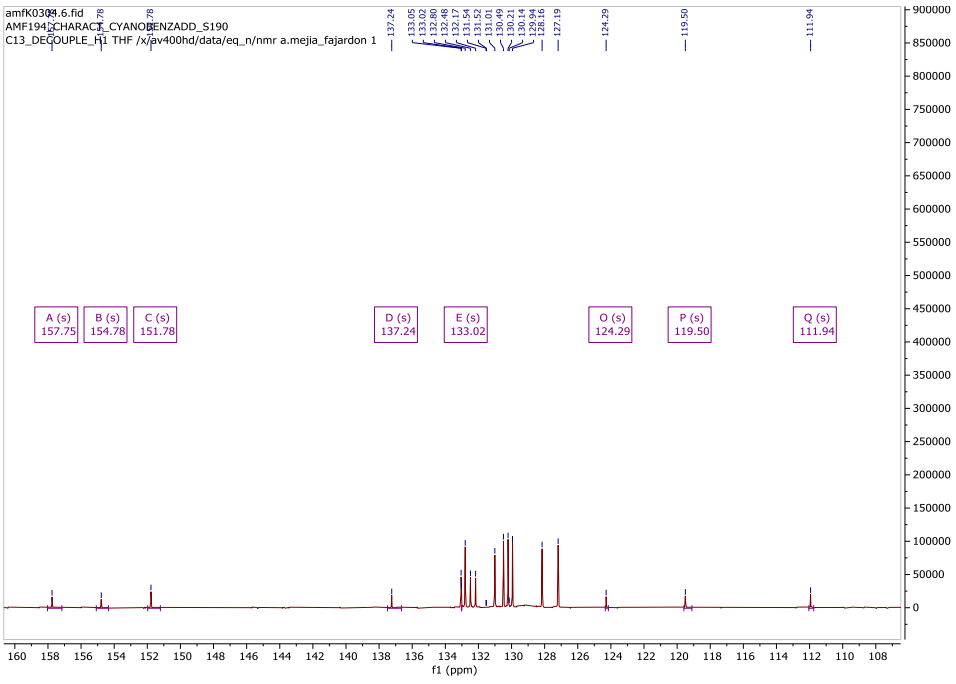

Figure 154. ^{13}C NMR spectrum observed for 15. Zoom on the 108 to 159 ppm area to emphasize the quaternary aromatics.

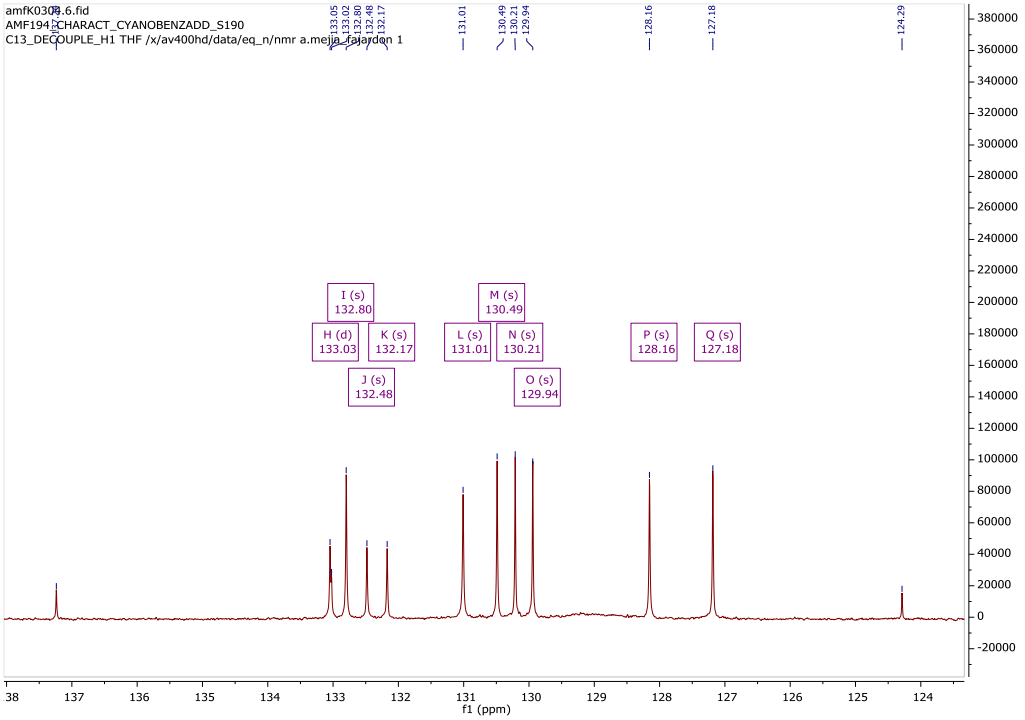

Figure 155. ^{13}C NMR spectrum observed for 15. Zoom on the 123 to 138 ppm area to emphasize the aromatic carbons.

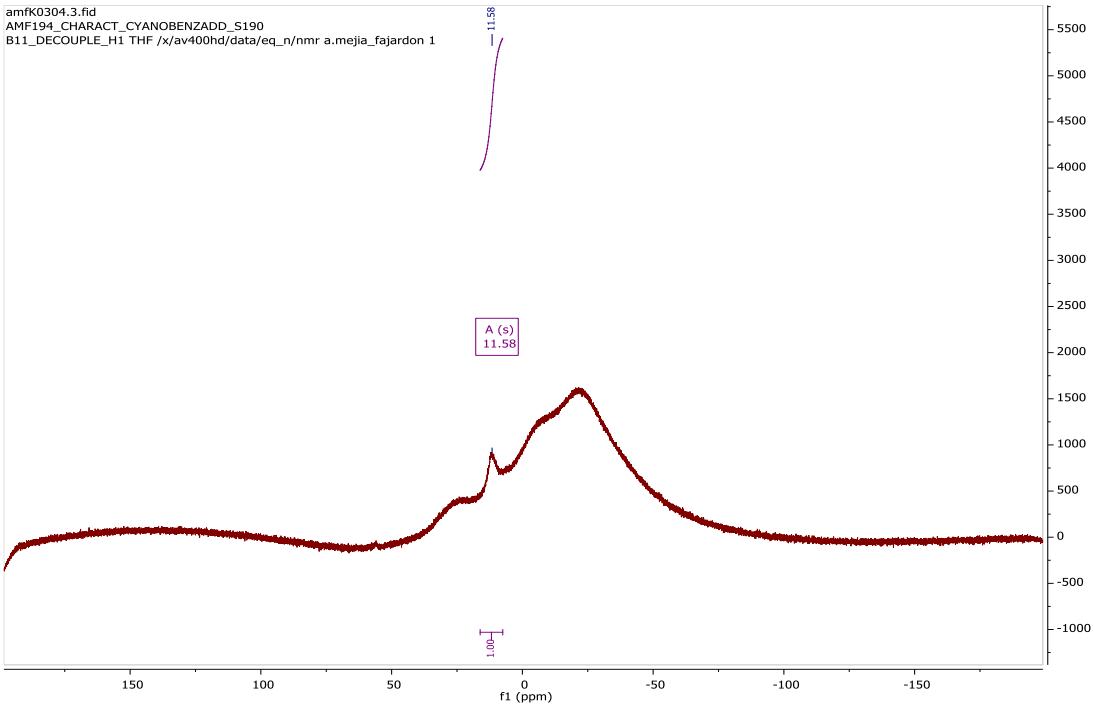

Figure 156. 11B{1H} NMR spectrum of **15** at 298 K in THF-d8.

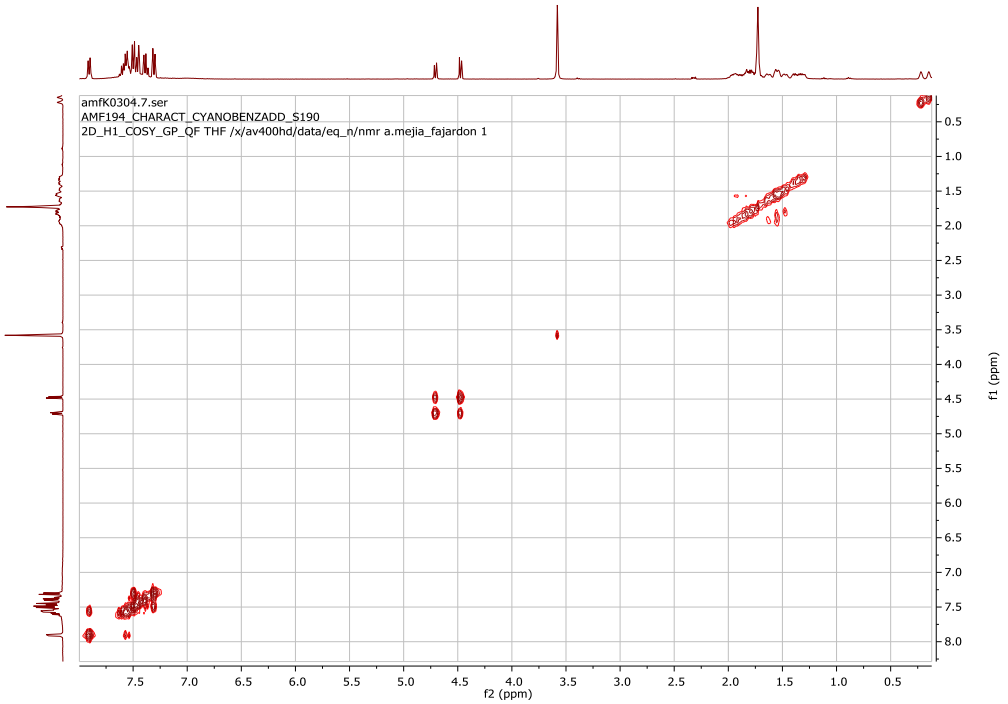

Figure 157. ^{1}H / ^{1}H NMR COSY experiment at 298 K for compound **15** in THF-d8.

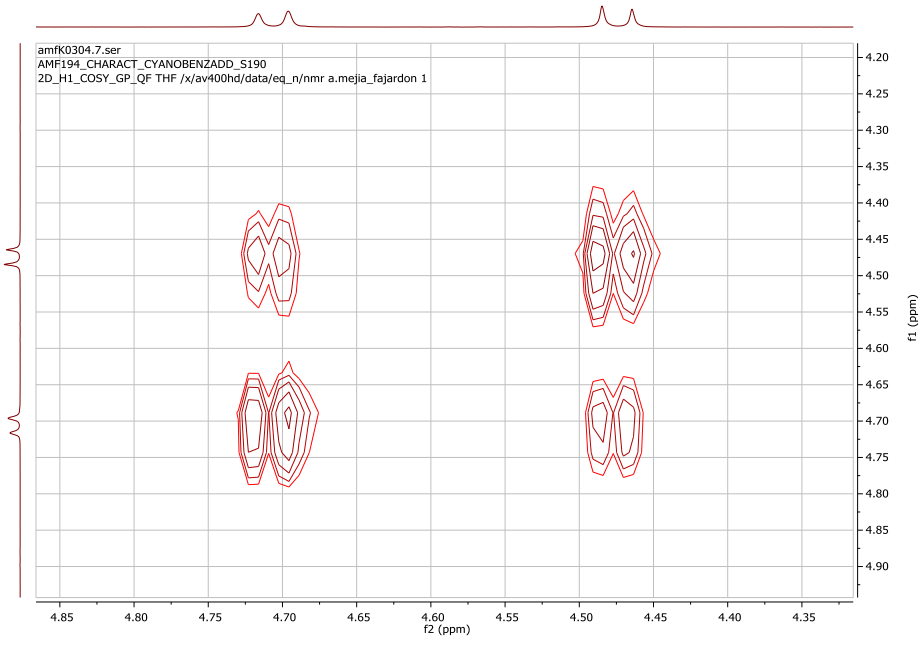

Figure 158. ^{1}H / ^{1}H NMR COSY experiment at 298 K for compound **15** in THF-d8. Zoom on the 4.3 to 4.9 ppm area.

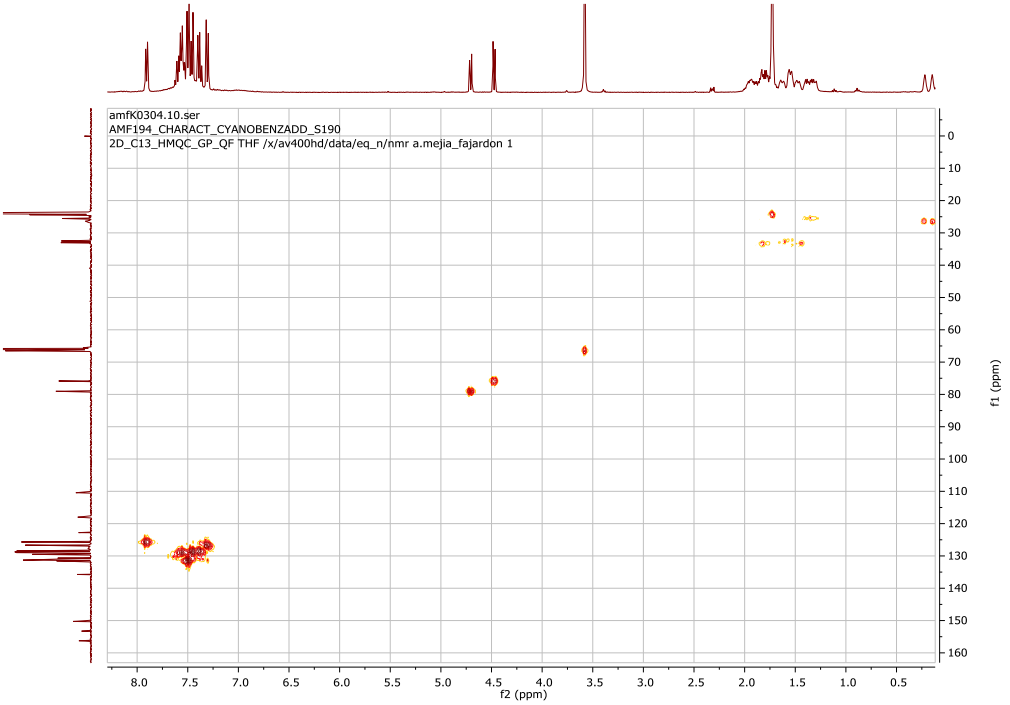

Figure 159. HMQC 13C{¹H}/¹H NMR spectrum of **15** at 298 K in THF-d8.

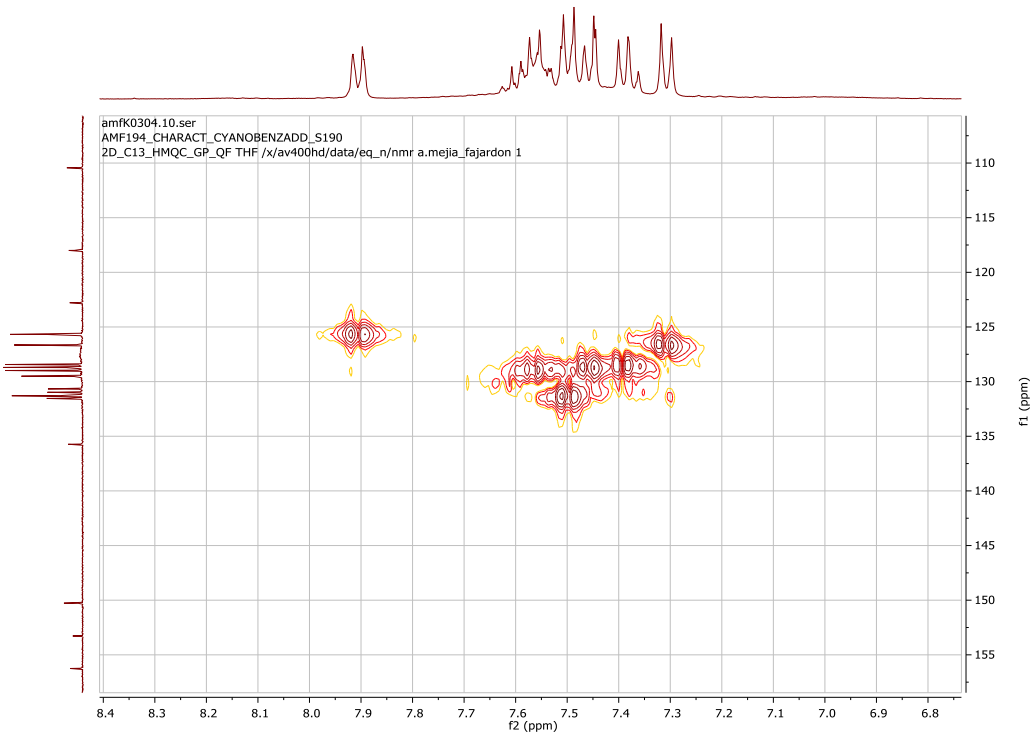

Figure 160. HMQC 13C{¹H}/¹H NMR spectrum of **15** at 298 K in THF-d8. Zoom on the aromatic area

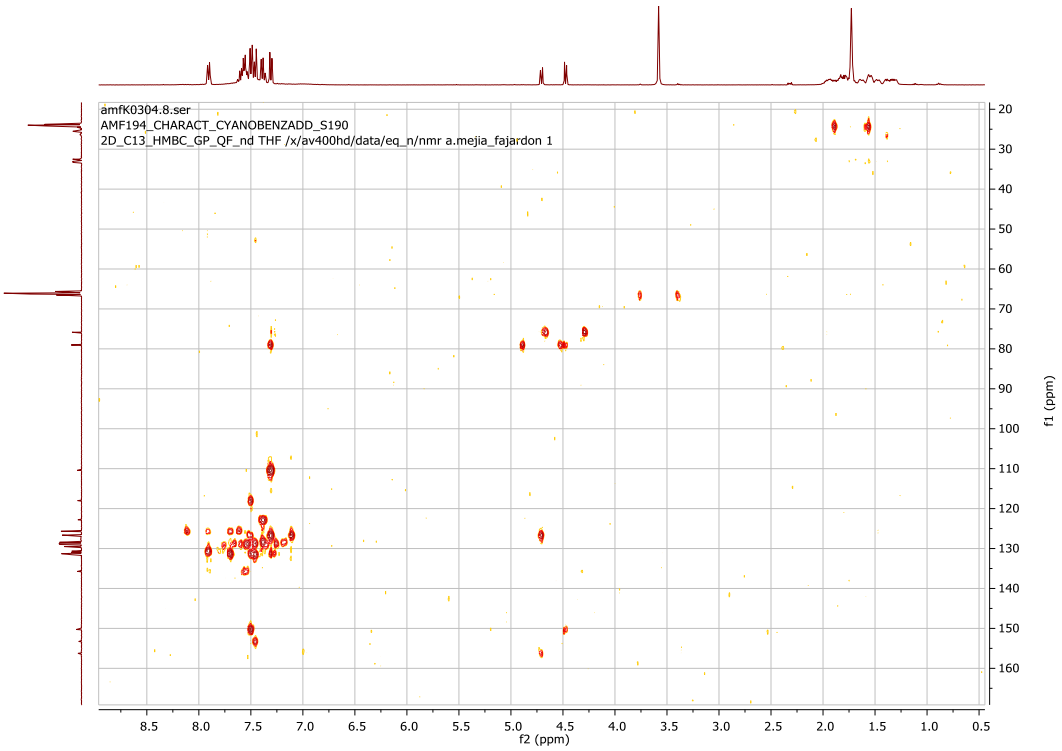

Figure 161. HMBC: long-range $^{13}C\{^1H\}/^1H$ NMR spectrum for **3** at 298 K in THF-d8

Mass Spectra

Monoisotopic Mass, Odd and Even Electron Ions
255 formula(e) evaluated with 3 results within limits (all results (up to 1000) for each mass)
Elements Used:
C: 0-100 H: 0-100 B: 1-1 N: 0-5 O: 0-5

DCI-CH4
20191008-AMF205-10 31 (0.517) Cm (31:33-122:123x5.000)

GCT Premier CAB109

08-Oct-201911:17:47
TOF MS CI+
6.51e+002

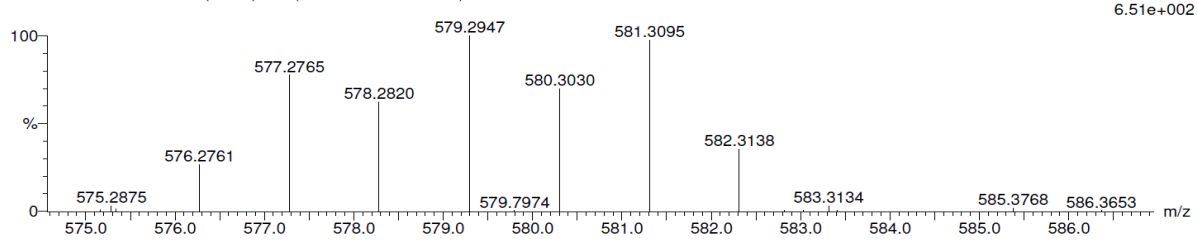

Minimum:				-1.5	
Maximum:		1.4	5.0	50.0	
Mass	Calc. Mass	mDa	PPM	DBE	i-FIT
579.2947	579.2972	-2.5	-4.3	26.5	265.4

Figure 162. ESI DCI-CH4 mass spectrum for compound **3.**

8. IR COMPOUNDS

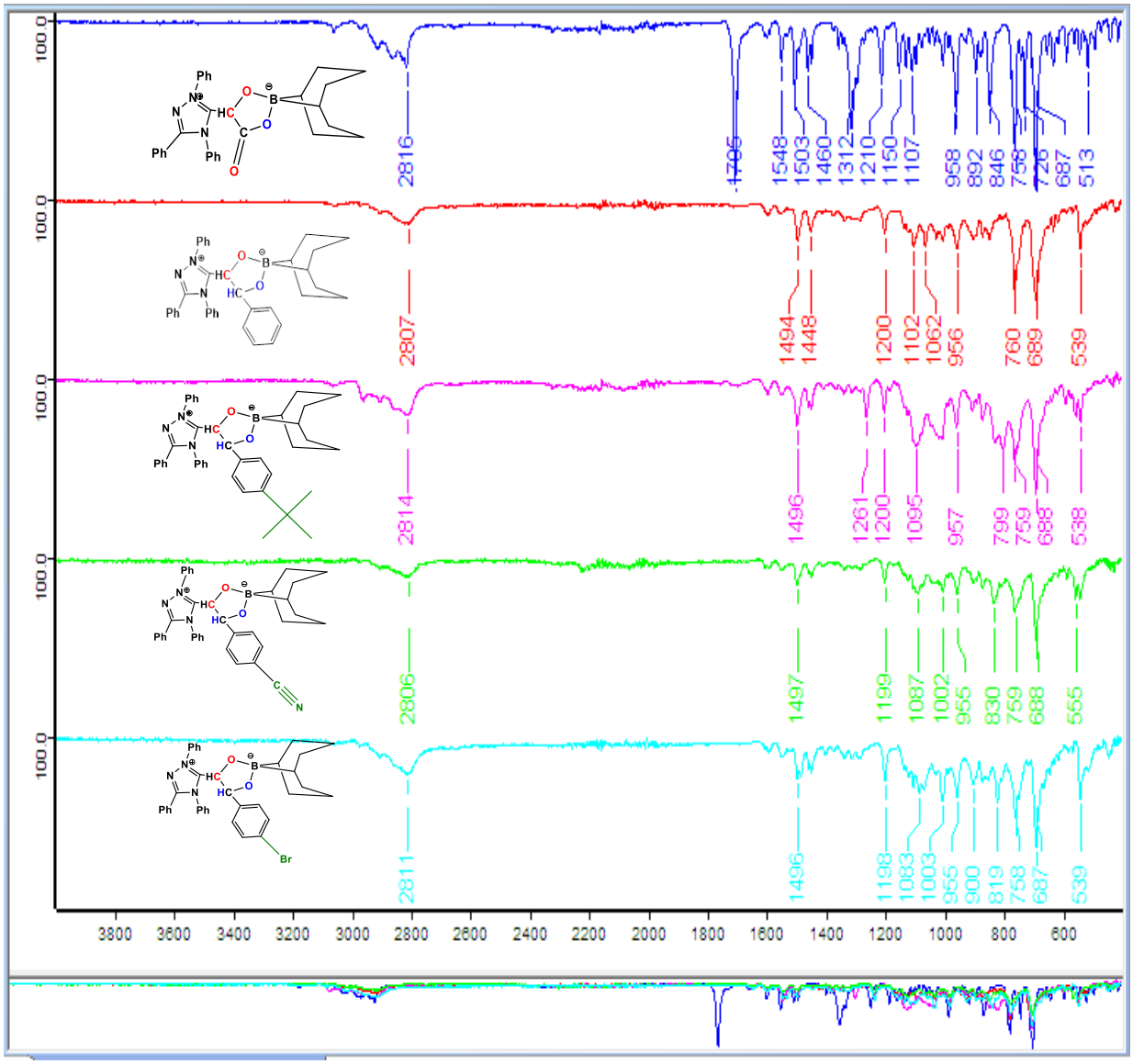

Figure 163. Powder ATR-FTIR spectrum for compounds 1, 3, 5, 15 and 11.

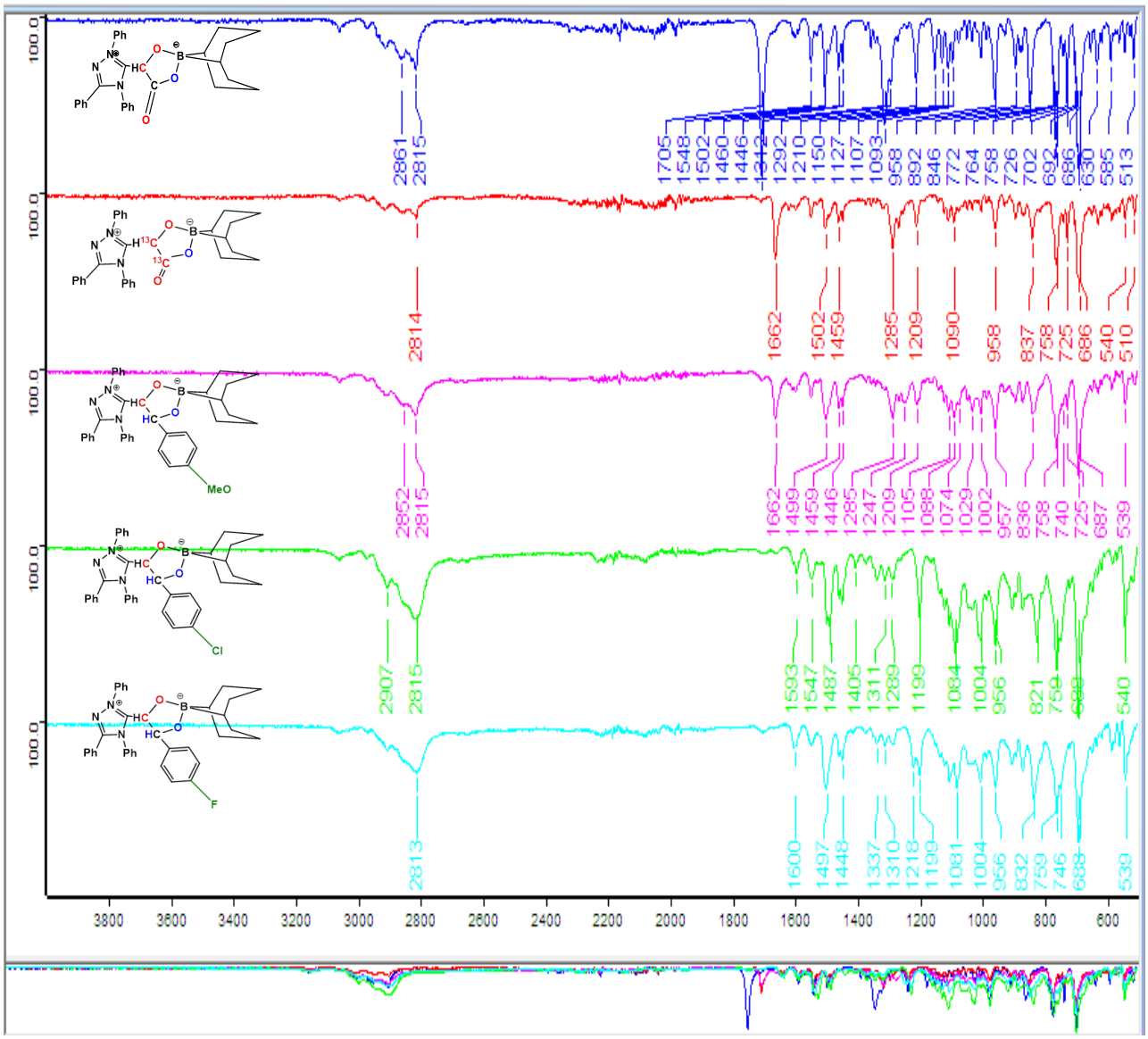

Figure 164. Powder ATR-FTIR spectrum for compounds 1, 7, 9 and 13.

RÉSUMÉ DÉTAILLÉ

NOUVEAU TYPE DE PAIRES DE LEWIS FRUSTREÉS (FLP) POUR L'ACTIVATION INTRAMOLÉCULAIRE DIASTÉRÉOSÉLECTIVE DES ALDÉHYDES

RÉSUMÉ

INTRODUCTION

La surexploitation des combustibles fossiles a entraîné un excès de dioxyde de carbone dans l'atmosphère, créant un déséquilibre dans le cycle du carbone. En conséquence, l'augmentation de la température mondiale et l'acidification des océans ont eu un impact direct sur tous les écosystèmes et, par conséquent, sur l'économie et la qualité de la vie humaine. [1] Des accords internationaux ont été conclus pour atténuer ces émissions. Le plus pertinent, l'Accord de Paris, la 21e Conférence des Parties (COP 21) de la Convention-cadre des Nations Unies sur les changements climatiques (CCNUCC), a été adopté le 12 décembre 2015.[2] Lors de cette réunion historique, pour la première fois, 195 nations ont convenu de limiter l'augmentation de la température moyenne mondiale au cours de ce siècle à bien moins de 2 degrés Celsius et d'être neutre en carbone au plus tard dans la seconde moitié du siècle - tous ces pays bénéficiant d'un financement et d'obligations internationales avec des actions spécifiques.

Dans ce contexte, la communauté scientifique est poussée à trouver de nouvelles possibilités et méthodes de capture et de réduction du dioxyde de carbone pour le stockage de l'énergie. [3,4] Dans le domaine de la chimie, l'approche pour la résolution de ces nouveaux défis liés au changement climatique s'oriente vers des solutions de chimie verte et durable, visant à concevoir et synthétiser des produits compétitifs en termes de coûts avec de meilleurs processus, en réduisant la pollution. Parmi ces principes, citons la prévention des déchets, la réalisation de synthèses moins dangereuses, la conception pour l'efficacité énergétique, l'utilisation de matières premières amovibles, la réduction des dérivés et l'amélioration de la catalyse par rapport à la stœchiométrie, entre autres. [5,6]

Le présent travail s'inscrit dans le cadre du Groupe d'Activation des Petites Molécules (SmAC), Laboratoire de Chimie de Coordination LCC-CNRS. Ce groupe étudie les principes fondamentaux de la catalyse homogène et les performances de leurs réactions, en activant des molécules abondantes et stables comme le dioxyde de carbone, l'oxygène, le dioxyde de carbone azoté, et d'autres types de

matières premières facilement disponibles, notamment le formaldéhyde, les alcanes, les alcènes et les aromatiques simples. À cet égard, l'équipe pourrait fournir des études fondamentales pour réduire l'empreinte écologique et améliorer le stockage d'énergie.

Les systèmes de paires de Lewis frustrées (FLP) sont un nouveau concept dans la chimie verte en raison de leur capacité à fonctionner comme un catalyseur sans métal pour l'activation de petites molécules comme l'hydrogène,[7] le dioxyde de carbone, les aldéhydes et toutes sortes de petites molécules. Bien que l'un des résumés les plus marquants du développement et des perspectives de la FLP ait été une revue de Stephan en 2015,[8] le domaine s'est considérablement développé depuis. Ces systèmes ont trouvé de nouvelles réactivités dans des conditions douces, ce qui les rend attractifs pour une solution de processus chimique pratique et sûr.

Le présent document vise à étudier la réactivité et l'utilisation potentielle de l'adduit du CO_2 = composé **1** (figure 1) (nommé ainsi car il provient de 2 molécules de CO_2). Cette molécule est particulièrement fascinante en raison de ses caractéristiques qui incluent :

Une base de Lewis à base de carbone qui ne provient pas d'un carbène, **F1**.

Un acide de Lewis, le borane **F2**.

Ces caractéristiques ont conduit à explorer l'utilisation potentielle du composé comme un nouveau système FLP, mentionné par le groupe de Bontemps [9], donnat lieu à des questions à aborder dans le présent travail (Figure 1) :

Peut-on le considérer comme une forme **Q1** de FLP masquée ?

Pourrait-il avoir le potentiel d'activer de petites molécules telles que les fonctions carbonyles **Q2** ?

Le chapitre 1 présente deux sections principales. La première porte sur les concepts généraux qui seront utilisés au cours de la présente étude. La deuxième partie concerne l'état de l'art, y compris les réactions et les publications les plus pertinentes.

Le chapitre 2 est divisé en deux parties essentielles. La première est consacrée à l'exploration du champ de réactivité des adduits du CO_2 avec les fonctions polaires et carbonyles et à la synthèse de

nouveaux composés. La seconde est consacrée à l'étude électronique et cinétique de la réaction de l'adduit du benzaldéhyde.

Le chapitre 3 est la compilation expérimentale de la présente étude.

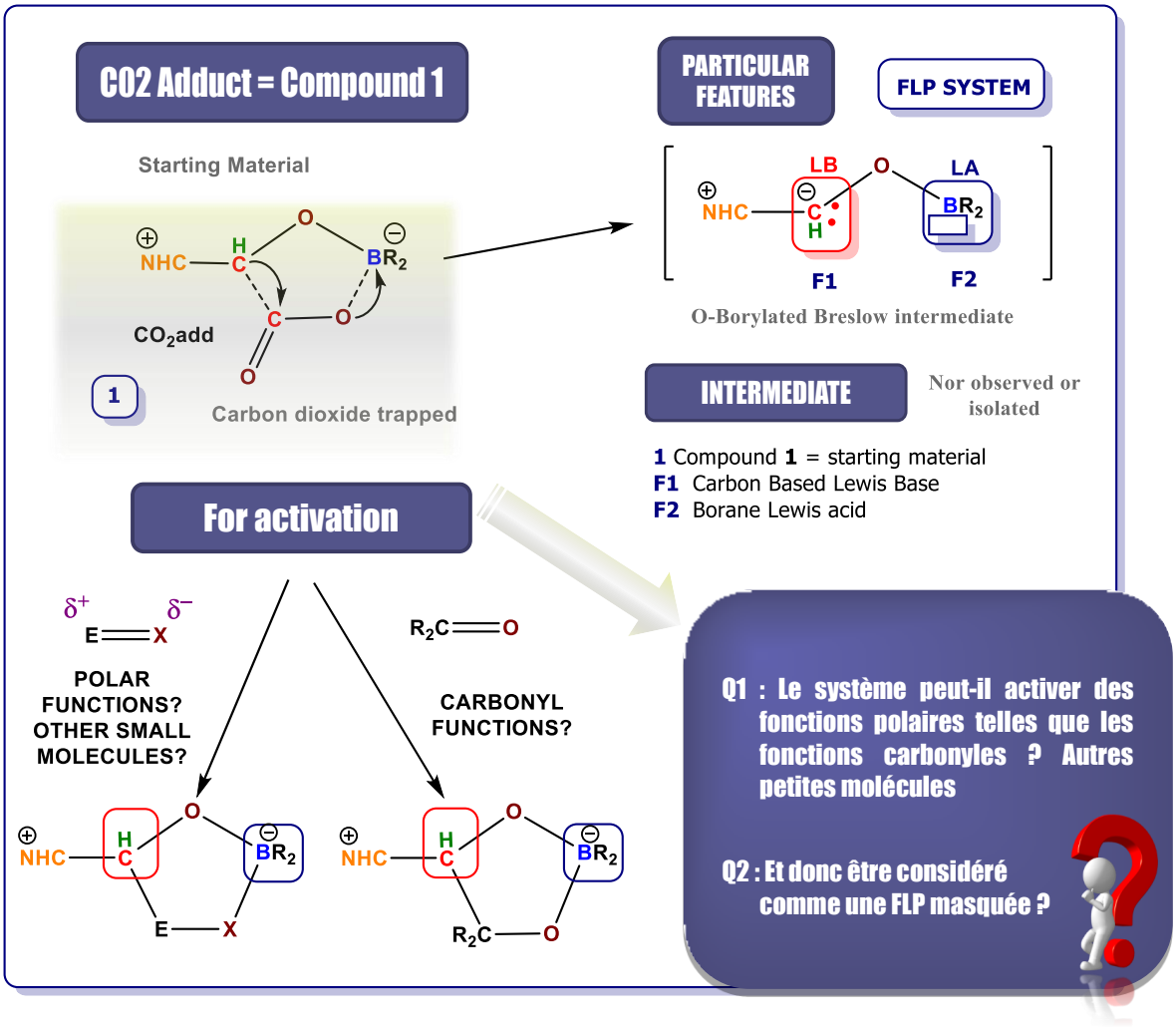

Figure 1. Adduit de CO2 = Composé 1. Nouvelle activation potentielle de type FLP et ses caractéristiques particulières.

Le présent travail étudiera une version de l'intermédiaire de Breslow, l'intermédiaire de Breslow O-Borylé (**OBB**), masqué dans le produit **1** (Figure 2). Cet intermédiaire, qui contient du bore d'une part et le triazol-5-ylidène carbène (également connu sous le nom de Enders carbène) d'autre part, donne un carbone nucléophile dans un site et du bore acide dans l'autre, fournissant une paire acide-base de Lewis.

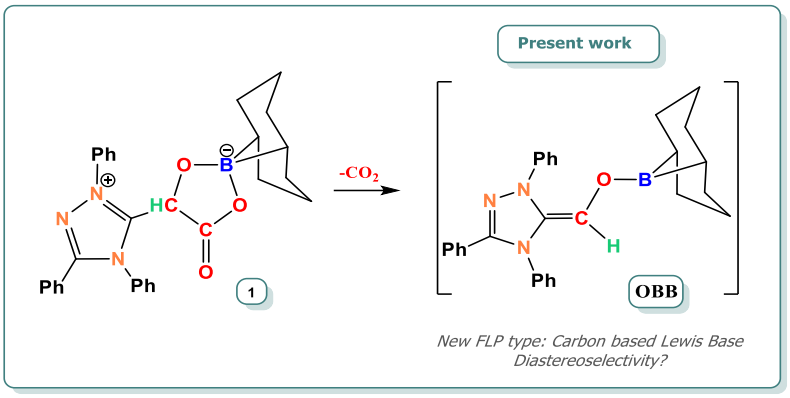

Figure 2. Intermédiaire de Breslow O-borylé masqué dans le produit 1.

CHAPITRE I : CONCEPT DE FLP ET ÉTAT DE L'ART

D'une manière générale, les FLP peuvent être classées en deux groupes principaux : les systèmes intermoléculaires et intramoléculaires (Figure 3). Essentiellement, le système intermoléculaire est une réaction bimoléculaire entre l'adduit et la molécule à activer, contrairement au système intramoléculaire, qui fait référence à la molécule qui présente une interaction interne de la paire de Lewis. [10]

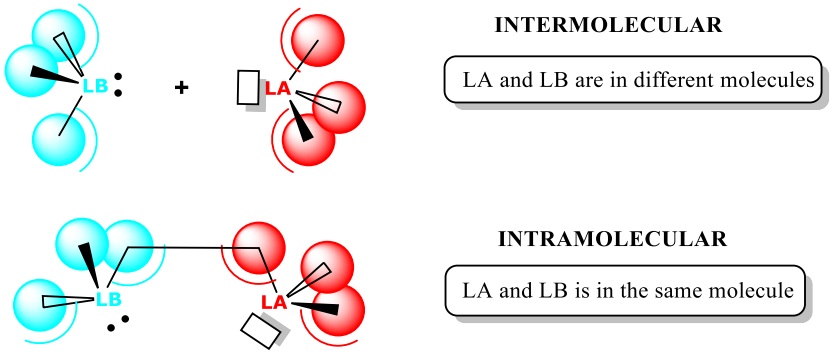

Figure 3. Schéma général de la FLP intermoléculaire et intramoléculaire.

3.6. Activation des aldéhydes

L'une des premières études concernant l'activation des aldéhydes par une FLP a été réalisée par Momming *et al.* (2009). [11] Le benzaldéhyde **I-46** et le cinnamaldéhyde **I-48** sont toutes deux des molécules polaires qui pourraient potentiellement réagir avec ce système FLP intramoléculaire **I-45**. Cependant, cette réaction d'addition (Figure 4) a montré une compétition directe entre les deux

aldéhydes, fortement entraînée vers le trans-cinnamaldéhyde, donnant le produit **I-49** plutôt que **I-47**. L'effet de résonance sur le cinnamaldéhyde pourrait expliquer cette réactivité, car ce dernier présente six structures de résonance (une de plus que le benzaldéhyde), fournissant un carbocation plus stable et favorisant ainsi le produit **I-49**.

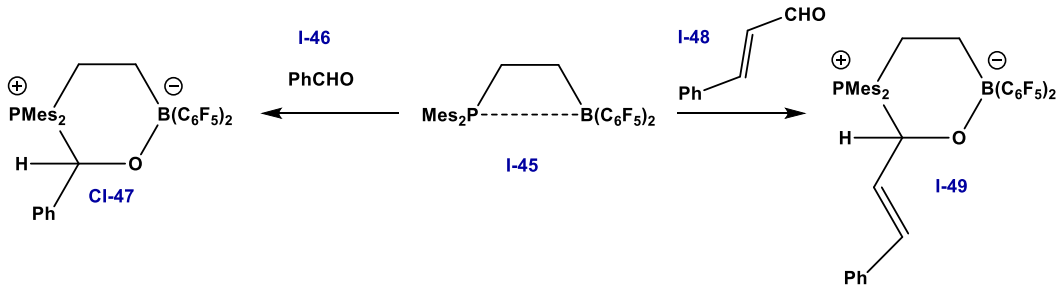

Figure 4. Système FLP avec benzaldéhyde et cinnamaldéhyde.

3.7. Base de Lewis à base de carbone

Ce groupe est constitué principalement des réactifs NHC et des composés suivants : les énamines et les ylures. Ils apportent un effet de résonance dans les structures, délocalisant les charges, et donnant des composés plus réactifs (Figure 5). Les ylures donnent des bases plus fortes, ce qui implique une application plus large que les énamines dans ce domaine. [12]

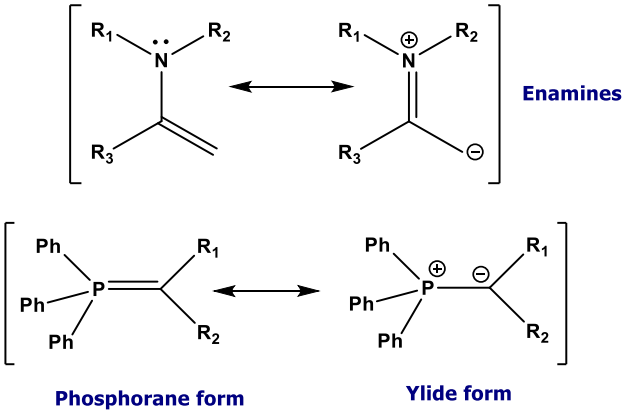

Figure 5. Formes de résonance des ylures et des énamines de phosphore.

En 2017, Erker et ses collègues[12,13] ont formé un système FLP C/B **I-52** avec une diénamine conjuguée (énamine) et le borane de Piers, activant de petites molécules telles que des nitriles, du dioxyde de soufre et du benzaldéhyde.

I-51 et **I-52** réagissent avec le benzaldéhyde **I-53** pour donner le produit **I-54**, par une formation de liaisons B-O et C-O. Ce type de liaisons peut être comparable au présent travail où le **composé 1** est généré par une formation de liaisons B-O et C-C lorsqu'il interagit avec le CO_2 et pourrait potentiellement réagir avec d'autres fonctions carbonyles. **I-54 a** produit différents stéréoisomères en raison de l'interaction stérique plus faible **I-54**, dans laquelle la configuration trans-CH-CH est obtenue (Figure 6).

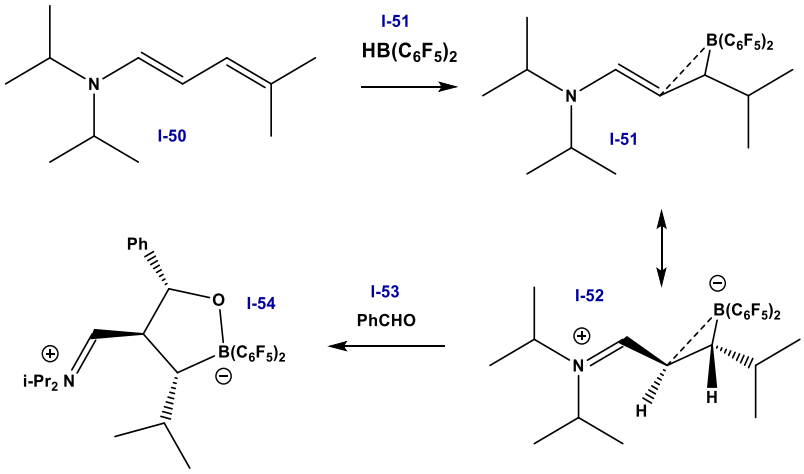

Figure 6. Système FLP avec du benzaldéhyde.

3.8. Les carbènes comme Bases de Lewis carbonées

Bertrand et ses collègues (2007),[14] Stephan (2008,[15] 2009[16]), et Tamm (2008)[17] ont travaillé sur l'interaction Carbènes/Boranes, notamment pour l'activation de H_2. Cependant, Stephan et Tamm, ont rapporté que la réaction entre $B(C_6F_5)_3$ et **I-55,** en présence d'hydrogène, forme une FLP **I-56** à basse température. Tamm et ses collègues ont décrit que si la réaction carbène/borane est effectuée à température ambiante en utilisant le THF au lieu de l'hydrogène, on obtient **I-53** (Figure 7). Cette réaction intermoléculaire pourrait donner la FLP à 20°C.

Sans surprise, les substituants *N* de ces bases de Lewis fortes sont dirigés vers la paire libre du carbène, générant une "pression stérique" significative. Lorsque $B(C_6F_5)_3$ est ajouté, l'interaction de ces systèmes conduit à une activation C-H en position 4 avec la formation irréversible d'une liaison B-C forte.

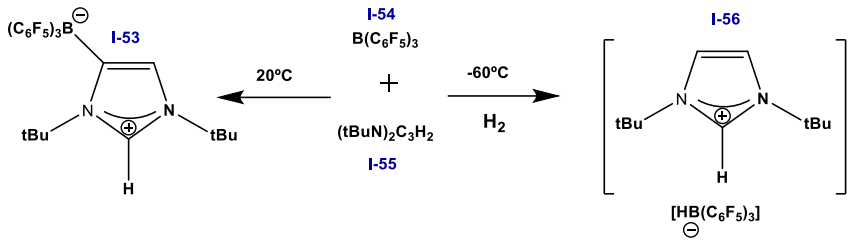

Figure 7. Réactions entre les carbènes et $B(C_6F_5)_3$.

Bien que la fixation du CO_2 soit largement utilisée dans les systèmes FLP phosphine/borane, il n'y a que quelques exemples avec les systèmes carbène/borane. Le système le plus appliqué **I-57**a été décrit par le groupe de Louie[18], qui a pu capturer le CO_2 avec un bon rendement. Cependant, il n'était pas assez stable au-dessus de 71°C. D'autre part, l'équipe de Tamm en 2012[19] a reporté un adduit **I-58** où le CO_2 est piégé par un système carbène/borane. Cet adduit était remarquablement stable en solution et à l'état solide (Figure 8).

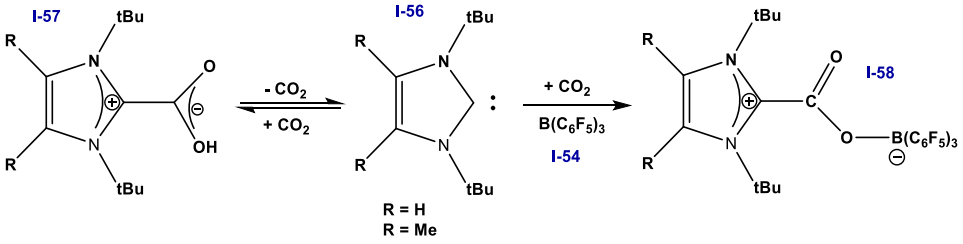

Figure 8. Réactions avec des carbènes.

3.9. *Systèmes FLP masqués*

Les systèmes FLP masqués sont des complexes intramoléculaires qui contiennent l'acide de Lewis et la base de Lewis, mais qui ne peuvent être vus comme un système FLP que lorsque la molécule activée est piégée. [20] Ce type de système est connu pour être instable jusqu'à ce qu'il forme le produit et n'est pas facile à isoler. Un exemple est le complexe **I-59,** qui forme une paire de Lewis classique entre le phosphore et l'aluminium. [21] Cependant, ce complexe est en équilibre avec une forme ouverte sans

l'interaction de la paire de Lewis. L'équilibre est largement déplacé vers la formation de la paire de Lewis, mais en présence de CO_2, les formes ouvertes se comportent comme un système FLP. Ceci conduit à deux isomères, avec une configuration cis (**I-60**) et une configuration trans (**I-61**). Cette FLP peut activer de petites molécules dipolaires comme l'isocyanate de phényle et le dioxyde de carbone. Dans le cas du dioxyde de carbone, deux isomères sont générés, les composés **I-60** et **I-61**. Le **I-60** comprend une disposition *cis* de Al et H au niveau de la liaison C=C, tandis que le **I-61** a une configuration *trans* (Figure 9). Cela montre que le système FLP peut dériver d'un complexe acide-base de Lewis classique, qui ne présente aucune preuve de dissociation et peut afficher un comportement de système FLP masqué.

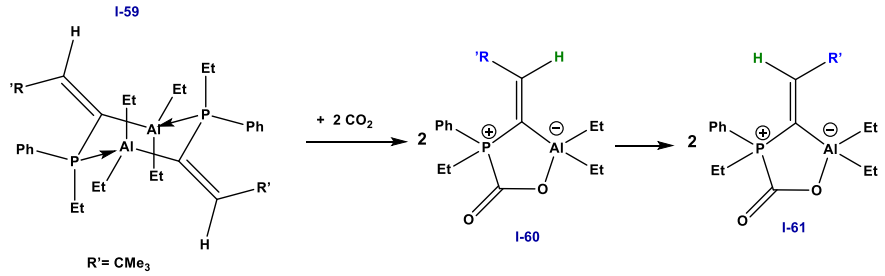

Figure 9. Système FLP masqué avec CO_2.

HYPOTHÈSE: ÉTUDE SUR LES ESPECES POTENTIELLES DE TYPE FLP MASQUEES INTRAMOLECULAIRES

Comme nous l'avons vu dans le premier chapitre, en 2019, Bontemps et ses collègues[9] suggèrent que le **composé 1**, peut-être formé via la formation transitoire de l'intermédiaire O-borylé de Breslow en raison de sa nature ambiphile, piège le dioxyde de carbone, avec unebase de Lewis carbonée et le bore comme acide de Lewis (figure 10).

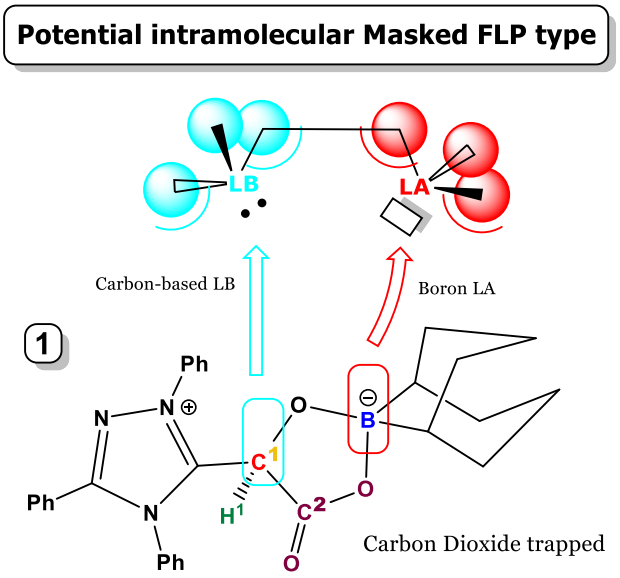

Figure 10. Système FLP intramoléculaire potentiel. Bleu : Base de Lewis à base de carbone ; rouge: acide de Lewis à base de bore.

CHAPITRE II : CHAMP D'APPLICATION DE LA RÉACTIVITÉ DE COMME SYSTÈME FLP

2.1. Synthèse du système FLP

Le composé **1** a été préparé selon le protocole décrit dans le groupe[9] en deux étapes principales. La première partie comprend la double hydroboration du CO_2 à partir de 2 équivalents de **9-BBN** sous CO_2 dynamique à température ambiante. 1 % de catalyseur au fer **FeCat** a été nécessaire pour obtenir le produit de réduction à 4e- **BBA**.

Le carbène d'Enders **E-carb** est ajouté pour l'étape de couplage C-C dans un rapport stœchiométrique à 60°C sous CO_2 dynamique. Pour obtenir le produit, il est lavé avec Et2O et filtré. Le solide blanc obtenu comme résidu est le composé pur (rendement= 50%).

Néanmoins, des ajustements du temps de réaction ont été nécessaires afin de pouvoir préparer davantage de matière première. Dans l'étape de couplage C-C, le temps a été modifié de 60 min à 120 min. Avec cette nouvelle procédure, l'adduit a pu passer de 318 mg à 3 grammes. Le carbène d'Enders nécessaire à la préparation de **1** a été produit au laboratoire (Figure 11).

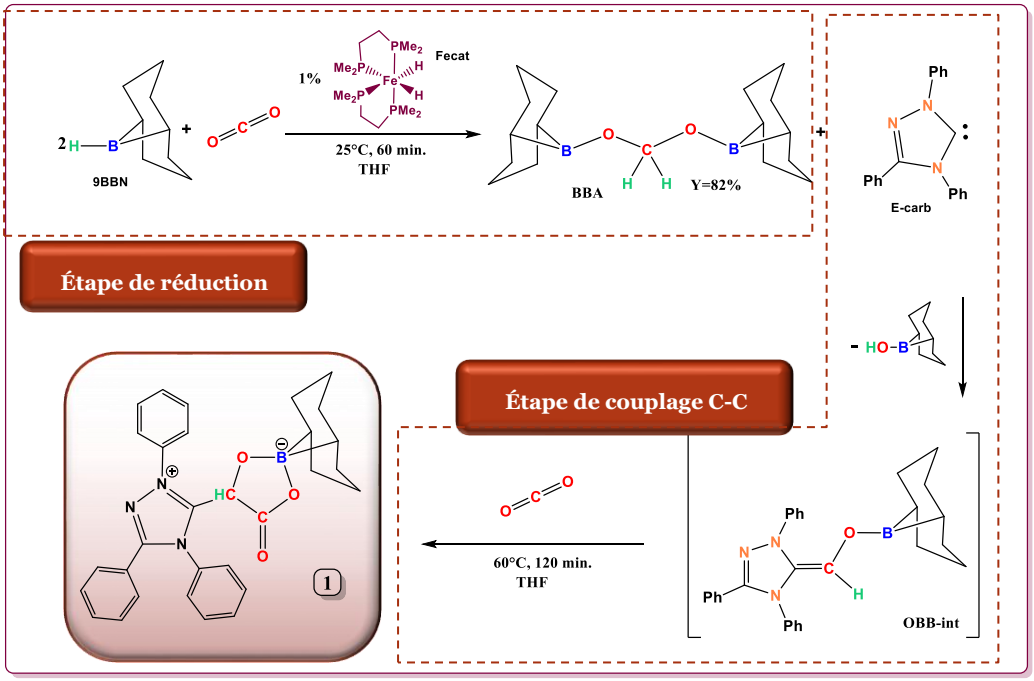

Figure 11. Produit de synthèse 1. Protocole utilisé dans le présent travail.

2.2. Réactivité avec les petites molécules

Dans le but de corroborer cette hypothèse (Système FLP intramoléculaire potentiel), différentes petites molécules telles que des alcynes, des cétones, des aldéhydes, des oléfines et d'autres petites molécules ont été utilisées pour le test d'activation.

En résumé, après avoir essayé les différentes fonctions (figure 12), le groupe fonctionnel carbonyle -CHO correspondant aux aldéhydes (figure 12) est activé avec succès. Le système piège l'aldéhyde et libère la molécule de dioxyde de carbone piégée. Cette réaction de substitution, spécifique au benzaldéhyde, confirme que le **composé 1** pourrait être considéré comme un nouveau type de FLP instable pouvant activer les aldéhydes de manière chimiosélective .

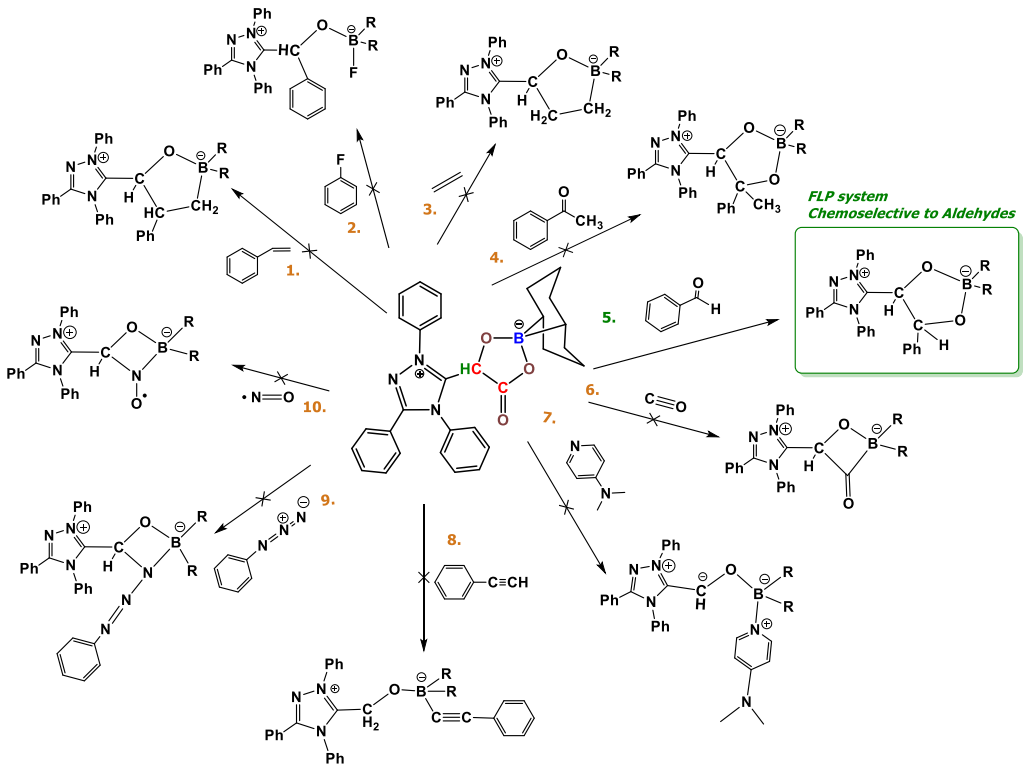

Figure 12. Petites molécules essayées avec le système FLP. Chimiosélectivité vis-à-vis des aldéhydes.

Sur la figure 13, il est possible d'observer la formation d'un nouveau produit. La réaction entre **1** et le benzaldéhyde (**2**) révèle l'apparition de deux nouveaux doublets à δ 4,44 et δ 4,67 avec une constante de couplage $^{3}J_{HH}$ de 8,2 Hz.

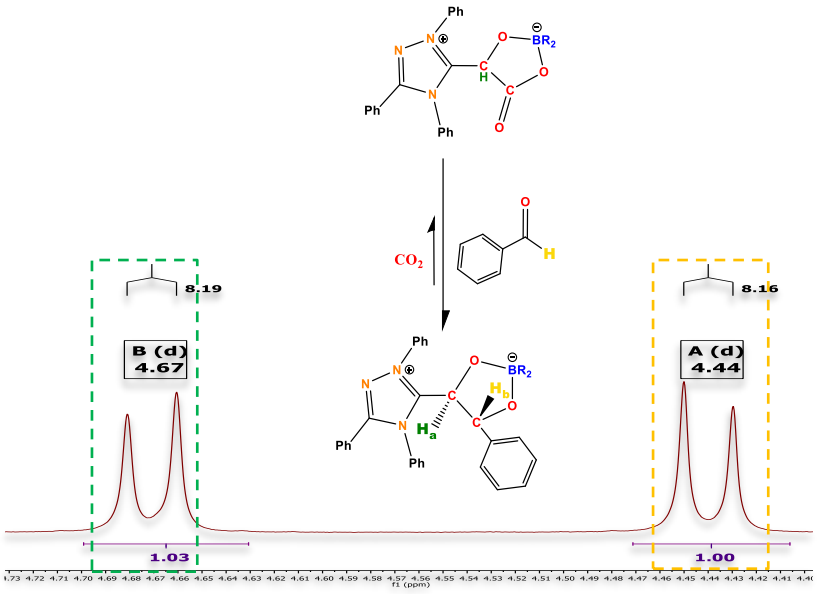

Figure 13. Réaction et détection spectrométrique du composé 1 avec le benzaldéhyde.

Ce jeune domaine des systèmes FLP a proliféré rapidement, donnant lieu à des découvertes remarquables dans l'activation de petites molécules. Nous avons montré que la chimie des FLPs moderne va au-delà de l'activation de dihydrogène et de la catalyse d'hydrogénation. Ce type de FLP élargit l'utilisation des études de bases de Lewis à base de carbone qui ne proviennent pas directement d'un carbène, une caractéristique unique de ce système, ouvrant de nouvelles options pour l'activation de petites molécules dans la chimie verte.

2.3. Champ d'application des aldéhydes : Réaction de référence

Pour comprendre la réactivité du nouveau type de FLP, entre l'acide et la base de Lewis avec le CO_2 et les aldéhydes, la réaction avec le benzaldéhyde a été prise comme référence (Figure 14) pour développer une méthodologie qui fonctionne comme un modèle à étendre à d'autres aldéhydes.

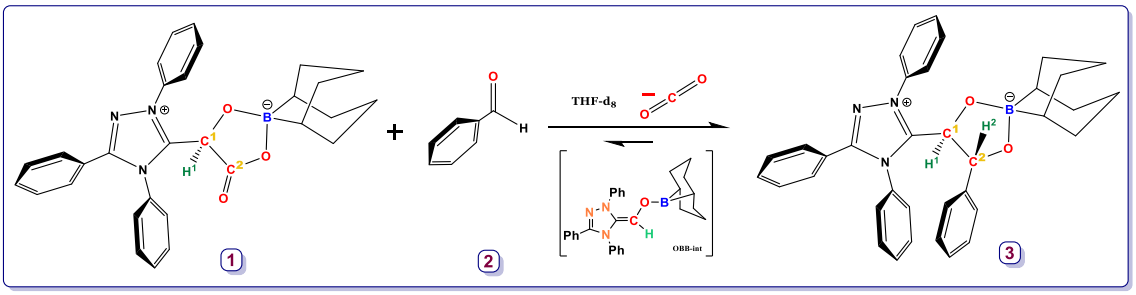

Figure 14. Réaction de référence.

L'étude cinétique sur la réaction de référence comportera les études à température ambiante (RT) avec un rapport stœchiométrique et des conditions de pseudo-ordre et les études à différentes températures pour comprendre l'effet de la température sur la constante de vitesse et permettant d'accéder aux paramètres d'activation $\Delta G^{\ddagger}$, $\Delta S^{\ddagger}$, et $\Delta H^{\ddagger}$. La deuxième partie étudiera les effets électroniques sur la réaction de référence, en modifiant les substituants sur le phényle du benzaldéhyde, fournissant un nouvel ensemble de réactions avec leurs synthèses et caractérisations respectives. La réaction dans des conditions de pseudo-ordre fournira la courbe de Hammett, permettant de comprendre la relation linéaire de l'énergie libre relative à la vitesse de réaction et à la constante d'équilibre.

Les études complémentaires ont été choisies pour approfondir les connaissances possibles sur la réactivité et le mécanisme.

2.4. Étude cinétique

Le modèle (Figure 15) pour le pseudo-premier ordre a expliqué 99,9 % des données cinétiques de **2** (benzaldéhyde) dans des conditions de pseudo-ordre. Ce résultat indique que les deux réactifs présentent un pseudo premier ordre pour une réaction globale d'ordre 2. En reprenant l'équation 1 :

Loi de vitesse = k [réactif 1]^{n} [réactif 2]^{m}

Où n=1 ; m= 1

Loi de vitesse = kr[réactif 1]^{1} [réactif 2]^{1}

Ordre de réaction global = n+m = 2

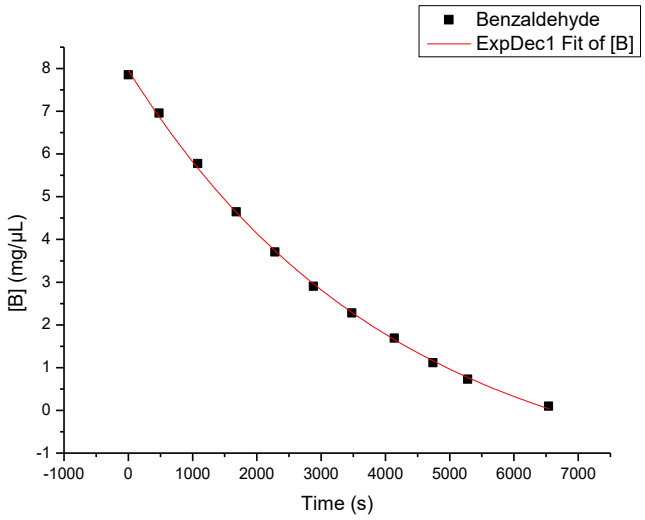

Equation	y = A1*exp(-x/t1) + y0		
Adj. R-Square	0,9992		
		Value	Standard Error
[B]	y0	-2,0327	0,232
[B]	A1	9,99284	0,21022
[B]	t1	4153,41852	184,50033

Figure 15. Analyse mon-exponentielle par ajustement des moindres carrés non linéaires avec l'équation proposée. La ligne rouge indique le modèle théorique avec une itération et les points noirs les données réelles.

Cette dépendance du résultat suggère que l'étape cinétiquement déterminante (rate-determining step , rds) implique une molécule de réactif **1** et une molécule de réactif **2**, soit une étape élémentaire. Cependant, il n'est pas possible de savoir si d'autres étapes élémentaires sont impliquées dans le mécanisme. Comme il existe un intermédiaire dans cette réaction, il est possible qu'il s'agisse d'une étape rapide et qu'elle ne puisse pas être observée.

L'énergie libre d'activation de Gibbs ($\Delta G^{\ddagger}$) pour l'adduit benzaldéhyde **3** est de 22,6 kcal/mol K à 25°C (298 K).

L'enthalpie, qui fait référence à la chaleur de la réaction, est de 17,7 kcal/mol, ce qui est en accord avec la réactivité à des températures douces. L'entropie associée à l'état de désordre pour le produit d'addition du benzaldéhyde est sensiblement négative (-16,2 kcal/mol) comme prévu

avec la formation du produit et suggère une étape cinétiquement déterminante de type associative.

2.4.1. Étude électronique : Analyse comparative

Afin d'étudier les effets électroniques sur la réaction de référence, il a été nécessaire de modifier les substituants sur le phényle du benzaldéhyde pour obtenir la relation entre les vitesses de réaction et les constantes d'équilibre par le biais du diagramme de Hammett. On a sélectionné 6 substituants différents : *t*Bu, MeO, F, Cl, Br, et CN.

La réaction met plus de temps à se terminer dans le cas de groupes attracteurs d'électrons (GAE) et les produits sont moins stables pour l'isolation. Tous les produits présentent la sélectivité pour les diastéréoisomères *trans* avec des constantes de couplage entre $^{3}J_{H\text{-}H}$ 8,0 et 8,2 Hz, une gamme étroite de +/- 0,2 Hz (Tableau 1).

Tableau 1. Tableau comparatif des substituants des aldéhydes.

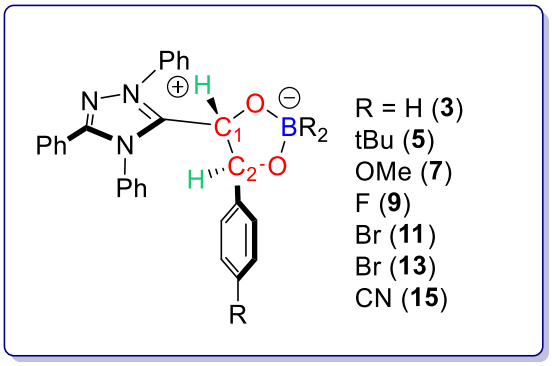

	Rendement (in-situ/isolé)	Temp °C	Temps (h) 1:1 Dans le porter de pêche (en remuant) 100 mg	Temps (h) 1:20 *In situ*	δH C1 et C2	$^{3}J_{HH}$ (Hz)
H (3)	83 % rdt.	25	1h	15.6	4.66 4.40	$^{3JH-H}$ = 8.2 Hz
tBu (5)	85 % rdt.	25	2 h	5	4.66 4.45	$^{3JH-H}$ = 8.2 Hz
MeO (7)	89 % rdt (*in situ*)	25	2 h	1.5	4.37 4.19	$^{3JH-H}$ = 8.1 Hz
F (9)	90% rdt (*in situ*)	25	4h	11.9	4.66 4.46	$^{3JH-H}$ = 8.0 Hz
Br (11)	97% rdt (*in situ*)	25	4h	6	4.62 4.44	$^{3JH-H}$ = 8.0 Hz
Cl (13)	96 % rdt (*in situ*)	25	4h	14.5	4.66 4.47	$^{3JH-H}$ = 8.0 Hz
CN (15)	95 % rdt.	25	2.5h	9.3	4.71 4.47	$^{3JH-H}$ = 8.1 Hz

Comparaisons des structures rayons X

D'une manière générale, les liaisons O-B dans les adduits aldéhydes sont plus fortes (distances plus courtes) que dans **1**, l'adduit avec le CO_2 piégé. Contrairement aux liaisons C-C qui sont plus faibles (plus longues) dans les aldéhydes que dans l'adduit **1**. Les distances des liaisons C-C sont dans les distances habituelles pour une liaison simple (tableau 2).

Tableau 2. Tableau comparatif des distances de cristal.

	COMP 1	COMP 3	COMP 5	COMP 7
LONGUEURS DE LIAISON (Å)				
C1-C2	1.5464(18)	1.5681(15)	1.561(6)	1.578(3)
C2-O2	1.2907(17)	1.3928(13)	1.398(5)	1.399(3)
O2-B	1.5737(18)	1.5150(15)	1.511(6)	1.512(3)
O1B	1.5233(17)	1.5213(14)	1.525(5)	1.527(3)
C1-O1	1.3774(16)	1.3849(13)	1.390(5)	1.390(3)

ANGLES DE LIAISON (°)				
C1C2O2	108.77(10)	103.41(8)	105.3(3)	103.60(16)
C2O2B	111.34(10)	110.96(8)	104.4(3)	111.40(16)
O2BO1	100.5(10)	102.35(8)	102.4(3)	102.15(16)
BO1C1	109.02(10)	105.96(8)	110.8(3)	106.59(16)
O1C1C2	107.45(10)	105.50(8)	102.5(3)	105.30(16)
ΣB	334.5	330.57	332.5	329.17
Anneau à 5 chaînons de Σ	537.12	528.18	525.4	529.04

Σ= somme des angles de liaison intérieurs (anneau spécifié).

2.5. Etude mécanistique : Calcul de la constante de vitesse avec les dérivés du benzaldéhyde

L'impact des benzaldéhydes para-substitués sur la cinétique a été réalisé. Grâce aux informations fournies par la variation du logarithme des constantes de vitesse en fonction des paramètres σ de Hammett[22] des benzaldéhydes sélectionnés (Tableau 3), il a été possible de dessiner le graphe de Hammett à 20 équivalents (Figure 15).

Tableau 3. K, log K, et σp pour les différents dérivés à 10 et 20 équivalents.

EQ	SUBS	σp	[B]mM/µL	K_r($M^{-1}.s^{-1}$)
20	Cl	0,232	$3,39 \times 10^{-4}$	$1,3 \times 10^{-4}$
20	tBu	-0,197	$3,39 \times 10^{-4}$	$5,8 \times 10^{-4}$
20	OMe	-0,268	$3,39 \times 10^{-4}$	$7,8 \times 10^{-4}$
20	CN	0,66	$3,39 \times 10^{-4}$	$1,8 \times 10^{-4}$
20	H	0	$3,39 \times 10^{-4}$	$1,7 \times 10^{-4}$

L'électronique dans cette réaction suit une tendance linéaire avec une pente négative pour les substituants OMe, tBu, H et Cl, ce qui indique que les groupes donneurs d'électrons (GDE) en position para du benzaldéhyde accélèrent la réaction en diminuant la barrière cinétique de l'étape cinétiquement déterminante (rate-determining step, rds) (Figure 16).

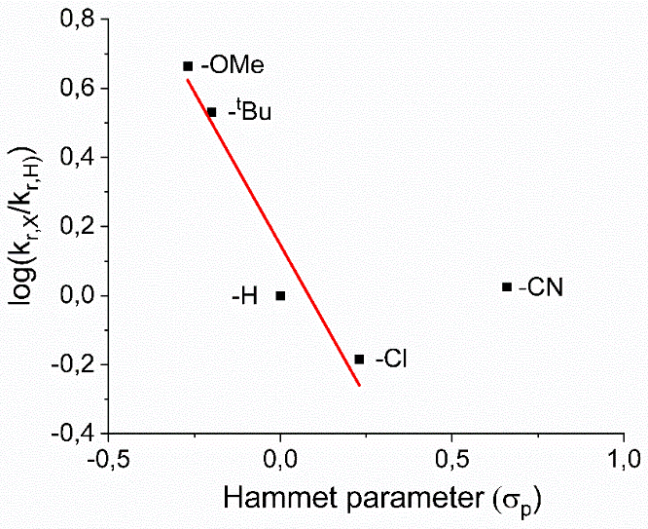

Figure 16. Graphe de Hammett pour les différents adduits du benzaldéhyde à 20 équivalents.

Les résultats expliquent que l'effet inductif a modifié la vitesse de la réaction. Lorsqu'il y a un GAE tel que Cl, de la densité électronique va être retirée. Cela signifie que le carbone sera plus électrophile et, de ce fait, retirera des électrons à l'oxygène. Dans ce cas, la réaction est plus lente, ce qui signifie qu'un GDE sera plus rapide, fournissant un oxygène plus nucléophile. Ce comportement nous donne un indice intriguant sur l'importance de l'oxygène, qui semble être l'élément qui entreprend l'attaque nucléophile initiale.

Cependant, le dérivé cyano conduisant au composé **15** diffère significativement de la tendance observée. Cette caractéristique pourrait provenir d'un changement de l'étape cinétiquement déterminante avec ce GAE ou de l'implication du groupement CN dans la réaction. Le groupe cyano est en effet une fonction base de Lewis. Dans cette optique, nous avons testé l'influence de l'ajout d'une base de Lewis sur les paramètres cinétiques de la réaction. Lorsque 20 et 70 équivalents de DMAP (DMAP = 4-diméthylaminopyridine) sont ajoutés à un mélange de **1** et 4-tBu-benzaldéhyde, une augmentation de la valeur de k_{obs} est observée (de 1,9 x 10^{-4} s^{-1} en l'absence de DMAP à 3,3 x10^{-4} s^{-1} en sa présence). Un tel résultat suggère que la présence de bases de Lewis pourrait aider cinétiquement l'étape déterminant la vitesse. La vitesse de réaction avec le 4-CN-benzaldéhyde serait alors influencée par des effets opposés : une diminution de la vitesse due à la nature électroattractrice du CN et une augmentation de la vitesse due à sa propriété de base de Lewis. Il est utile de mentionner qu'aucune réactivité de **3** envers le DMAP n'a été observée.

2.6. Compréhension du mécanisme

Les hypothèses suivantes ont été formulées sur la base des résultats expérimentaux obtenus dans ce travail et des études théoriques préliminaires menées par le Laboratoire de Physique et Chimie des Nano-Objets (LPCNO).

Comme hyphotèse, on peut dire que la molécule 1a existe sous une autre forme 1b plus réactive, où l'oxygène du CO2 reprend l'électron engagé avec le bore (Figure 80). Cette forme instable est élucidée à partir de la réversibilité de la réaction. L'oxygène du benzaldéhyde (2) déclenche la réaction, et 1b réagit avec 2, comme le suggère l'étude électronique. Une liaison hydrogène apparaît entre l'oxygène de 1b et l'hydrogène de l'aldéhyde, permettant une géométrie optimale conduisant à la décarboxylation. L'oxygène de l'aldéhyde donne son doublet d'électrons pour réaliser la liaison O-B . Le carbanion généré attaque le carbone électrophile de l'aldéhyde, conduisant au produit 3, et le dioxyde de carbone est libéré du système (Figure 80). L'intermédiaire OBB n'est jamais libéré complètement, et cela pourrait expliquer pourquoi il n'a pas été observé ou isolé les ts. Enfin, le Benzadd est formé de manière complètement diastéréosélective, donnant lieu au trans-diastéréoisomère de 3.

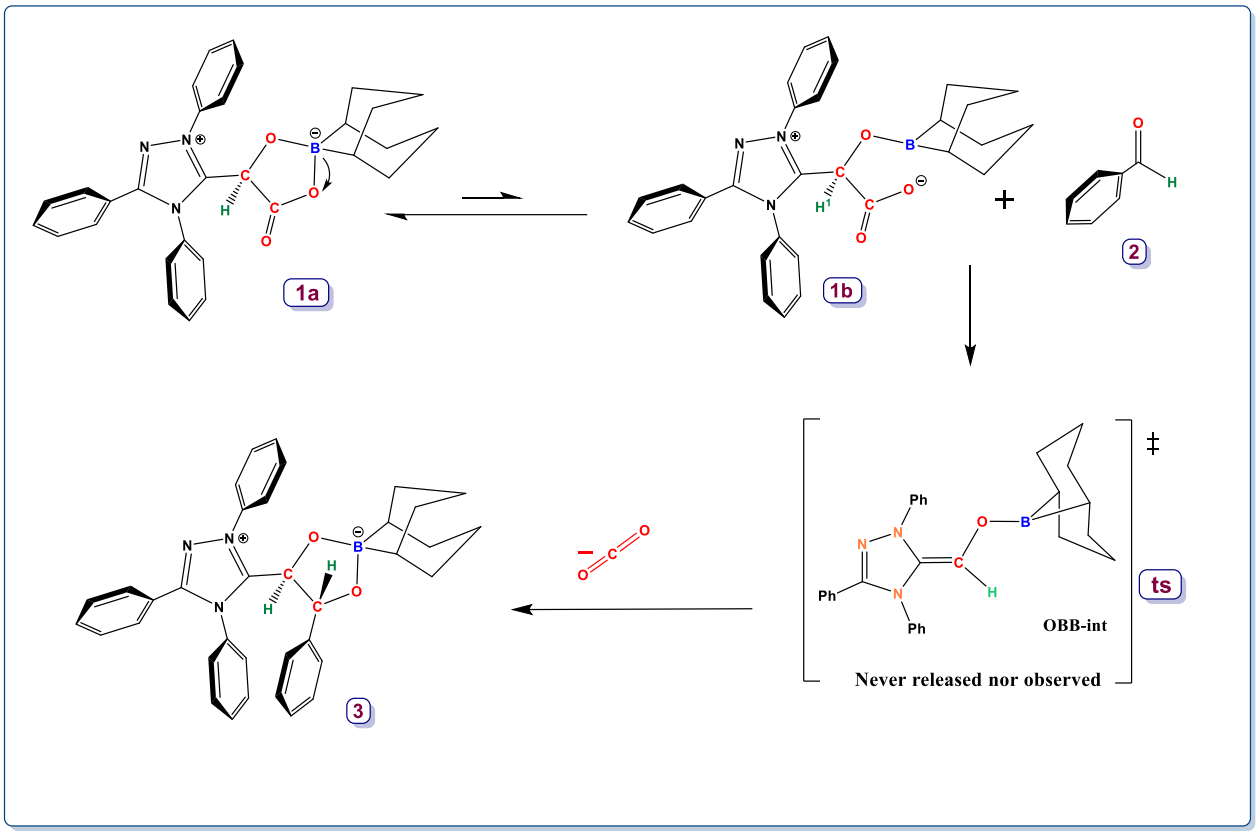

Figure 17. Le mécanisme proposé pour le système FLP pour l'activation des aldéhydes.

D'après l'énoncé, « *un produit cinétique est le produit qui se forme plus rapidement, et un produit thermodynamique est le plus stable* », et en tenant compte du fait que pendant la présente étude cinétique et mécanistique, le cis-diastéréoisomère n'a été observé à aucun moment., la diastéréosélectivité du système pourrait être dirigée à la fois par un contrôle thermodynamique et cinétique. Ce comportement du système permet un contrôle complet de la diastéréosélectivité pour la configuration trans observée expérimentalement, ce qui suggère que l'étape cinétiquement déterminante est associée à la barrière d'activation et évite par conséquent la formation de la structure cis.

CONCLUSIONS

Nous avons étudié la réactivité de divers types de petites molécules sur le système, y compris des molécules polaires et non polaires, et constaté que le système est chimiosélectif pour les aldéhydes. Ce

nouveau type de FLP intramoléculaire avec une diastéréosélectivité complète sans précédent a été révélé, conduit par un contrôle cinétique et thermodynamique pour le diastéréoisomère trans.

L'utilisation du **CO2add** a permis d'accéder à un intermédiaire de Breslow O-borylé (OBB) comme système FLP dans des conditions douces. Ce nouvel intermédiaire OBB est obtenu à partir d'une nouvelle voie de synthèse. Le mécanisme proposé pour cette réaction est le résultat d'études expérimentales et théoriques préliminaires, grâce auxquelles nous savons que l'intermédiaire OBB n'est jamais libéré pendant l'activation. Ceci explique pourquoi il n'est pas possible de l'observer dans le système conduit par contrôle cinétique et thermodynamique, étant suffisamment stable pour toute étude ultérieure sous sa forme masqué.

La relation d'énergie libre reliant les vitesses de réaction et les constantes d'équilibre par le biais du diagramme de Hammett a montré que l'étape cinétiquement déterminante comprend une molécule de **1** et une molécule de **2**, ce qui signifie qu'il s'agit d'une étape élémentaire (Figure 18). Les aldéhydes comportant des groupements électrodonneurs (GDE) favorisent le système, réduisant la barrière cinétique, et ceux possédant des groupements électroattracteurs (GAE) déstabilisent le système. Cependant, la vitesse de réaction est affectée par l'assistance éventuelle d'un acide de Lewis externe (comme dans le cas du groupe cyano ou du DMAP). L'équation de la loi de vitesse = kr [**react 1**]^1 [**react 2**]^1 fournit un ordre global de la réaction de 2.

Cette étude s'est accompagnée de difficultés dans les voies de synthèse. Travailler avec cette FLP qui comprend un carbène d'Enders rend le composé très sensible à l'air et à l'eau, ce qui complique les processus d'isolation et de cristallisation. Néanmoins, il a été possible de caractériser entièrement tous les produits et d'obtenir trois structures cristallographiques. La solubilité et stabilité a également constitué un défi, le THF étant le seul solvant à offrir une solubilité et stabilité suffisante pour mener à bien les réactions. Par exemple, dans d'autres solvants comme le benzène, certaines composés étaient solubles mais perdaient rapidement leur stabilité, ce qui entraînait leur décomposition.

Comme principale conclusion de ce travail, nous avons prouvé l'hypothèse selon laquelle le **CO2add** : est un nouveau système FLP intramoléculaire masqué avec des caractéristiques originales en tant que base de Lewis à base de carbone ; est chimiosélectif pour activer les aldéhydes ; conduit à

une diastéréosélectivité sans précédent, et ceci a amené des idées originales sur la cinétique et son mécanisme (Figure 18).

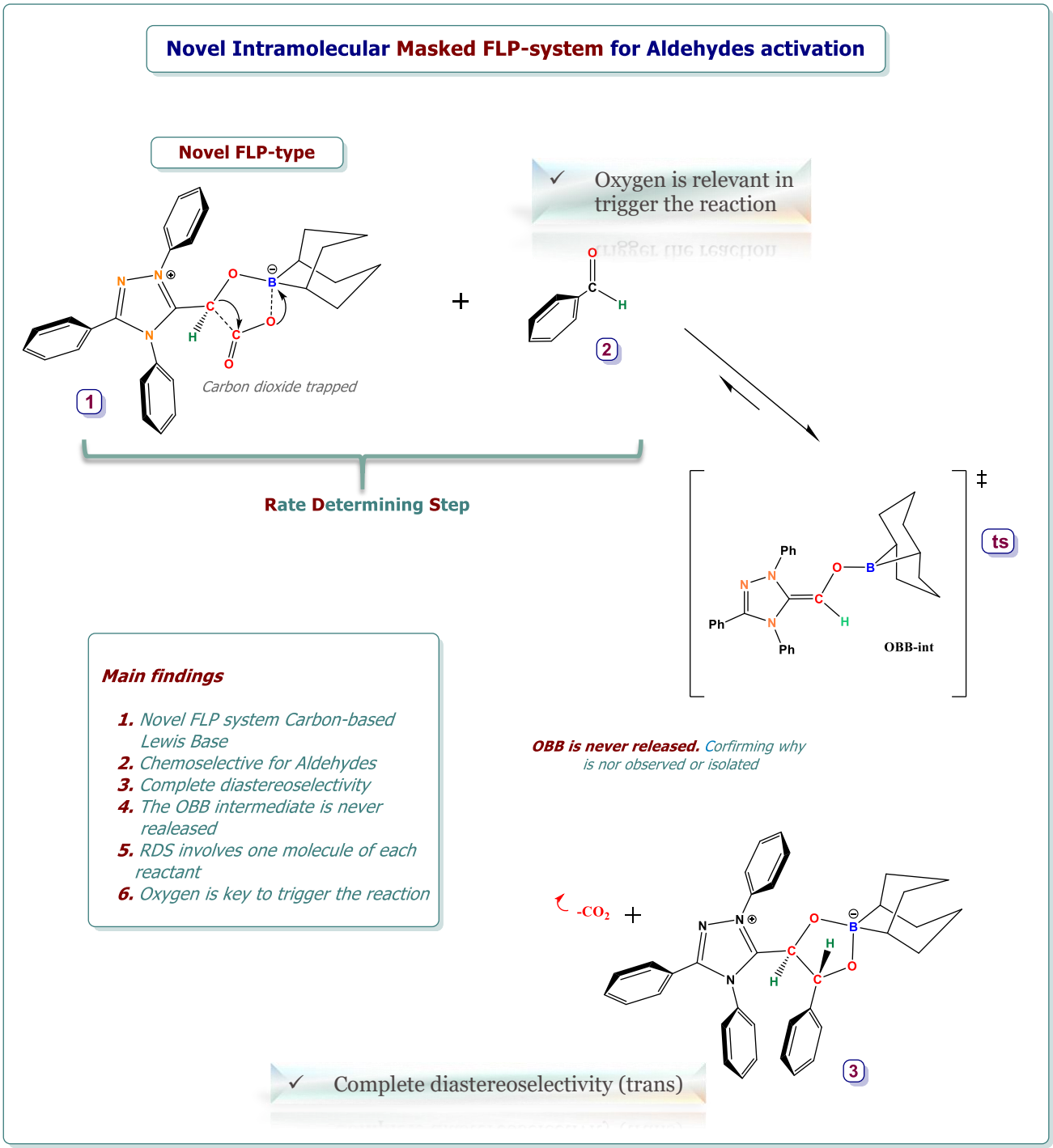

Figure 18. Principaux résultats pour le nouveau type de FLP intramoléculaire masqué pour l'activation des aldéhydes.

REFERENCES

(1) Appel, A. M. ; Bercaw, J. E. ; Bocarsly, A. B. ; Dobbek, H. ; DuBois, D. L. ; Dupuis, M. ; Ferry, J. G. ; Fujita, E. ; Hille, R. ; Kenis, P. J. A. ; Kerfeld, C. A. ; Morris, R. H. ; Peden, C. H. F. ; Portis, A. R. ; Ragsdale, S. W. ; Rauchfuss, T. B. ; Reek, J. N. H. ; Seefeldt, L. C. ; Thauer, R. K. ; etc. R. ; Ragsdale, S. W. ; Rauchfuss, T. B. ; Reek, J. N. H. ; Seefeldt, L. C. ; Thauer, R. K. ; Waldrop, G. L. Frontiers, Opportunities, and Challenges in Biochemical and Chemical Catalysis of CO 2 Fixation . *Chem. Rev.* **2013**, *113* (8), 6621-6658. https://doi.org/10.1021/cr300463y.

(2) CCNUCC. *Convention-cadre sur les changements climatiques. Adoption de l'accord de Paris, 21e conférence des parties, Paris : Nations Unies. Publication officielle* ; 2015.

(3) D'Alessandro, D. M. ; Smit, B. ; Long, J. R. Carbon Dioxide Capture : Prospects for New Materials. *Angew. Chem. Int. Ed.* **2010**, *49* (35), 6058-6082. https://doi.org/10.1002/anie.201000431.

(4) GIEC. *Rapport spécial du GIEC sur le CSC* ; 2011 ; Vol. 45. https://doi.org/10.1021/es200619j.

(5) Anastas, P. ; Warner, J. *12 Principles of Green Chemistry - American Chemical Society* ; 1998.

(6) Lapkin, A. ; Constable, D. J. C. *Green Chemistry Metrics : Measuring and Monitoring Sustainable Processes* ; John Wiley and Sons, 2009. https://doi.org/10.1002/9781444305432.

(7) lei, L. Mini - Review Reaction Mechanism of Hydrogen Activation by Frustrated Lewis Pairs.

(8) Stephan, D. W. ; Erker, G. Frustrated Lewis Pair Chemistry : Development and Perspectives. *Angew. Chem. Int. Ed.* **2015**, *54* (22), 6400-6441. https://doi.org/10.1002/anie.201409800.

(9) Béthegnies, A. ; Escudié, Y. ; Nuñez-Dallos, N. ; Vendier, L. ; Hurtado, J. ; del Rosal, I. ; Maron, L. ; Bontemps, S. Reductive CO_2 Homocoupling : Synthèse d'un glucide en C_3 borylé. *ChemCatChem* **2018**, *11* (2), cctc.201801875. https://doi.org/10.1002/cctc.201801875.

(10) Stephan, D. W. ; Erker, G. *Frustrated Lewis Pairs I : Découvrir et comprendre* ; 2013 ; Vol. 332. https://doi.org/10.1007/978-3-642-36697-0.

(11) Mömming, C. M. ; Frömel, S. ; Kehr, G. ; Fröhlich, R. ; Grimme, S. ; Erker, G. Reactions of an Intramolecular Frustrated Lewis Pair with Unsaturated Substrates : Evidence for a Concerted Olefin Addition Reaction. *J. Am. Chem. Soc.* **2009**, *131* (34), 12280-12289. https://doi.org/10.1021/ja903511s.

(12) Möricke, J. ; Wibbeling, B. ; Daniliuc, C. G. ; Kehr, G. ; Erker, G. Design and Reactions of a Carbon Lewis Base/Boron Lewis Acid Frustrated Lewis Pair. *Philos. Trans. R. Soc. A Math. Phys. Eng. Sci.* **2017**, *375* (2101). https://doi.org/10.1098/rsta.2017.0015.

(13) Dureen, M. A. ; Stephan, D. W. Reactions of Boron Amidinates with CO2 and CO and Other Small Molecules. *J. Am. Chem. Soc.* **2010**, *132* (38), 13559-13568. https://doi.org/10.1021/ja1064153.

(14) Frey, G. D. ; Lavallo, V. ; Donnadieu, B. ; Schoeller, W. W. ; Bertrand, G. Facile Splitting of Hydrogen and Ammonia by Nucleophilic Activation at a Single Carbon Center. *Science (80-.).* **2007**, *316* (5823), 439-441. https://doi.org/10.1126/science.1141474.

(15) Chase, P. A. ; Stephan, D. W. Activation d'hydrogène et d'amine par une paire de Lewis frustrée d'un carbène N-hétérocyclique volumineux et $B(C_6F_5)_3$. *Angew. Chem. Int. Ed.* **2008**, *47* (39), 7433-7437. https://doi.org/10.1002/anie.200802596.

(16) Chase, P. A. ; Gille, A. L. ; Gilbert, T. M. ; Stephan, D. W. Frustrated Lewis Pairs Derived from N-Heterocyclic Carbenes and Lewis Acids. *Dalton Trans.* **2009**, *0* (35), 7179. https://doi.org/10.1039/b908737k.

(17) Holschumacher, D. ; Bannenberg, T. ; Hrib, C. G. ; Jones, P. G. ; Tamm, M. Activation dihydrogène hétérolytique par une paire de Lewis Carbène-Borane frustes. *Angew. Chem. Int. Ed.* **2008**, *47* (39), 7428-7432. https://doi.org/10.1002/anie.200802705.

(18) Van Ausdall, B. R. ; Glass, J. L. ; Wiggins, K. M. ; Aarif, A. M. ; Louie, J. A Systematic Investigation of Factors Influencing the Decarboxylation of Imidazolium Carboxylates. *J. Org. Chem.* **2009**, *74* (20), 7935-7942. https://doi.org/10.1021/jo901791k.

(19) Kolychev, E. L. ; Bannenberg, T. ; Freytag, M. ; Daniliuc, C. G. ; Jones, P. G. ; Tamm, M. Reactivity of a Frustrated Lewis Pair and Small-Molecule Activation by an Isolable Arduengo Carbene-B{3,5-(CF3)2C6H3}3 Complex. *Chem. - Eur. J.* **2012**, *18* (52), 16938-16946. https://doi.org/10.1002/chem.201202840.

(20) Erker, G. ; Stephan, D. W. *Frustrated Lewis Pairs II : Expanding the Scope* ; 2013 ; Vol. 334. https://doi.org/10.1007/978-3-642-37759-4.

(21) Roters, S. ; Appelt, C. ; Westenberg, H. ; Hepp, A. ; Slootweg, J. C. ; Lammertsma, K. ; Uhl, W. Dimeric Aluminum-Phosphorus Compounds as Masked Frustrated Lewis Pairs for Small Molecule Activation. *Dalton Trans.* **2012**, *41* (30), 9033-9045. https://doi.org/10.1039/c2dt30080j.

(22) Hansch, C. ; Leo, A. ; Taft, R. W. A Survey of Hammett Substituent Constants and Resonance and Field Parameters. *Chem. Rev.* **1991**, *91* (2), 165-195. https://doi.org/10.1021/cr00002a004.

Frustrated Lewis Pairs systems (FLP) are a new concept in green chemistry due to their ability to function as free metal catalyst activation such as hydrogen, carbon dioxide, aldehydes, and all kinds of small molecules. The present document seeks to study the reactivity and potential use of a molecule as a masked FLP that, in its inner features, includes a nonclassical carbon-based Lewis base that is not coming from a carbene, and a borane as Lewis acid (compound **1**). Three parts were developed into this analysis strategy. The first was the reactivity study of various small molecule types on the system. The second part was to comprehend the benzaldehyde adduct reaction, identifying that the use of **1** enabled access to an O-Borylated Breslow intermediate as an FLP system for the product. In the third part, benzaldehyde adduct reaction was taken as a reference model to develop a methodology to be extended to other aldehydes. It has been proved that compound **1**: is a novel intramolecular masked FLP system with unique features; is chemoselective to activate aldehydes; has unprecedented diastereoselectivity, and this study brings original insights about the kinetics and the reaction mechanism.

Keywords: FLP – aldehydes – small molecules – diastereoselectivity – Breslow intermediate.

Les systèmes de paires de Lewis frustrées (FLP) constituent un nouveau concept en chimie verte en raison de leur capacité à fonctionner comme un catalyseur sans métal pour l'activation de composés tels que l'hydrogène, le dioxyde de carbone, les aldéhydes et toutes sortes de petites molécules. Ce document vise à étudier la réactivité et l'utilisation potentielle d'une molécule en tant que FLP masquée qui, dans ses caractéristiques internes, comprend une base de Lewis non classique à base de carbone qui ne provient pas d'un carbène, et un borane comme acide de Lewis (composé **1**). Trois parties ont été développées dans cette stratégie d'analyse. La première était l'étude de la réactivité de divers types de petites molécules sur le système. La deuxième partie consistait à comprendre la réaction de l'adduit du benzaldéhyde, en identifiant que l'utilisation de **1** permettait d'accéder à un intermédiaire de Breslow O-borylé comme système FLP pour le produit. Dans la troisième partie, la réaction de l'adduit du benzaldéhyde a été prise comme modèle de référence pour développer une méthodologie pouvant être étendue à d'autres aldéhydes. Il a été prouvé que le composé **1**: est un nouveau système FLP intramoléculaire masqué avec des caractéristiques originales; est chimiosélectif pour activer les aldéhydes; a une diastéréosélectivité sans précédent, et cette étude apporte un nouvel éclairage sur la cinétique et le mécanisme de la réaction.

Mots clés : FLP - aldéhydes - petites molécules - diastéréosélectivité - intermédiaire de Breslow.